

Surface Engineering Solutions for Scale Resistance

By

Mohammad Mohsen Vazirian

Submitted in accordance with the requirements for the degree of

Doctor of Philosophy

The University of Leeds

School of Mechanical Engineering

Leeds, UK

March, 2017

The candidate confirms that the work submitted is his/her own, except where work which has formed part of jointly-authored publications has been included. The contribution of the candidate and the other authors to this work has been explicitly indicated below. The candidate confirms that appropriate credit has been given within the thesis where reference has been made to the work of others.

In all papers listed below, the primary author completed all experimental studies, evaluation of data and preparation of publications. All authors contributed to proof reading of the articles prior to publication. Due to the radiation hazards of scale deposits in the oilfield, Mr. Felipe Batista Alvim (PETROBRAS R&D group – CENPES, Rio de Janeiro, Brazil) provided field data.

- **Vazirian, Mohammad Mohsen**, Thibaut VJ Charpentier, Mônica de Oliveira Penna, and Anne Neville. "Surface inorganic scale formation in oil and gas industry: As adhesion and deposition processes." *Journal of Petroleum Science and Engineering* 137 (2016): 22-32.
- **Vazirian, Mohammad Mohsen**, Thibaut TJ Charpentier, Anne Neville, Felipe Batista Alvim, and Mônica de Oliveira Penna. "Assessing Surface Engineering Solutions for Oilfield Scale; Correlating Laboratory Tests to Field Trials." In *SPE International Oilfield Scale Conference and Exhibition*. Society of Petroleum Engineers, 2016.
- **Vazirian, Mohammad Mohsen**, Felipe Batista Alvim, Mônica de Oliveira Penna, Thibaut VJ Charpentier, and Anne Neville. "Scale Deposition in the Oil and Gas Industry: From a Systematic Experimental Scale Study to Real-Time Field Data." In *CORROSION 2016*. NACE International, 2016.

This copy has been supplied on the understanding that it is copyright material and that no quotation from the thesis may be published without proper acknowledgement.

The right of “Mohammad Mohsen Vazirian” to be identified as Author of this work has been asserted by him in accordance with the Copyright, Designs and Patents Act 1988.

© 2017 The University of Leeds and Mohammad Mohsen Vazirian

Acknowledgements

Firstly, I would like to express my sincere gratitude to Professor Anne Neville, for the opportunity she gave me in doing this research project, for her trust, continued support, enthusiasm, encouragement and advice throughout my studies.

Secondly, I am particularly grateful for the assistance given by Victoria Masters during the transition of PhD programs, as I am sure without her support I could not have a chance to pursue my educations.

I would like to thank PETROBRAS for their financial support and technical contribution. I am also very grateful to Dr Thibaut Charpentier for his helpful advice and support. I cannot forget friends who went through hard times together, cheered me on, and celebrated each accomplishment: Erfan, Faezeh and Mahyar. Many thanks to my fellow research scale groups, Ogbemi, Laura, Jide, Michal, Bello, Loubna and William; and also members of iFS research group and the technicians, especially to Fiona, Nasim, Nasser, Ali, Farnaz, Siavash, Pourya, Frederick, Doris, Shahriar, Lukman, MacDonald, Zahra, James, Earle, Evan, Thawhid, Vishal, Ashley, Wassim, Danny, Rick, Sikiru, and Rachael Spraggs.

Special thanks to my sister, Marjan and her husband, Ali and my brother, Mohammad and his wife, Mahsa for having faith in me, without your help, I could not embark my PhD program in the UK.

Special gratitude to my mother (Fariba) and father (Reza) for their continuous love and encouragement, without whom I would never have the chance to accomplish any successes.

I would finally like to express my profound appreciation to my beloved wife, Aalam for her love and understanding during the past few years. A journey from Shiraz to Leeds, We did it together on our 2nd anniversary!

Abstract

Scale formation on surfaces can normally be divided into two distinct processes: a “deposition process” which refers to the process of heterogeneous nucleation and growth at the asperities of the surface in the bulk solution and an “adhesion process” which refers to the sticking of pre-existing crystals, which have nucleated in the bulk solution, and which build up as a layer on the surface. The presented work represents an experimental study of scaling tests to assess the effect of hydrodynamic conditions in a complex scaling environment, supersaturated with sulphate/carbonate-dominated brine solutions, on the stainless steel substrate coated with a range of commercially-available coatings. Due to the complexity of the brine solutions, the formed scale deposits are the product of the co-precipitation process. The morphology of the scale deposits along with the chemical composition of the surface scale deposits in different conditions was analysed and characterised.

In addition, the effect of the surface energy and surface roughness on both processes have been studied. The thesis provides data that will assist in the understanding of the controlling parameters in scale formation in different conditions, and also describes what characteristics of the surface can make it a good anti-scaling surface for inorganic scale; however, the results have shown that merely one parameter cannot assure a surface as a good antifouling surface.

Since most of the surface scaling studies have been focused on laboratory experiments and very little data are available to demonstrate such results are relevant and can be scaled-up to field environment, the current study focuses on correlating the systematic laboratory results with field trials. The current study shows that if properly selected, surface engineering offers great promise as an approach to prevent mineral scale deposition in the piping system of oilfields.

Table of Contents

Acknowledgements.....	IV
Abstract.....	V
Table of Contents	VI
List of Tables	X
Table of Figures.....	XII
Nomenclature & Abbreviations.....	XIX
Chapter 1 Introduction.....	1
1.1. Introduction.....	1
1.2. Oil and gas formation and extraction.....	2
1.3. Scaling in oil and gas	4
1.4. Objectives of the thesis	6
1.5. Overview and outline of the thesis.....	7
Chapter 2 Background and Literature Review.....	9
2.1. Introduction.....	9
2.2. Scaling in the oil and gas industry	9
2.3. Type of scales and scale formation.....	10
2.3.1. Calcium carbonate scale forms and its polymorphism	12
2.3.2. Sulphate scale formation.....	13
2.4. Scale formation process/ theories of crystal growth.....	15
2.4.1. Expression of supersaturation.....	16
2.4.2. Nucleation	18
2.4.3. Primary nucleation	18
2.4.4. Induction time	24
2.4.5. Scale crystal growth.....	26
2.4.6. Adhesion	27
2.5. Factors affecting scale formation.....	28
2.5.1. Effects of temperature.....	29
2.5.2. Effects of saturation ratio.....	30
2.5.3. Effects of pressure.....	30
2.5.4. Effects of bulk alkalinity (pH value).....	32
2.5.5. Effects of CO ₂	34
2.5.6. Effects of water composition	35
2.5.7. Effects of impurities.....	35
2.5.8. Effects of hydrodynamic conditions of the bulk solution.....	36

2.6.	Effect of nature of substrate	37
2.6.1.	Surface roughness	37
2.6.2.	Surface energy.....	39
2.6.3.	Scale control at surfaces.....	42
2.6.4.	Surfaces inspired by nature	45
2.7.	Co-precipitation and co-deposition.....	46
2.8.	Methods to remove and prevent scale in the oil and gas industry	50
2.8.1.	Mechanical removal techniques.....	51
2.8.2.	Chemical removal techniques	52
2.8.3.	Scale inhibitors.....	52
2.9.	Summary and gaps in the literature.....	52
Chapter 3	Experimental Methodology.....	55
3.1.	Introduction.....	55
3.2.	Chemical reagents	55
3.3.	Substrates	57
3.4.	Surface roughness measurements	62
3.5.	Surface energy measurements.....	66
3.6.	Dynamic scale deposition tests	70
3.7.	Surface scale deposition tests.....	73
3.7.1.	Limitations of surface scaling tests.....	74
3.8.	Turbidity meter.....	75
3.9.	Scanning Electron Microscopy (SEM)	76
3.10.	Inductively Coupled Plasma (ICP).....	78
Chapter 4	Results of Carbonate-dominated Brine	79
4.1.	Introduction.....	79
4.2.	Surface scale <i>deposition</i> of carbonate-dominated brine.....	80
4.3.	Surface scale <i>adhesion</i> of carbonate-dominated brine.....	82
4.4.	SEM scale deposits for <i>adhesion</i> and <i>deposition</i> processes in laminar and turbulent regimes.....	83
4.4.1.	SEM images in the <i>adhesion</i> process.....	84
4.4.2.	SEM images in the <i>deposition</i> process.....	99
4.5.	EDX analysis of scale deposits	109
4.6.	ICP analysis of scale deposits	112
4.7.	Summary	116
Chapter 5	Results of Sulphate-dominated Brine	119
5.1.	Introduction.....	119

5.2.	Surface scale deposition of sulphate-dominated brine.....	119
5.2.1.	SEM and EDX study of scale deposits	123
5.2.2.	Inductively Coupled Plasma (ICP) of scale deposits	137
5.3.	Summary	141
Chapter 6	Field Data.....	144
6.1.	Introduction	144
6.2.	Oilfield rig.....	144
6.3.	Oilfield results.....	146
6.4.	Summary	154
Chapter 7	Discussion of the Results	155
7.1.	Introduction	155
7.2.	Hydrodynamic effects on surface scale deposition.....	156
7.2.1.	Carbonate-dominated scale formation	156
7.2.2.	Sulphate-dominated scale formation.....	162
7.2.3.	Conclusion summary.....	167
7.3.	Surface roughness/energy effects on surface scale deposition	168
7.3.1.	Carbonate-dominated scales.....	168
7.3.2.	Sulphate-dominated scales	174
7.3.3.	Conclusion summary.....	177
7.4.	Morphology of scale deposits	178
7.4.1.	Carbonate-dominated scales.....	178
7.4.2.	Sulphate-dominated scales	181
7.5.	Co-precipitation of scale deposits	182
7.5.1.	Carbonate-dominated scales.....	182
7.5.2.	Sulphate-dominated scales	184
7.6.	Field data.....	186
7.6.1.	Mass gain	187
7.6.2.	Conclusion	189
Chapter 8	Conclusion	190
8.1.	Conclusion summary.....	190
8.2.	Surface scale formation.....	190
8.3.	Good anti-fouling surfaces.....	191
8.4.	Morphology and co-precipitation of scale deposits	192
8.5.	Correlating the laboratory studies to field data.....	194
8.6.	Future work	195

Bibliography 197

List of Tables

Table 2.1. Common scales in oil and gas industry (conditions: T = 100°C, at pH = 7) [10-12]	11
Table 2.2. A summary of investigations of calcium carbonate polymorphs [21, 22]......	13
Table 3.1. Ion composition of both brines.....	55
Table 3.2. Brine composition of both brines.....	56
Table 3.3. Saturation ratio of brine solutions calculated by Multiscale® software.....	56
Table 3.4. Modified substrates with their corresponding coating code	57
Table 3.5. The molecular structures of different fluoropolymers	60
Table 3.6. The surface roughness for all the substrates used in the scaling tests, presented in the form of R_a, R_{sk}, R_{ku}, and R_{pc}.	65
Table 3.7. Surface tension (mN/m) components of liquid probes [122].	68
Table 3.8. Hydrodynamic conditions of RCE test cases	72
Table 6.1. The order number of the commercial coatings positioned from the inlet of the oilfield rig.	145
Table 6.2. Ion composition of the water in the oilfield rig.....	146
Table 6.3. Saturation ratio calculations of the oilfield water composition.	146
Table 6.4. The scale deposits mass gain of the pipes along the pipeline.....	147
Table 6.5. Images of the modified pipe spools in the flow rig before (Stage 1) and after (Stage 2&3) running the test along with post processing (Stage 4).....	148
Table 6.6. Elemental results of the surface scale deposits on surface “B5891” and uncoated (or “UC”) on three random points along with their whole mapping area.....	150
Table 6.7. The mass gain of the modified pipe spools without the presence of iron-based compounds.	151
Table 6.8. The scaling tendency performance efficiency of modified substrates with regard to (a) the average performance of uncoated substrates and (b) hypothetical SR value along the piping system.	153
Table 7.1. The comparison of the surface scale mass gains ratio for different flow regimes and surface scale processes, in carbonate-dominated brine.	160
Table 7.2. The comparison of the surface scale mass gain ratio for different flow regimes and surface scale processes in sulphate-dominated brine.	165

Table 7.3. The chemical compound of the carbonate-dominated scale deposits on the surface, analysed by ICP in turbulent and laminar flow conditions in the <i>adhesion</i> and <i>deposition</i> processes.....	183
Table 7.4. The chemical compound of the sulphate scale deposits on the surface, analysed by ICP in turbulent and laminar flow conditions in the <i>deposition</i> process.....	185
Table 7.5. The comparison between the supersaturation ratio of the brine composition tested in the laboratory setup and the field data.....	186
Table 7.6. The comparison of the flow regimes between the laboratory setup and the field data.....	187
Table 7.7. The comparison of scale deposits growth in the oilfield with the laboratory setup for both carbonate/sulphate-dominated brine compositions for <i>adhesion</i> and <i>deposition</i> processes.	188
Table 7.8. The scale tendency performance ranking of the epoxy coating in the oilfield and the laboratory.	188

Table of Figures

Figure 1.1. Enhanced oil recovery (EOR) using CO ₂ injected into oil reserves will boost oil production [4].....	3
Figure 1.2. Flowline clogged by scale [6].....	4
Figure 1.3. The formation of carbonate scale in an oilfield: (a) Before the drill bit reaches and cracks the reservoir (the reservoir is at high pressure) and (b) After the drill bit cracks the reservoir, oil production is on-going and the downhole pressure is decreasing.	5
Figure 1.4. The formation of sulphate scale in the oilfield: (a) Oil production at an optimum rate, (b) Oil production depletion, (c) pumping seawater into the oil well, rich in sulphate ions and (d) EOR with seawater.	6
Figure 2.1. SEM images of scales: (a) calcite, (b) aragonite, (c) vaterite; and (d) vaterite (spherical), aragonite (needle-like), and calcite (rhombic) [19].....	12
Figure 2.2. SEM images of normal crystal form of barite: Orthorhombic (a) and (b) [26]; Bipyramidal (c) and (d) [27].....	14
Figure 2.3. SEM images of strontium sulphate at (a) 298K and (b) 308K [30].....	15
Figure 2.4. Schematic representation of the most important steps in the pathway from soluble ions to a microscopic calcium carbonate scale deposit [31].....	15
Figure 2.5. Homogeneous nucleation process: ion pairs in supersaturation system and then cluster start to grow [2].....	17
Figure 2.6. Free energy diagram with regard to the radius of the particle [38].....	19
Figure 2.7. The nucleation induced by surface defects or rough spots, called as “heterogeneous” nucleation [2].	21
Figure 2.8. Interfacial tension at the boundaries between two solids and one liquid [32].....	22
Figure 2.9. A de-supersaturation curve (diagrammatic): c^* = equilibrium saturation, t_n = nucleation time, t_{ind} = induction time, t_{lp} = latent period [32].	25
Figure 2.10. Plot of the induction time versus the SR_{CaCO_3} for different temperatures based on an empirical equation [45].....	26
Figure 2.11. Reaction rate constant of barium sulphate with regard to supersaturation in different temperatures [51].....	29
Figure 2.12. Average coverage estimated by electrochemical technique versus pressure [56].	30

Figure 2.13. Prediction of BaSO ₄ (above) and CaCO ₃ (below) scale formation with regard to temperature, pressure and supersaturation [55].	31
Figure 2.14. The effect of pH on corrosion and scale [58].	32
Figure 2.15. Specification diagram for CO ₂ in seawater showing the relative proportion of each species.	33
Figure 2.16. Schematic representation of the carbonic scale system [60].	34
Figure 2.17. The amount of deposited scale from different mixtures of formation water and injected water (seawater) [2].	35
Figure 2.18. Efficiency of Mg ²⁺ on bulk precipitation and surface deposition [62].	36
Figure 2.19. Wall shear stress versus deposition weight (mild steel). Condition: CaSO ₄ conc. = 1000ppm, T=40°C, pH=8 [58], q=31082.03 W/m ² , time-48hr.	37
Figure 2.20. The effect of surface roughness (R _a) on calcite layer adhesion strength [63].	38
Figure 2.21. Scheme representing the contact angle (θ) between the vapour, liquid and solid phases for a liquid on a solid.	39
Figure 2.22. An average mass gain of scale deposit vs. water contact angle [64].	43
Figure 2.23. Induction time prediction for stainless steel and copper under batch conditions [80].	44
Figure 2.24. Plant surface structures and wettability, (a) to (c) representing SEM images with a different resolution of the surface structure of a lotus leaf [84].	46
Figure 2.25. Schematic representing the pathways of scale prevention [31].	51
Figure 3.1. Ternary phase diagram of bonding in amorphous carbon-hydrogen alloys [117].	61
Figure 3.2. Evaluation of the surface roughness profile.	62
Figure 3.3. The distribution curve of the surface profile: (a) surface skewness and (b) surface kurtosis.	63
Figure 3.4. Illustration of the stylus profilometer sketch[118].	64
Figure 3.5. Kurtosis value for two modified surfaces: (a) B1341 and (b) DHS.	65
Figure 3.6. The surface roughness along with the number of peaks per centimetre of each modified substrate.	66
Figure 3.7. Illustration of contact angle formed by a sessile liquid drop on a smooth homogeneous solid surface[120].	67
Figure 3.8. Illustration of a contact angle measurement using sessile drop technique [121].	67

Figure 3.9. Typical results obtained from the contact angle measurement tests using the sessile drop technique for (a) the most hydrophobic coating and (b) the most hydrophilic.	68
Figure 3.10. The surface energy of modified surfaces along with their polar and dispersive components with two sets of liquid probes: (a) diiodomethane and water and (b) diiodomethane and ethylene glycol.	69
Figure 3.11. Rotating Cylinder Electrode (RCE) components and its experimental setup.	71
Figure 3.12. Schematic of scale formation in different regions of an oilfield: region A: heterogeneous nucleation and crystal growth, and region B: adhesion of particles to the surface [124].	74
Figure 3.13. Illustration of turbidity measurement using the light scattering technique [125].	75
Figure 3.14. Turbidity measurement of the brine solutions for both the carbonate-dominated (blue dots) and sulphate-dominated (red crosses) brines. “Deposition” process starts at 0 min and “Adhesion” process starts at 90 min.	76
Figure 3.15. Schematic diagram of SEM.	77
Figure 4.1. Mass gain of modified surfaces in the <i>deposition</i> process in (a) laminar flow regime, (b) turbulent flow regime.	81
Figure 4.2. Mass gain of modified surfaces in adhesion process in (a) laminar flow regime, (b) turbulent flow regime.	83
Figure 4.3. SEM images of the scale deposits formed on different modified surfaces at different magnification range in the adhesion process for laminar flow regime.	92
Figure 4.4. SEM images of the scale deposits formed on different modified surfaces at different magnification range in the adhesion process for turbulent flow regime.	98
Figure 4.5. The SEM image of scale deposits in the adhesion process in the turbulent conditions. Heterogeneous nucleation and crystal growth still occurring onto the surface: (a) DLC and (b) TiN.	99
Figure 4.6. The SEM image of scale deposits on the “B1341” coating in the <i>deposition</i> process.	100
Figure 4.7. The SEM image of scale deposits on the “B1391” coating in the <i>deposition</i> process.	101
Figure 4.8. The sharp edges of calcite are rounded on different modified surfaces: (a) ETFE and (b) PFA.	101
Figure 4.9. The formation of needle-like aragonite bundle with low aspect ratio and calcite formation and dissolution at their edges in the <i>deposition</i> tests on the fluoropolymer surfaces: (a) ETFE, (b) FEP, (c) PFA and (d) PTFE.	102

Figure 4.10. The formation of rounded edges calcite, needle-like aragonite with low aspect ratio and round shape and/or di-pyramidal vaterite formed in the <i>deposition</i> tests on different modified surfaces: (a) CrN, (b) DLC, (c) TiN, (d) DLC, (e) DHS and (f) Stainless steel.	103
Figure 4.11. SEM images of CaCO ₃ deposited on DLC: showing deformity at the centre of the cubical structure.....	104
Figure 4.12. SEM images of the crystal morphologies of scale deposits on a specific substrate (TiN) in different flow regimes: (a) Turbulent conditions (b) Laminar conditions	105
Figure 4.13. SEM images of carbonate scale formation in laminar conditions (zoomed out): (a) DHS, (b) TiN, (c) Stainless steel, and (d) DLC.	106
Figure 4.14. SEM images of scale formation in turbulent conditions (zoomed out): (a) DLC, (b) DTi, (c) B1541 and (d) Black.....	106
Figure 4.15. SEM images of scale deposits on different modified surface, the formation of polyhedron calcite due to the existence of Mg ²⁺ crystals: (a) B5891, (b) CrN, (c) Stainless steel, and (d) DHS.....	107
Figure 4.16. SEM images of scale deposits on modified surfaces: (a) DHS and (b) Stainless steel; formation of aragonite (needle-like bundles) with low aspect ratio with an orientation parallel to the surface.	108
Figure 4.17. EDX images of scale deposits: the presence of magnesium in the lattice of calcium carbonate (aragonite).	108
Figure 4.18. EDX analysis of surface scale formation (surface deposition of CaCO ₃ , SrCO ₃ and BaSO ₄).....	109
Figure 4.19. EDX images of scale deposited on the stainless steel surface: the incorporation of strontium in the lattice of aragonite, but not the calcite.....	110
Figure 4.20. EDX images of scale deposits on DHS surface: incorporation of strontium in the lattice of aragonite is higher compared to both calcite and vaterite.	111
Figure 4.21. ICP results of the scale deposits in the <i>deposition</i> tests presented in mass gain: (a) Laminar and (b) Turbulent flow conditions.	112
Figure 4.22. ICP results of the scale deposits in the <i>adhesion</i> tests presented in mass gain: (a) Laminar and (b) Turbulent flow conditions.....	113
Figure 4.23. Mole percentage of barium, calcium, strontium and magnesium existing on the surface as scale deposits in the <i>deposition</i> process: (a) Laminar and (b) Turbulent flow conditions.	114
Figure 4.24. Mole percentage of barium, calcium, strontium and magnesium existing on the surface as scale deposits in the <i>adhesion</i> process: (a) Laminar and (b) Turbulent flow conditions.	115

Figure 5.1. Scale deposits formed on different modified substrates in the <i>deposition</i> tests, where the focus is on heterogeneous nucleation and crystal growth, in (a) laminar and (b) turbulent conditions.	120
Figure 5.2. Scale deposits thickness growth of different modified substrates in the <i>adhesion</i> tests, where the focus is on <i>adhesion</i> of pre-precipitated of scale crystals, in (a) laminar and (b) turbulent conditions.	121
Figure 5.3. SEM images of the scale deposits formed on different modified surfaces at different magnification range in the <i>adhesion</i> process for turbulent flow regime.	128
Figure 5.4. SEM images of the scale deposits formed on different modified surfaces at different magnification range in the <i>adhesion</i> process for laminar flow regime.	131
Figure 5.5. The SEM images of the scale deposits on different modified surfaces in the <i>deposition</i> tests in the turbulent flow conditions.	132
Figure 5.6. The SEM images of the scale deposits on different modified surfaces in the <i>deposition</i> tests in the laminar conditions.	135
Figure 5.7. The SEM images of scale deposits on different modified surfaces: the size of each morphology of the sulphate-dominated scale deposits is in the same range.	135
Figure 5.8. EDX images of the sisal-like hierarchical structure morphology.	136
Figure 5.9. EDX images of the bowtie structure morphology.	137
Figure 5.10. ICP results of the scale deposits in the <i>deposition</i> tests presented in mass gain: (a) Laminar and (b) Turbulent flow conditions.	138
Figure 5.11. ICP results of the scale deposits in the <i>adhesion</i> tests presented in mass gain: (a) Laminar and (b) Turbulent flow conditions.	139
Figure 5.12. Mole percentage of calcium, barium and strontium existing on the surface as scale deposits in the <i>deposition</i> process: (a) Laminar and (b) Turbulent flow conditions.	140
Figure 5.13. Mole percentage of calcium, barium and strontium existing on the surface as scale deposits in the <i>adhesion</i> process: (a) Laminar and (b) Turbulent flow conditions.	141
Figure 6.1. Onshore oilfield flow rig.	144
Figure 6.2. Schematic of oilfield site flow rig: green lines are coated pipes, red lines are uncoated pipes.	145
Figure 6.3. The scale deposits mass gain of each substrate along the flow rig.	147
Figure 6.4. SEM images of scale deposits formed on the pipe surfaces along with three random points analysed by EDX technique.	149
Figure 6.5. The X-ray diffraction analysis of the scale deposits in the rig: (a) coated pipe and (b) uncoated pipe.	150

Figure 6.6. The comparison of the mass gain of each substrate with regard to hypothetical SR: (1) SR does not change, (2) SR decreases linearly, (3) SR decreases non-linearly along the piping system.....	152
Figure 7.1. The comparison of the surface scale mass gain between the <i>deposition</i> and <i>adhesion</i> processes for (a) Laminar and (b) Turbulent flow conditions.....	157
Figure 7.2. The comparison of the surface scale mass gain between the laminar and turbulent flow conditions for (a) <i>Deposition</i> and (b) <i>Adhesion</i> processes.	158
Figure 7.3. The summary mass gain comparison of the <i>adhesion</i> and <i>deposition</i> processes with regard to the flow regimes in carbonate-dominated brine: (a) the flow regimes have different behaviour toward the <i>adhesion/deposition</i> processes, (b) the processes have the same effect on the flow regimes of the bulk solution with different magnitude.	161
Figure 7.4. Comparison of scaling tendency in different levels of agitation in the (a) <i>Adhesion</i> and (b) <i>Deposition</i> processes.....	162
Figure 7.5. Comparison of scaling tendency in different processes of scale formation in (a) Laminar and (b) Turbulent flow conditions.....	164
Figure 7.6. The summary mass gain comparison of the <i>adhesion</i> and <i>deposition</i> processes with regard to the flow regimes in sulphate-dominated brine: (a) the flow regimes have the same behaviour toward the <i>adhesion/deposition</i> processes, (b) the processes have the same effect on the flow regimes of the bulk solution with different magnitude.	166
Figure 7.7. The effect of surface roughness on a number of surface scale deposits in the <i>deposition</i> process in (a) laminar, and (b) turbulent flow conditions.....	168
Figure 7.8. The effect of surface roughness on a number of surface scale deposits in the <i>adhesion</i> process in (a) laminar, and (b) turbulent flow conditions.	169
Figure 7.9. The effect of surface peaks density on a number of surface scale deposits in the <i>deposition</i> process in (a) laminar, and (b) turbulent flow conditions; and in the <i>adhesion</i> process in (c) laminar, and (d) turbulent flow conditions.	169
Figure 7.10. The effect of surface peaks density on ceramic surface scale deposits in laminar flow conditions in the <i>deposition</i> process for (a) all the ceramic coatings, and (b) ceramic coatings except DTi.	170
Figure 7.11. Schematic of two surfaces with a different number of peaks in a specific length.	171
Figure 7.12. The effect of surface energy components on the scaling tendency rate in the <i>deposition</i> process using liquid probes for diiodomethane and water for laminar (left column) and turbulent (right column) flow conditions.....	171

Figure 7.13. The effect of surface energy components on the scaling tendency rate in the <i>deposition</i> process using liquid probes for diiodomethane and ethylene glycol for laminar (left column) and turbulent (right column) flow conditions.....	172
Figure 7.14. The effect of surface energy components on the scaling tendency rate in the <i>adhesion</i> process using liquid probes for diiodomethane and water for laminar (left column) and turbulent (right column) flow conditions.....	173
Figure 7.15. The effect of surface roughness and peak distribution on the surface scale growth rate in the <i>adhesion</i> process, for (a) & (c) Turbulent and (b) & (d) Laminar flow conditions respectively.	174
Figure 7.16. The effect of surface roughness and peak distribution on the surface scale growth rate in the <i>deposition</i> process for (a) & (c) Turbulent and (b) & (d) Laminar flow conditions, respectively.	175
Figure 7.17. The effect of surface energy on the surface scale growth rate in the <i>adhesion</i> process for (a) Turbulent and (b) Laminar flow conditions.	176
Figure 7.18. The effect of surface energy on the surface scale growth rate in the <i>deposition</i> process for (a) Turbulent and (b) Laminar flow conditions.	177
Figure 7.19. Schematic illustration of the formation process of the SrSO₄ sisal-like hierarchical structures [29] and the natural shape of a sisal plant.....	181
Figure 7.20. The SEM image of the scale deposits showing the evolution steps of the bowtie structure morphology.....	181

Nomenclature & Abbreviations

a	initial concentration of the precipitate
b	initial concentration of the solution
A	Arrhenius constant, or surface area
C	actual concentration of solute
C_e	equilibrium concentration of solute
D	diffusion coefficient
J	rate of nucleation
K	solubility
K_{sp}	solubility of product
K_{Sr}^A	distribution coefficient of strontium in aragonite
K_{Sr}^C	distribution coefficient of strontium in calcite
P	pressure
Re	Reynolds number
R_a	arithmetic mean of the absolute departure of the roughness profile
R_{ku}	Kurtosis value, spikiness of the measure profile
R_{sk}	measured profile skewness
R_{pc}	peaks number in a certain length
S_a	surface roughness average
S_{sk}	surface skewness
SI	supersaturation index
SR	supersaturation ratio
T	temperature
U_{cyl}	linear velocity of cylinder
a_i	ion activity of anion or cation
c	solution concentration
c^*	solution concentration at equilibrium saturation at a given temperature
d_{cyl}	diameter of cylinder
dm/dt	mass of the solute deposited on the crystal surface during time
k	Boltzman constant
l_m	total measured length of the profile
r	radius of the particle

r^* or r_{crit}	nucleus critical radius
t_g	grow time of nucleus
t_{ind}	induction time
t_n	nucleation time
t_r	relaxation time
v	molecular volume
z_x	sampling length
Δc	concentration driving force
ΔG	overall free energy change
ΔG_{crit}	overall critical free energy change (homogeneous nucleation)
$\Delta G'_{crit}$	overall critical free energy change (heterogeneous nucleation)
ΔG_S	free energy between the surface of the particle and the bulk
ΔG_V	free energy change of transformation
γ	interfacial tension (or surface energy)
γ_{cl}	interfacial tension between crystalline deposit and liquid
γ_{cs}	interfacial tension between crystalline deposit and the solid surface
γ_{sl}	interfacial tension between the solid surface and the liquid
γ^{lv}	liquid surface free energy
γ^{sl}	solid/liquid interfacial free energy
γ^{sv}	solid surface free energy
γ_i^d	dispersion energy of testing drop i
γ_i^p	polar energy of testing drop i
γ_s^d	dispersion energy of testing surface
γ_s^p	polar energy of testing surface
γ_s^+	surface tension contributed by acid
γ_s^-	surface tension contributed by base
δ	thickness of the stagnant layer at the vicinity of crystal surface
σ	relative supersaturation
λ	distribution coefficient
θ	contact angle
μ	viscosity

ρ	density
τ_{cyl}	surface shear stress of the cylinder
φ	nucleation correction factor
<i>ASTM</i>	American Society for Testing and Materials
<i>CCS</i>	Carbon Capture and Sequestration
<i>EDS</i>	Energy Dispersive X-ray spectroscopy
<i>EDX</i>	Energy Dispersive X-ray
<i>EOR</i>	Enhanced Oil Recovery
<i>FTU</i>	Formazin Turbidity Unit
<i>ICP</i>	Inductively Coupled Plasma
<i>RCE</i>	Rotating Cylinder Electrode
<i>SEM</i>	Scanning Electron Microscope
<i>TDS</i>	Total Dissolved Solid

Chapter 1

Introduction

1.1. Introduction

Calcium carbonate is an abundant inorganic mineral comprising approximately 4% of the earth's crust which is widely developed both by nature and humankind [1]. However, the formation of calcium carbonate in the industry is not favourable and is called fouling or “scaling” in the industry. It causes the blockage of the pipes, reduces the heat transfer in boilers and condenser and affects the vulnerability of the equipment in contact with water e.g. pump failure. Other than calcium carbonate scale which is the most common scale in the industry, there are other types of scales such as barium sulphate that is extremely resistant to both chemical and mechanical removal [2].

Conventionally scale studies have involved in the evaluation of bulk scaling which describes the process of scale forming in a solution, here referred to as precipitation. Deposition or formation of scale at a surface has received much less attention. The surface deposition phenomenon is not well understood so far, therefore the main focus of this research will be on the surface deposition and the parameters that affect this phenomenon.

Inhibition has been by far the most commonly employed and effective means of controlling scale but nowadays the surface engineering has received some attention, however, it is still in its early stages for scale control.

There are many approaches to remove scaling, however, prevention is recognised as a more efficient and preferable method of management.

Surface engineering is a critical technology behind major industries including aerospace, automotive, construction, the off-shore industries, power generation and bio-medical applications. Appropriate coatings can solve a diverse collection of engineering problems and provide protection against corrosion, wear damage or high temperature, but these can also supply added-value, increasing economic and environmental benefits. In this study, we will introduce surface engineering strategies for the management of scale deposition in valve and pipe components.

1.2. Oil and gas formation and extraction

The oil and gas that we use today began as microscopic plants and animal living in the ocean million years ago. These microscopic plants and animals absorbed the energy from the sun and stored them as carbon molecules in their bodies. When these creatures died, they sank to the bottom of the sea. Over millions of years, plants, sediment and bacteria accumulated over layer by layer, and as they buried deeper and deeper, the heat and pressure began to rise. High pressure and temperature turn the decaying plants and micro-organisms into useful hydrocarbons (i.e. oil and natural gas). A percentage of these formed oil and gas escaped through the pores of the layer to the atmosphere, but other were trapped under the impermeable layers of rocks or clay. These trapped deposits are where we find oil and natural gas reservoirs as today.

After geologists find the right place to be potential for oil and gas extraction, a hole is drilled and a casing is lowered down into the hole. Then cement is pumped through the bottom of the casing to fill the area between the casing and the side of the well, in order to prevent oil, gas and brines from entering and contaminating the underground fresh water (aquifers). Since the casing should be in the oil well for a long time and the maintenance is costly, a pipe which is called tubing is placed in the casing which the oil and gas are produced through this pipe.

- The amount of extracted oil and natural gas from deep underground varies depending on factors like porosity of the rock and the viscosity of the deposits which hinder the free flow of the product into the well. Oil and gas can be recovered in three main stages as follows [3]:
 1. Primary recovery: This technique relies on the pressure of the underground to drive fluids to the surface. There are some other methods to artificially lift the oil up such as pumping back the gas to the well to push the oil up. In this method, just 10% of the oil in the deposits is recoverable.
 2. Secondary recovery: In this technology the water that is produced and separated from the oil in the initial phase of drilling is pumped into the oil-bearing to boost oil recovery with an additional 20% of the oil in place to the surface.
 3. Enhanced recovery: There are three main approaches to extract the remaining oil in the reservoir: thermal recovery, gas injection and chemical flooding. By employing these techniques, 60% of the reserve can be recovered to the surface.

(a) Thermal recovery: In this technique, steam is injected into the reservoir. Steam increases the pressure of the reservoir and also the heat from steam reduces the viscosity of the oil which makes the flow easier to flow.

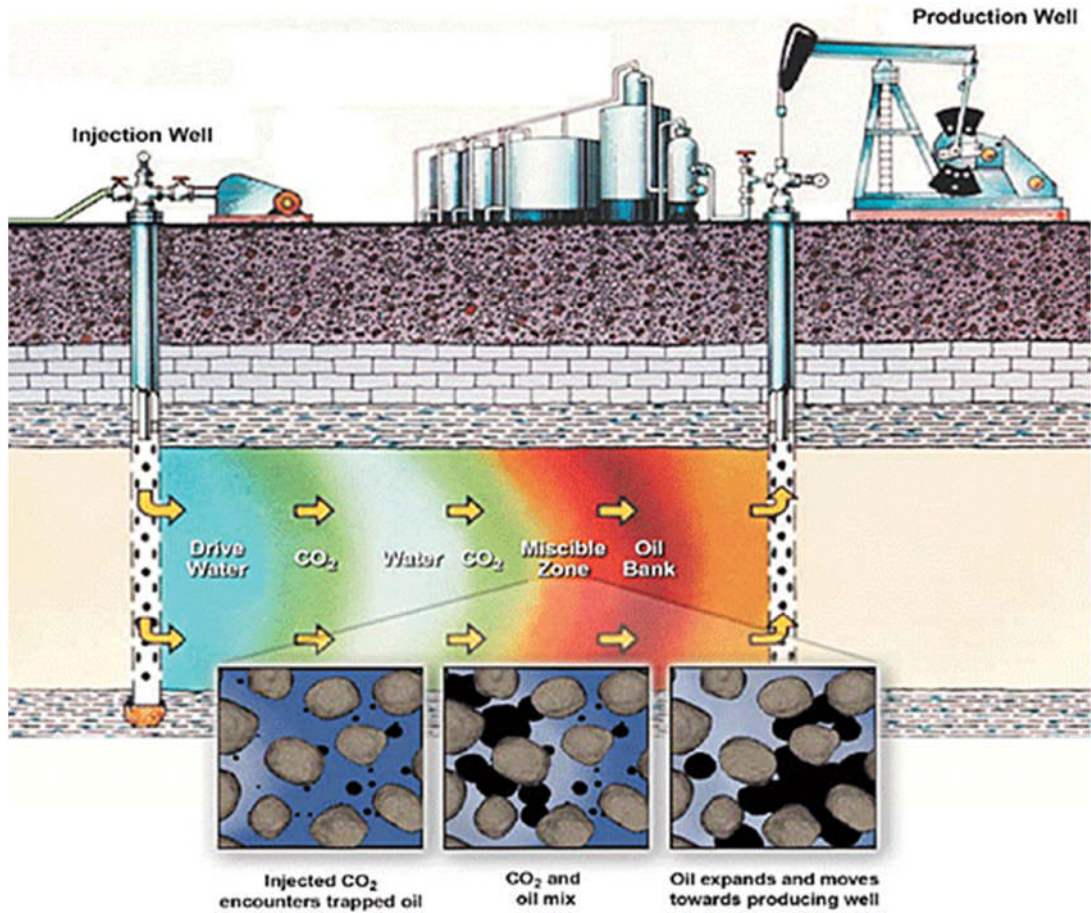


Figure 1.1. Enhanced oil recovery (EOR) using CO₂ injected into oil reserves will boost oil production [4].

(b) Gas injection: The aim of this technique is the same as thermal recovery technique but with different methodology. By injecting miscible gases into the reservoir, gases such as CO₂, methane, propane or other gases dissolve in the oil to lower the viscosity and increase flow, and by injecting immiscible gases which do not mix with oil, it increases the pressure of the reservoir instead. This technique is nowadays widely used by CO₂ flooding not only for the purpose of Enhanced Oil Recovery (EOR) but also for reducing the emissions from the fossil fuels as a part of global warming scope. The schematic

of EOR as part of Carbon Capture and Sequestration (CCS) technique is shown in Figure 1.1.

- (c) Chemical flooding: This technique involves in injecting mixing dense, water soluble polymers to the reservoir which has an identical effect like the other techniques [3].

1.3. Scaling in oil and gas

Generally, the accumulation of dissolved minerals and deposition on equipment surfaces is called scaling. Scale formation is recognised as one of the major flow assurance problems affecting production in the oil and gas sector. The main problem of scaling is clogging the wellbore and preventing fluid from flowing easily, which could be so costly. For instance, in the North Sea well in the Miller field, the production fall from 30,000 Barrel per day to zero in just 24 hours. The scale can be deposited all along the water paths [5].



Figure 1.2. Flowline clogged by scale [6].

The scale is mostly originated either from the precipitation of water that is naturally in the reservoir or as a result of produced oversaturated water with scale component when two incompatible water streams meet in the downhole. As a result, wherever

water is injected into the oil well to enhance recovery, there is a possibility of scale to form [2].

As shown in Figure 1.2, the thickness of the scale deposit is about 3 inches which have reduced the pipeline cross-sectional area by more than 58% in every three to five months depending on the water cut.

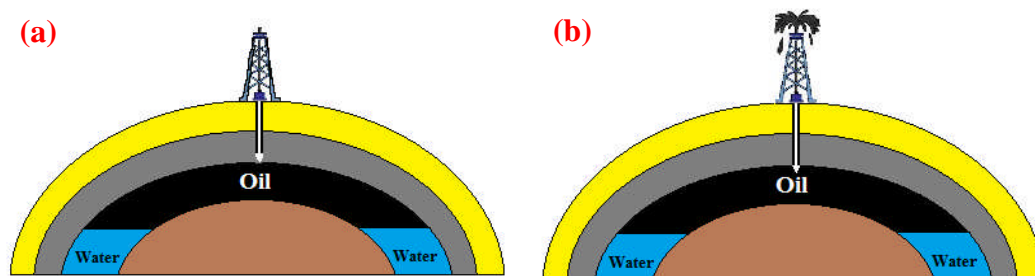


Figure 1.3. The formation of carbonate scale in an oilfield: (a) Before the drill bit reaches and cracks the reservoir (the reservoir is at high pressure) and (b) After the drill bit cracks the reservoir, oil production is on-going and the downhole pressure is decreasing.

Inorganic scale deposits (e.g. CaCO_3 , BaSO_4 and SrSO_4) can deposit all along the water paths in the pipeline applications. Oil industries normally encounter two types of scale formation: [7, 8] carbonate scales and sulphate scales.

Carbonate-dominated scale deposits: It happens due to a change in temperature and pressure, and mainly happens in early stages of the oil extraction process. As shown in Figure 1.3, the oil reservoir is at its highest natural pressure until the drill bit cracks the reservoir and the pressure and temperature of the reservoir drastically changes which lead to a change in the chemical composition of the brine solution in the downhole and the formation of carbonate scale deposits.

Sulphate-dominated scale deposits: This occurs as a result of the mixture of two incompatible brines, and mainly happens in the latest stages of the oil extraction, specifically Enhanced Oil Recovery (EOR) process. As shown in Figure 1.4, after a time interval of oil production, the output rate of the oil well depletes due to the reduction of natural pressure of the reservoir. To recover such reductions, seawater which is both cheap and abundant is pumped into the downhole. Seawater is rich in sulphate ions and reacts with aquifer which is rich in cation ion (such as Ba^{2+} and Sr^{2+}) and results in the formation of sulphate scales.

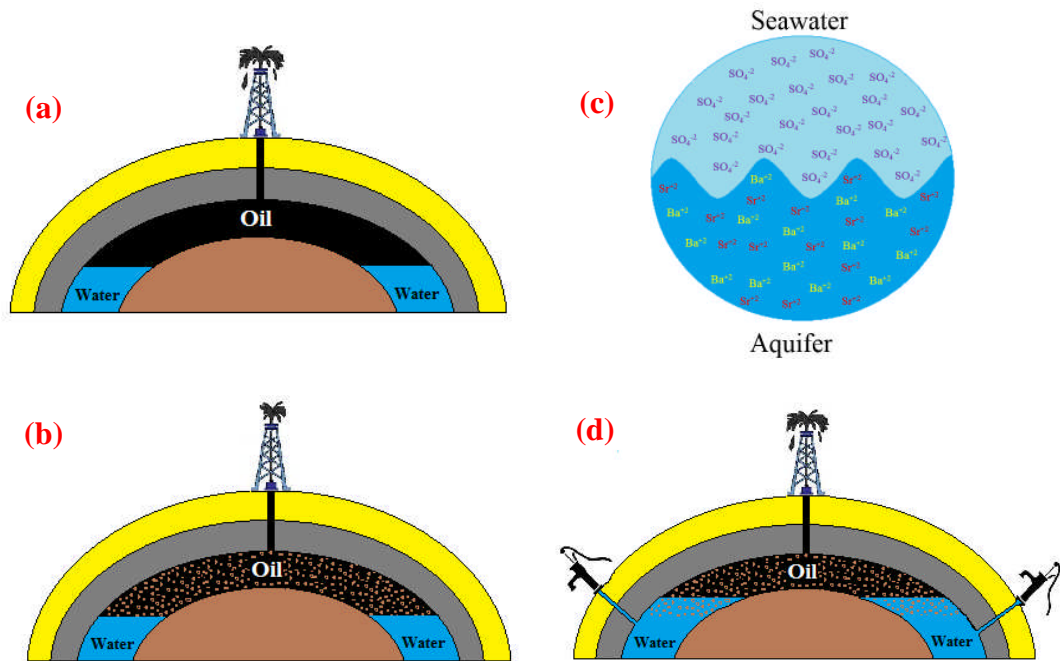


Figure 1.4. The formation of sulphate scale in the oilfield: (a) Oil production at an optimum rate, (b) Oil production depletion, (c) pumping seawater into the oil well, rich in sulphate ions and (d) EOR with seawater.

1.4. Objectives of the thesis

The principal goal of this study is to understand and predict the process of surface scaling in the valve and pipe applications in the oil and gas industry. To characterise the type of scale forming on the surface in the downhole and the ground level of the oilfield, two laboratory setup has been designed as *deposition* and *adhesion* processes. In the *deposition* setup, the coated samples are immersed in the brine solution from the beginning of the tests in the laboratory while in the *adhesion* setup the coated samples are immersed in the brine solution when the rate of crystallisation is in balance with the rate of dissolution.

The main objectives of this thesis are:

- To understand and characterise a good anti-scaling surface, diverse types of existing commercial coatings are selected and tested based on operational conditions in terms of the chemical and flow conditions.
- To understand and assess the surface scaling tendency in both the carbonate-dominated and sulphate-dominated brine compositions in laminar and turbulent flow regimes.

- To evaluate the surface scale formation for a wide range of modified surfaces in two processes: “Deposition” and “Adhesion”, where the former one can be referred to the process which the nucleated growth of scale for the asperities at the surface in a heterogeneous form, and the latter one can be referred as the process that the pre-existing crystals that are formed in the bulk would stick to the surface.
- To assess the morphology and chemical composition of the scale deposits formed in such complex brine compositions.
- Analysing the scale crystals that are the product of co-precipitation and co-deposition processes for both of the complex brine compositions.
- A surface engineering study to bridge a systematic experimental scale study to field data.

The current study shows that if properly selected, surface engineering offers a great promise as an approach to prevent mineral scale deposition in the piping system of oilfields.

1.5. Overview and outline of the thesis

The first chapter gives an insight into the scale formation processes along with its associating problems it faces in the oil and gas industry. The mechanism of different types of scale formation in the oil production systems have been addressed, as well as presenting the objective and the highlight of this work.

A comprehensive literature review on the type of scales and its formation in the oil and gas industry, as well as the theories of crystal growth and the parameters that affect the rate of crystallisation and surface scale formation, are given in chapter two. This chapter also encompasses the surface parameters that affect the surface scaling tendency.

Chapter 3 mainly provides the details of the experimental setup and the methodologies that have been employed to conduct the scaling research as well as the analysis techniques to study the surface scale formation.

In chapter four, the hydrodynamic effects on modified surfaces in the carbonate-dominated brine conditions have been studied, as well as the morphology and chemical composition of the scale deposits. Similarly, the same study has been conducted and reported in chapter five. The same methodology has been applied but in sulphate-dominated brine composition.

In chapter 6, field data has been presented, where scaling tests have been conducted in one of the oil production sites in Brazil and the surface scale tendency of modified surfaces in the re-injection oil facility site is observed.

The discussion of the results and the performance of the modified surfaces in the sulphate/carbonate-dominated brine composition in the laminar/turbulent flow conditions for the *adhesion/deposition* processes, as well as the effect of surface roughness/surface energy of the modified surfaces on the rate of surface scaling tendency is provided in chapter 7. Also, the scale deposit crystals as the product of co-precipitation have been studied for both water compositions. In addition, the field data has been compared with the results obtained from the systematic laboratory surface scaling test.

In the end, the summary, conclusions and recommended future work are presented in chapter 8.

Chapter 2

Background and Literature Review

2.1. Introduction

In many industrial systems, scale formation causes significant problems, not only when it precipitates in a bulk solution but when it deposits on surfaces. In the oil and gas industry, many oil wells suffer from flow reduction due to scale deposition within the downhole utilities and pipe and valve applications, generally in oil recovery operations. The shared disadvantage of both chemical and mechanical treatments is that they do not only remove scale from the formation, and thus they ignore all formation damages. Strategies to prevent surface deposition are of interest. Surface analysis is the first step towards understanding the scale deposition on the surfaces. Although surface deposition and precipitation are interlinked, they have very different kinetics. In developing a surface engineering strategy for scale it is particularly important to understand some parameters in scaling such as surface parameters, e.g. the roughness and the wettability, kinetics of surface depositions, and the induction time for surface scaling which is dependent on the flow regime and the supersaturation rate.

2.2. Scaling in the oil and gas industry

The process of scale formation is a result of several chemical and physical relations which tend to bring the whole system to equilibrium; and scale formation happens when the solubility of different compounds in the water is exceeded, for instance in reservoir fluids total dissolved solids can reach 400,000 (mg/l). However, this number is so dependent on thermodynamic and chemical parameters such as temperature, pressure, pH, water composition, etc., and so determining the extent to which compounds can be dissolved or will come out of solution is not trivial.

Groundwater and water in the near surface environment are usually different from the subsurface water associated with gas and oil fields. Normally, water is a good solvent for many materials and can carry a lot of ions and scaling minerals. Water is used during the oil recovery process to enhance the production rate. Water treatment and analysis are of primary importance in scaling in an oilfield environment.

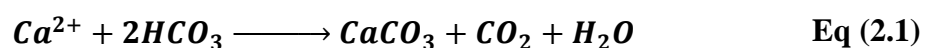
The subsurface water in carbonate and calcite-cemented sandstone reservoirs is rich in magnesium (Mg^{2+}) and calcium Ca^{2+} , and sandstone formation fluids contain barium (Ba^{2+}) and strontium (Sr^{2+}). Most scale found in oil fields forms either from precipitation in the reservoir rocks or as a result of two incompatible waters meeting downhole which majorly results in the scale formation of calcium carbonate ($CaCO_3$), barium sulphate ($BaSO_4$) and strontium sulphate ($SrSO_4$) that is costly to remove either physically or chemically in the oil and gas applications. In order to effectively manage these scales forming on surfaces we need to comprehensively understand (a) type of scales and scale formation rates; (b) process of scaling; (c) parameters which affect the scaling rate; and (d) surface characterisation.

2.3. Type of scales and scale formation

Generally, there are two different types of scaling (or fouling): organic scaling (biofouling) and inorganic scaling. Biofouling refers to the accumulation of micro-organisms, plants algae, or animal on wetted surfaces which causes the degradation of surfaces. Inorganic scaling may occur by one or the combinations different mechanisms, such as precipitation or crystallisation fouling, particulate fouling, chemical reaction fouling, corrosion fouling, and solidification fouling.

Depending on water chemistry and composition, and the environmental conditions in the oil and gas fields, various types of scales can form. Sulphate and carbonate, due to their low solubility, are the dominant scales.

It is estimated that more than 60% of the world's oil and 40% of the world's gas reserves are held in carbonate reservoirs. Also in the Middle East, these numbers escalate to 70% and 90%, respectively[9]. In such reservoirs, as the aquifer water passes through the bubble point and the carbon dioxide evolves, the carbonate scale would form, according to Equation 2.1.



As carbon dioxide evolves the solubility with respect to carbonate drops quickly and forms a precipitate with divalent ions such as calcium, or iron in some special circumstances. In cases where the water cut rises to compensate the oil production,

the injected water (seawater, aquifer) contains sulphate which consequently results in the formation of sulphate scales, as follows:



Depending on the cation, sulphate and carbonate scales have a wide range of solubility. Common scale minerals that are found in oil and gas industry, their composition, relative solubility and physical conditions that cause their formation are shown in Table 2.1.

Table 2.1. Common scales in oil and gas industry (conditions: T = 100°C, at pH = 7) [10-12]

Mineral type	Composition	Relative solubility (mg/L)	Causes of solubility change
Calcite	CaCO ₃	196	P _{CO2} , P _{tot} , TDS, T, pH
Barite	BaSO ₄	44	P, T, TDS
Celestite	SrSO ₄	520	P, T, TDS
Anhydrite	CaSO ₄	3270	P, T
Gypsum	CaSO ₄ .2H ₂ O	6300	P, T
Siderite	FeCO ₃	100	P _{CO2} , P _{tot} , TDS, T, pH
P _{CO2} : Partial pressure of CO ₂ , P _{tot} : Total pressure, TDS: Total Dissolved Solids, T: Temperature, P: Pressure			

The main types of scale that are normally found in oil and gas fields are carbonate and sulphate scales. Whilst the formation of carbonate scale [13, 14] is associated with the pressure and pH changes of the fluid, the sulphate scale occurrence is due to the mixing of incompatible brines [2, 15]. Normally the reduction of pressure leads to the release of CO₂ into the gas phase leaving the solution which is supersaturated in calcium carbonate; and the increase in temperature leads to the formation of calcium sulphate scale, i.e. gypsum and anhydrite.

Due to the lower solubility of barium sulphate compared to calcium carbonate and sulphate scales of strontium and calcium, it is one of the main barriers of flow assurance, although the amount of sulphate within the formation water or in seawater

is low. In one glance, one of the strategies that can be employed is de-sulphating of seawater, which normally reduces the amount of sulphate to 40ppm; however, the sulphate level must be lower than 10 ppm in order to eliminate barite scale completely from the whole production system, which seems that it is not economically feasible [16].

2.3.1. Calcium carbonate scale forms and its polymorphism

Calcium carbonate is the most common type of scale that occurs in oil and gas fields. It has the capability to crystallise in three hydrate forms: (a) amorphous calcium carbonate, (b) monohydrate and (c) hexahydrate calcium carbonate; and in three anhydrate forms as (a) calcite, (b) aragonite, and (c) vaterite. The solubility of these anhydrate crystal are $K_{Calcite} = 1.9 \times 10^{-9}$, $K_{Aragonite} = 4.78 \times 10^{-9}$, and $K_{Vaterite} = 12.6 \times 10^{-9}$ at 20°C, respectively [17]. The rareness of the vaterite can be explained by its higher solubility comparing to other two calcium carbonate polymorphs. Calcite is thermodynamically the most stable crystal with the least crystal defects in its crystal among these polymorphs, while the vaterite crystal is the most instable crystal and forms as porous crystal, since it is not a single crystal and is the result of the agglomeration of the vaterite crystals together [18].

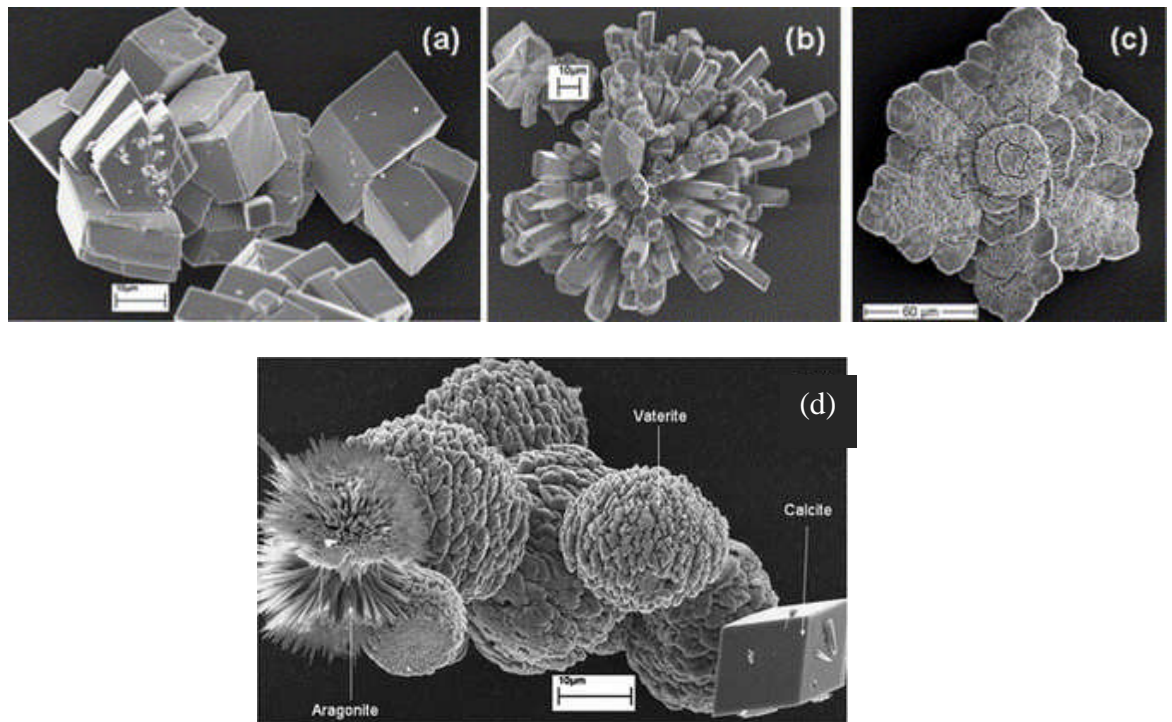
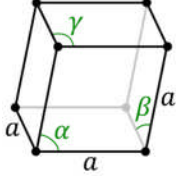
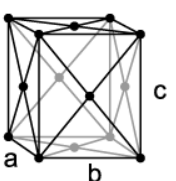
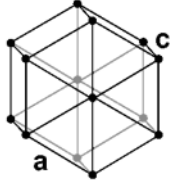


Figure 2.1. SEM images of scales: (a) calcite, (b) aragonite, (c) vaterite; and (d) vaterite (spherical), aragonite (needle-like), and calcite (rhombic) [19].

Brevecic and Kralj [20] referred to some studies that showed vaterite is the first polymorph of calcium carbonate that forms and due to its instability it changes to calcite and aragonite, acting as a “precursor”. In Figure 2.1, different crystal shapes of calcium carbonate are illustrated by Scanning Electron Microscope (SEM). Summary information of different calcium carbonate crystals is given in Table 2.2.

Table 2.2. A summary of investigations of calcium carbonate polymorphs [21, 22].

	Calcite	Aragonite	Vaterite
Crystal system	Rhombohedral $\alpha=\beta=\gamma \neq 90^\circ$ 	Orthorhombic $a \neq b \neq c$ 	Hexagonal $a < c$ 
Morphology	Cubic to rhombohedral	Needle-like	Hexagonal Hemispherical Apricot kernel
Favourable condition	Instantaneous nucleation, Room temperature, Harassed by foreign ions (Mg), High oxygen concentration oxygen	Temperature above 50°C, High pH value (above 13.5)	High supersaturation, Low concentration of oxygen, Strong tendency to spread laterally
State	Excellent quality Single crystal Most stable	Excellent quality Single crystal More porous	Metastable Microcrystalline Porous

2.3.2. Sulphate scale formation

Many researchers [2, 8, 23] have surveyed on operational problems and difficulties associated with sulphate scales which lead to additional capital and operational costs. Sulphate scales are hard, adherent and almost insoluble in most acids and common solvents, and also are difficult to remove mechanically.

The existence of sulphate in the injected seawater will also cause the formation of hydrogen sulphide (H₂S), in certain conditions, which results in reservoir souring and corrosion, and more importantly is toxic and lethal. Furthermore, it escalates the HSE concerns regarding the radioactive waste disposal (adherence of radioactive species,

radium isotopes) to such scales [24]. The treatment of sulphate scales is (a) very expensive, (b) field dependent, (c) a trial-error procedure (necessarily cannot be generalised for all oil fields), and (d) only successful in less severe cases of scaling.

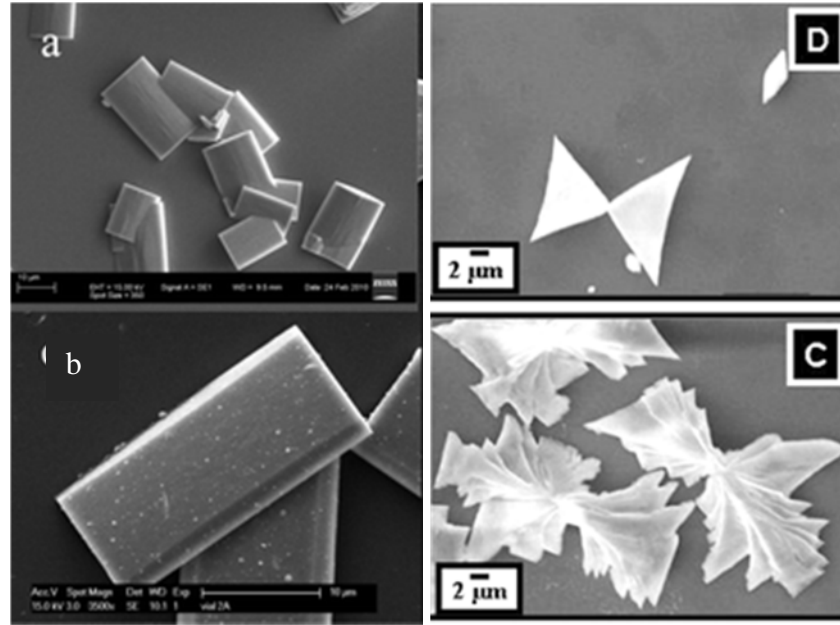


Figure 2.2. SEM images of normal crystal form of barite: Orthorhombic (a) and (b) [26]; Bipyramidal (c) and (d) [27].

Barium sulphate (barite) and strontium sulphate (celestite) are the most common types of sulphate scales, due to their low solubility, that occur in oil and gas industry.

Barite, BaSO_4 , a member of a large class of isomorphous crystals and is described as orthorhombic bipyramidal [25]. The crystal shape of barite is not well defined and its shape would be dependent on the conditions that it is processed. Figure 2.2 illustrates the common shapes of barite crystals.

Blount [28] has shown in his report that barite has its maximum solubility between 100°C and 150°C . Pressure and temperature effects on barite solubility above 150°C are similar to solubility trends of anhydrite and celestite. However, the author believes that only in this work such results are presented and not supported by other research teams.

The morphology of strontium sulphate crystals is shown in Figure 2.3. The morphology of strontium sulphate is also so dependent on the formation process. In some studies, its morphology would be sisal-like hierarchical structures [29].

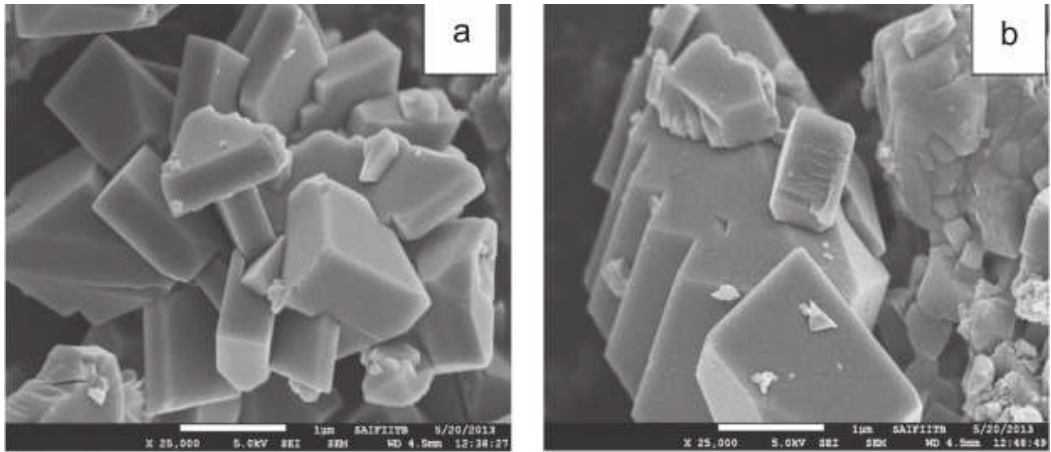


Figure 2.3. SEM images of strontium sulphate at (a) 298K and (b) 308K [30].

2.4. Scale formation process/ theories of crystal growth

The scale formation process can be divided into two different processes: nucleation and crystal growth. However, to have scale formation, the solution itself should have the ability to form nuclei and increase their size. So the solution should be supersaturated with ions. In other words, the saturation ratio is thermodynamically the driving force of scale formation. The schematic representation of the calcium carbonate scale formation is shown in Figure 2.4.

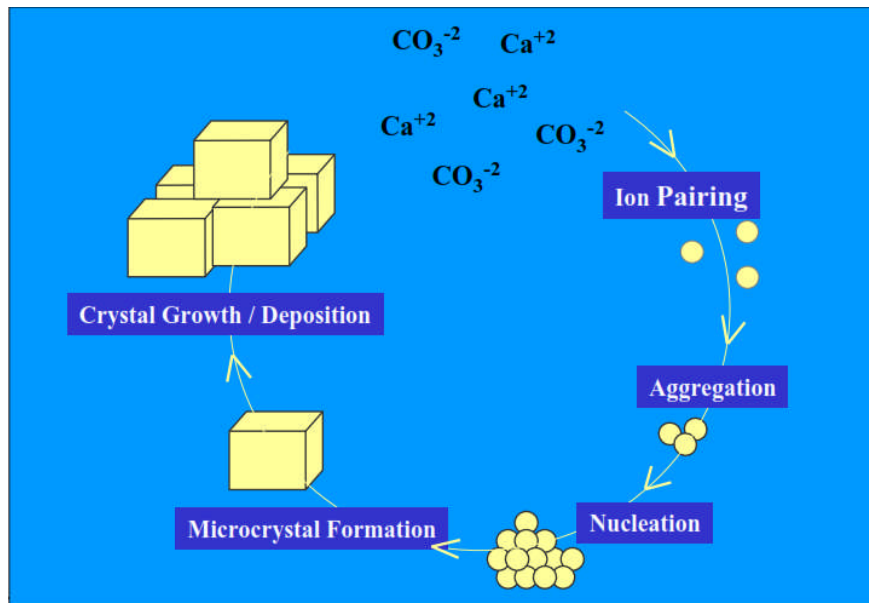


Figure 2.4. Schematic representation of the most important steps in the pathway from soluble ions to a microscopic calcium carbonate scale deposit [31].

2.4.1. Expression of supersaturation

The term “supersaturation” of a system may be expressed in many different ways and it is essential to quote the temperature when expressing the supersaturation of a system since the equilibrium saturation concentration is temperature dependent. There are some basic units that are commonly used: concentration driving force, Δc , the supersaturation ratio, SR , and a quantity sometimes referred to as the absolute, or relative supersaturation, σ [32]. These quantities are described as the following equations:

$$\Delta c = c - c^* \quad \text{Eq (2.3)}$$

$$SR = \frac{c}{c^*} \quad \text{Eq (2.4)}$$

$$\sigma = \frac{\Delta c}{c^*} = SR - 1 \quad \text{Eq (2.5)}$$

where, c is the solution concentration, and c^* is the equilibrium saturation at the given temperature. However, for practical purposes, the supersaturation ratio can be expressed directly in terms of solution concentration such as molarity (mol/lit of solution, c), molality (mol/kg of solvent, m), mole fraction, x , or even ion activity (which in our study is more common). For example, based on the scale that we would have the saturation ratio can be expressed as:

$$SR_{\text{calcite}} = \frac{(a_{Ca^{2+}}) \times (a_{CO_3^{2-}})}{K_{sp,CaCO_3}} \quad \text{Eq (2.6)}$$

$$SR_{\text{barite}} = \frac{(a_{Ba^{2+}}) \times (a_{SO_4^{2-}})}{K_{sp,BaSO_4}} \quad \text{Eq (2.7)}$$

$$SR_{\text{celestite}} = \frac{(a_{Sr^{2+}}) \times (a_{SO_4^{2-}})}{K_{sp,SrSO_4}} \quad \text{Eq (2.8)}$$

where, $a_{i,j+}$ and $a_{i,j-}$ are the ion activities of the anion and cation respectively, and K_{sp} is the solubility product which is a constant number and is defined as the product of ions reactants either dissolved or un-dissolved in equilibrium conditions. The supersaturation ratio would be different in different conditions, since the ion activity and solubility product are pressure and temperature dependent. The supersaturation of an aqueous solution refers to how much of a certain salt is currently dissolved in the solution, above that which would be present at equilibrium [33].

Also, in some studies the saturation index, SI , is frequently used which corresponds to the logarithm of SR , to express scaling tendency.

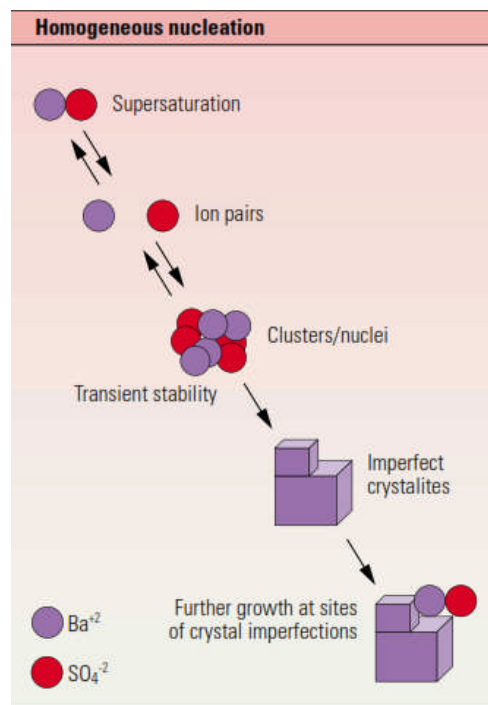


Figure 2.5. Homogeneous nucleation process: ion pairs in supersaturation system and then cluster start to grow [2].

The scale formation can be expressed by saturation ratio which can be any of these cases:

- if $SR < 1$, then the solution is considered as undersaturated and it can still dissolve any deposits and the scale formation is not possible.
- if $SR = 1$, then the solution is considered to be in equilibrium condition, which means that the rate of scale formation is equal to the dissolution of the deposits.

- if $SR > 1$, then the solution is considered as supersaturated and the scale formation is thermodynamically likely to happen.
- if $SR > 40$, then the precipitation of calcium carbonate would be spontaneous [34].

2.4.2. Nucleation

Although the driving force for scale formation can be temperature, pressure, pH shift, outgassing, supersaturation, or the contact of incompatible waters, the scale always does not form. Before crystals can form, there should be some tiny solid bodies, nuclei or seeds in the system that act as centres of crystallisation. There is no general rule to categorize the nucleation process, but researchers [32, 35, 36] categorized them as (a) primary nucleation which is expressed as all sorts of nucleation provided that the system does not contain any crystalline matter, and (b) secondary nucleation where the nuclei are generated in the vicinity of the crystals existing in a supersaturation system. Furthermore, if the primary nucleation occurs without any external stimuli, it is homogeneous nucleation (Figure 2.5), on the other hand, if the primary nucleation happens by the influence of external stimuli (such as pipe surface roughness, or joints and seams in the production line) it is known as heterogeneous nucleation.

2.4.3. Primary nucleation

2.4.3.1. Homogeneous nucleation

In a homogeneous fluid, the formation of the nucleus is not well understood but the Gibbs free energy can explain the nucleation and crystallisation process at some point. The overall free energy change (ΔG) required for the formation of small particle of the solute (for simpler cases it is considered as spherical with the radius, r), is defined as the sum of the free energy change for the formation of a solid surface (ΔG_S), i.e. the free energy between the surface of the particle and the bulk of the particle, and the free energy change of transformation (ΔG_V), i.e. the free energy change between a very large particle ($r = \infty$) and the solute in solution, as the following equation [37]:

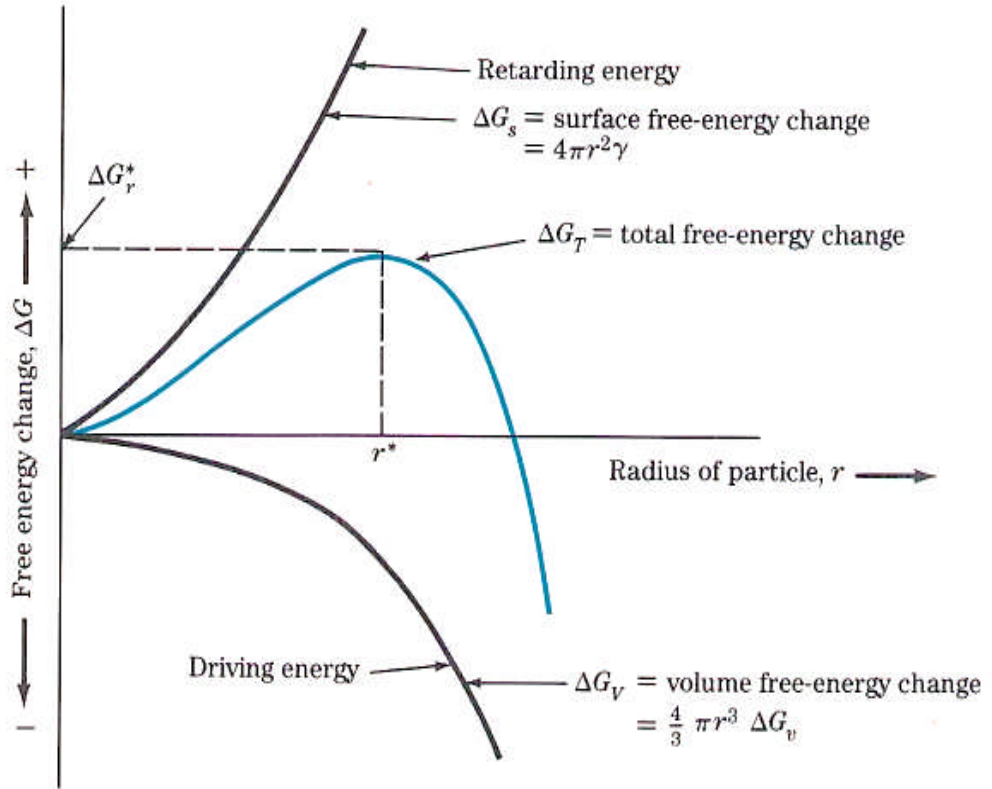


Figure 2.6. Free energy diagram with regard to the radius of the particle [38].

$$\Delta G = \Delta G_S + \Delta G_V \quad \text{Eq (2.9)}$$

where, the magnitude of ΔG_S is proportional to r^2 , and is a positive quantity, and the magnitude of ΔG_V is proportional to r^3 and is a negative quantity. Equation 2.9 can be rewritten as:

$$\Delta G = 4\pi r^2 \gamma + \frac{4}{3} \pi r^3 \Delta G_v \quad \text{Eq (2.10)}$$

where, ΔG_v is the free energy change of transformation per unit of volume and γ is the interfacial tension (or surface energy), i.e. between the supersaturation solution and developing crystalline surface.

As shown in Figure 2.6, the two components of the free energy are of opposite sign and as a result, the total free energy passes through a maximum number, ΔG_{r^*} , which corresponds to the critical nucleus, r^* (or r_{crit}), and can be calculated as follows:

$$\frac{d\Delta G}{dr} = 8\pi r\gamma + 4\pi r^2\Delta G_v = 0 \quad \text{Eq (2.11)}$$

Therefore

$$r^* = \frac{-2\gamma}{\Delta G_v} \quad \text{Eq (2.12)}$$

By referring to Figure 2.6, ΔG_v is intrinsically a negative number, so:

$$\Delta G_{r^*} = \frac{16\pi\gamma^3}{3(\Delta G_v)^2} = 0.75\pi\gamma(r^*)^2 \quad \text{Eq (2.13)}$$

The critical size r^* is the minimum size of a stable nucleus. In other words, particles smaller than r^* will either dissolve or evaporate (in a supersaturated vapour), and particles larger than r^* will continue to grow [32].

Apart from the size, the rate of nucleation, J , is also important. The rate of nucleation is the number of nuclei formed per unit of time per unit volume, and can be expressed by the modified format of the Arrhenius reaction velocity equation, as follows:

$$J = A. \exp \left[-\frac{16\pi\gamma^3 v^2}{3k^3 T^3 (\ln Sr)^2} \right] \quad \text{Eq (2.14)}$$

where, A is constant and will vary depending on the order of the reaction, v is the molecular volume, k is the Boltzman constant, T is the temperature and Sr is the degree of supersaturation. This equation shows that the rate of nucleation is mainly depending on three factors: temperature, saturation ratio and surface energy of the

particle. There are other modifications to this equation which is out of the scope of this study but for more information the reader can refer to the crystallization book by Mullin [32].

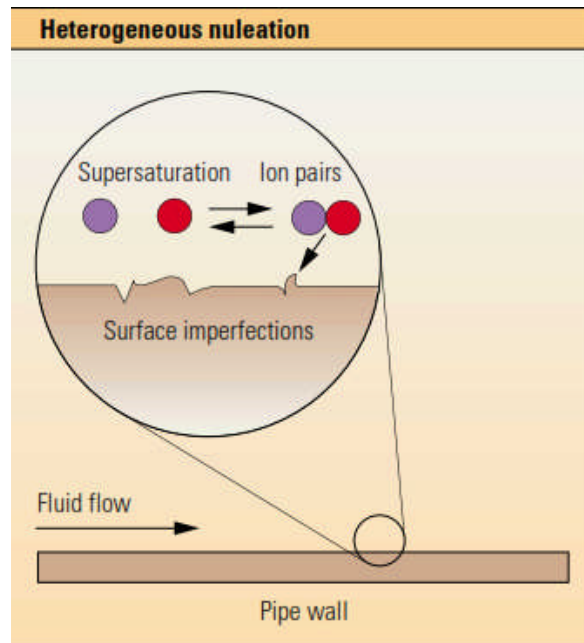


Figure 2.7. The nucleation induced by surface defects or rough spots, called as “heterogeneous” nucleation [2].

2.4.3.2. Heterogeneous nucleation

In a nucleation process, even pure homogeneous nucleation is induced in some way, which accentuates that the homogeneous nucleation is not a common process, i.e. at the nanoscale, the homogeneous nucleation is considered as a heterogeneous nucleation due to the existence of nanoparticles. For instance, in an aqueous solution that normally prepared in the lab, there are roughly more than million particles with the size of less than $1\mu\text{m}$ in the solution. Filtration can reduce this number, but still some particles can exist in the solution. Heterogeneous nucleation is greatly affected by the impurities in the solution.

In general, homogeneous nucleation occurs mainly at high supersaturation brine solution while the heterogeneous nucleation is dominant at low supersaturation brine solutions[32]. The general description of heterogeneous nucleation is shown in Figure 2.7, which the nucleation is dominantly induced by surface imperfections or surface roughness.

As seen in Equations 2.13 and 2.14, the surface energy (or interfacial tension), γ , plays a major role in the nucleation process. In the process of scale deposition occurring on a surface, there are three phases in contact, and consequently three interfacial tensions between surfaces, comprising as: (a) γ_{cl} , the interfacial tension between the crystalline deposit and the liquid, (b) γ_{sl} , the interfacial tension between the solid surface and the liquid, and (c) γ_{cs} , the interfacial tension between the crystalline deposit and the solid surface.

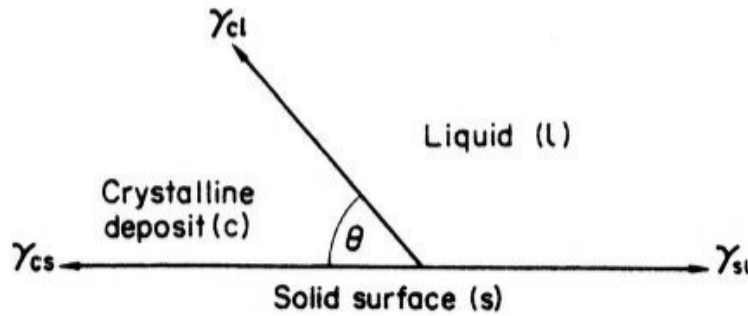


Figure 2.8. Interfacial tension at the boundaries between two solids and one liquid [32].

As shown in Figure 2.8, by resolving these forces in a horizontal direction will lead to:

$$\cos\theta = \frac{\gamma_{sl} - \gamma_{cs}}{\gamma_{cl}} \quad \text{Eq (2.15)}$$

where, θ is the angle of contact between the solid surface and the crystalline deposit.

The overall critical free energy change with the formation of heterogeneous nucleation, $\Delta G'_{crit}$ can be expressed by the overall critical free energy change with the formation of homogeneous nucleation, ΔG_{crit} , as follows:

$$\Delta G'_{crit} = \phi \Delta G_{crit} \quad \text{Eq (2.16)}$$

where, ϕ is less than unity and expressed as:

$$\varphi = \frac{(2 + \cos\theta)(1 - \cos\theta)^2}{4} \quad \text{Eq (2.17)}$$

These are the conditions [32]:

- If $\theta = 180^\circ$, i.e. complete non affinity between the crystalline and the surface (or non-wetting in liquid solid base) then $\varphi = 1$ and $\Delta G'_{crit} = \Delta G_{crit}$ which means that the overall free energy of nucleation needed is the same as for homogeneous nucleation.
- If $0 < \theta < 180$, then easier nucleation can be achieved, since the free energy change required is less than that in a homogeneous nucleation.
- If $\theta = 0$, i.e. complete affinity (or complete wetting) then $\varphi = 0$ and $\Delta G'_{crit} = 0$ which means that no nuclei have to be formed in the solution.

The critical supersaturation number for the homogeneous nucleation is about 40, while in the case of heterogeneous nucleation, this value is lower compared to the homogeneous nucleation[32, 39]. As a result, the nucleation rate of heterogeneous nucleation is higher which affects the crystal morphology of scale deposits[40].

2.4.3.3. Secondary nucleation

The term secondary nucleation is normally used to investigate in particular the nucleation in a supersaturation solution that the crystals are already formed in the solution while in the primary nucleation there is no formed crystal. So many theories have been proposed for the secondary nucleation which can be mainly categorised into two categories [41, 42]:

1. The origin of the formation of nuclei can be referred to the parent crystal. This type of nucleation can be: (a) initial or dust breeding, (b) needle breeding, or (c) collision breeding. In dust breeding, minute crystallites are formed on the crystal surface which act as nucleation sites. Needle (or dendritic) breeding occurs at high supersaturation where needle-like pieces of crystals form as nucleation sites. Collision (or attrition) breeding happens in high stirring speeds which result in the rounding of edges and corners of crystals, the remaining bits are considered as nucleation sites. Such mechanism is dependent on crystal hardness and the concentration of suspension.

2. The origin of the formation of nuclei can be referred to the solute being in the liquid phase, and the attributed mechanisms in this category could be: (a) due to impurity concentration gradient nucleation; or (b) nucleation due to fluid shear. In the impurity concentration gradient nucleation theory, it is assumed that the whole fluid is structured and the area near to the surface of the crystals is more supersaturated; impurities are either dissolved in the solution or unite with the formed crystals. So there are impurity concentration gradients in the solution which increase the rate of nucleation. It is predictable that stirring the solution reduces the impurity concentration gradient which leads to lower nucleation rates. The fluid shear mechanism is expressed in high supersaturation solution where dendritic crystals are formed and due to either flow shear or dendrite coarsening mechanism break, which will be the source of the nucleation sites.

In short, the secondary nucleation originates due to either from the boundary layer near the growing crystal or from the seed crystal. There are some parameters that affect the secondary nucleation such as the supersaturation ratio, the degree of agitation and the presence of impurities. For instance, the size of the critical nuclei decreases as the degree of supersaturation increases; the stirring the solution decreases the absorbed layer around the crystals which leads to a lower rate of nucleation; or the effect of the existence of impurities in the solution will vary but normally by an increase [32, 42].

2.4.4. Induction time

Sonhel and Mullin [43] describe the induction period as the time elapses between the achievement of supersaturation and the first observable changes in the physical property of the precipitation system. These changes could be the variations of solution composition or conductivity, or the turbidity which is affected by the appearance of the crystals, depending on the experimental setup or equipment that is employed to detect this interval. As a consequence, the accuracy of the experimental induction period depends on the equipment sensitivity.

The induction time encompasses three periods of time, as follows [32]:

- (a) **Relaxation time, t_r** , the time needed for the molecule clusters to distribute within the solution to reach to a quasi-steady- state conditions. The relaxation

time depends on the viscosity of the solution, or consequently the diffusivity of the solution.

- (b) **Nucleation time, t_n** , the time needed to form stable nuclei. Nucleation time depends on the supersaturation which affects the size of critical nucleus.
- (c) **Grow time, t_g** , the time needed for a nucleus to reach to a recognizable size. Grow time depends on the size at which nuclei are detectable, and the equipment that are employed.

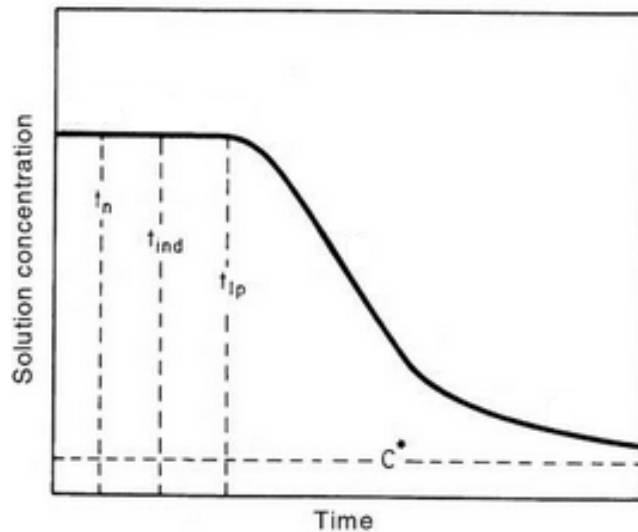


Figure 2.9. A de-supersaturation curve (diagrammatic): c^* = equilibrium saturation, t_n = nucleation time, t_{ind} = induction time, t_{lp} = latent period [32].

At lower supersaturation systems another time lag may be observed, expressed as the latent period. The latent period is defined as the beginning of a significant change in the system; for instance, some clear evidence of the solution de-supersaturation. A de-supersaturation curve is illustrated in Figure 2.9.

The induction time, t_{ind} , is affected by either thermodynamic parameters such as temperature or pressure, or solution composition and saturation ratio. He et al. [44] demonstrated that the nucleation induction time of CaCO_3 is delayed in the presence of inhibitors, and also showed that the logarithm of the induction time of CaCO_3 is inversely proportional to SI at a given temperature and proportional to $1/T$ at a given saturation index. Stamatakis et al. [45] reported that the induction time of calcium carbonate at 25°C decreases exponentially as the saturation ratio increases. They also

conducted the precipitation test for calcium carbonate at different temperatures and proposed the following semi-empirical equation, which is illustrated in Figure 2.10.

$$\log t_{ind} = 3.2 - \frac{3.0}{SI} - \frac{959.8}{T} + \frac{1849.9}{SI \times T} \quad \text{Eq (2.18)}$$

where, T , is the temperature and SI is the saturation index.

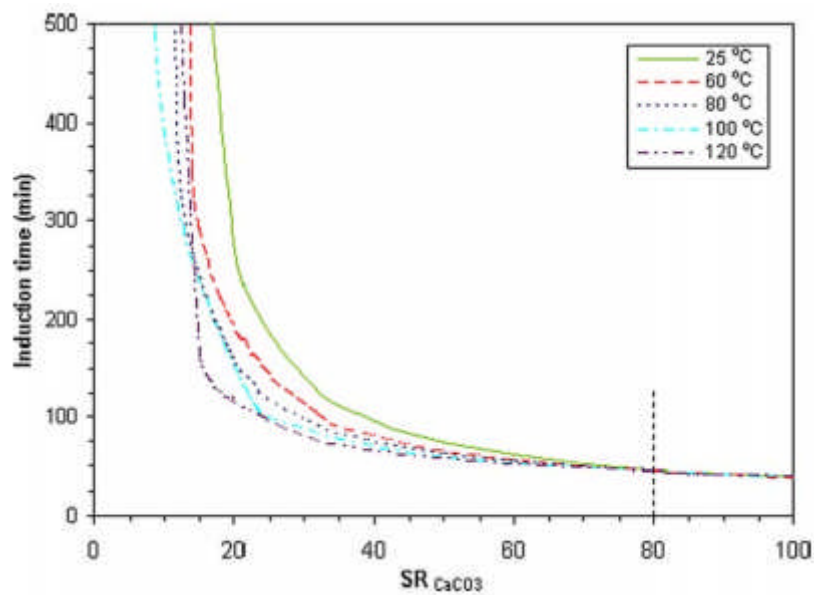


Figure 2.10. Plot of the induction time versus the SR_{CaCO3} for different temperatures based on an empirical equation [45].

2.4.5. Scale crystal growth

As presented in the nucleation section, the nucleus needs to reach to a certain magnitude, i.e. critical sized cluster of molecules, to grow based on Gibbs free energy, and if it does not reach that, it will dissolve into the solution. Koutsoukows and Kontoyannis [46] have shown that the precipitation at the initial stage has rapidly grown in a number of crystals, while at later stages the crystals formed grow without an increase in their quantity. In order to understand different mechanisms and kinetics of the cluster growth, different theories have been developed such as surface energy theory and diffusion theory.

The surface energy theory governs when the differences in solubility are small, i.e. between the solute and the solution; growth is mainly governed by surface energy. According to this theory, as the supersaturation enhances, the growth becomes rapid in all directions and consequently, the shape of the crystals should be spherical. But in experiments, it has been noted that in high supersaturation, well-defined faces are propagated [47].

The diffusion theory was first proposed by Noyes and Whitney [48] based on these assumptions:

1. In the vicinity of a growing surface, there is a concentration gradient.
2. Dissolution process is the reverse process of the crystal growth.

They also proposed the following expression for the solute that will get deposited over the crystal surface:

$$\frac{dm}{dt} = \frac{D}{\delta} A(C - C_e) \quad \text{Eq (2.18)}$$

where, dm is the mass of the solute deposited on the crystal surface of area A during time dt , D is the diffusion coefficient of the solute, δ is the thickness of the stagnant layer at the vicinity of the crystal surface, and $(C - C_e)$ is the difference between the actual and equilibrium concentration of solute. Like the other theory, there are some observations that does not support the diffusion theory [47].

2.4.6. Adhesion

The word “adhesion” means “stick to”, and the use of adhesion is expressed as the state or phenomenon where two entities are stuck together. It is accepted by American Society for Testing and Materials (ASTM D 907) that the definition of adhesion is referred to “the state in which two surfaces are held together by interfacial forces, which may consist of valence forces or interlocking forces or both”. The magnitude of adhesion is expressed in different ways depending on where the term is used. Adhesion can be measured by either the forces between atoms at the interface or the number that results from shear stress, tensile stress and so on. The first term is known as “fundamental” adhesion and tied to one of the theories of adhesion to a particular model for the interfaced problem; and the latter term is known as “practical” adhesion and can be referred to the strength of a joint or coating, known as peel strength [49].

The adhesion of the particulate matter onto the surface is one of the stages in which the fouling develops. The concepts of adhesion of inorganic particles onto the surface due to the size of the particulate matters (e.g. less than $1\mu\text{m}$, known as colloidal size) can be referred to colloidal concepts. In such conditions, the hydrodynamic and gravitational forces are negligible since shear forces are not as effective as they are when the particle sizes are small. The dominant forces between the colloids are *van der Waals* forces (considered as attractive forces), and *electrostatic double layer* forces (considered as repulsive forces). Van der Waals forces correspond to the attractions and repulsion between atoms, molecules and surfaces, as well as other intermolecular forces; while the electrostatic double layer forces appear on the surface of an object when it is exposed to a fluid. As a result, the process of adhesion between particulates in a liquid medium and the surface is determined by the balance between the attractive *van der Waals* forces and the repulsive *electrostatic double layer* forces, known as Derjaguin-Landau-Verwey-Overbeek (DLVO) theory. There are other forces depending on the conditions play a major role in the adhesion process, such as hydrophobic interactions in polar media; ion bridging with the presence of positively charged ions, and steric forces in the presence of polymers [50].

2.5. Factors affecting scale formation

One of the main reasons not to have a clear idea about the process of scale deposition is that there are so many factors influencing the scale formation in the bulk solution and on the surface. These factors could be either the operating conditions of the bulk solution such as: hydrodynamics of the flow, solution composition, pH, temperature, dissolved and suspended impurities, the presence of gas bubbles, CO_2 content in the water, etc.; or the surface parameters such as surface roughness, surface energy, complexity of the surface (defined by fractal dimension), etc. At a glance, it seems to be practical to analyse each factor that is affecting the scale formation solely, but in real conditions, there is a combination of factors affecting the scale formation which make the process of scale deposition on the surface unpredictable. For instance, the crystallization process in the bulk can be either inhibited by impurities (having scrubbing effect) or escalate the nucleation process (acting as nucleation sites); or in surface deposition, higher the velocity have higher deposition rate up to a point where the shear stress (induced by hydrodynamic conditions) acts as scale removal factor. So many case studies have been conducted by researchers to study the effect of various parameters on the scale formation rates which are presented as follows:

2.5.1. Effects of temperature

The fluid temperature plays a major role in scale formation due to its effect on the supersaturation of different salts. For instance, calcium carbonate solubility is inversely proportional to the temperature, i.e. as the temperature increases, there are more deposited crystals formed on the surface. On the other hand, the solubility of barium sulphate is proportional to temperature in the range of 25-100°C and then the solubility decreases up to 200°C [2].

Merdhah and Yassin [51] have reported that the solubility rate of barium sulphate with regard to temperature is so affected by the ion concentration of barium. They measured the solubility of the barium ions at 250 and 2200 ppm, and they found that as the ion concentration increases the solubility of barium sulphate increases by increasing the temperature, which leads to lower precipitation.

There are some studies that have proved that temperature also affects the morphology of calcium carbonate scale [52, 53]. At high temperature (e.g. 60°C) the dominant morphology of calcium carbonate scale is aragonite, whereas for low temperature (e.g. 25°C) the deposits are mostly composed of calcite and vaterite. Some surveys have also conducted regarding the size of the crystals formed at different temperatures. Yu et al. [54] have reported that as the temperature increases the size of the formed crystals decreases, e.g. the deposited crystals size range 6 to 12 μm at 25°C, while the crystals size slightly decrease to about 4 to 10 μm at 80°C.

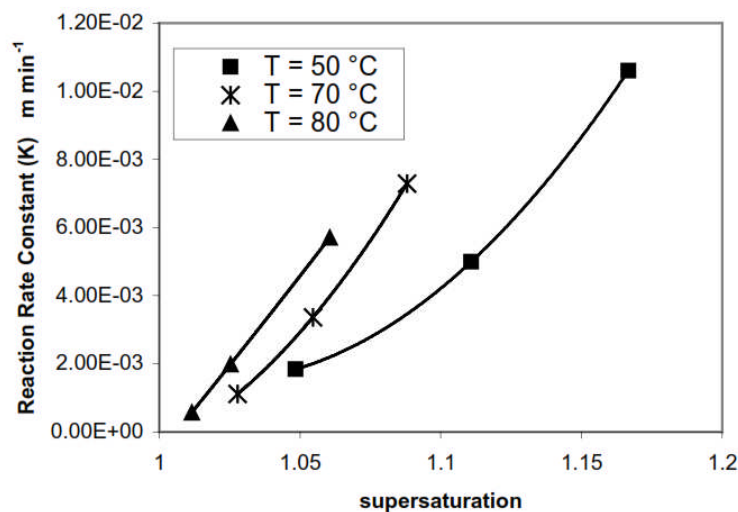


Figure 2.11. Reaction rate constant of barium sulphate with regard to supersaturation in different temperatures [51].

2.5.2. Effects of saturation ratio

Supersaturation ratio is known as the driving force to scale formation. Therefore, the higher the supersaturation the higher the scale formation rate is. As mentioned in the supersaturation section, for supersaturation value more than one the scale formation thermodynamically is possible. As shown in Figure 2.11, the reaction rate constant of barium sulphate increases proportionally with supersaturation and, of course, temperature.

The reaction rate constant of barium sulphate increases linearly with supersaturation at 50°C, but as temperature increases, the reaction rate constant of BaSO₄ increases at lower speed comparing to lower temperatures. The reason can be explained as the solubility of BaSO₄ increases proportionally with temperature, so less scale will form, and this trend is more effective where the supersaturation of barium is higher. But eventually, for higher supersaturation value (more than 1.15), it can overcome the temperature effect and consequently the scale will form with a higher rate.

2.5.3. Effects of pressure

Pressure changes, as a physical parameter, would definitely affect the scale form, but its impact is not as high as some other parameters such as supersaturation and temperature. Some studies have been conducted [2, 55, 56] to investigate the pressure effect.

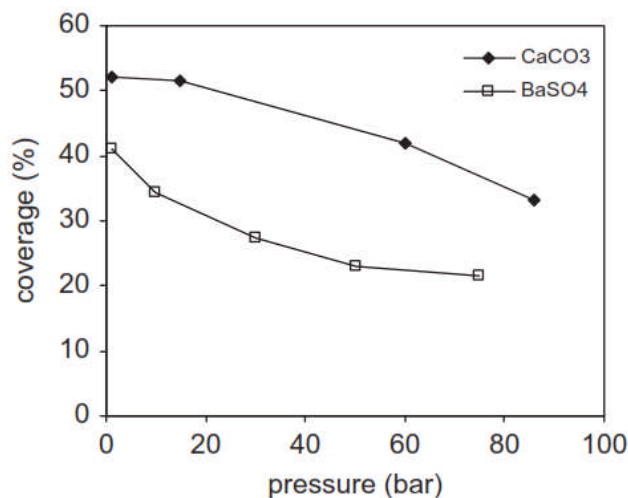


Figure 2.12. Average coverage estimated by electrochemical technique versus pressure [56].

Generally, pressure raise would increase the solubility of barium sulphate and decrease the supersaturation; As a matter of fact, the same trend for carbonate scaling system is true, as shown in Figure 2.12

Peyvandi et al. [56] have reported that by increasing the pressure, both the number of nucleation sites and the size of the crystals decrease, and also they have investigated the polymorphism of calcium carbonate and found that the dominant polymorph of calcium carbonate at high pressure is calcite.

Dyer and Graham [55] investigated for systems with low and high sulphate brine system for different pressure cases, as shown in Figure 2.13; and they found that the effect of pressure is not as much as temperature and supersaturation; however, they mentioned that the effect of pressure on the formation of both scales at 180°C is more significant than at lower temperatures.

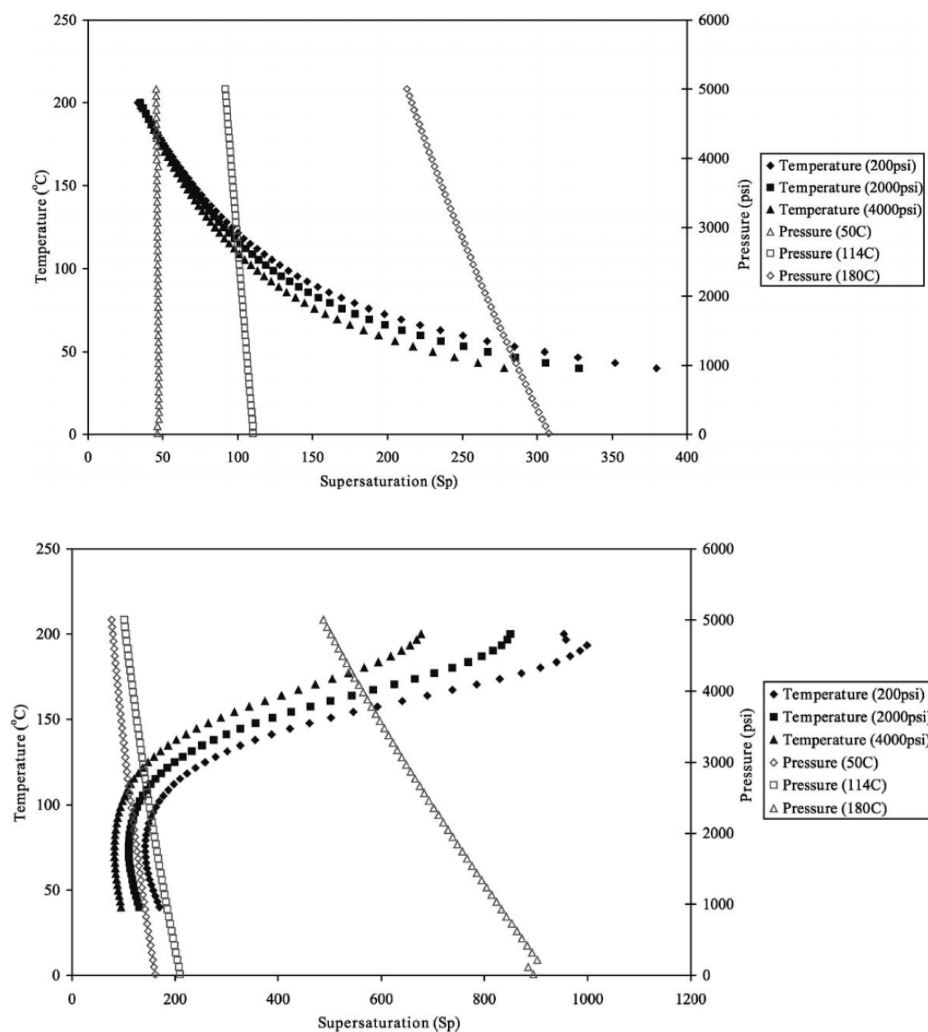


Figure 2.13. Prediction of BaSO₄ (above) and CaCO₃ (below) scale formation with regard to temperature, pressure and supersaturation [55].

2.5.4. Effects of bulk alkalinity (pH value)

There are some difficulties in understanding the concept of pH. But in a simple explanation, pH shows the number of hydrogen ions (H^+ , also referred as “protons”) in a solution. The effect of pH value is one of the major concerns, especially in oil and gas industry. In applications where the flow assurance is the main concern, dosing acid to the system (reducing the pH value) will minimise the scale; however, low pH value makes the system prone to corrosion problems. Therefore, the pH value should be monitored carefully throughout the system to minimise both the scale and corrosion problems. As shown in Figure 2.14, studies have shown that the scaling process occurs even in lower pH, but the corrosion increases sharply as the pH decreases, so the optimum number of pH to avoid the scale and corrosion problem is between 6 and 7 [57].

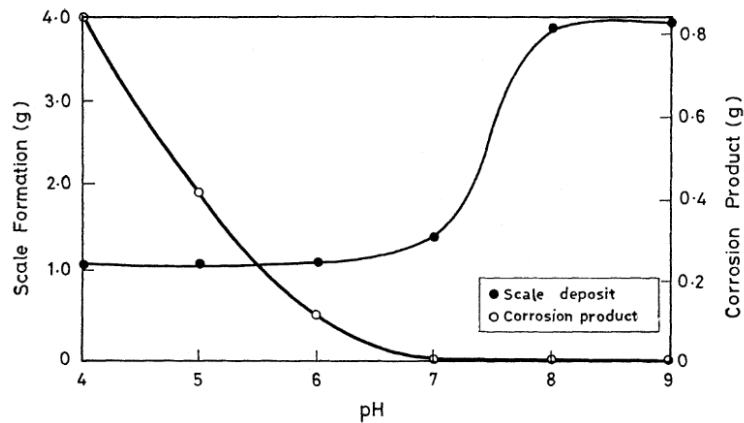
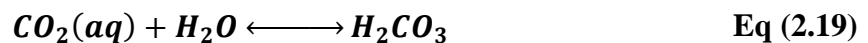


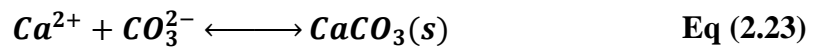
Figure 2.14. The effect of pH on corrosion and scale [58].

The effect of CO_2 in the solution on the rate of scale formation will be discussed in another section, but the amount of CO_2 dissolved in a solution is not as straightforward as some ions like Ca^{2+} , Sr^{2+} and Ba^{2+} since in water CO_2 can form as carbonic acid (H_2CO_3), bicarbonate ion (HCO_3^-), or carbonate ion (CO_3^{2-}), as the following equations:





By referring to the equations, it is obvious that these four different chemical species forms interact with H^+ . Therefore, the proportion of each chemical species depends on the pH. For instance, when we have high amount of H^+ in the solution (pH is low) then the CO_3^{2-} and HCO_3^- ions interact with H^+ and will form CO_2 ; on the other hand, where there is few H^+ in the solution (pH is high) then CO_2 and HCO_3^- will lose H^+ and we mostly have CO_3^{2-} . This trend is shown in Figure 2.15. This is the main reason in carbonate scale systems that at higher pH, the amount of scale is higher due to the abundance of carbonate ions which interact with Ca^{2+} as the following equation:



The specification at normal seawater condition ($pH = 8.2$, $P = 1atm$, $T = 25^\circ C$) is indicated by the dashed line in Figure 2.15, where the proportions are 88.4% (HCO_3^-), 11.0% (CO_3^{2-}), and only 0.54% (CO_2); Indeed, these proportions would be easily changed by variations of physical and chemical conditions [59].

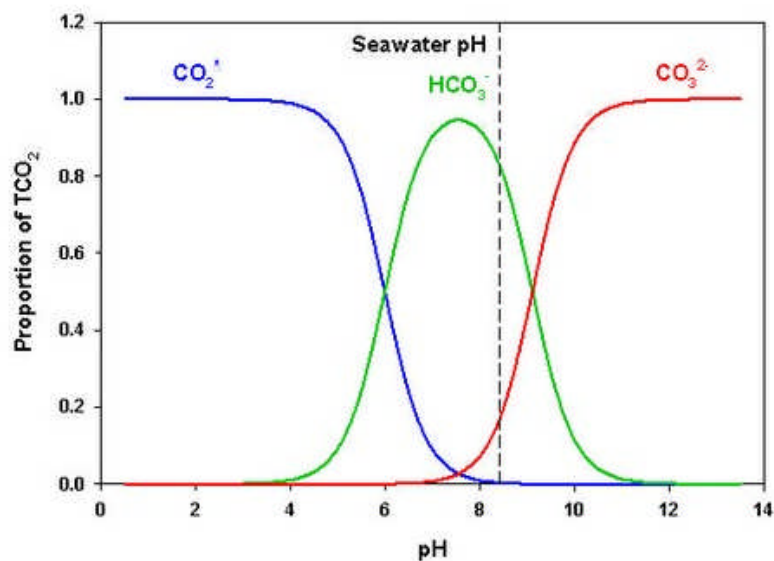


Figure 2.15. Specification diagram for CO₂ in seawater showing the relative proportion of each species.

2.5.5. Effects of CO₂

In a supersaturated brine solution which is prone to carbonic scale formation, carbon dioxide affects the rate of scale formation. As shown in Figure 2.16, the carbonic scale formation encompassing carbon dioxide, carbonic acid, bicarbonate ions, carbonate ions, calcium ions and calcium carbonate, is sketched.

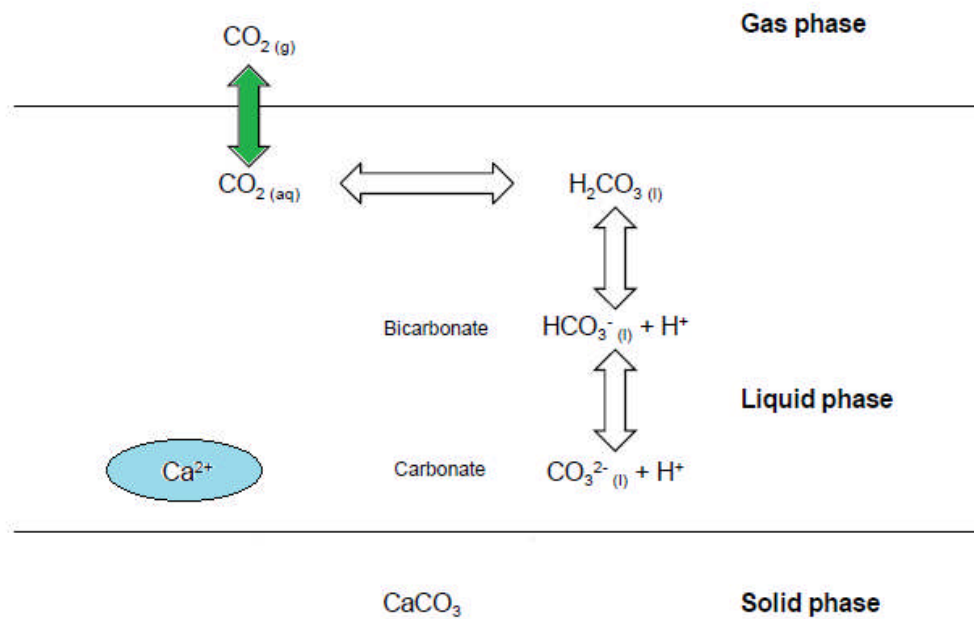
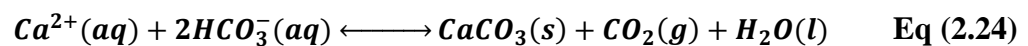


Figure 2.16. Schematic representation of the carbonic scale system [60].

In a carbonic scale system the following equation governs:



As a result, any changes in the system would induce the system to shift the reaction in a way to reach to equilibrium. With regard to carbon dioxide, there are two scenarios:

1. **The decrease in CO₂:** In oil fields in the downhole, the chemical species are in equilibrium till the drill reaches to the reservoir and breaks this equilibrium which leads to a pressure release. As the pressure reduces abruptly, the carbon

dioxide releases into the formation water resulting in carbonic acid formation. The formation water is rich in calcium ions which interacts with carbonate and precipitate as calcium carbonate.

2. **The increase in CO₂:** The nature of CO₂ is acidic and its increase in water leads to the decrease in pH which inhibits the scale formation.

2.5.6. Effects of water composition

Sulphate scale normally happens at the enhanced oil recovery stage in oil and gas fields due to the incompatible mixing of the injected water and the formation water. Seawater is one of the most abundant and cheap liquids that can be employed to enhance the oil production. The problem is that the seawater is rich in sulphate anions which have the potential to react with cations (such as Ca^{2+} , Ba^{2+} and Sr^{2+}) and form the sulphate scale (e.g. $CaSO_4$, $BaSO_4$ and $SrSO_4$). The two latter ones due to lower solubility are of main concerns in oil and gas scale problems, which their formation with regard to the percentage of seawater is sketched in Figure 2.17.

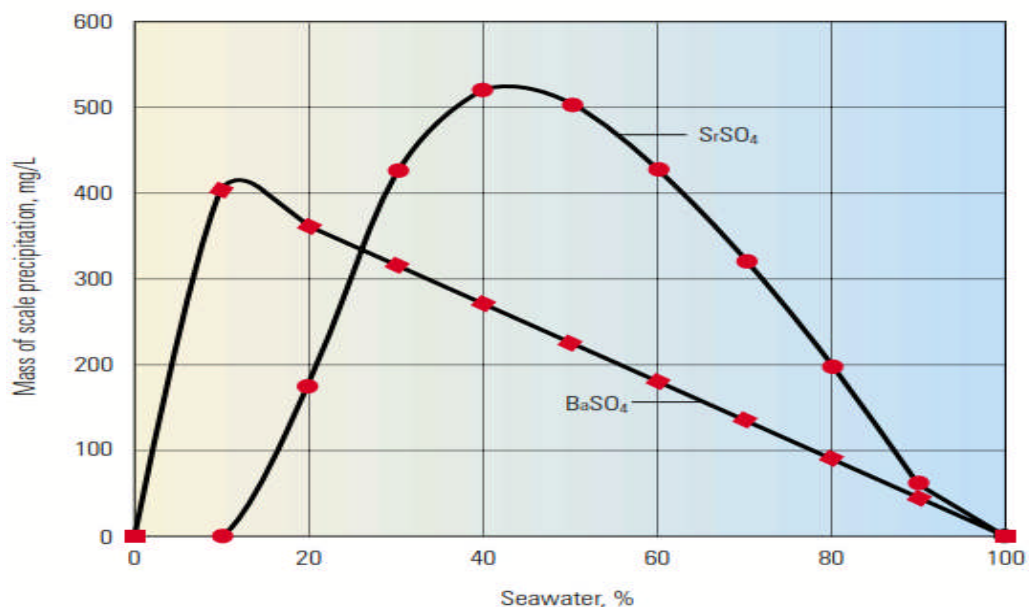


Figure 2.17. The amount of deposited scale from different mixtures of formation water and injected water (seawater) [2].

2.5.7. Effects of impurities

Many studies have been conducted to assess the effect of impurities on the bulk scale formation and surface deposition. It has been reported that by increasing the charge

of the cations ($Cr^{3+} > Fe^{3+} > Ni^{2+} > Na^+$) in the solution the inhibition effect of such impurities would increase [32, 42].

Wada et al. [61] have assessed the effect of different divalent cations (e.g. Fe^{2+} , Mg^{2+} , Ni^{2+} , Co^{2+} , Cd^{2+} , Zn^{2+} and Cu^{2+}) in the solution on different aspects of carbonate scale formation (i.e. induction time, crystal growth, morphology etc.). The existence of such impurities in the solution did not affect the induction time but they inhibit the crystal growth; and to compensate the crystal growth, the supersaturation ratio should be higher. They also found that aragonite is the dominant morphology that is formed in the existence of such impurities in the solution.

Chen et al. [62] have studied the effect of Mg^{2+} on both the precipitation and surface deposition of the calcium carbonate. They found that the existence of Mg^{2+} in solution would inhibit more the bulk precipitation than the surface deposition, as shown in Figure 2.18. So it could be concluded that these processes are two different processes. They have also reported that by increasing the concentration of Mg^{2+} in the solution, the crystals that are formed (i.e. calcite and vaterite), the calcite become more dominant crystal that is formed.

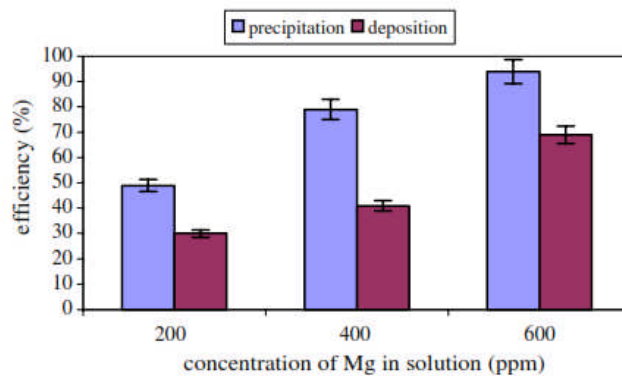


Figure 2.18. Efficiency of Mg^{2+} on bulk precipitation and surface deposition [62].

2.5.8. Effects of hydrodynamic conditions of the bulk solution

Hydrodynamics of the fluid is one of the most important parameters in both scale formation and the removal of scale. Shear stress is the main factor to remove the deposited scale from the surface. Alahmad et al. [58] surveyed that in a system prone to $CaCO_3$ and $CaSO_4$ scales, how the fluid velocity and consequently Reynolds

number (ranging 400-29,600) and wall shear stress decreases the deposited scale, as shown in Figure 2.19.

The stirring (or agitation) rate also affects the particles configuration. The calcium carbonate particles that formed at low stirring rate seems to be dense compared to particles formed at high stirring rate looked loosely; the author explains this occurrence due to the effect of hydrodynamics conditions on the formation of amorphous calcium carbonate crystals, which are unstable and easily affected [52].

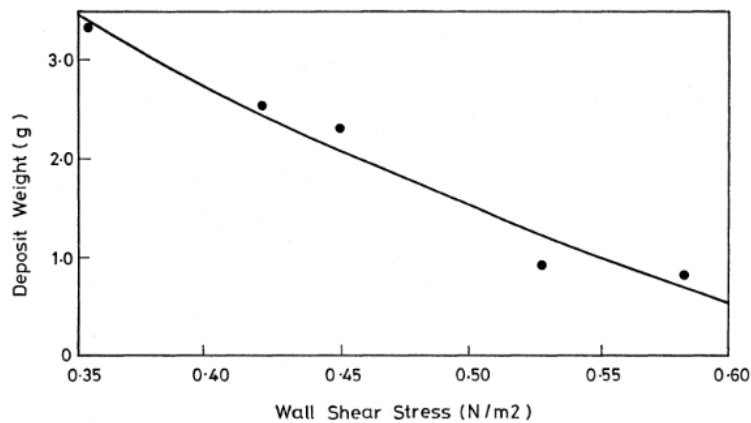


Figure 2.19. Wall shear stress versus deposition weight (mild steel). Condition: CaSO₄ conc. = 1000ppm, T=40°C, pH=8 [58], q=31082.03 W/m², time-48hr.

2.6. Effect of nature of substrate

2.6.1. Surface roughness

There have been so many surveys conducted to assess the effect of surface roughness on the scale formation [63-66]. Rankin and Adamson [65] have mentioned that roughness increases contact surface area; therefore, a rough surface has a greater effective surface energy comparing to a smooth surface, and as a result, a stronger adhesion can occur on rough surfaces. They also have reported that the scaling rate is independent of surface roughness and surface material, while scale adhesion is higher for rough surfaces and is also higher for metallic surfaces comparing to Teflon surfaces.

Keysar [63] has tested the effect of roughness (0.1µm - 24µm) of the mild steel under well-controlled conditions on the calcite scale formation. As shown in Figure 2.20, he

found that the adhesion force of rough surface is much higher than that of the smooth surface. On the other hand, he has reported that the porosity of scales form on a smooth surface is higher than that of the rough surface.

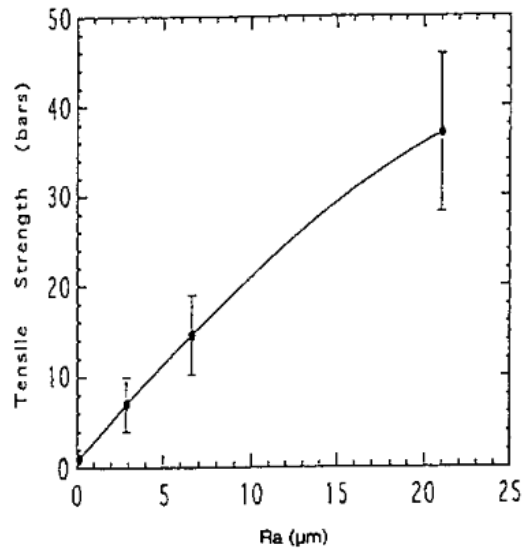


Figure 2.20. The effect of surface roughness (R_a) on calcite layer adhesion strength [63].

However, recently Cheong [64] has reported that rougher surfaces do not necessarily end up with higher scale deposits. The report has indicated that in polymer surfaces the roughness effects found to be of secondary importance and other characteristics such as surface chemistry and surface energy could be more important. Herz et al. [66] have also conducted the scale deposition test on a substrate with roughnesses range $0.18 \mu\text{m}$ to $1.55 \mu\text{m}$ and accentuate that as the surface roughness increases the deposited scale enhances on the surface. They have reported that such behaviour can be contributed to the reduction of local shear forces at the valleys and the increase in primary heterogeneous nucleation rate on the surface.

Most surfaces have roughnesses at many different length scales, ranging from the macro to the molecular. Normally, each unit area of the substrate has a finite number of nucleation active sites and the probability of nucleation depends on the number of free sites. On the other hand, if the surface presents a microroughness, a minimal number of contact points may reduce the possibility of adhesion since it reduces the contact area between the bodies [50, 67]. Surfaces may possess a roughness at several

length scales, but due to the short range of the van der Waals interaction, roughness at the nanoscale ultimately determines the strength of adhesion. [68]

2.6.2. Surface energy

The surface energy of a liquid is similar to its surface tension, but the surface energy determination of solids is not as easy as liquids but can be calculated indirectly. The surface energy of solids is calculated by a set of liquid/solid contact angles, established by bringing various types of liquids in contact with the solid. As a result, there is not a universal set of liquids for use to characterise a specific surface energy of a specific solid, and subsequently, there is not an exact value of surface energy for a specific solid.

To determine the solid surface energy indirectly with the shape of a drop placed on the surface, three interfacial forces balance at the edge of the drop exist. As shown in Figure 2.21, two of these forces are in opposite direction and the third one forms a particular angle to the surface, which is called contact angle.

The wettability of a solid surface can be expressed by the well-known Young equation as follows:

$$\gamma^{sv} = \gamma^{sl} + \gamma^{lv} \cos\theta \quad \text{Eq (2.25)}$$

where, θ is contact angle, γ^{lv} is the liquid surface free energy, γ^{sl} is the solid/liquid interfacial free energy and γ^{sv} is the solid surface free energy.

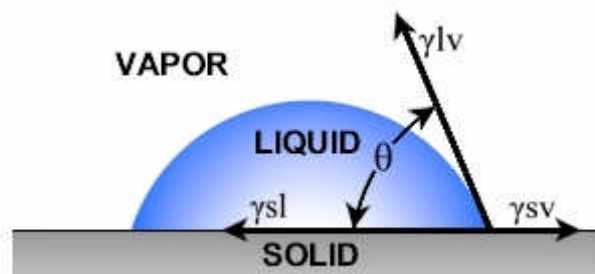


Figure 2.21. Scheme representing the contact angle (θ) between the vapour, liquid and solid phases for a liquid on a solid.

Surface energy is the combination of dispersion (non-polar) and polar energy. The polar energy exists only when polar groups are present while the dispersion energy exists between all molecules. The polar energy can be initiated by (a) Dipole-Dipole interactions (b) Dipole-Induced Dipole Interactions, (c) Hydrogen Bonding, or (d) Acid-Base Interactions.

There are two independent variables that will affect the surface energy: (a) the liquids that are used, and (b) the theory that is chosen. Normally, for non-polar surfaces such as poly(ethylene) and poly(propylene), the liquids are chosen that are non-polar (e.g. toluene or ethylene glycol) and surface energy theories that do not accentuate on specific molecular interactions. For polar surfaces such as glasses, ceramics and metals, the polar liquids (e.g. pure water) are selected along with the surface energy theories which emphasise on molecular interactions between the solid and two or three test liquids.

There are common surface energies theories that are normally employed to measure the surface energy of the solids:

- (a) **Zisman[69] Theory:** A one component model for solid surface energy which is widely used in surface energy theories. Zisman defines the surface energy of a solid to be equal to the surface tension of the highest surface tension liquid that completely wet the surface, with a contact angle of 0° . This theory works best for non-polar surfaces; as a result, if the surface is marginally polar the Zisman method becomes inadequate. Polymers can be calculated by this theory provided that they themselves do not contain heteroatoms, since heteroatoms make such surfaces polar, such as polyamides, polyesters, polyacrylates, polycarbonates, etc. Zisman theory characterises the surface energy of surfaces and the surface tension of liquids by only one overall value, as a result, it ignores the specific liquid-solid interactions. This method is suitable for testing surfaces with low contact angle and requires at least two drops of low contact angle:

$$\cos\theta_i = \frac{\gamma_s}{\gamma_i} \quad i = 1, 2 \quad \text{Eq (2.26)}$$

where θ_i is contact angle of testing drop, γ_i is surface tension of testing drop and γ_s is surface tension of testing surface.

- (b) **Fowkes [70] Theory:** A two-component model for solid surface energy which is known as “Geometric Mean” method. This method divides the surface energy into two components, dispersive and polar, and uses a geometric mean approach to combine their contributions.

$$\gamma_i(1 + \cos\theta_i) = 2 \left(\sqrt{\gamma_i^d \gamma_s^d} + \sqrt{\gamma_i^p \gamma_s^p} \right) \quad i = 1, 2 \quad \text{Eq (2.27)}$$

$$\gamma_i = \gamma_i^d + \gamma_i^p \quad i = 1, 2 \quad \text{Eq (2.28)}$$

$$\gamma_s = \gamma_s^d + \gamma_s^p \quad \text{Eq (2.29)}$$

where γ_i^d and γ_i^p are dispersion and polar energy of testing drop i , and γ_s^d and γ_s^p are dispersion and polar energy of testing surface. This equation is also rearranged by Owens/Wendt [71] to form the equation to the type of $y=mx+b$ which the slope is $(\gamma_s^p)^{1/2}$ and the y-intercept will be $(\gamma_s^d)^{1/2}$. By doing so, the total free surface energy is merely the sum of its two component forces.

- (c) **Wu [72] Theory:** Another two-component model for solid surface energy which is known as “Harmonic Mean” method. This model is suitable for non-polar low energy surfaces and requires at least two kinds of drops with different surface tensions. Like the previous method, it divides the surface energy into two components, dispersive and polar which are presented as follows:

$$\gamma_i(1 + \cos\theta_i) = 4 \left[\frac{\gamma_i^d \gamma_s^d}{\gamma_i^d + \gamma_s^d} + \frac{\gamma_i^p \gamma_s^p}{\gamma_i^p + \gamma_s^p} \right] \quad i = 1, 2 \quad \text{Eq (2.30)}$$

- (d) **Van Oss [73] Theory:** A three-component model for solid surface energy. In this method, the surface energy is divided into three components (a dispersive component, an acid component, and a base component). Like the previous method, the dispersive component is intended to characterise all of the non-specific interactions, such as van der Waals type, that the surface would have a wetting liquid. The acid component, in theory, is the tendency of the surface interacting with wetting liquid to donate the electron density (act basic), while

the base component is the tendency of the surface interacting with wetting liquid to accept electron density (act acidic). This method is suitable for materials with polar surfaces and requires at least three drops of different surface tensions, at least two of them must be polar fluid.

$$\gamma_i(1 + \cos\theta_i) = 2 \left(\sqrt{\gamma_i^d \gamma_s^d} + \sqrt{\gamma_i^+ \gamma_s^-} + \sqrt{\gamma_i^- \gamma_s^+} \right) \quad \text{Eq (2.31)}$$

$$\gamma_i = \gamma_i^d + 2\sqrt{\gamma_i^+ \gamma_i^-} \quad \text{Eq (2.32)}$$

$$\gamma_s = \gamma_s^d + 2\sqrt{\gamma_s^+ \gamma_s^-} \quad \text{Eq (2.33)}$$

where, γ_i is surface tension of testing drop i , γ_i^d is dispersion portion of surface tension, γ_s^+ is surface tension contributed by acid, γ_s^- is surface tension contributed by base, and subscript s denotes the solid surface.

2.6.3. Scale control at surfaces

The accumulation of unwanted crystalline deposits, known as fouling, reduce the efficiency of the system; for instance, the scale formed in the tubes of the heat exchanger will reduce the heat transfer coefficient and eventually increases the maintenance cost. So many studies have been conducted to assess the surface deposition and the ways to decrease the scale formation on the surfaces.

In general, the parameters such as surface chemistry, surface roughness, surface energy, and surface hydrophobicity of the surface known as the criteria that play a major role in scale deposition process, but it is not fully understood the effects of such parameters all together in a process. For instance, low surface energy is known as one of the parameters which decrease the scale deposition rate on a surface. Forster et al. [74] have shown that the deposition rate of a substrate with Polytetrafluoroethylene (PTFE) coating is higher than that with Diamond Like Carbon (DLC) coating, although the latter one has higher surface energy.

Eroini et al. [75] have surveyed surface resistance test over seven diverse substrates, such as stainless steel, stainless steel pre-treated with Polyphosphineocarboxylic Acid (PPCA), PTFE, DLC, ceramic, polymer coated stainless steel, and isotropic super-finished (ISF) stainless steel. They have reported that there is no strong correlation

between the surface roughness/hydrophobicity with the scaling deposits. For instance, ISF stainless steel which is the most hydrophilic surface had a better performance in scaling deposition (CaCO_3) comparing to other surfaces. Although they could not identify a unique parameter (such as surface roughness, surface chemistry, etc.) to make a surface efficient in terms of scaling, they have reported that non-directional R_a profile is a quite efficient parameter in terms of scaling.

Cheong et al. [64] have reported the scale deposition of CaCO_3 on different coatings such as stainless steel, six different polymer surfaces, two ceramic coatings and DLC. They have reported that for polymer surfaces the scale deposition rate proportionally increases by water contact angle while for other surfaces this trend is inversely proportional, as shown in Figure 2.22. They have reached a conclusion that the surface deposition rate decreases as the surface roughness increases, which is opposite to the general philosophy.

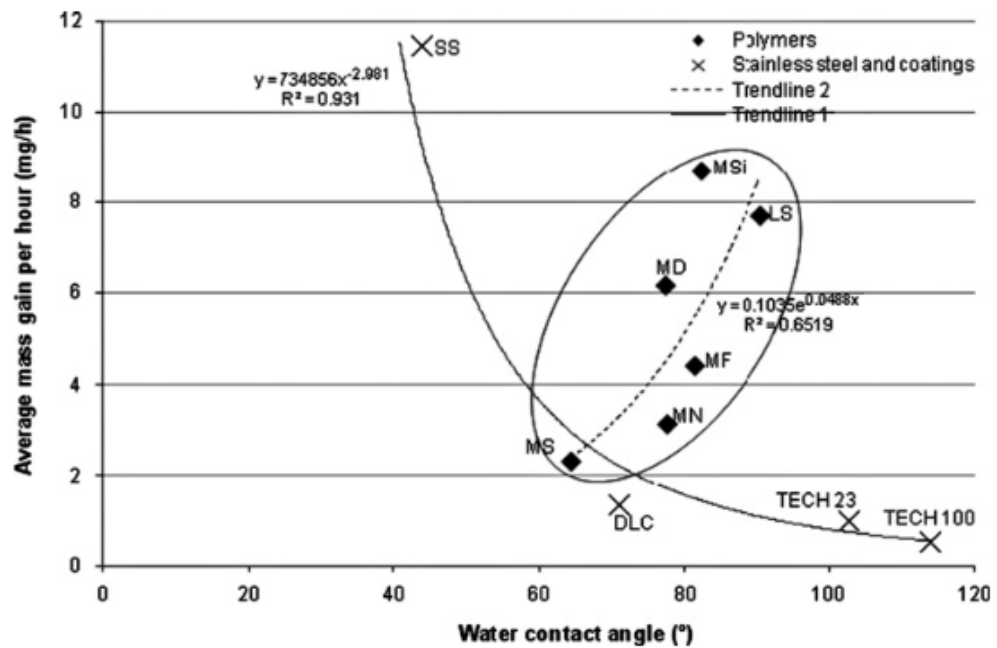


Figure 2.22. An average mass gain of scale deposit vs. water contact angle [64].

Some researchers have focused on the surface chemistry and modify the substrate to reduce the scale deposition rate. Zhao and Wang [76] have fluorinated the DLC coating and investigated its effect on the surface energy and the scale adhesion and subsequent scale formation. The substitution of hydrogen atoms with fluorine atoms will lead to a significant reduction of surface free energy [77, 78]. Zhao and Wang found that by increasing the C_2F_4 : C_2H_2 ratio, there has been a significant reduction

in the Lifshitz-van der Waals (or dispersive) component (γ^{LW}), while there is no change in the Lewis acid-base (or polar) component (γ^{AB}). They also found that the scale deposits (CaSO_4) rate of fluorinated DLC is lower than the untreated DLC.

Bargir et al. [79] have studied the theoretical work of adhesion (CaCO_3) with different types of substrates, including metallic and non-metallic, with the average mean roughness value no more than 100 nm. They have reported that the theoretical work of adhesion is influenced by surface topography or its polar surface free energies or both, depending on the chemical and physical homogeneity of the surface. They also found that the Lewis base component, γ^- , had the greatest effect on scaling rate, while the Lewis acid component, γ^+ , did not have any effect.

There are some studies that show that by surface modifications the induction time can be extended and predictable [80, 81]. Geddert et al. [81] in 2009 have shown that by the modification of surface and decreasing the nucleation sites by the electrochemical treatment the induction time has extended. They mention that this treatment does not change the mechanical surface characteristics like topography and roughness, but change the energetic property of the substrate. Geddert et al. [80] in 2011 have predicted the induction time of CaSO_4 based on surface parameters and supersaturation of the salt solution, as follows:

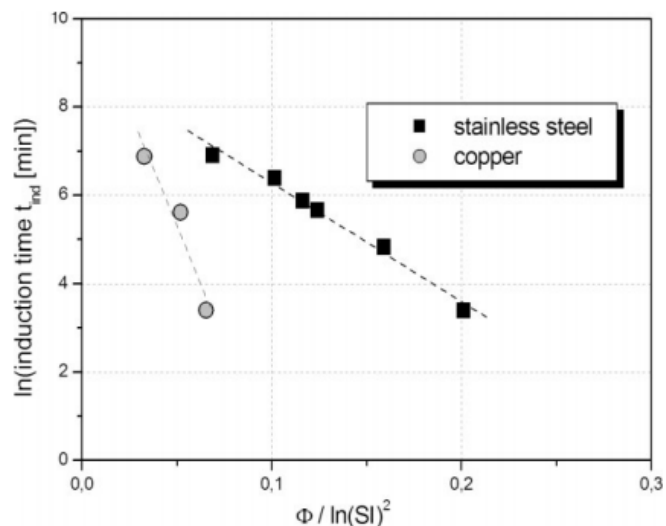


Figure 2.23. Induction time prediction for stainless steel and copper under batch conditions [80].

$$\ln(t_{ind}) \propto \frac{\varphi}{\ln(SI)^2} \quad \text{Eq (2.34)}$$

where, t_{ind} is the induction time, φ is the nucleation correction factor, and SI is the saturation index. They presented the prediction for stainless steel and copper in Figure 2.23. One of the drawbacks of their approach is that the induction time of calcium sulphate is based on the assumption that the induction process is dominated by heterogeneous nucleation.

Jaouhari et al. [82] have reported that the nature of the substrate has a significant effect on the nucleation process of the scaling rate of calcium carbonate. They have used an electrochemical test based on oxygen reduction technique for the calcium carbonate deposition on a different metallic substrate: stainless steel, bronze, and gold. They found that with different solution composition gold had the fastest scale followed by bronze and stainless steel had the slowest scale rate. The authors believe that the presence of oxide on the surface would slow down the oxygen reduction process which results in the decrease in the nucleation rate. The Same technique has been conducted on stainless steel by Gabriellie et al. [83]. They found that the presence of passivating layer (i.e. OH^- formation through local oxygen reduction) on non-noble metal (i.e. metals prone to corrosion and oxidation in moist air) would decrease the density of nucleation sites on the surface and consequently lower deposition rate.

2.6.4. Surfaces inspired by nature

Surface chemistry and structure play major roles in the scaling process. There are different surface characteristics that can be inspired by nature that can be implemented and developed into technology. Leaves of plants are one the surfaces that have been modified and developed during million years to adapt themselves to the environment. Koch et. al. [84] have reported the most prominent functions of the plant boundary layer such as mass transfer of water as hydration and dehydration, surface wettability, anti-adhesive/self-cleaning properties, surface self-cooling to reduce the surface temperature, etc.

2.6.4.1. Lotus effect – self-cleaning surfaces

Leaves of the Lotus plant are extremely water repellent (or superhydrophobic). As shown in Figure 2.24, the schematic of the wettability of plant surface with regard to its structure is illustrated. The contact angle of Lotus plant is more than 150° which can be categorised as superhydrophobic. The surface structure of Lotus leaf is made

up of convex cells (micro level) superimposed by hydrophobic tubules (nano-level hair like). In such configuration, air is trapped in the cavity of the convex cells which reduce the interface of solid-water and consequently the wettability of the surface decreases. Therefore, water gains less energy from the surface (adsorption energy) and forms as a spherical droplet. As a result, both the contact angle and the adhesion to the surfaces reduce. Cheng et al. [85] have reported the importance of nano- hair like waxes on the self-cleaning behaviour of the lotus leaf. They have heated up the Lotus leaf, so the nano- hair like waxes would melt, and the contact angle would reduce by a magnitude of 20°.

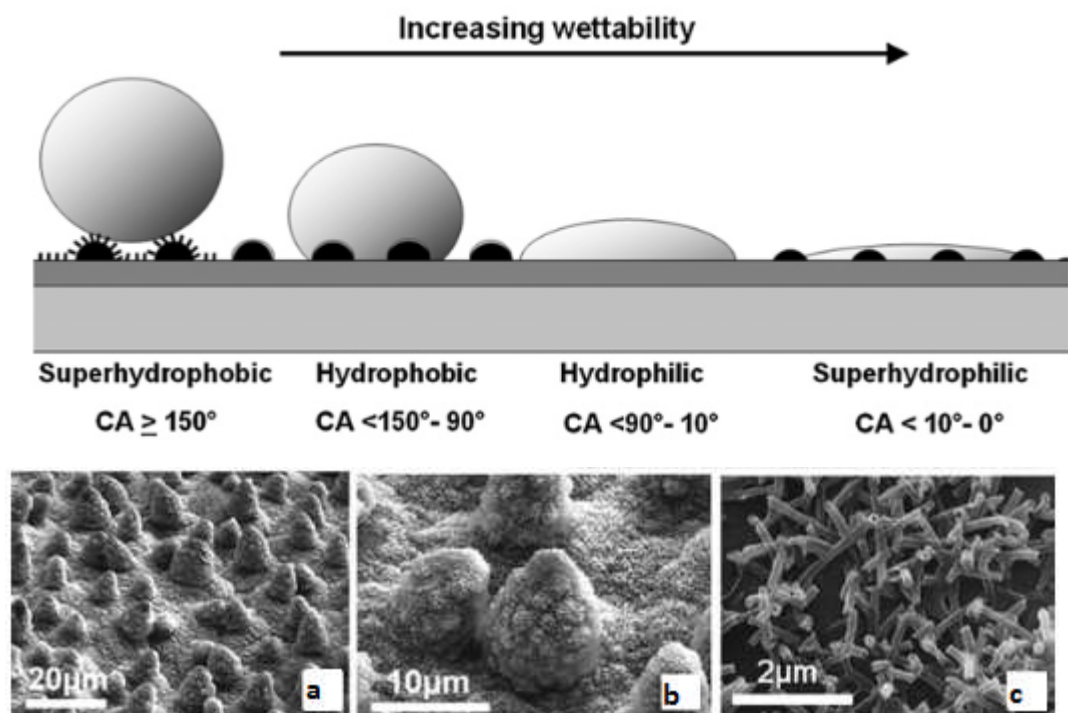


Figure 2.24. Plant surface structures and wettability, (a) to (c) representing SEM images with a different resolution of the surface structure of a lotus leaf [84].

2.7. Co-precipitation and co-deposition

The mechanism of precipitation in the bulk solution has been studied extensively and in most case scenarios the solo scale formation is studied, although the co-precipitation theory has been demonstrated for a long time. As Kolthoff [86] has established his co-precipitation theory, there are mainly three different types of co-precipitation:

1. The formation of mixed crystal; the incorporation of the impurities in the crystal lattice; the structure of the crystal does not change.
2. Occlusion; the impurities are absorbed during the crystal growth of the crystals and would affect the structure of the crystals, i.e. increase the formation of imperfections in the crystal and known as “real co-precipitation”.
3. Surface adsorption by the precipitate after it has been formed or separated; this co-precipitation only happens when the precipitate has a large surface area where the precipitate has a similar microcrystalline character.

In short, the co-precipitation of impurities can either be incorporated in the crystal lattice or formed imperfections inside of the crystals or absorbed on the surface of the precipitate.

Distinguishing of such mechanisms is not normally straight forward. For instance, it was believed that there is a co-precipitation of zinc with copper sulphide or co-precipitation of magnesium with calcium oxalate, while further studies proved that these mechanisms are called post-precipitation mechanisms and due to its slight differences, it is normally misunderstood by co-precipitation mechanisms[86]. Sheikholeslami [87] reported that the standard Gibbs free energy of formation for an impure salt, as well as the thermodynamic solubility product, and the morphology of precipitates, are different from that of a pure salt.

The logarithmic Doerner-Hoskins law [88] is one of the models describing the distribution between the precipitate and the solution as follows:

$$\ln \frac{a}{a-x} = \lambda \ln \frac{b}{b-y} \quad \text{Eq (2.35)}$$

where, a and b are the initial concentrations of the precipitate and the solution, respectively; and $a-x$ and $b-y$ are the concentration of the precipitate and the solution after the separation, and λ is the distribution coefficient which for λ greater than unity will result in the formation of solid scale in the solution.

Kushnir [89] has studied the co-precipitation of gypsum with cations (e.g. Na^+ , K^+ , Mg^{2+} , Sr^{2+}) and anions (e.g. Cl^-) as a function of temperature, brine supersaturation rate and crystal kinetics. An increase in the kinetics of gypsum would increase the concentration of cations in the gypsum up to a limit, while has little effect on chloride

concentration. An increase in the temperature would decrease the partition coefficient of the cations in the gypsum. He explained in this study that the co-precipitation behaviour can be defined as the relation between the rate of desorption of the cations from the surface of gypsum, and the rate of gypsum co-precipitating crystal growth with cations. Lorens [90] found that the distribution coefficient of metal ions (e.g. Co^{2+} , Mn^{2+} and Cd^{2+}) in calcite decreases in a co-precipitation process as the precipitation ratio increases, while strontium acts quite opposite.

Brower [91] has conducted a research to synthesise the homogeneous barium strontium sulphate as the $(\text{Ba}_x\text{Sr}_{1-x})\text{SO}_4$ where $0.1 < x < 0.9$ for a range of temperature from 35-150°C. She found that an increase in temperature would change the “x” from 0.86 to 0.50.

The presence of other cations can adversely affect the distribution coefficient in the lattice of calcium carbonate by temperature. For instance, Dietzel et al. [92] have reported in a system with possible co-precipitation of aragonite with Ba^{2+} and Sr^{2+} , the distribution coefficient of both cations decreases as the temperature increases.

The co-precipitation of strontium in the calcium carbonate has been studied extensively [93-96].

The distribution coefficient of Sr^{2+} in calcite (k_{Sr}^{C}) or aragonite (k_{Sr}^{A}) is defined as the ratio of Sr^{2+} to Ca^{2+} , ($m_{\text{Sr}^{2+}}/m_{\text{Ca}^{2+}}$), in the precipitated calcite (or aragonite) divided by $m_{\text{Sr}^{2+}}/m_{\text{Ca}^{2+}}$ in the solution which the calcite (or aragonite) was precipitated, as indicated in Equation 2.36 for the distribution coefficient of strontium in nearly pure aragonite: [93]

$$\frac{m_{\text{Sr}^{2+}}^{\text{A}}}{m_{\text{Ca}^{2+}}^{\text{A}}} = k_{\text{Sr}}^{\text{A}} \frac{m_{\text{Sr}^{2+}}^{\text{L}}}{m_{\text{Ca}^{2+}}^{\text{L}}} \quad \text{Eq (2.36)}$$

if the calcite (or aragonite) precipitated from a homogeneous solution and if during the precipitation a surface equilibrium condition maintained between the solution and the crystals (i.e. the co-precipitation process is controlled by surface processes), then the Doerner-Hoskins relation [88] can be applied as indicated in Equation 2.37. [94]

$$\log \frac{(m_{Sr^{2+}}^L)_i}{(m_{Sr^{2+}}^L)_f} = k_{Sr}^A \log \frac{(m_{Ca^{2+}}^L)_i}{(m_{Ca^{2+}}^L)_f} \quad \text{Eq (2.37)}$$

or

$$\log \left(1 + \frac{(M_{Sr^{2+}}^A)_i}{(M_{Sr^{2+}}^L)_f} \right) = k_{Sr}^A \log \left(1 + \frac{(M_{Ca^{2+}}^A)_i}{(M_{Ca^{2+}}^L)_f} \right) \quad \text{Eq (2.38)}$$

where, “*m*” refers to the concentration of ions and subscripts “*i*” and “*f*” denotes the initial and final solutions, respectively, and “*M*” refers to a total number of moles with respect to its corresponding super/sub-scripts. Equation 2.38 describes the distribution of trace elements co-precipitated in carbonate minerals and has been found more accurate compared to Equation 2.37, where there is a small co-precipitation of Sr^{2+} with $CaCO_3$. [95]

Holland et al. (1963) [93] determined k_{Sr}^A by the ratio of solubility products $^{\circ}K^A$ (pure aragonite) and $^{\circ}K^S$ (pure strontianite or $SrCO_3$), by the ratio of the activity coefficients of calcium carbonate and strontium carbonate in the aragonite phase, by the ratio of the activity coefficient of Sr^{2+} to that of Ca^{2+} in the liquid phase, by the following equation:

$$k_{Sr}^A = \frac{^{\circ}K^A}{^{\circ}K^S} \cdot \frac{\gamma_{CaCO_3}^A}{\gamma_{SrCO_3}^A} \cdot \frac{\gamma_{Sr^{2+}}^L}{\gamma_{Ca^{2+}}^L} \quad \text{Eq (2.39)}$$

Holland et al. [93, 95] have shown that the k_{Sr}^A [93] and the k_{Sr}^C [95] in the solution is nearly independent even by the presence of large concentration of NaCl, however, Pingitore and Eastman [96] have demonstrated that the k_{Sr}^C decreases by the presence of Na^+ in NaCl. The importance of temperature is evident in the dependency of strontium distribution coefficient on the existence of the NaCl in calcite, i.e. the former reports by Holland et al. [93, 95] are done in a temperature range of 90-100°C, while the latter one has conducted at 25°C. Oomori et al. [97] have reported that the distribution coefficient of magnesium ions in calcite increases as the temperature rises, while this value does not change by temperature increase in aragonite.

The k_{Sr}^C in the temperature range of 95°-100°C is around 0.076, [95] while the same study was carried out in the same range of temperature demonstrating that the k_{Sr}^A is around 0.593 to 0.798 depending on the concentration of strontium in the solution. [93] Holland et al. [95] have reported that the k_{Sr}^C is independent of ionic strength of the solution up to 1.4M, while the k_{Sr}^A is adequately large and is affected by the mol fraction of Sr^{2+} in the solution. In other words, depending on the mole fraction of Sr^{2+} in the solution, the ratio k_{Sr}^A/k_{Sr}^C in the temperature range of 95°-100°C can vary from 7.8 to 10.5.

Kinsman and Holland [94] have demonstrated that the k_{Sr}^A linearly decreases from 1.17 to 0.88 by an increase in temperature from 16° to 80°C, respectively. They have attributed such a matter to the solubility products ratio of pure aragonite to the pure strontianite (or $SrCO_3$), as mentioned in Equation 2.39. The $K^A/°K^S$ is around 11 at 25°C which decreases to unity at 170°C. The activity coefficient ratio for pure aragonite is equal to unity and the $\gamma_{Sr^{2+}}^L/\gamma_{Ca^{2+}}^L$ is equal to unity, except for the solution with very high ionic strength. The $\gamma_{SrCO_3}^A$ seems the only parameters that increases with an increase in temperature that its magnitude cannot compete with the decrease of $K^A/°K^S$ in the temperature range between 0° to 100°C.

2.8. Methods to remove and prevent scale in the oil and gas industry

As scales form on the surface, the only option which is costly and in some cases ineffective is the scale removal either mechanically or chemically. Scale removal techniques should not be damaging to the surface and environment, and be effective at re-precipitation. Depending on the nature of the scale, the technique that should be applied is different. For instance, calcium carbonate can be dissolved with acids, while some hard scales, e.g. barium sulphate, is extremely resistant to chemical additives and is so rigid to be removed by mechanical equipment. Pure barium sulphate has a very low acid solubility with a low degree of porosity and can be removed by modern mechanical removal techniques. However, the mixture of other scales such as strontium sulphate, calcium sulphate or calcium carbonate with barium sulphate will widen the approaches to remove the scale.

2.8.1. Mechanical removal techniques

The mechanical removal normally applied where there is a thick non-porous layer of scale should be treated, wherein such conditions, chemical removal techniques are ineffective. One of the earliest techniques that were applied in the oil industry was using the explosive to shed off the brittle scales by its wave impact. However, such technique would also damage the wall itself. On the other hand, safe explosive removal would not be effective where there is a thick layer of scale. Water jetting is the other option to implement, but it is not so effective even for carbonate scales that have lower adhesion force comparing to other scales. By adding a small ratio of solid particulates, 1% to 5% by weight, the performance of water jet would significantly increase and is called abrasive water jet. Although such equipment has higher cutting performance compared to a water jet, there is a high possibility of damage to the wall. There are so many mechanical removal methods that can be employed but due to a limited range of applicability of such methods, chemical removing treatment would be the first choice to remove scale [2].

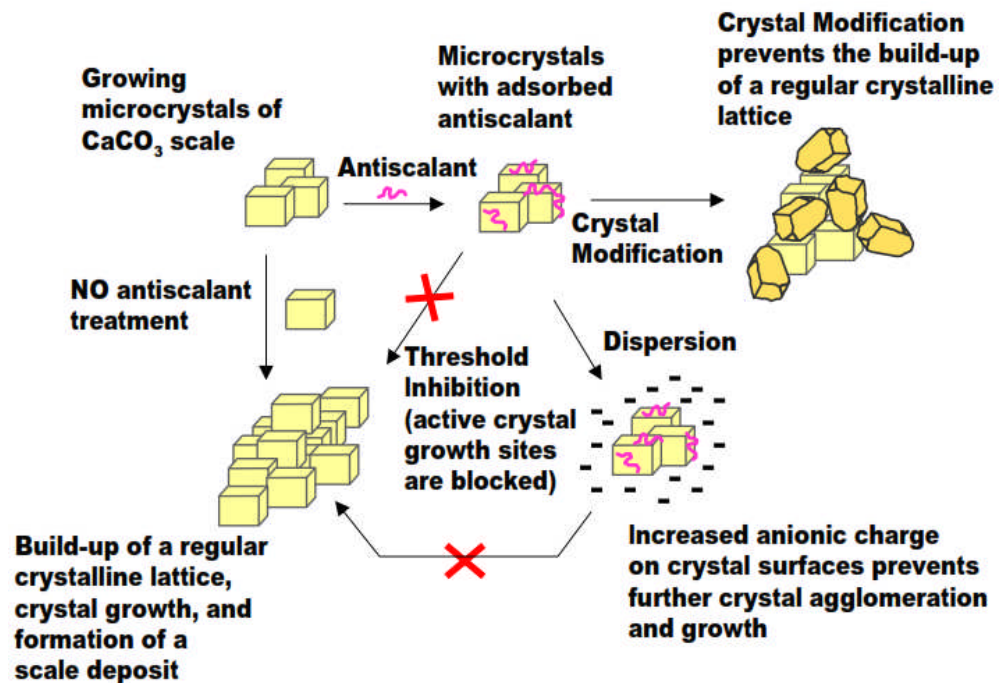


Figure 2.25. Schematic representing the pathways of scale prevention [31].

2.8.2. Chemical removal techniques

Using chemical removal scale techniques are more conventional where mechanical removal methods are ineffective or costly. Carbonate scales are well soluble in hydrochloric acids, while hard sulphate scales are more difficult to dissolve in acids due to their low acid solubility characteristics. As a result, there should be chemical additives to be applied to have another effect rather than solubility. Ethylenediaminetetraacetic acid (EDTA) is one of the acids that are widely used for such purposes. EDTA is a chelate compound which shares electrons from oxygen and nitrogen with barium ions, forming a barium EDTA chelate compound which helps the dissolution of solid barium sulphate [2].

2.8.3. Scale inhibitors

There are different ways to inhibit the crystallisation growth. Adding some inhibitors (e.g. EDTA, DTPA), known as chelants, in controlling the scale deposits is widely used. Chelants are molecules that isolate soluble cationic scaling species (such as Ca^{2+} , Ba^{2+} and Sr^{2+}) to prevent their reaction with counter-ions (such as CO_3^{2-} and SO_4^{2-}). The disadvantage of such additives is that they interact on a stoichiometric level (i.e. one molecule of chelant reacts with just one cationic species); therefore, a high dosage of additives is required to attain satisfactory performance, which is costly. Duggirala [31] has introduced in his report a polymeric antiscalant that react on sub stoichiometric level, and as a result demands lower dosage of inhibitor. As shown in Figure 2.25, this type of antiscalant operates in one or three possible mechanisms: threshold inhibition, crystal dispersion, or crystal modification.

2.9. Summary and gaps in the literature

Scale formation is recognised as one of the major flow assurance problems affecting production in the oil and gas sector. The main problems of scale deposits in oil and gas industries are clogging the wellbore; reducing equipment lifetime; impairing the oil applications, particularly subsurface control valve (SSCV), Electrical Submersible Pumps (ESPs) and hydraulic actuators; and preventing fluid flow, which could be so costly for not only lower oil production but also the huge maintenance cost of the production line in oilfields.

In the oil and gas industry, many oil wells suffer from flow reduction due to scale deposition within the downhole utilities, valve applications, and tubular components, especially during the oil recovery operations.

At the early stages of the oil extraction process, due to high differences in temperature and pressure carbonate scales are the dominant type of scales to form, while at the late stages of oil extraction sulphate scales are the dominant types. The reason is that in the Enhanced Oil Recovery (EOR) process seawater, which is abundant and cheap, is pumped down to the reservoir to increase the oil production. Seawater is rich in sulphate ions and reacts with cations (such as Ba^{2+} and Sr^{2+}) in the reservoir which leads to the formation of sulphate scales. Although in some cases to prevent the sulphate scale problems, the de-sulphated seawater is injected into an oilfield, it is not economically efficient [10].

Inorganic scale deposits (e.g. CaCO_3 , BaSO_4 and SrSO_4) can be deposited all along the water paths in the pipeline applications. Oil industries normally are encountering two mechanisms of scale formation [7, 8, 11, 12] as follows:

- (a) Carbonate-dominated scales (CaCO_3 and FeCO_3) take place where there is a change in temperature and pressure which results in the release of carbon dioxide from aqueous form to gas form from the flowing fluid.
- (b) Sulphate-dominated scales (BaSO_4 , SrSO_4 , CaSO_4 and $\text{CaSO}_4 \cdot \text{H}_2\text{O}$) come about where there is a mixture of two incompatible brines.

Surface analysis is the first step that should be surveyed to have a better understanding about the scale deposition on the surface. In developing a surface engineering strategy for scale, it is particularly important to understand some parameters in scaling such as: surface parameters (e.g. the roughness [63, 64, 98] and the wettability [64, 79, 99-103], kinetic of crystallization and surface deposition [2, 53, 54, 56, 104], and the induction time [80-83] for surface scaling which is depending on the flow regime [51, 58, 105].

Surface deposition and bulk precipitation are interlinked processes. However, they have very different kinetics [106]. In an oilfield, the type of the scale that deposits on the surface would be different from place to place i.e. the mechanism of scale deposition on the surface at the downhole would be different from that of on the ground level components due to (a) the difference in water composition and saturation ratio between these two regions, and (b) the formation of crystals and particles in the

brine solution while reaching to the ground level valves and pipe components. In so many studies [107-113] the hydrodynamic effects on the process of scale formation on the surface have been surveyed as one mechanism referred to as “deposition” on the surface. In the presented thesis, the scale deposits on the surface are divided into two mechanisms which are interlinked as: “deposition process” which refers to the process of nucleated growth of scale for the asperities at the surface in a heterogeneous form and “adhesion process” which refers to the sticking of pre-existing crystals that are already nucleated in the bulk solution and built up as a layer on the surface; and the experimental setup are designed accordingly.

Understanding the flow assurance problems in the oilfield is not an easy task, and selecting a right procedure to mitigate the surface scaling is dependent on the type of the scale deposits. Although the importance of mixed precipitates in real flow assurance problems is clear, only a few studies have been focused on the co-precipitation of scale deposits [87, 88, 91, 94, 114].

Despite much recent attention to the surface scale formation, there is still no solid unanimous awareness on characterising a good anti-fouling surface. This necessitates a comprehensive study of the surface scale deposition for a different type of mixed scale deposits with different scale mechanisms.

In this study, a systematic laboratory setup has been designed to test the modified surfaces that are commercially-available, based on the real flow conditions in the oilfield. This study is divided into two types of scale deposits: carbonate-dominated brine (Chapter four) and sulphate-dominated brine (Chapter five). Since the type of surface scale deposited in the downhole is different from the surface scale formed on the ground level, the scaling process has two scenarios as *adhesion* and *deposition* processes. The co-precipitation of the scale deposits and their corresponding co-deposition on the modified surfaces are studied, as well. To correlate the scaling tendency tests in the laboratory to real conditions, a surface scaling rig has been designed, and the obtained data is analysed and compared with the experimental results.

Chapter 3

Experimental Methodology

3.1. Introduction

In order to study the surface scale formation and characterization of various modified surfaces, a combination of methods, analyses and techniques have been used. This chapter provides a description of the experimental methodology.

3.2. Chemical reagents

The brine solutions investigated were based on the properties of common brine solutions found in the Brazilian basins, provided by PETROBRAS.

Table 3.1. Ion composition of both brines

Sulphate-dominated brine		Carbonate-dominated brine	
Ion	Amount (mg/l)	Ion	Amount (mg/l)
Na ⁺	71,131	Na ⁺	71,131
K ⁺	2,469	K ⁺	2,469
Mg ²⁺	1,678	Mg ²⁺	1,678
Ca ²⁺	11,541	Ca ²⁺	11,541
Ba ²⁺	157	Ba ²⁺	157
Sr ²⁺	2,686	Sr ²⁺	2,686
Cl ⁻	138,400	Cl ⁻	138,400
Br ⁻	1,024	Br ⁻	1,024
CH ₃ COO ⁻	14	CH ₃ COO ⁻	58
SO ₄ ²⁻	562	SO ₄ ²⁻	14
HCO ₃ ⁻	58	HCO ₃ ⁻	562

In the laboratory, the scale tendency tests have been carried out based on two different brine compositions for sulphate-dominated and carbonate-dominated brine solutions, as shown in Table 3.1 and Table 3.2.

The supersaturated brine used in the study is composed of two complex brines (as shown in Table 3.2) which were prepared separately by weighing the appropriate quantity of salts and mixing with distilled water, and then mixed in the ratio of 1:1.

Table 3.2. Brine composition of both brines

Brine 1 (g/l)			Brine 2 (g/l)		
Salt	Sulphate	Carbonate	Salt	Sulphate	Carbonate
CaCl ₂ .2H ₂ O	84.6521	84.6521	Na ₂ SO ₄	1.6604	0.0414
BaCl ₂ .2H ₂ O	0.5598	0.5598	NaBr	2.6372	2.6372
MgCl ₂ .6H ₂ O	28.0756	28.0756	NaHCO ₃	0.1598	1.5484
SrCl ₂ .6H ₂ O	16.3241	16.3241	NaCH ₃ COO	0.0741	0.3068
KCl	9.4228	9.4228	NaCl	228.0267	228.0267
NaCl	180.825	180.825			

Both brine solutions were filtered by a membrane with pore size of 0.45µm, and before mixing the two brine solutions, they were heated up to 56°C. “Brine 1” solution was buffered by CO₂. The process of buffering the solution with CO₂ is called the “oxygen reduction” process which is applied in such experiments due to (a) simulating the real conditions inside the wellbore and production line which is oxygen-free and (b) to maintain the level of pH at a constant level throughout the experiment.

The initial saturation ratio, calculated by Multiscale® software, is shown in Table 3.3.

Table 3.3. Saturation ratio of brine solutions calculated by Multiscale® software

Sulphate dominant brine		Carbonate dominant brine	
Species	Saturation Ratio	Species	Saturation Ratio
CaCO ₃	10.79	CaCO ₃	12.54
BaSO ₄	121.50	BaSO ₄	3.03
SrCO ₃	4.09	SrCO ₃	4.67
SrSO ₄	11.70	SrSO ₄	0.29

As a result, thermodynamically there is a possible scale formation of calcium carbonate, barium sulphate and strontium sulphate in the bulk solution of the sulphate-dominated brine solution, and a formation of calcium carbonate, barium sulphate and strontium carbonate in the bulk solution of carbonate-dominated brine solution. Kan and Tomson [115] have shown that with the saturation ratio of barite higher than 3,

the precipitation and crystal growth can happen even without the existence of seed crystals of barite.

3.3. Substrates

A standard austenitic stainless steel (UNS S31603) is selected as a metallic reference material.

The stainless steel (SS316) samples are coated with 21 different commercially available types of coatings which cover a variety of surface roughness and surface energy values with different surface compositions, as shown in Table 3.4.

Table 3.4. Modified substrates with their corresponding coating code

No.	Coating name	Company name	Type
1	DTi	Danish Technological Institute	Si-O ₂ -amorphous carbon
2	B1341	Belzona	Epoxy
3	B1381	Belzona	Epoxy
4	B1391	Belzona	Epoxy
5	B1541	Belzona	Epoxy
6	B5891	Belzona	Epoxy
7	B5892	Belzona	Epoxy
8	B5891exp	Belzona	Epoxy
9	B5892 exp	Belzona	Epoxy
10	PTFE	DuPont	Zonyl (3-layers)
11	PFA	DuPont	Teflon (3-layers)
12	FEP	DuPont	Teflon (3-layers)
13	ETFE	DuPont	Tefzel (3-layers)
14	One	DuPont	3 in 1 fluoropolymer
15	Black	DuPont	3 in 1 fluoropolymer
16	DHS	Diamond Hard Surfaces	Diamond Like Carbon
17	TiN	Tecvac	TiN
18	TiN-Al	Tecvac	TiN-Al
19	CrN-Ag	Tecvac	CrN-Ag
20	CrN	Tecvac	CrN
21	DLC	Tecvac	Amorphous carbon

Stainless steel grade 416 has also been tested in scale tendency tests (carbonate-dominated brine) due to its applicability in the oilfield applications.

Commercially-available coatings selected in this study can be categorised based on their applicability in the oilfield applications. In other words, the fluoropolymer and epoxy coatings can be applied inside the pipeline systems while the DLC and ceramic coatings due to their comparative higher cost of surface treatment and production complexities are not viable choices. On the other hand, due to the higher relative thickness of fluoropolymer and epoxy coatings compared to DLC and ceramic coatings, the applicability of former coatings in valve component (e.g. subsurface safety valves) is not feasible and leads to malfunction of the valve.

CORE Coat 010™ is produced by Danish Technological Institute (DTi) that has excellent repellent properties with low surface energy and smooth surface. The technology employed to produce this coating is called “Sol-Gel” technology, which is a method for the synthesis of glass ceramic-like coatings from liquid reagents. Although the thickness of such coatings is 5µm, it is both chemical and heat resistance.

Belzona Polymeric Ltd. produces and develops epoxy and resin-based coatings, such as:

- Belzona® 1341 has a very smooth, slick surface designed to improve fluid flow. It has a maximum wet heat resistance of 60°C, but may not be effective/appropriate at higher temperatures.
- Belzona® 1381 is a new erosion-corrosion resistant coating that does not wear spray equipment during application. It also benefits from a relatively low surface energy. This coating is suitable for wet immersion temperatures up to 95°C.
- Belzona® 1391 is a very popular Belzona high-temperature coating with an excellent reputation in the Oil & Gas industry. The maximum wet heat resistance is ~100°C.
- Belzona® 1541 is a developmental coating designed for ‘non-stick’ applications at elevated temperatures. The maximum wet heat resistance will be ~90°C.

- Belzona® 5891 is a two component coating system for corrosion protection of metallic surfaces, against attack from aqueous solutions operating at a temperature up to 90 °C.
- Belzona® 5892 is a two part epoxy coating for corrosion and chemical protection of high-temperature equipment operating under constant immersion up to 95°C.
- Both Belzona® 5891-exp and Belzona® 5892-exp coatings are experimental coatings that are the mixture of their corresponding resins with silicon carbide to amend the surface topography of the samples with the same surface chemical composition.

DuPont Company is known for the discovery of fluoropolymers. Fluoropolymers are defined as a polymer consisting of carbon (C) and fluorine (F), known for their non-stick properties (e.g. Teflon®). The fluoropolymer coatings employed in this study are as follows [116]:

- **Polytetrafluoroethylene (PTFE):** This is an example of a linear fluoropolymer with the chain of (CF₂-CF₂-) with strong bonds of C-C (607 KJ/mole) and C-F (552 KJ/mole). Furthermore, it has a low surface energy (18 dynes/cm) with the electrical inertness characteristic and relatively high melting point (320-342°C). It is also categorised as a *homopolymer*, a polymer made from a single monomer. By different applications and needs, different modifications have been applied to PTFE to reach to a certain level of chemical and thermal characteristics.
- **Fluorinated Ethylene Propylene (FEP):** It is categorised as a *copolymer*, a polymer made from other monomers. If instead of one of the fluorine atoms on tetrafluoroethylene, there is a trifluoromethyl group (-CF₃), then the new monomer would be called *hexafluoropropylene* (HFP) which encompasses five percent or less of the molecule. Depending on how much trifluoromethyl is added and the molecular weight, it has a lower melting point (274°C) comparing to PTFE. Worth to mention that, one of the main reasons for such occurrence is the decrease in crystallinity of 70% while PTFE is 98%.

- Ethylene-Tetrafluoroethylene (ETFE) Copolymers:** If the monomer contains other atoms such as chlorine or hydrogen instead of fluorine atoms then these polymers are categorised as partially fluorinated polymers (e.g. ETFE which is a copolymer of ethylene and tetrafluoroethylene). It has an excellent electrical and chemical resistance with excellent dielectric properties and non-stick characteristic. Its mechanical properties are superior to those of PTFE and FEP.

Table 3.5. The molecular structures of different fluoropolymers

Fluoropolymer	Molecular Structure
PTFE	$\left[\begin{array}{cccccccc} \text{F} & \text{F} \\ & & & & & & & \\ -\text{C} & -\text{C}- \\ & & & & & & & \\ \text{F} & \text{F} \end{array} \right]_n$
FEP	$\left[\begin{array}{cccccccc} \text{F} & \text{F} \\ & & & & & & & \\ -\text{C} & -\text{C}- \\ & & & & & & & \\ \text{F} & \text{F} & \text{F} & \text{F} & \text{F} & \text{CF}_3 & \text{F} & \text{F} \end{array} \right]_n$
ETFE	$\left[\begin{array}{cccccccc} \text{F} & \text{F} & \text{H} & \text{H} & \text{F} & \text{F} & \text{H} & \text{H} \\ & & & & & & & \\ -\text{C} & -\text{C}- \\ & & & & & & & \\ \text{F} & \text{F} & \text{H} & \text{H} & \text{F} & \text{F} & \text{H} & \text{H} \end{array} \right]_n$
PFA	$\left[\begin{array}{cccccccc} \text{F} & \text{F} \\ & & & & & & & \\ -\text{C} & -\text{C}- \\ & & & & & & & \\ \text{F} & \text{F} & \text{F} & \text{F} & \text{F} & \text{O} & \text{F} & \text{F} \end{array} \right]_n$ $\begin{array}{c} \text{F}-\text{C}-\text{F} \\ \\ \text{F}-\text{C}-\text{F} \\ \\ \text{F}-\text{C}-\text{F} \\ \\ \text{F} \end{array}$

- Perfluoroalkoxy (PFA) Polymers:** By making more changes to PTFE molecule by adding perfluoro alkoxy (typically as $-\text{O}-\text{CF}_2-\text{CF}_2-\text{CF}_3$) we would have PFA polymer. This polymer still retains its chemical resistance,

low surface energy and good electrical insulation properties, like other fully fluorinated polymers, but its melting point is between 305-310°C (as shown in Table 3.5).

For a better understanding about the fluoropolymers, the molecular structures of these fluoropolymers are shown in Table 3.5.

Both the fluoropolymer coatings named as “Black” and “One” are the new coatings that are in the development phase in DuPont’s R&D. Both of these coatings have an identical chemical composition with different topographical properties.

Diamond-Like Carbon (DLC) is an amorphous carbon coating comprising a network of sp^3 (diamond-like), sp^2 (graphite-like) and hydrogen bonds, and with regard to the mixture ratio of sp^2 and sp^3 , its physical and chemical properties would change. For instance, a significant fraction of sp^2 of DLC provides low friction properties similar to graphite, while the fraction of sp^3 provides tremendous mechanical properties like a diamond. DLC coatings are widely used in different industrial applications (e.g. aerospace, biomedical coatings, oil and gas industries, etc.) due to their exceptional characteristics such as: low friction properties, high wear resistance, high thermal and chemical stability, high corrosion resistance, high hardness, etc. [117]. There are various forms of DLC that can be processed by the phase ternary diagram as shown in Figure 3.1.

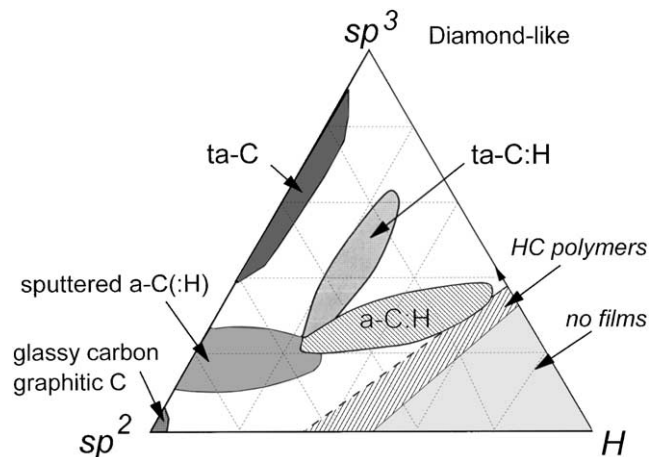


Figure 3.1. Ternary phase diagram of bonding in amorphous carbon-hydrogen alloys [117].

This type of coating is prepared by two different coating companies: Diamond Hard Surfaces (DHS) and Tecvac.

There are other types of ceramic coatings employed in this study, e.g. chromium nitride (CrN), titanium nitride (TiN), chromium nitride doped with silver (CrN-Ag), titanium nitride doped with aluminium (TiN-Al) are provided by Tecvac company. These types of ceramic coatings are hard and extremely resistant to corrosion which can be applied as a thin coating. As referred to the manufacturer, the CrN-Ag coating is made particularly for organic fouling, but its performance on inorganic fouling conditions has not been tested, yet.

3.4. Surface roughness measurements

Each component's surface according to its structure and the way it has been made has different forms of texture. These surfaces can be broken down into three main categories: Surface Roughness, Waviness and Form. In order to study the surface texture, it is necessary to quantify the surface characteristics.

Surface roughness, R_a , refers to the irregularity of the surface texture formed by peaks and valleys, and the quantity of R_a is referred to the arithmetic mean of the absolute departure of the roughness profile from the mean line and expressed as:

$$R_a = \frac{1}{l_m} \int_0^{l_m} |z(x)| dx \quad \text{Eq (3.1)}$$

Where the l_m is defined as the total measured length of the profile for the five consecutive sampling lengths.

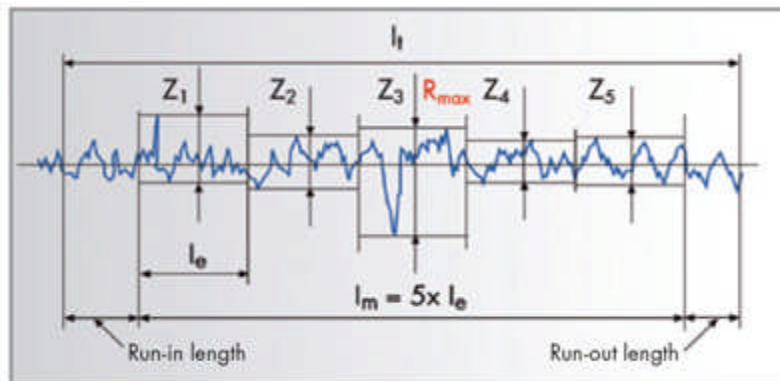


Figure 3.2. Evaluation of the surface roughness profile.

There are also three parameters to characterise the topography of the surfaces and are measured in this study, as follows:

- The surface skewness (R_{sk}) which measures the symmetry of peaks and valleys using the average line as the centre. The normal distribution or symmetrical about the average line is expressed as: $R_{sk}=0$. A negative skew indicates a predominance of valleys, while positive skew will be seen on surfaces with ample peaks (Figure 3.3a).

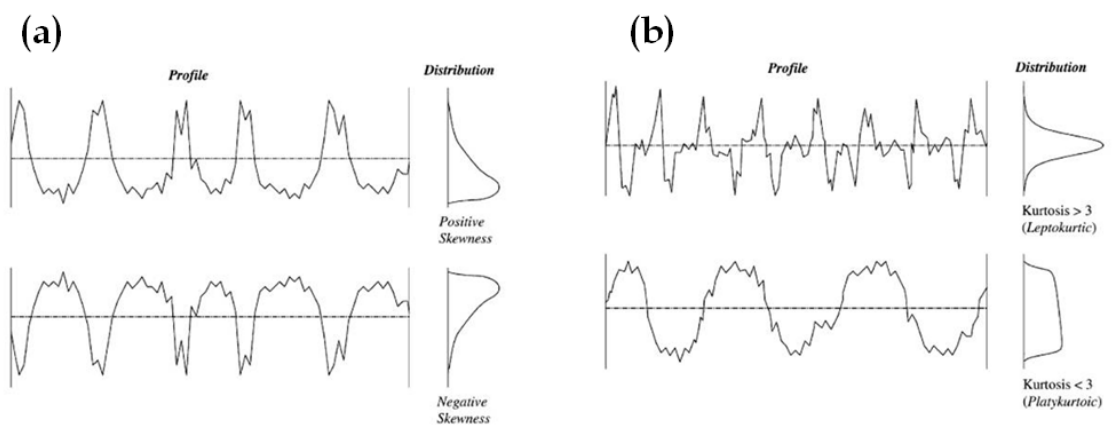


Figure 3.3. The distribution curve of the surface profile: (a) surface skewness and (b) surface kurtosis.

- The Kurtosis value (R_{ku}) is a measure of the distribution of the spikes above and below the mean line. It provides a measure of the sharpness of the surface profile. The normal distribution has the kurtosis value of 3. For kurtosis value of more than 3, the surface profile is considered as spiky, whereas for kurtosis value of less than 3, the surface profile is considered as not sharp(Figure 3.3b).
- RP_c is the peak count and is the number of local peaks in an assessment length. This value is normally denoted as peaks/cm (or per inch).

The surface roughness measurements of each substrate in this study are measured by the Taylor Hobson Talysurf stylus profilometer.

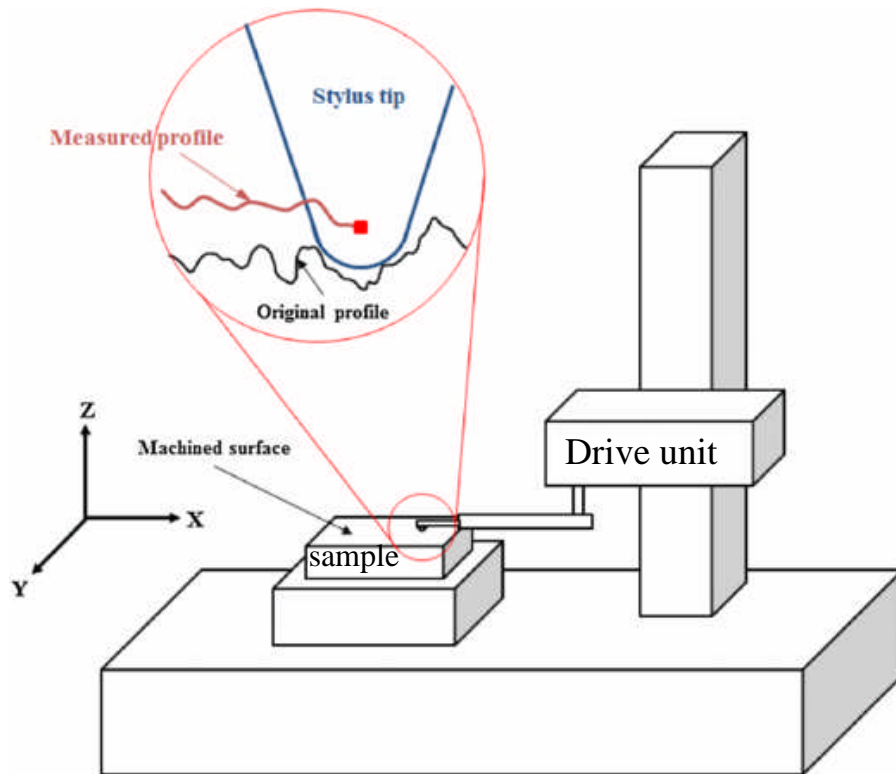


Figure 3.4. Illustration of the stylus profilometer sketch[118].

As shown in Figure 3.4, a profilometer is equipped with a diamond stylus tip that traverses onto the surface of the samples to characterise its topography. The transducer in the profilometer records the vertical and horizontal coordinates of the stylus tip. As a result, the obtained data is composed of a series of discrete coordinate pairs of (x,z) which can be post-processed and translated into the surface topography characterization of the analysed sample.

As shown in Table 3.6, the surface roughness of all modified surfaces used in the scaling tests are presented in the form of arithmetic mean of a line profile on a surface, “ R_a ”, the symmetry of the line profile on a surface, “ R_{sk} ”, the spikiness of the line profile on a surface, “ R_{ku} ” and the number of peaks in one centimetre, “ R_{pc} ”.

As shown in Table 3.6, the surface roughness of the ceramics coatings is relatively lower compared to the other modified surfaces, while the fluoropolymer and epoxies are rougher. The level of the skewness, kurtosis value and the number of the peaks of the surfaces cannot be categorised according to their coatings types, i.e. chemical composition.

The lowest (B1341) and highest (DHS) kurtosis value measured by the Talysurf for the modified surfaces are shown in Figure 3.5.

Table 3.6. The surface roughness for all the substrates used in the scaling tests, presented in the form of R_a , R_{sk} , R_{ku} , and R_{pc} .

No.	Coating	R_a (μm)	R_{sk}	R_{ku}	$R_{pc}(\text{peaks.cm}^{-1})$
1	B1341	0.546 ± 0.256	0.193	2.120	20.54 ± 6.48
2	B1381	1.032 ± 0.458	-0.128	6.124	44.43 ± 4.53
3	B1391	1.590 ± 0.639	0.717	3.618	102.22 ± 12.60
4	B1541	0.897 ± 0.373	0.987	4.703	108.82 ± 29.47
5	B5891	0.840 ± 0.364	-0.864	4.254	244.46 ± 3.91
6	B5891xp	4.807 ± 1.929	0.944	5.067	40.95 ± 4.85
7	B5892	0.219 ± 0.095	0.136	3.422	44.95 ± 9.86
8	B5892xp	2.971 ± 1.403	1.405	6.050	20.00 ± 2.97
9	Black	1.258 ± 0.509	0.203	3.278	81.97 ± 2.38
10	CrN	0.119 ± 0.048	-1.211	7.943	121.16 ± 10.64
11	CrN-Ag	0.126 ± 0.048	2.346	35.714	174.60 ± 14.75
12	DHS	0.231 ± 0.100	5.754	42.161	181.46 ± 7.39
13	DLC	0.141 ± 0.054	-0.268	7.538	110.30 ± 6.84
14	Dti	0.063 ± 0.025	-0.248	2.618	46.90 ± 4.63
15	ETFE	1.697 ± 0.645	-0.027	2.275	34.72 ± 11.68
16	FEP	0.420 ± 0.169	0.152	2.977	44.10 ± 8.73
17	One	3.603 ± 0.098	-0.480	3.122	75.03 ± 6.60
18	PFA	1.010 ± 0.418	-0.211	3.059	39.28 ± 9.58
19	PTFE	0.890 ± 0.337	-0.515	3.047	52.54 ± 7.70
20	SS316	0.080 ± 0.030	-0.246	3.877	107.74 ± 10.75
21	SS416	0.135 ± 0.060	-0.223	5.625	165.56 ± 18.39
22	TiN-Al	0.160 ± 0.060	1.946	20.701	116.18 ± 12.68
23	TiN	0.148 ± 0.055	-0.225	3.355	91.42 ± 16.68

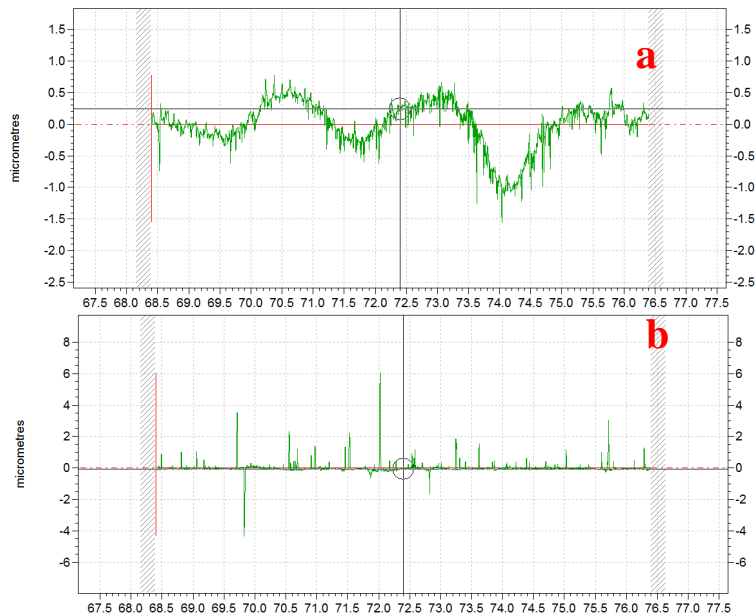


Figure 3.5. Kurtosis value for two modified surfaces: (a) B1341 and (b) DHS.

The surface roughness of each modified substrates along with the number of peaks per a specific distance (e.g. centimetre) is shown in Figure 3.6. The number of peaks shows the number of nucleation sites on the surface that play a major role in the heterogeneous nucleation, which is independent of the surface roughness as shown in Figure 3.6.

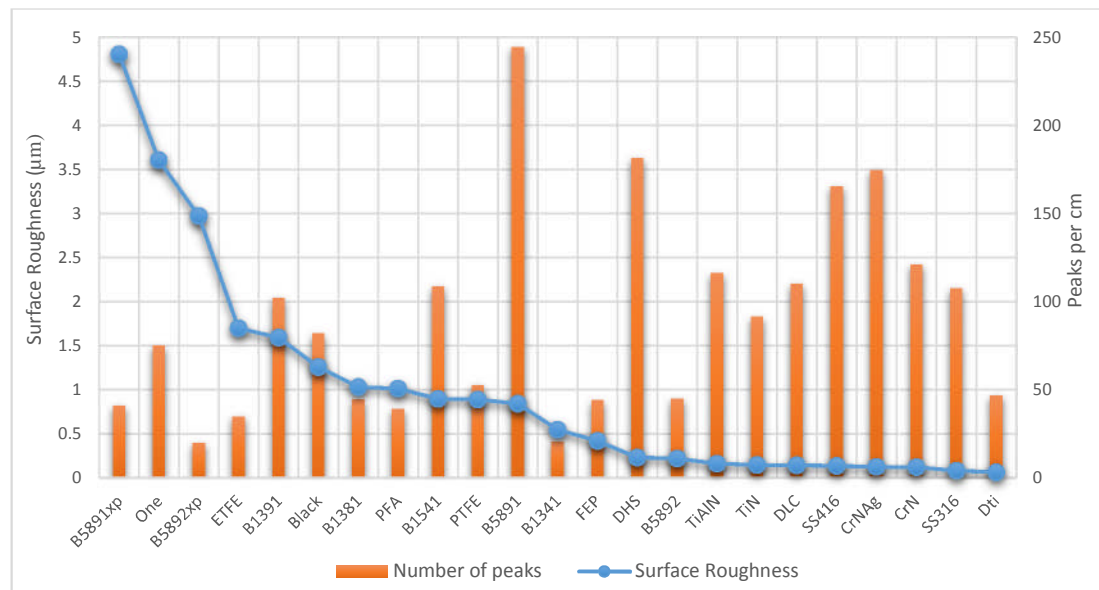


Figure 3.6. The surface roughness along with the number of peaks per centimetre of each modified substrate.

3.5. Surface energy measurements

The surface energy of a solid surface can be associated with the contact angle or wettability behaviour of the surface. The chemical composition and the roughness of the solid surface affect the wettability behaviour of the surface[119]. Calculations based on the contact angle measurements produce the solid surface tension, i.e. quantifies the wetting characteristics of the solid surface material.

The contact angle is defined as an angle formed onto the solid surface between the intersection of the liquid/gas interface and the liquid/solid interface, as shown in Figure 3.7.

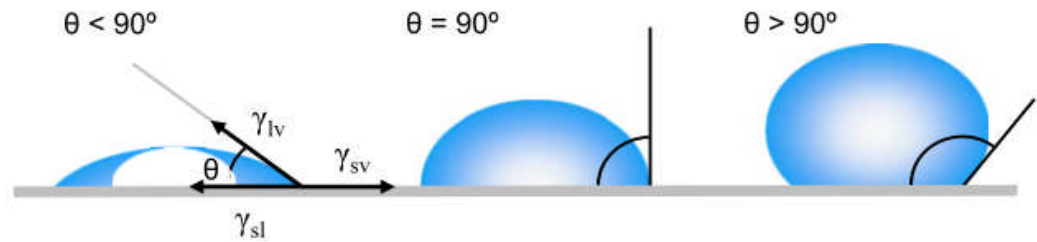


Figure 3.7. Illustration of contact angle formed by a sessile liquid drop on a smooth homogeneous solid surface[120].

Contact angle measurements of each substrate were performed by the sessile drop method which measures the contact angle of a series of liquid probes on the solid substrate.

As shown in Figure 3.8, the sessile drop image is captured with the camera and the angle is measured with the help of a goniometer.

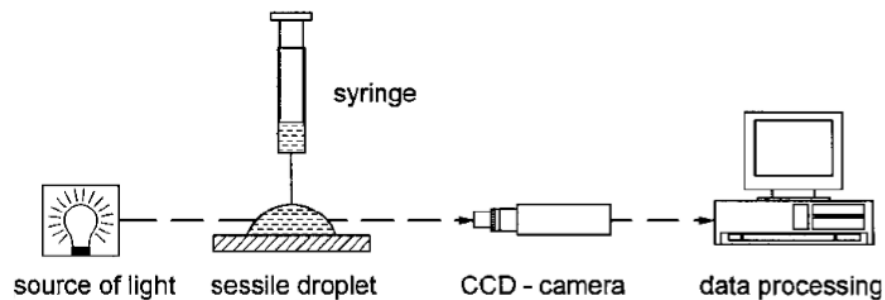


Figure 3.8. Illustration of a contact angle measurement using sessile drop technique [121].

Typical results obtained from the contact angle measurement tests for the most hydrophobic coating (DuPont-One) with the highest contact angle value and the most hydrophilic coating (Belzona 5891) is shown in Figure 3.9.

The contact angle measurement tests are performed in an open air condition at a room temperature of 20°C, a relative humidity of approximately 40%. The liquid probes used are ultrapure water (18 MV), diiodomethane, and ethylene glycol; and their corresponding surface tension components are shown in Table 3.7.

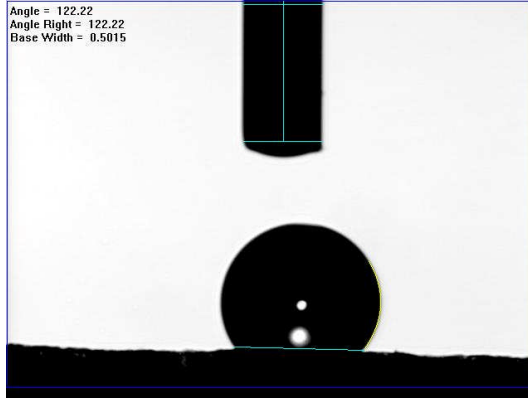


Figure 3.24a - One

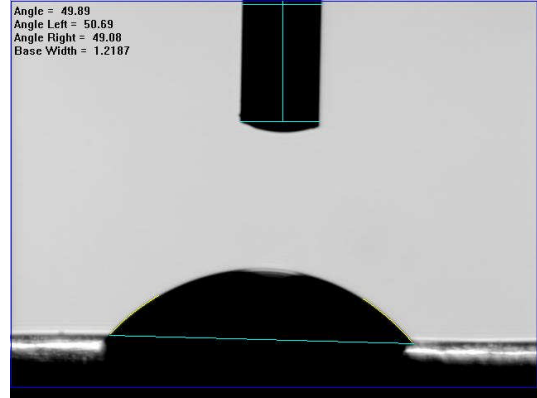


Figure 3.24b – B5891

Figure 3.9. Typical results obtained from the contact angle measurement tests using the sessile drop technique for (a) the most hydrophobic coating and (b) the most hydrophilic.

The dispersive and polar components of surface energy calculations are based on a two-component model for solid surface energy referred as Fowkes theory [70], as follows:

$$\gamma_i(1 + \cos\theta_i) = 2 \left(\sqrt{\gamma_i^d \gamma_s^d} + \sqrt{\gamma_i^p \gamma_s^p} \right) \quad i = 1, 2 \quad \text{Eq (3.2)}$$

$$\gamma_s = \gamma_s^d + \gamma_s^p$$

$$\gamma_i = \gamma_i^d + \gamma_i^p \quad i = 1, 2$$

Where θ_i is contact angle of testing drop, γ_i^d and γ_i^p are dispersion and polar energy of testing drop i , and γ_s^d and γ_s^p are dispersion and polar energy of testing surface.

Table 3.7. Surface tension (mN/m) components of liquid probes [122].

Liquid	Total (mN/m or mJ/m ²)	Dispersive	Polar	Acid	Base
Water	72.8	21.8	51.0	25.5	25.5
Diiodomethane	50.8	50.8	0.0	0.0	0.0
Ethylene Glycol	48.0	29.0	19.0	3.0	30.1

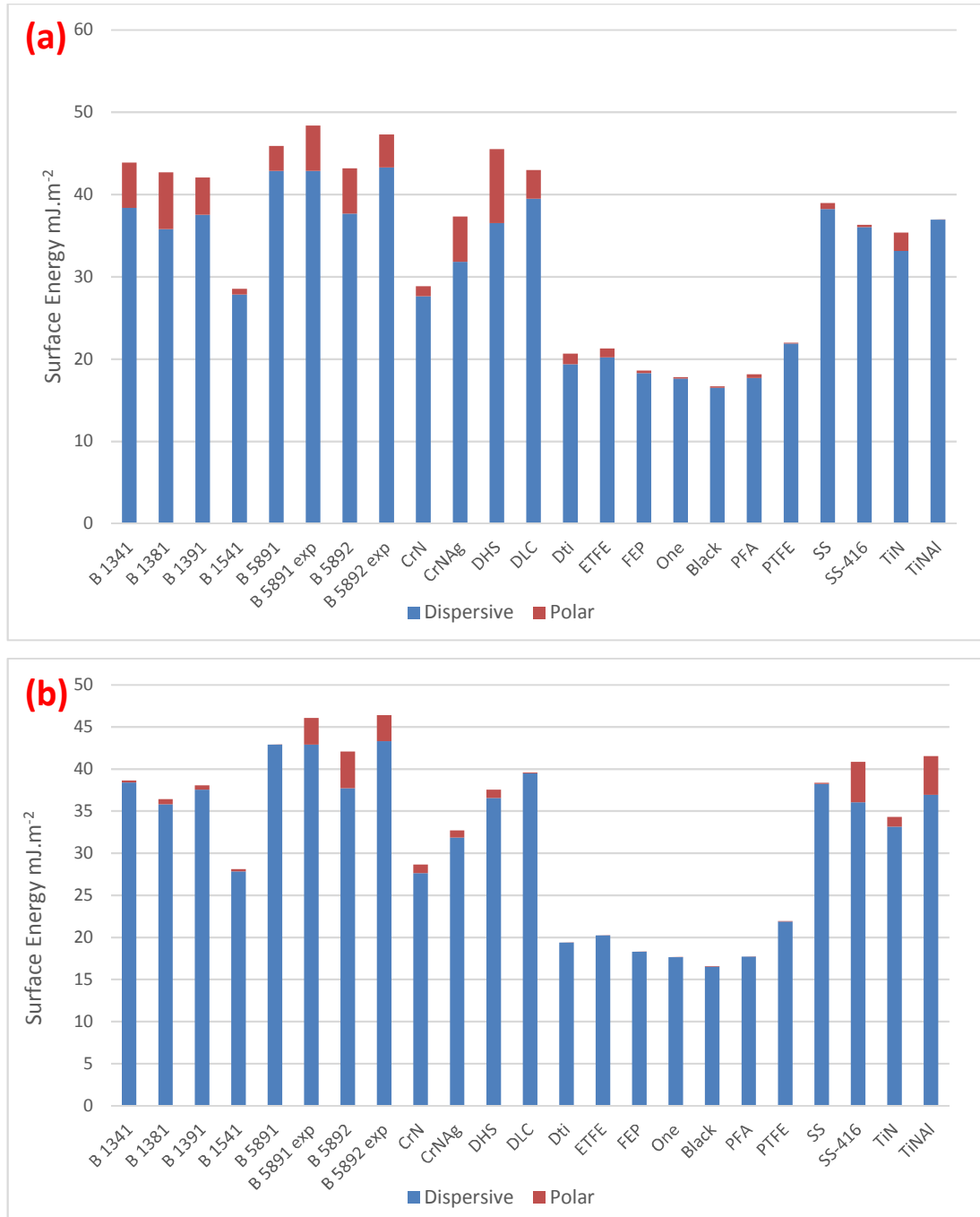


Figure 3.10. The surface energy of modified surfaces along with their polar and dispersive components with two sets of liquid probes: (a) diiodomethane and water and (b) diiodomethane and ethylene glycol.

The surface energy of each modified substrates along with their dispersive and polar components for different sets of liquid probes are shown in Figure 3.10. The sets of results with different liquid probes have been selected due to the fact there is no universal protocol to take the surface energy measurements. As a result, one fully dispersive (e.g. diiodomethane) and two polar (e.g. water and ethylene glycol) liquid probes have been chosen to compare the results together. Therefore, the dispersive

component of both sets are similar and the only difference is the polar component of the surface energy (see Figure 3.10). As a result, the interpretation of the surface energy results would be highly dependent on the nature of the liquid probes.

3.6. Dynamic scale deposition tests

The scaling process depends on parameters such as pressure, temperature and fluid flow. The latter two conditions can be adjusted in the lab equipment using the Rotating Cylinder Electrode (RCE) apparatus. The RCE equipment consists of an electrode rotator and a control unit which can control the rotational speed of the electrode in the vessel. The coupon is mounted on the tip of the shaft between two Teflon based rings which are chemically and electrically inert. The sample used in the static batch jar test is cylindrical with the diameter of 12mm and the height of 10mm, as shown in Figure 3.11.

The RCE is ideal to simulate turbulent conditions at a low velocity around the vertically positioned shaft, i.e. the sample. By adjusting the rotational speed of the shaft the hydrodynamic conditions around the sample can be replicated. The main aim of using the RCE is to match the laboratory fluid flow conditions to those found in the field.

At low rotational speed, the flow conditions of the brine solution around the sample are called laminar flow. As the rotational speed increases, the flow conditions of the brine solution around the shaft become more complex. The shear stress at the vicinity of the surface induces vortices to spin off from the surface to the brine solutions. At this point, the flow conditions are called transitional from the laminar conditions to turbulent conditions. As the rotational speed increases more, the formed vortices themselves create more vortices and the flow conditions become quite chaotic which is called turbulent conditions.

Reynolds number is a dimensionless quantity which expresses the flow regime. This quantity is the ratio of inertial forces to viscous forces. In such setup, the Reynolds number will be calculated to determine the shear stress at the vicinity of the surface. Reynolds number of the rotating cylinder electrode with outer diameter, d_{cyl} (cm), can be computed as:

$$Re = U_{cyl} \cdot d_{cyl} \cdot \rho / \mu \quad \text{Eq (3.3)}$$

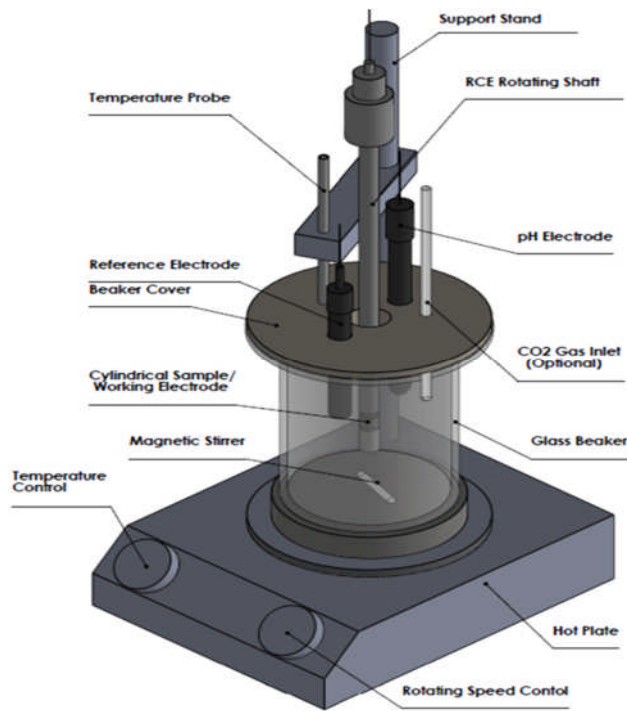


Figure 3.11a. Illustration of Rotating Cylinder Electrode (RCE) and its components.

Figure 3.11b. RCE tip; the coated sample is positioned in between of Teflon rings.

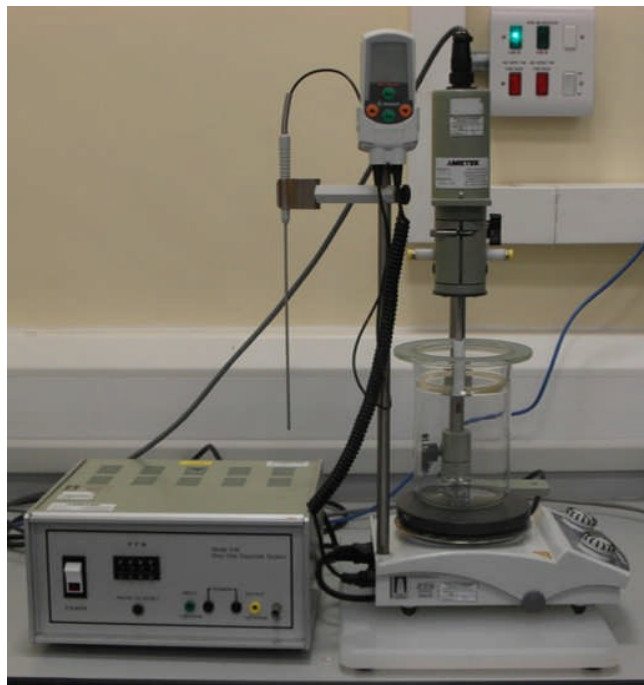


Figure 3.11c. RCE experimental setup; variable rotational speed of the RCE can be set by a control unit; the RCE tip is immersed into a 1L vessel at 56°C.

Figure 3.11. Rotating Cylinder Electrode (RCE) components and its experimental setup.

where, U_{cyl} (cm.s^{-1}) is the linear velocity, ρ is the solution density (g.cm^{-3}) and μ is the viscosity of the solution ($\text{gr.cm}^{-1}.\text{s}^{-1}$). The linear velocity at the outer diameter (i.e. surface velocity) can be calculated as:

$$U_{cyl} = \pi \cdot d_{cyl} \cdot F / 60 \quad \text{Eq (3.4)}$$

where, F is expressed by rpm.

Hydrodynamic conditions can be predetermined using the RCE at different rotational velocities to have turbulent flows. Consequently different shear stresses at the vicinity of the surface. The shear stress on the cylinder surface can be calculated as follows[123]:

$$\tau_{cyl} = 0.0791 \rho Re^{-0.3} U_{cyl}^2 \quad \text{Eq (3.5)}$$

where, τ_{cyl} is the shear stress ($\text{g.cm}^{-1}.\text{s}^{-2}$) at the vicinity of the surface. The unit of shear stress is normally expressed as Pascal, so:

$$1Pa = 1 \frac{N}{m^2} = 1 \frac{kg}{m.s^2} = 10 \frac{g}{cm.s^2} \quad \text{Eq (3.6)}$$

The sample was rotating in the brine at two rotational speeds: (a) 2000 rpm ($Re \sim 17,800$) which represents the fully turbulent flow regime and (b) 20 rpm ($Re \sim 178$) which represents the laminar flow regime for 90 minutes. The test results are then calculated as shown in Table 3.8.

Table 3.8. Hydrodynamic conditions of RCE test cases

Rotational Speed F (rpm)	Surface Velocity U_{cyl} (cm/sec)	Reynolds Number	Surface Shear Stress, τ_{cyl} (Pa)
2000	125.6	17845	7.851
20	1.256	178	0.003

3.7. Surface scale deposition tests

The surfaces have been tested using a bulk jar test where precipitation occurred at 56°C and at atmospheric pressure. Two scenarios are designed to perform the dynamic scale tests, as follows:

- In scenario-1 (or *adhesion* process), the sample was immersed in the batch vessel, where the crystals are already formed into the mixed brine. The mixed brine is kept at 56°C for 90 minutes which is enough time for the system to equilibrate. This test measures how the presences of pre-formed crystals from the turbid solution form on the surface. It assumes that adhesion dominates and deposition is minimal.
- In scenario-2 (or *deposition* process), as soon as the anions and cations are mixed, the sample is immersed in the brine for 90 minutes. As such, there is a high driving force for heterogeneous nucleation which can occur at the surface asperities. The deposition can occur by the growth of scale at these asperities. So the sample would be in the beaker during the crystallisation.

After each test, the sample was rinsed with distilled water and dried by compressed air and put in an oven. Repeated measurements have shown the ability of the polymer coatings to uptake liquid within themselves after the tests. McKeen [116] has reported that the water absorption of fluoropolymer, such as FEP, PFA and ETFE within 24 hours are around 0.01%, 0.03% and 0.03% by weight, respectively. In order to obtain the scaling tendency, the samples were weighed before and after an experiment with a mass balance having a resolution of 0.001mg in a controlled condition room with the temperature of 21°C and the relative humidity of 42%. Typically, two coupons were tested for each type of surface but in the cases where the results were different, a third coupon to experiment was done for each surface.

In an oilfield, as shown in Figure 3.12, the process of scale formation on the surface is different from one region to another. For instance, the type of scale formation down in the wellbore is different from the formed scale on the surface of valves and pipe applications on the ground level. The main reason is due to the time that it takes for

the bulk (or brine solution) to reach from the downhole to the ground level. Normally, in the downhole areas there are no particles formed in the brine solution and the process of scale formation dominantly occurs as heterogeneous nucleation and crystal growth on the surface (region-A in Figure 3.12); while at the ground level, due to the time interval, the crystals are already formed in the bulk and the process of scale formation is dominantly occurs as the adhesion of the so-called pre-precipitated crystals on the surface (region-B in Figure 3.12).

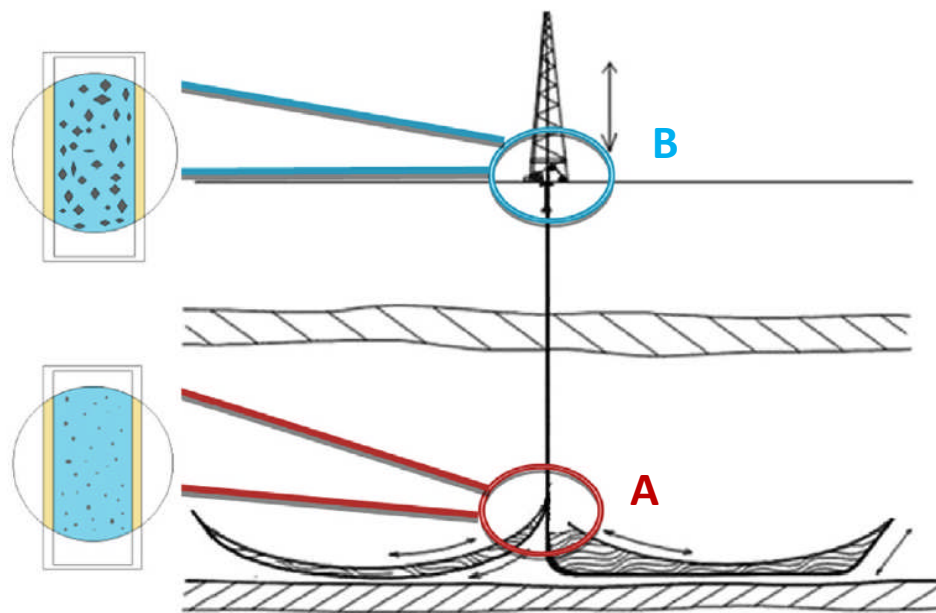


Figure 3.12. Schematic of scale formation in different regions of an oilfield: region A: heterogeneous nucleation and crystal growth, and region B: adhesion of particles to the surface [124].

To replicate these conditions in the laboratory we have proposed two different scenarios, as scenario-1 (or *adhesion* process) and scenario-2 (or *deposition* process).

3.7.1. Limitations of surface scaling tests

The following limitations can be addressed in the methodology that has been used in this study:

- Using the standard bulk jar test to assess the surface scaling tendency has its own advantages such as simulating the flow conditions with high precision, however it has some drawbacks at some points. Controlling the parameters in such methodology where another phase is present (e.g. oil) is not quite

straightforward. In order to maintain a homogeneous brine solution, another propeller needs to be used that will disturb the main flow stream which result in less control over the flow conditions at the vicinity of the surface.

- During the surface scale test, a fraction of scale deposits form on the wall of the beaker that at some point will affect the rate of surface scaling, however such effect is the same for all the tested modified surfaces.
- The brine solution is saturated with CO₂ to maintain the condition of the test throughout the whole process and remove the oxygen ions from the brine solution. In order to improve such methodology, the addition of NaOH to the brine solution to preserve the level of the pH is advisable.

3.8. Turbidity meter

Turbidity is caused by suspended particles such as sludge, limestone, yeast or microorganisms. The level of the turbidity is associated with the level of cloudiness of the water solution. Turbidity does not measure the suspended substances in a sample but instead, measure the scattering effect of such particles on the light. In other words, the results obtained from the turbidity meter is the ratio between the scattered light and the transmitted light, and the difference between these two values is in proportion to the concentration of suspended substances in the sample, as shown in Figure 3.13.

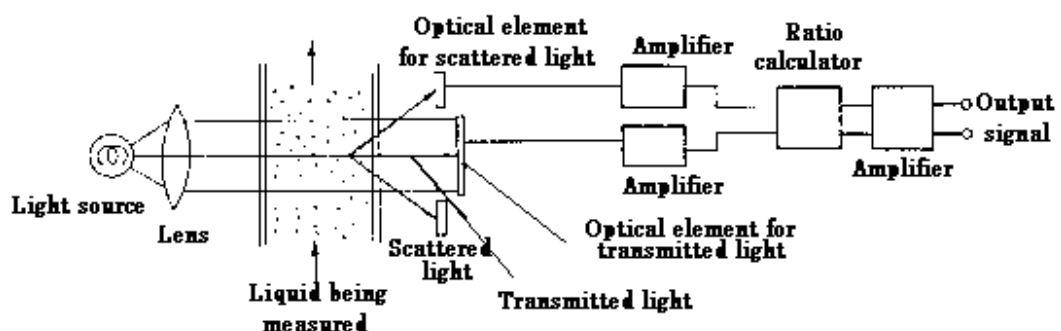


Figure 3.13. Illustration of turbidity measurement using the light scattering technique [125].

A Hach DR/890 Colorimeter was used to measure the turbidity of the scaling solution once the Brine-1 and Brine-2 were mixed. The calorimeter acts by measuring the reduction of light as it passes through the sample column of water and shows the results as Formazin Turbidity Unit (FTU).

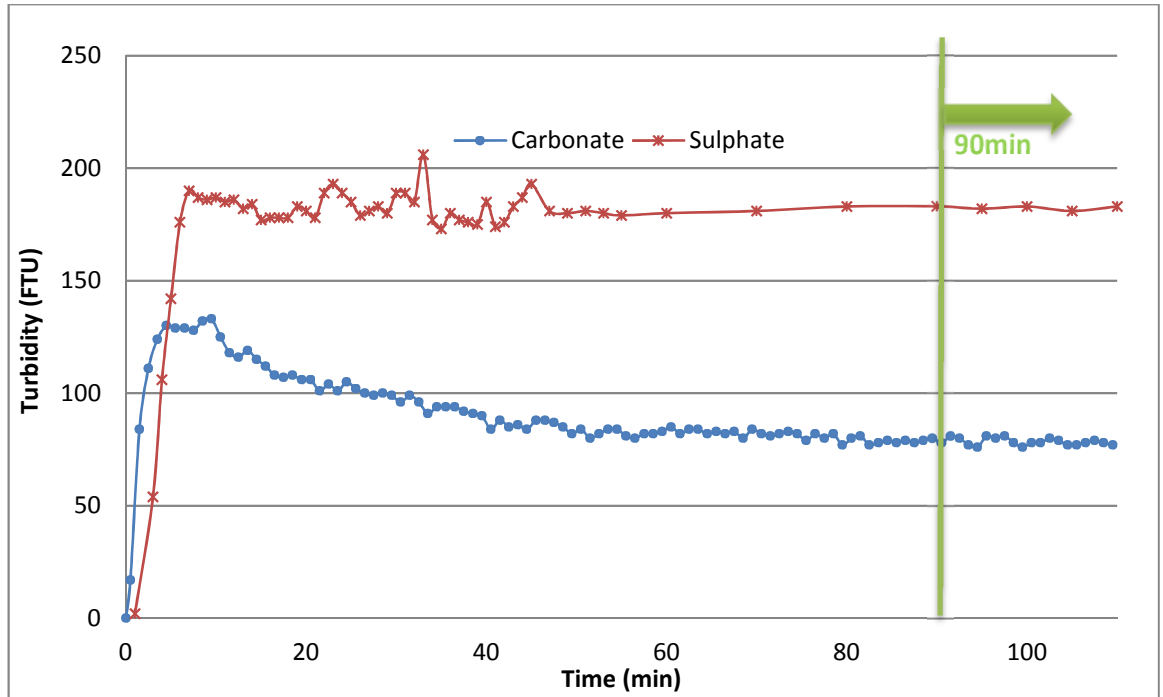


Figure 3.14. Turbidity measurement of the brine solutions for both the carbonate-dominated (blue dots) and sulphate-dominated (red crosses) brines. “Deposition” process starts at 0 min and “Adhesion” process starts at 90 min.

The induction time for such a solution is so fast due to the high supersaturation index that can be neglected. The turbidity increases rapidly in the first 10 minutes, and after some fluctuations, it is stable.

As shown in Figure-1, the “deposition” test starts from minute “0”; and the “adhesion” test starts from minute “90” where the speed of the crystallisation is in balance with the dissolution rate of the particles in the brine solution. The turbidity as a function of time of both solutions is plotted in Figure 3.14. The measurements have been done for 110 minutes as the brine 1 and brine 2 are mixed together. The behaviour of the carbonate-dominated brine is different from the sulphate-dominated brine. In the carbonate-dominated brine, the cloudiness of the brine reaches a certain level and then it decays by time until it reaches a certain amount, while in the sulphate-dominated brine, the turbidity reaches to a certain level and then it remains stable.

3.9. Scanning Electron Microscopy (SEM)

As part of the qualitative assessment, Scanning Electron Microscopy (SEM) has been applied to study the morphology of the crystals and the way that they are formed on the surfaces. The SEM Carl Zeiss EVO MA15 and Hitachi TM3030 Bench Top SEM

were used after the scaling tendency tests to capture images revealing details less than 1nm in size. The majority of the SEM images taken are from signals produced by secondary electrons (SE) and a few of them are from the back-scattered electrons (BSE). The signals result from interactions of the electron beam (around 20keV) with atoms at a different depth within the sample. Signals from the SE are electron emitted from the vicinity of the sample surface, while the signals from the BSE are beam electron that is reflected from the sample. The schematic of the SEM is shown in Figure 3.15.

The specimen surface needs to be electrically conductive and electrically grounded to prevent electrostatic overcharge at the surface. In order to prevent any fault scanning in SEM image for the nonconductive specimens (e.g. epoxy and fluoropolymer coatings), the specimens were coated with ultrathin conductive materials (e.g. gold or platinum) using the low vacuum sputter coating technique.

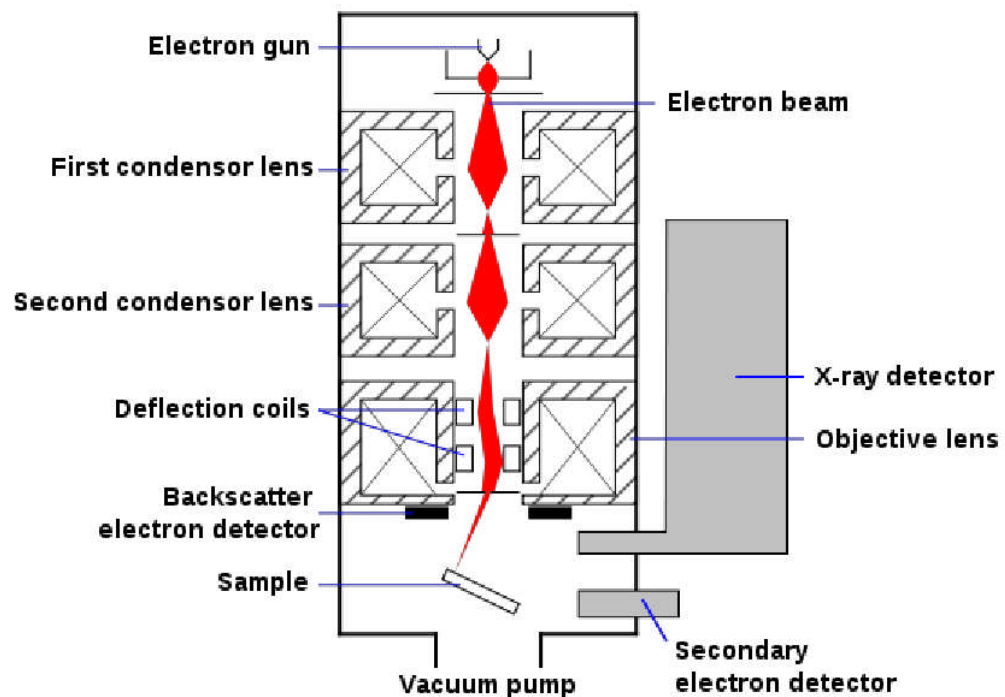


Figure 3.15. Schematic diagram of SEM.

The elemental analysis or chemical characterization of the scale deposits on the surface has been done by Energy Dispersive X-ray spectroscopy (EDX) technique (Oxford instrument Aztec Energy EDX) coupled by Carl Zeiss EVO MA15 SEM. In this technique, a high energy beam of charged particles strikes the specimen to stimulate the emission of characteristic X-ray from the specimen. The number and

energy of the X-ray emitted from the specimen will be measured to calculate the elemental composition of the specimen.

3.10. Inductively Coupled Plasma (ICP)

To understand more about the chemical composition of the deposited crystals on the surface, the Inductively Coupled Plasma Atomic Emission Spectroscopy (ICP-AES) spectroscopy technique is employed to measure the relative amount of calcium, barium and strontium by either mass or mole percentage by dissolving the deposited scale formed on the surface of the coatings.

ICP-AES is a multi-element analysis technique that uses inductively coupled plasma, normally uses ionised argon at high temperature as a source, to stimulate atoms and ions of the sample to emit electromagnetic radiation at wavelength characteristics of a particular element. The emitted light is separated into different wavelengths that the specific wavelength of interest can be detected by a monochromator and its intensity by a detector. The data is then used to calculate the concentration of that element of interest.

Chapter 4

Results of Carbonate-dominated Brine

4.1. Introduction

In many industrial systems, scale formation causes significant problems, mainly relating to the process efficiency in the oil and gas industry, where fouling by mineral scaling can cause problems relating to the flow assurance. Carbonate scale deposition (mainly formed as CaCO_3 and SrCO_3) on the surfaces is one of the most common scale types which can impair the oil production by blockage of pipelines and tubing, fouling equipment and concealment of corrosion. Therefore, understanding the mechanism and rates of scale deposition (i.e. where and how much carbonate scale deposited) is vital to predict and manage the potential scale deposition. This knowledge would facilitate the design of more effective treatment of carbonate scale as well as minimise the scale deposition tendency during the oilfield production.

The origin of scale is often complicated. It can be from crystals pre-precipitated in the bulk solutions or can be from crystallisation on a solid surface. The mechanisms need to be understood to properly manage scale problems. Conventionally scale studies have involved the evaluation of bulk scaling which describes the process of scale formation in a solution, referred to as precipitation; while scale deposition, or formation of scale at a surface, has received much less attention.

One of the main difficulties in anticipating the process of scale deposition is that there are so many factors influencing the scale formation in the bulk and on the surface:

- **Bulk solution parameters.** The factors could be the operating conditions of the bulk solution such as the hydrodynamics of the flow, solution composition, pH, temperature, dissolved and suspended impurities, the presence of gas bubbles, and CO_2 content in water.
- **Surface parameters.** The surface parameters such as surface roughness, surface energy, and surface chemical composition can affect the rate of surface scale formation.

Surface scale formation would be affected by a combination of both bulk solution and surface parameters which make the prediction of scale formation on the surfaces difficult [124].

Zhang et al. [126] reported that in a gas lift well, the carbonate scale thickness found at the gas entry point in the downhole is at its highest rate and gradually decreases. Therefore, in this chapter, the results of two surface deposition processes, i.e. as “adhesion process” and “heterogeneous nucleation and crystal growth process”, of carbonate-dominated brine on different commercially-available modified surfaces are assessed. The amount of scale mass gain deposited on the modified surfaces was recorded in two scenarios.

The polymorphs, size and shape of crystals formed on the surface were observed by Scanning Electron Microscope (SEM) and the elemental composition of the scale deposits are studied by Energy Dispersive X-rays spectroscopy (EDX). The existence of ions in the scale deposits on the surfaces is also studied by the Inductively Coupled Plasma (ICP) by dissolving the scale deposits on the surface. In addition, the effect of the surface energy and surface roughness on both processes has been studied.

4.2. Surface scale *deposition* of carbonate-dominated brine

As shown in Figure 4.1, different modified substrates are subjected to 2-hour surface scale deposition experiments in laminar and turbulent flow conditions, respectively. It can be concluded from the results that the ceramic coatings (e.g. TiN, CrN, DLC, DHS and TiAlN) along with the stainless steel 316 and 416 have generally the best performance amongst other coatings in both laminar and turbulent conditions, although in turbulent conditions some epoxies have shown promising results (e.g. B1381 and B1341). Surprisingly, the fluoropolymer coatings with relatively lower surface energy have higher scaling tendency compared to other types of coatings. Charpentier et al. [127] have reported that modified surfaces such as fluoropolymer coatings with low surface energy do not have necessarily good anti-scaling performance.

By comparing the performance of the modified surfaces with reference materials (Stainless Steel 316 or 416), it would raise one question as what is the use of surface engineering and the application of modified surfaces. It should be noted that using such stainless steel samples with such a high-quality surface finish is not normally used in industry, and if it is used the cost would be so high.

As shown in Figure 4.1, the measured mass gain values for a unit of area on the modified surfaces in laminar flow regime conditions ranges from 0.125 mg/cm² (TiN)

to 0.546 mg/cm² (B5891-Exp), while in the turbulent flow regime the mass gain values for a unit of area ranges from 0.231 mg/cm² (SS-316) to 0.800 mg/cm² (FEP). It is evident from the results that flow regime can change the anti-scaling performance of the modified surfaces.

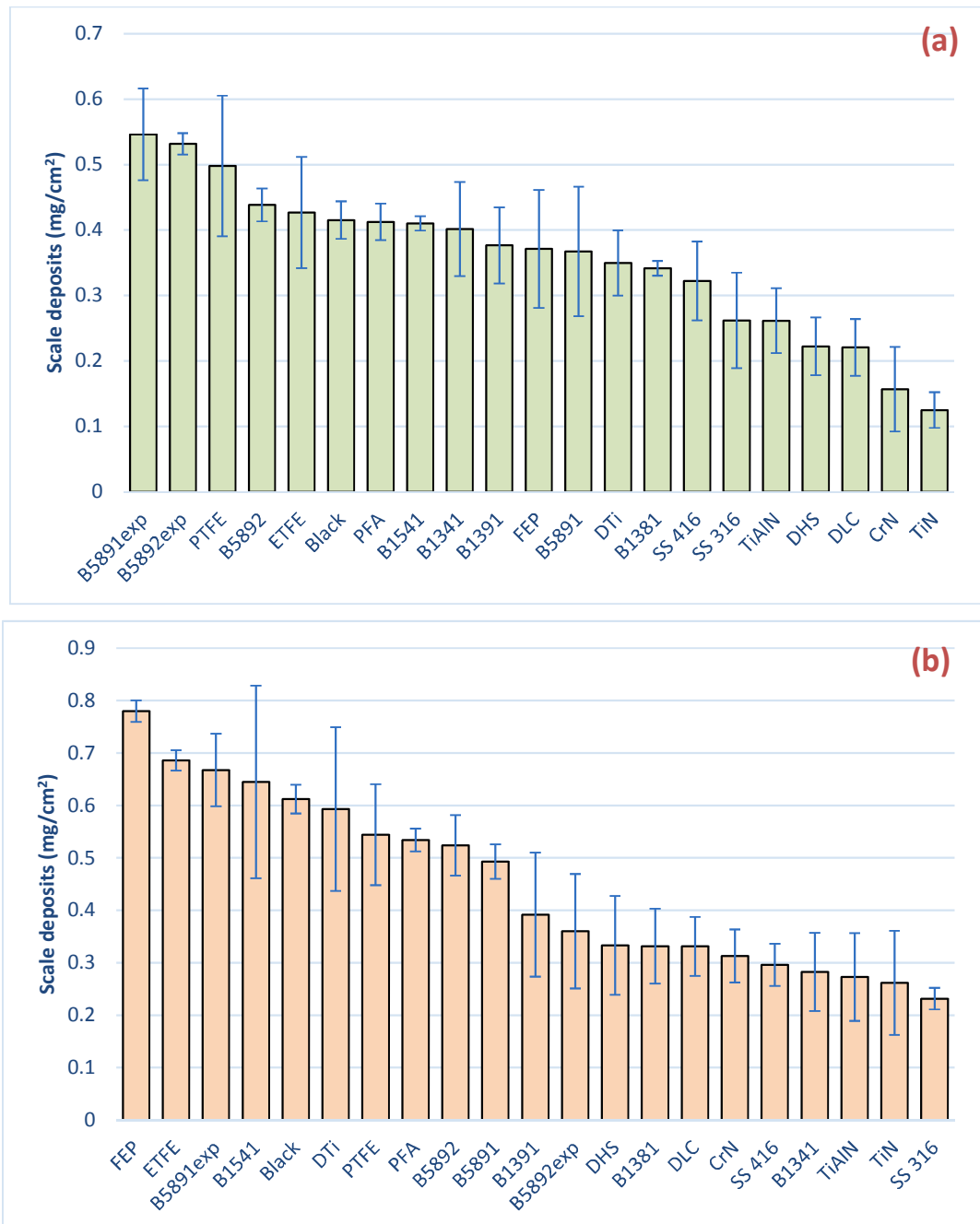


Figure 4.1. Mass gain of modified surfaces in the *deposition* process in (a) laminar flow regime, (b) turbulent flow regime.

In order to show the scaling tendency of each modified substrate to a better indicator, the results are interpreted as the scale deposits thickness increase in a year, provided that the scale deposits are fully dense.

Based on the ICP and SEM results, it has been assumed that the scale deposits are made of the mixture of 10% of SrCO_3 (with density of 3.5 g.cm^{-3}) and 90% of CaCO_3 where the morphologies of the formed crystals of the calcium carbonate is half calcite (with density of 2.71 g.cm^{-3}) and half aragonite (with density of 2.83 g.cm^{-3}). As a result, the density of the scale formed on the surface is around 2.843 g.cm^{-3} , provided that the deposited scale is fully dense. As a result, the highest scaling tendency in a year is in a range of 0.192 (TiN) to 0.841 (B5891exp) cm.year^{-1} and 0.357 (SS 316) to 1.202 (FEP) cm.year^{-1} in laminar and turbulent flow regimes, respectively. In short, each value of the mass gain per area can be multiplied by 0.65 to get the value as the growth rate of scale deposits on the surface in cm.year^{-1} .

4.3. Surface scale *adhesion* of carbonate-dominated brine

The mass gain results of different modified substrates per unit area for the adhesion tests are shown in Figure 4.2.

In the surface adhesion scaling tendency test, the brines were mixed together and after two hours the substrates were immersed in the brine solution for two hours. These experiments have been conducted for both laminar and turbulent flow regimes.

Like the surface *deposition* results, the performance of the ceramic coatings along with the stainless steel 316 and 416 in the carbonate-dominated brine is better compared to the epoxies and fluoropolymer coatings in both laminar and turbulent flow regimes.

The measured mass gain values for a unit of area on the modified surfaces in laminar flow regime conditions ranges from 0.110 mg/cm^2 (SS 316) to 0.430 mg/cm^2 (PFA), while in the turbulent flow regime the mass gain values for a unit of area ranges from 0.029 mg/cm^2 (DLC) to 0.334 mg/cm^2 (Black).

As explained in the surface scale *deposition* section, assuming the scale deposits formed on the surface in the adhesion process is fully dense, the annual rate of scale formation on different modified surfaces can be converted to surface scale growth by multiplying the mass gain in mg/cm^2 to 0.65. The results of the scaling tendency in a

year will be in a range of 0.169 (SS 316) to 0.663 (PFA) $\text{cm}\cdot\text{year}^{-1}$ and 0.045 (SS 316) to 0.514 (Black) $\text{cm}\cdot\text{year}^{-1}$ in laminar and turbulent flow regimes, respectively.

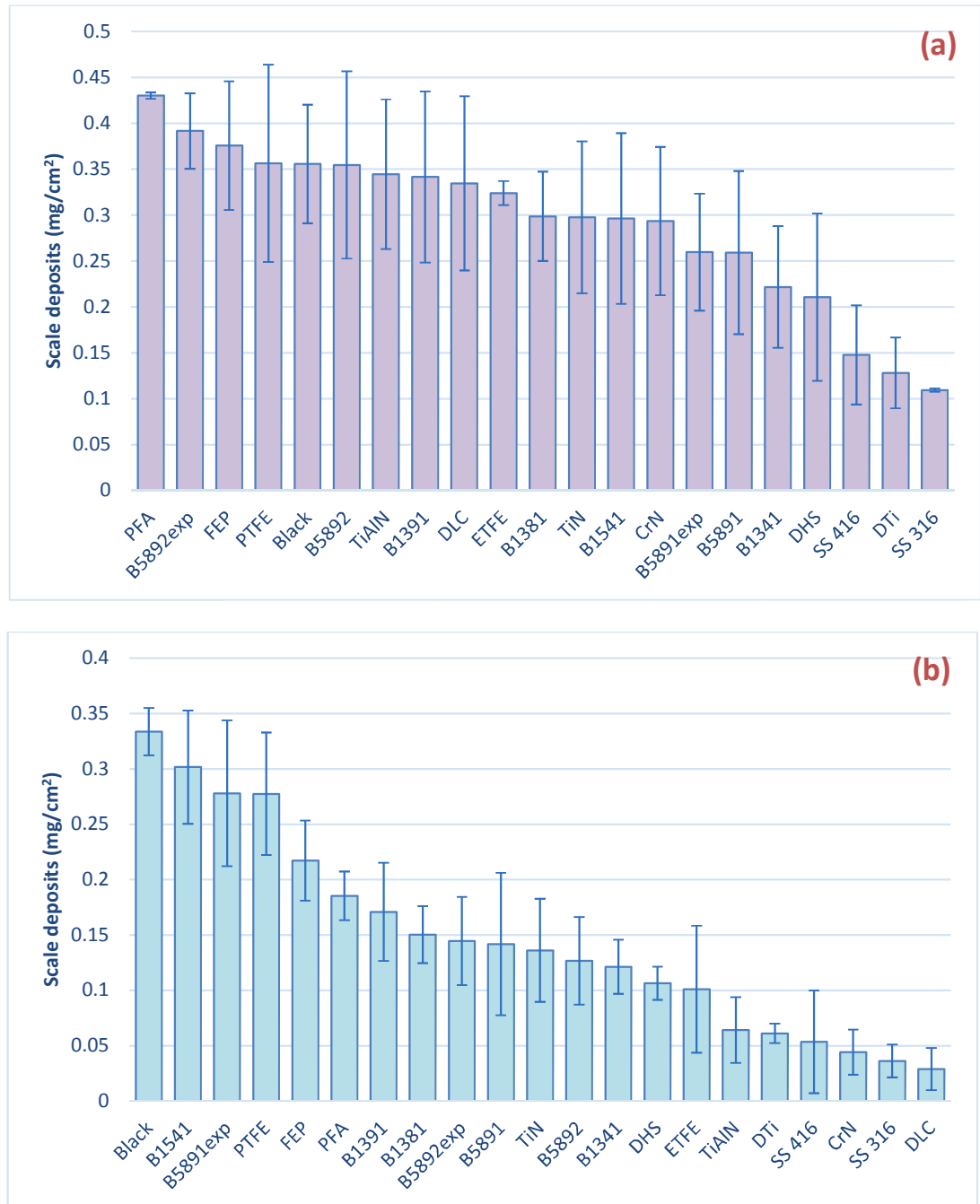


Figure 4.2. Mass gain of modified surfaces in adhesion process in (a) laminar flow regime, (b) turbulent flow regime.

4.4. SEM scale deposits for *adhesion* and *deposition* processes in laminar and turbulent regimes

Figure 4.3 shows the scale formation morphologies and elemental composition of scale deposits on different modified surfaces after a 2 hour experiment period. Based

on the initial saturation ratio calculation of the brine composition, scale precipitation of CaCO_3 , SrCO_3 and BaSO_4 in the bulk solution is thermodynamically possible.

In order to understand the morphology of the deposited scale on the surface, SEM images were taken for a range of modified surfaces experimented in both scenarios at laminar and turbulent flow regimes.

4.4.1. SEM images in the *adhesion* process

The presentation of the SEM images of scale deposits over a wide range of different modified substrates will enable us to understand more about the effect of the substrate on the scaling tendency rate and behaviour. To date, little research has been conducted to study the effect of substrate on the scale formation process and the morphology of scale deposits.

4.4.1.1. Laminar conditions

The SEM images taken from different modified surfaces in the laminar flow regime at different magnitude are shown in Figure 4.3. The images show both the mapping of the scale deposits (at zoomed out images) formed on substrates and also the morphology of them at zoomed-in images.

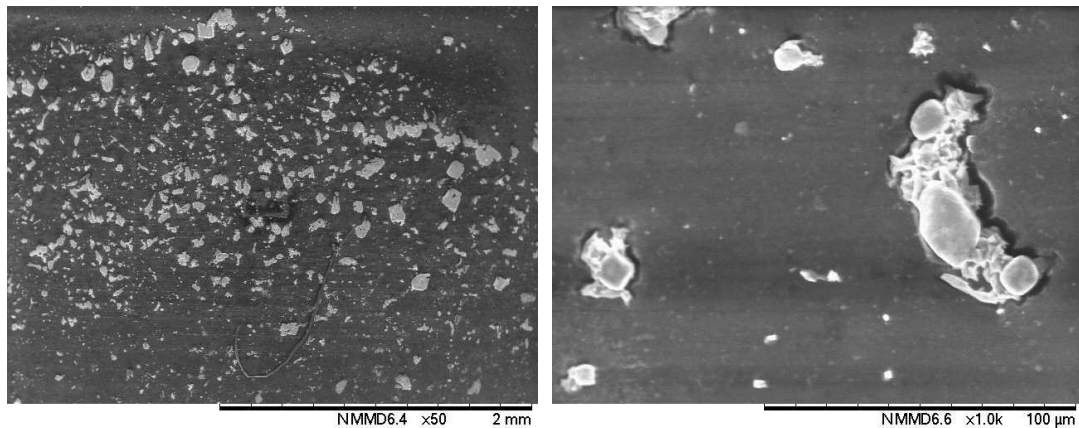


Figure 4.3a: B1341 – Scale deposits scattered all over the surface but have formed in accumulated clumps.

With the first glance by looking at the mapping formation of the scale deposits on the substrates, it shows that the scale deposits are almost deposited on the substrates in a scattered form. The morphology of the scale deposit crystals formed on the surfaces is mainly cubic calcite with round edges, needle-like aragonite, and with some rare

vaterite crystals. The presence of amorphous crystals is quite distinguishable on the surface of the majority of modified surfaces.

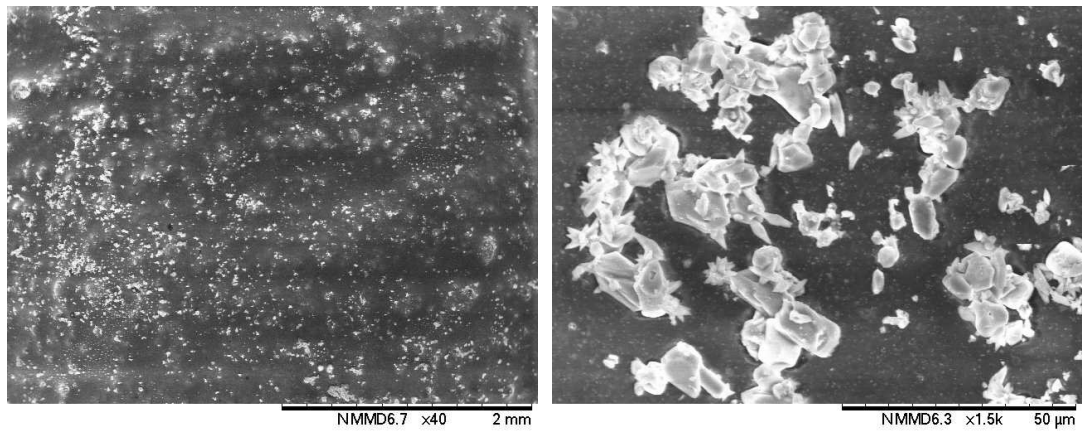


Figure 4.3b: B1381- Scale deposits scattered all over the surface but have formed in accumulated clumps.

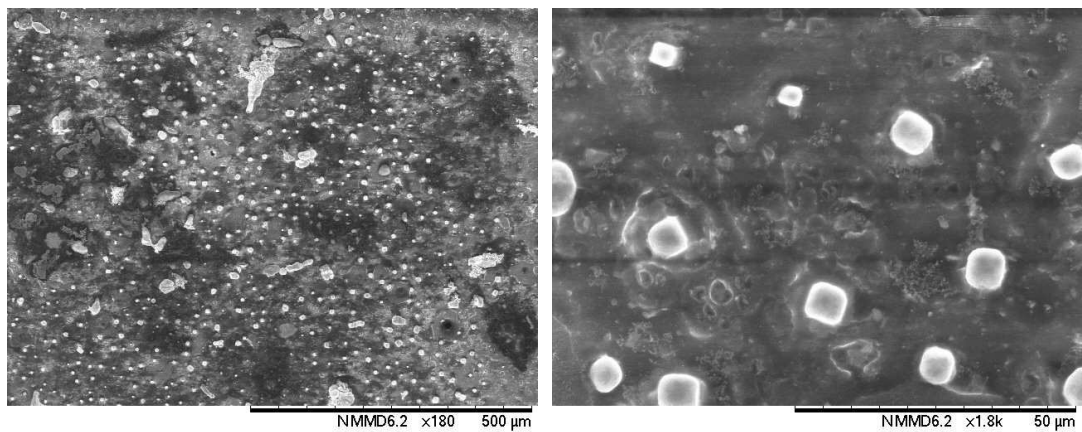


Figure 4.3c: B1391- Formation of calcite crystals with rounded edges.

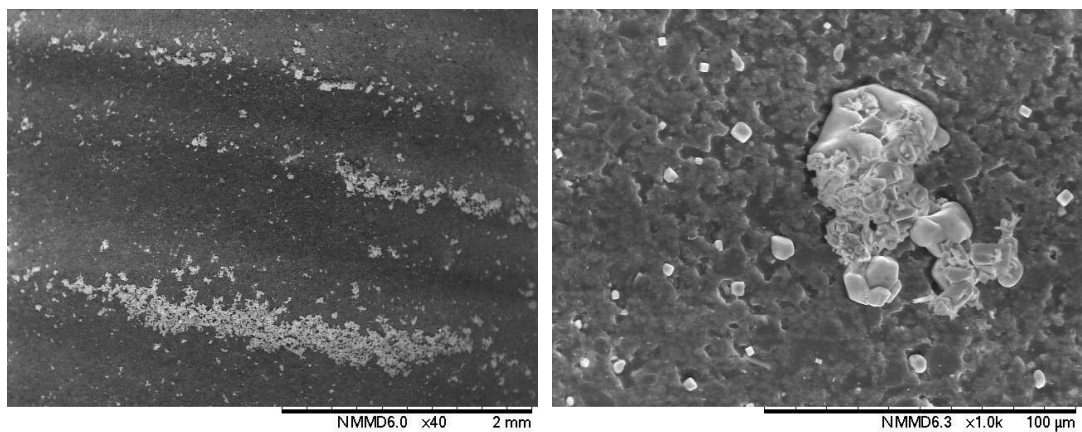


Figure 4.3d: B1541- The density of the scale deposits on the convex area of the surface is higher

Figure 4.3a to Figure 4.3h show the scale deposits on formed epoxy coatings. Due to the chemical composition complexity of the brine solution, the scale deposits formed on the surfaces are diverse in morphologies and scale pattern.

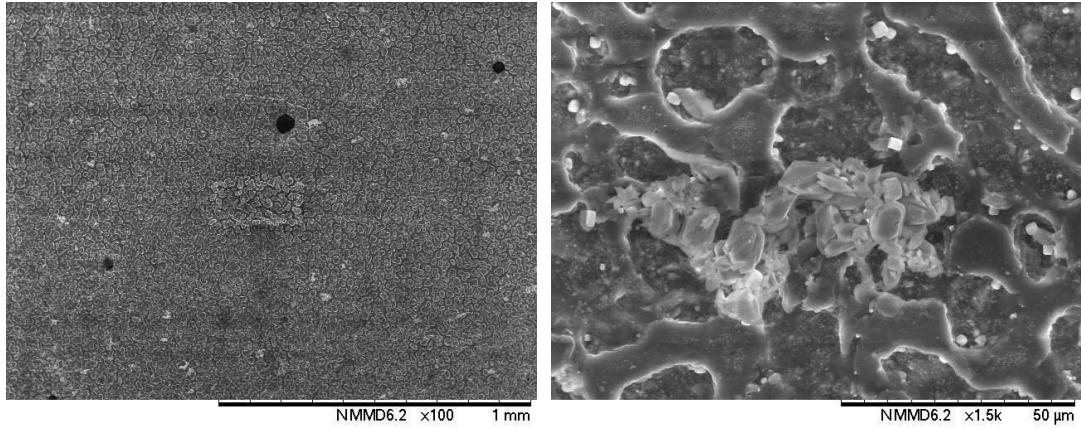


Figure 4.3e: B5891- Scale deposits scattered all over the surface but have formed in accumulated clumps.

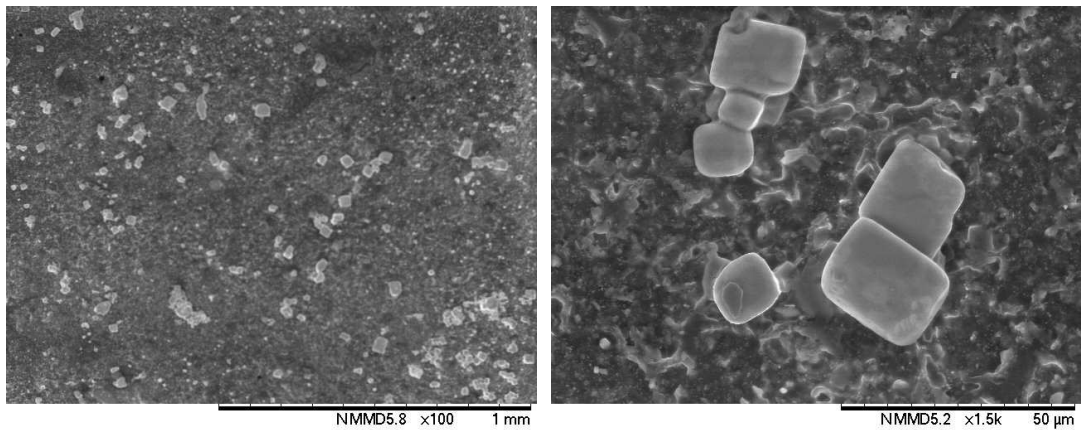


Figure 4.3f: B5891exp – The surface scale deposition as big calcite crystals with rounded edges scattered all over the surface.

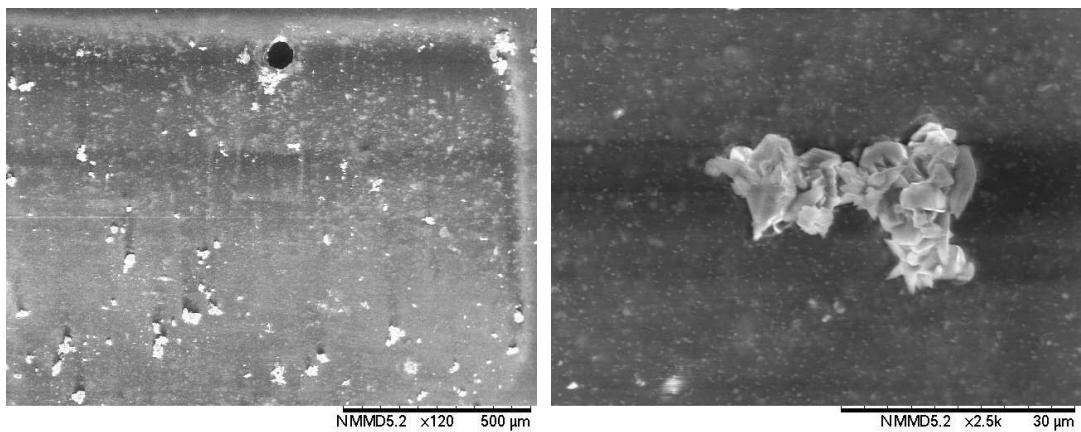


Figure 4.3g: B5892 - Scale deposits scattered all over the surface but have formed in accumulated clumps.

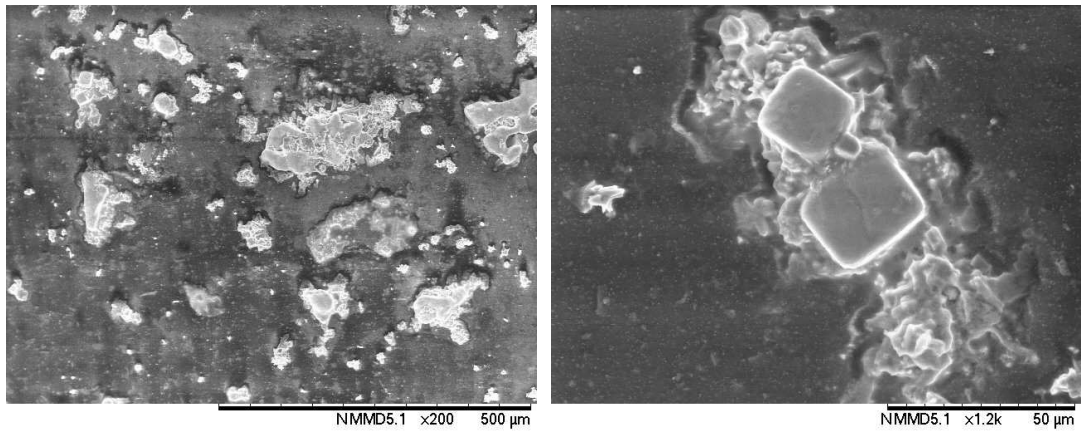


Figure 4.3h: B5892exp – Formation of scale deposits as clumps all over the surface, the dominant scale deposits can be categorised as amorphous crystals.

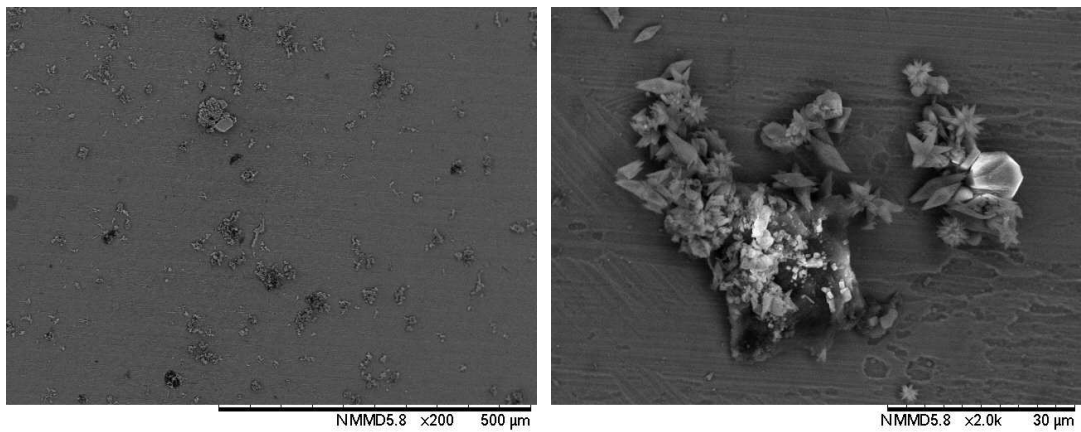


Figure 4.3i: CrN - Scale deposits scattered all over the surface but have formed in accumulated clumps, mixture of the amorphous and aragonite crystals

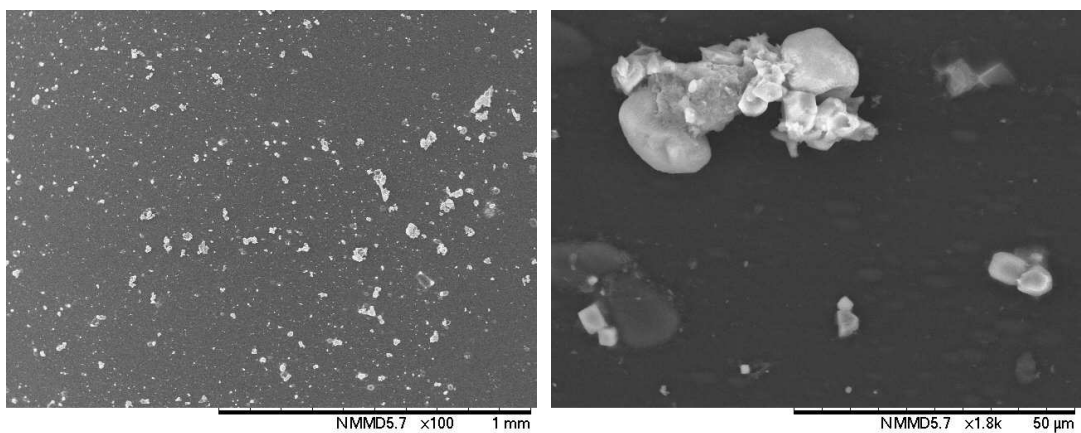


Figure 4.3j: DHS – The formation of amorphous crystals scattered all over the surface.

As shown in Figure 4.3d, the scale deposits are formed on the bulge of the surface. The magnitude of such convex area is normally omitted in the roughness measurement

techniques as a shape factor filter. Such convex areas are pretty scale-problematic regions where the mass transfer rate is controlled mainly by diffusion rather than convection (e.g. laminar conditions). In addition, these areas have a relatively higher surface energy compared to other locations on the surface. On the other hand, scale crystals adhere themselves in the valleys in between micro-grooves on the surface, where the relative surface energy is higher, as shown in Figure 4.3e.

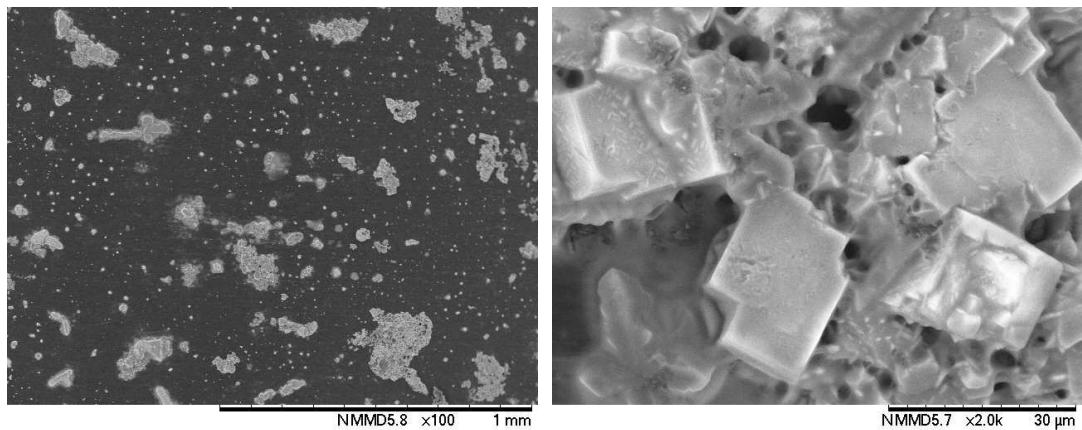


Figure 4.3k: DLC – The formation of amorphous and calcite crystals on the surface.

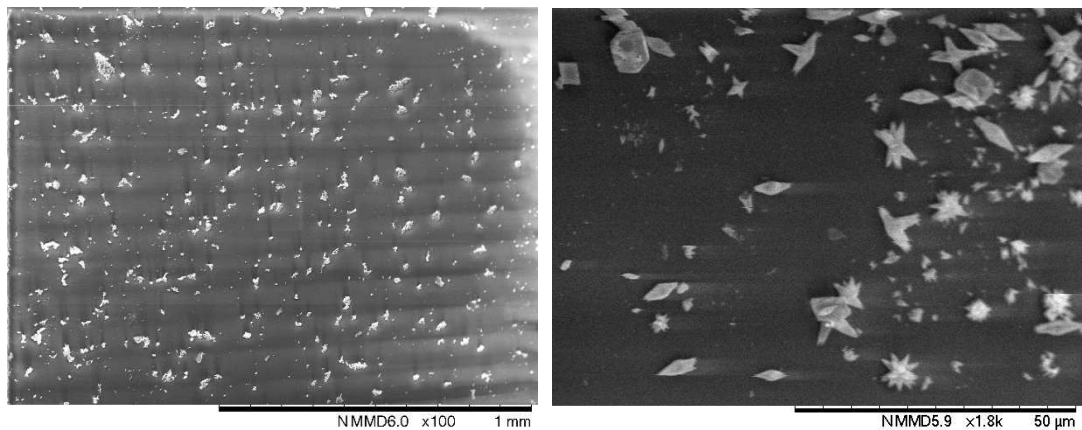


Figure 4.3l: Dti – Formation of aragonite crystals formed as either single or bundle crystals.

The SEM images of ceramic coatings along with the reference surfaces (stainless steel 316 & 416) are shown from Figure 4.3i to Figure 4.3p. In surfaces such as SS316 and SS 416, and TiN and TiAlN there are not much difference in the morphology of the scale deposits formed on the surface, e.g. in the former, mainly deformed calcite due

to the presence of magnesium ions, and in the latter, a combination of amorphous calcium carbonate and big crystals of calcite with round edges.

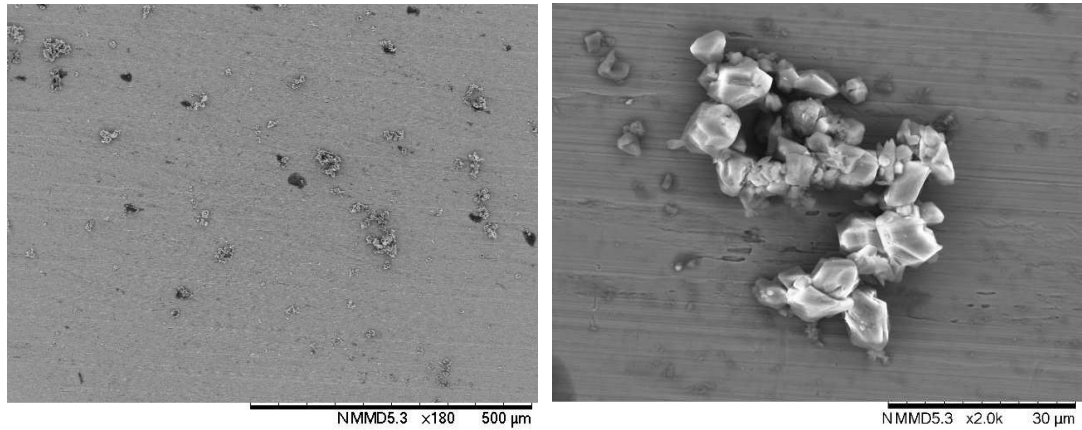


Figure 4.3m: SS 316 – The formation of amorphous crystals as a bundle and calcite with rounded edges.

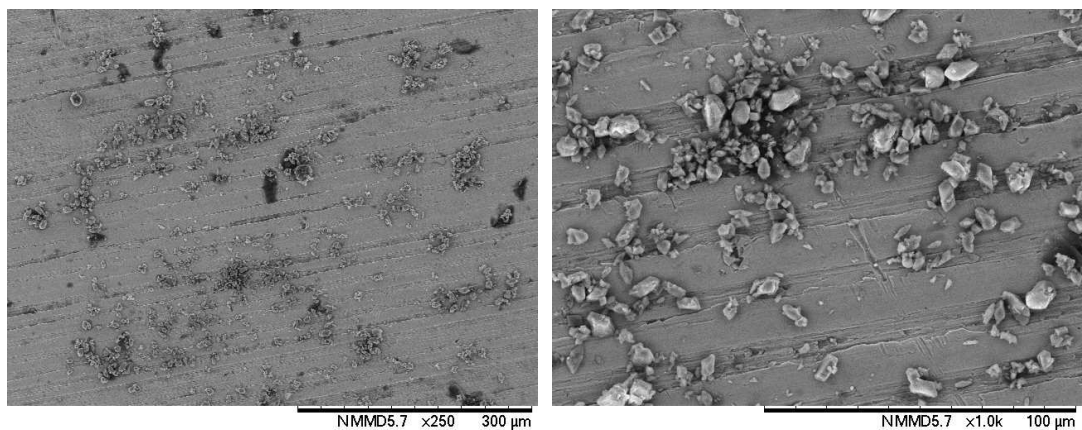


Figure 4.3n: SS 416 – Calcite with rounded edges are formed all over the surface.

The presence of aragonite crystals as single and bundle crystals are quite noticeable on CrN and Dti surfaces. Scale deposits on the DLC-based surfaces are different, in terms of both the morphology of the crystals and the scaling behaviour. In other words, the scale deposits formed on the DLC are mainly amorphous and deformed calcite crystals formed as agglomerated clumps of crystals, while on the DHS surface, the calcite crystals are relatively smaller and are scattered all over the surface.

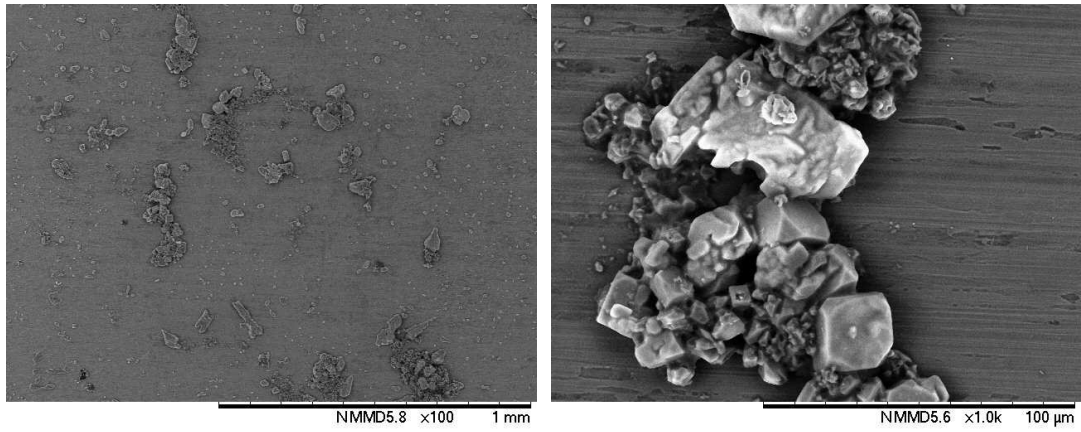


Figure 4.3o: TiN – A mixture of amorphous and calcite crystals formed on the surface as a clump.

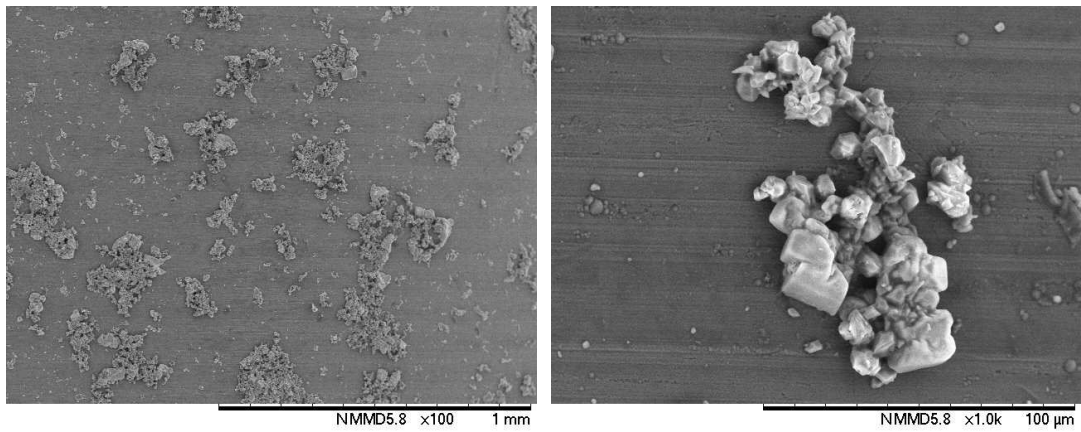


Figure 4.3p: TiAlN - A mixture of amorphous and calcite crystals formed on the surface as a clump.

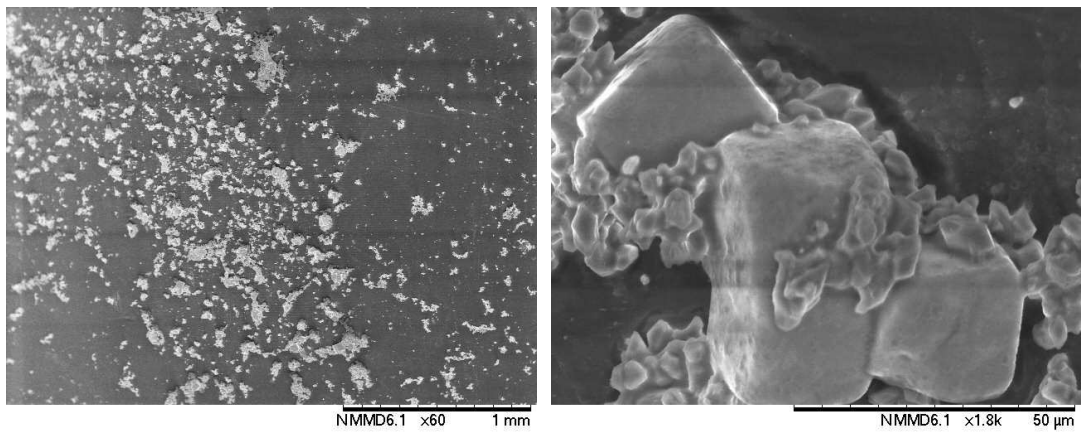


Figure 4.3q: ETFE - Formation of amorphous crystals all over the calcite crystals scattered all over the surface.

The SEM images of the scale deposits on the fluoropolymer coatings are shown from Figure 4.3q to Figure 4.3u.

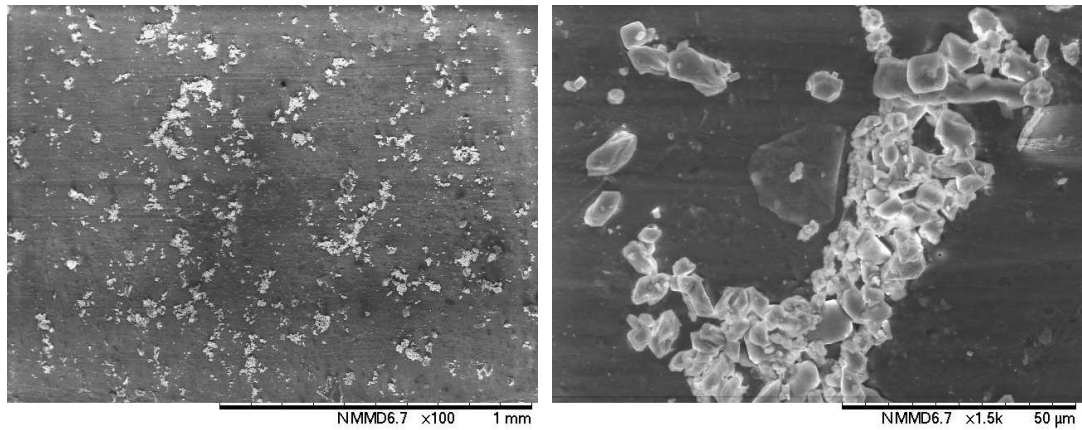


Figure 4.3r: FEP – Scattered crystals formed on the surface, mainly formed as calcite crystals with rounded edges.

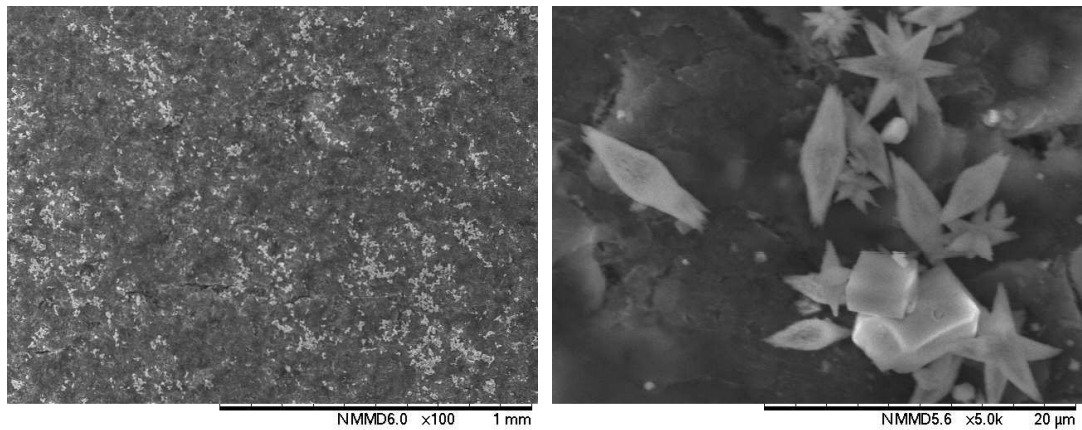


Figure 4.3s: One – Scattered crystals formed on the surface, mainly formed as calcite and aragonite.

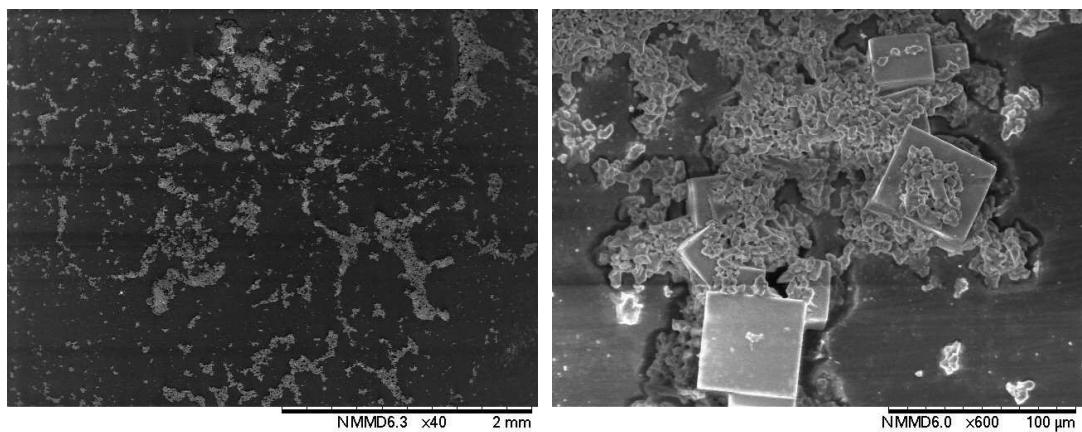


Figure 4.3t: PFA – The formation of perfect calcite crystals and amorphous crystals in between of them.

Unlike the “One” coating with calcite and aragonite (formed either singular or as a bundle), all the other surfaces are filled with amorphous calcium carbonate crystals with some calcite crystals in between. The fluoropolymer coatings are surfaces with relative lower surface energy, as a result, the formed scale deposits are rather attached together than attach themselves to the surface. In other words, the scale deposits in such surfaces are attached together as a lump of crystals.

In general, the scale deposits formed on the substrates in the adhesion process with laminar flow conditions are scattered all over the surface, mainly composed of calcite and amorphous calcium carbonate crystals with a minor portion of aragonite crystals in some surfaces. The surface scale formation behaviour of different substrates is different, and the author believes that apart from the bulk precipitation, at some point the surface scale formation is controlled by the substrate’s characteristics (such as the surface topography/texture/complexity/roughness/energy and chemical composition).

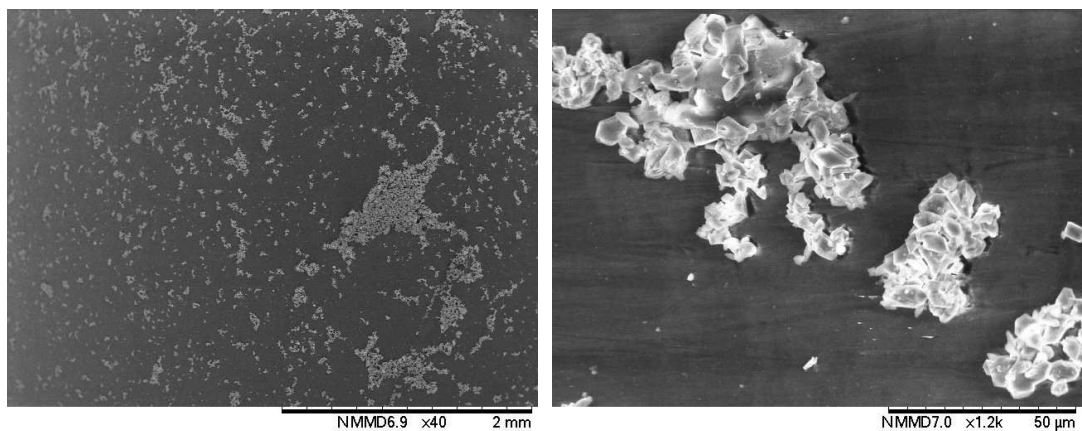


Figure 4.3*u*: PTFE – The formation of calcite crystals with rounded edges and amorphous crystals scattered all over the surface.

Figure 4.3. SEM images of the scale deposits formed on different modified surfaces at different magnification range in the adhesion process for laminar flow regime.

4.4.1.2. Turbulent Conditions

The SEM images of the scale deposits on different modified surfaces of the adhesion process in turbulent flow regime are shown from Figure 4.4*a* to Figure 4.4*o*.

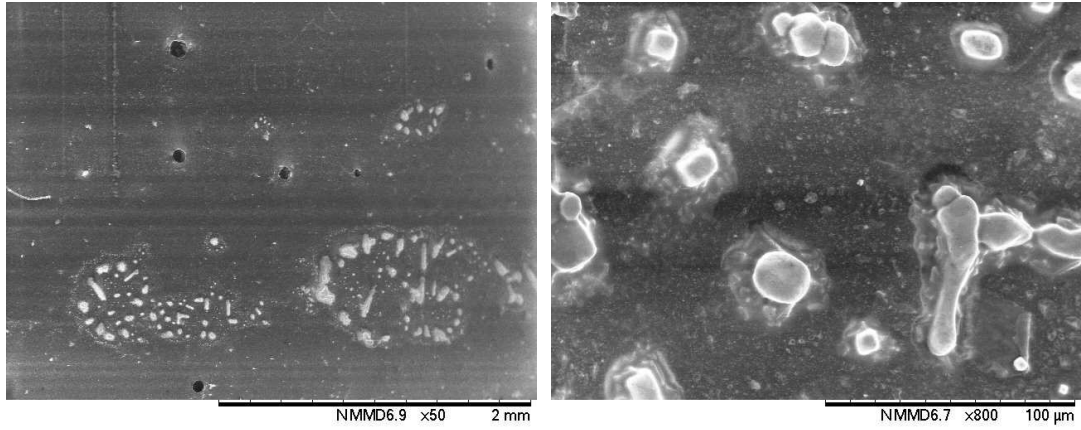


Figure 4.4a: B1381 – Amorphous crystal formed locally onto the surface, heterogeneous nucleation has occurred, although it is in the adhesion process.

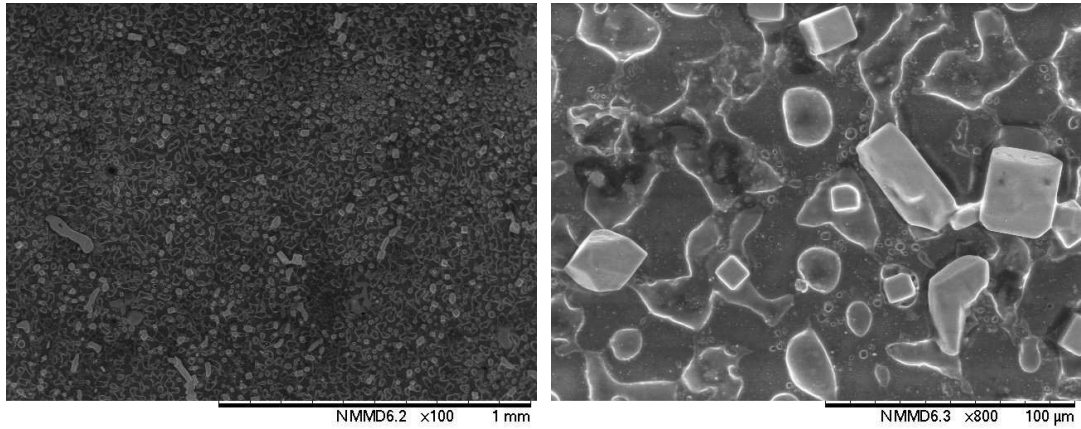


Figure 4.4b: B1391 – Calcite crystals with round edges are formed on the surface, they are scattered all over the surface as single crystals.

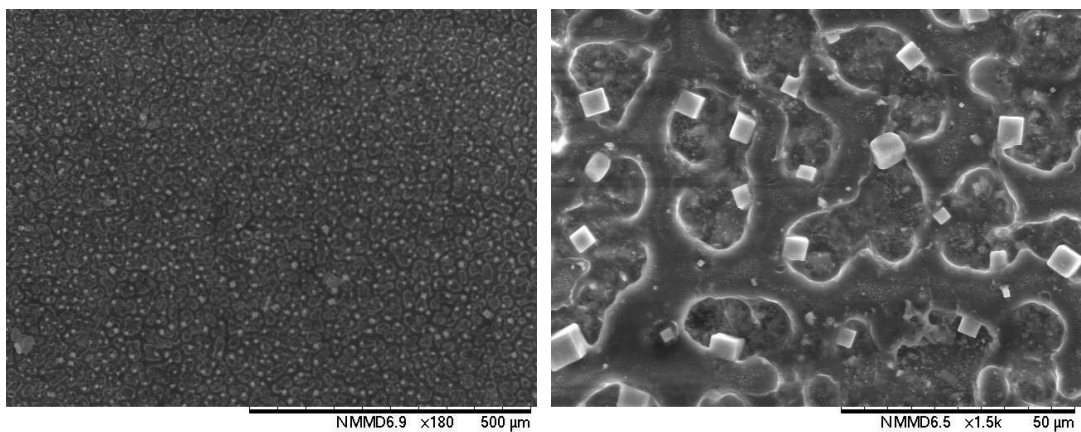


Figure 4.4c: B5891 - Calcite crystals are formed on the surface, they are scattered all over the surface as single crystals.

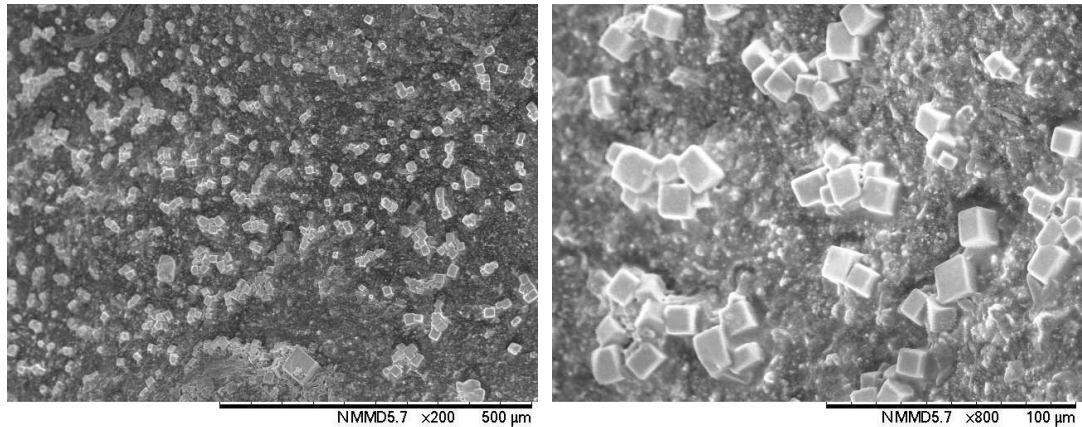


Figure 4.4d: B5891exp - Calcite crystals are formed on the surface, they are scattered all over the surface as both single and or accumulated crystals.

In turbulent flow regime, mass transfer is governed by advection rather than diffusion. As a result, in the adhesion process, where the pre-precipitation has already started and the crystals are formed, the adhesion of the bigger crystals onto the surface at higher shear forces induced by the flow is more difficult.

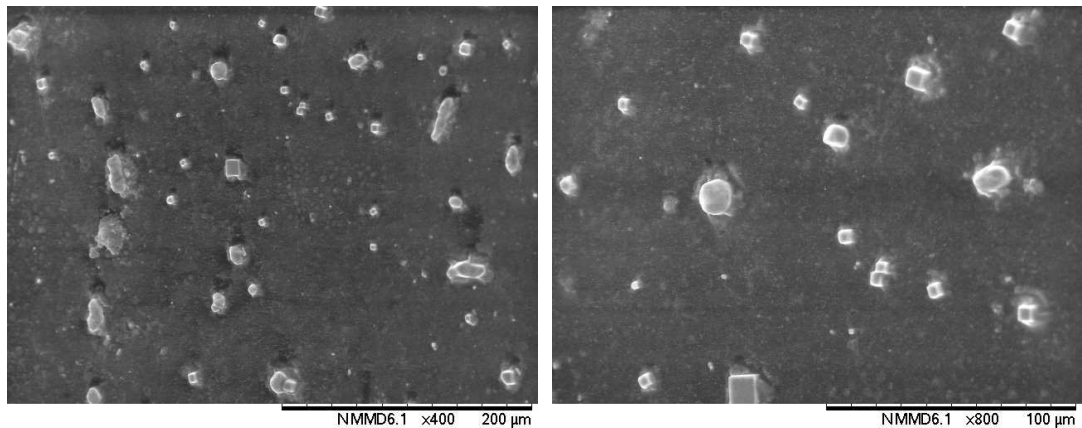


Figure 4.4e: B5892 – Heterogeneous nucleation occurring on the surface, although it is adhesion process.

In such conditions, there is a rivalry between the mass transfer rate which is in favour of scale formation and the gravitational forces which are against the surface scale formation. As a result, the crystals normally formed on the surface in turbulent conditions are smaller than in laminar conditions.

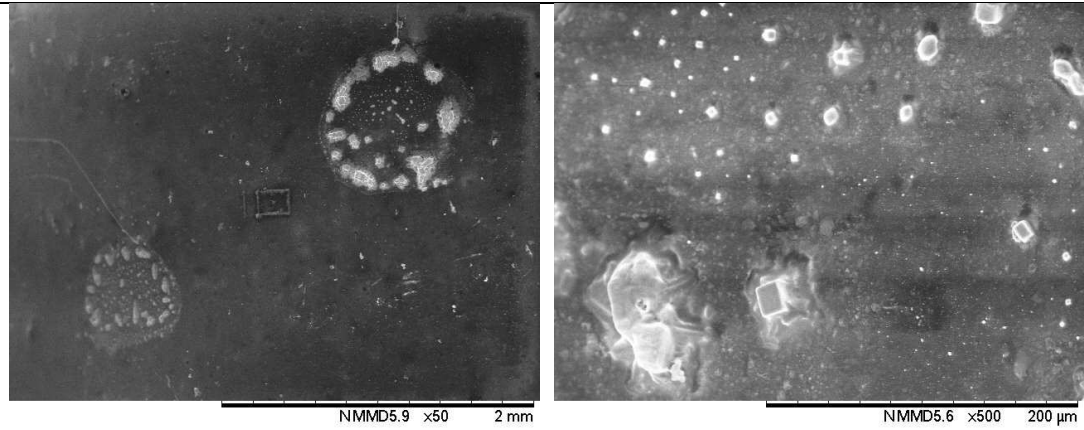


Figure 4.4f: B5892exp – Localised formation of crystals onto the surface, heterogeneous nucleation is in progress.

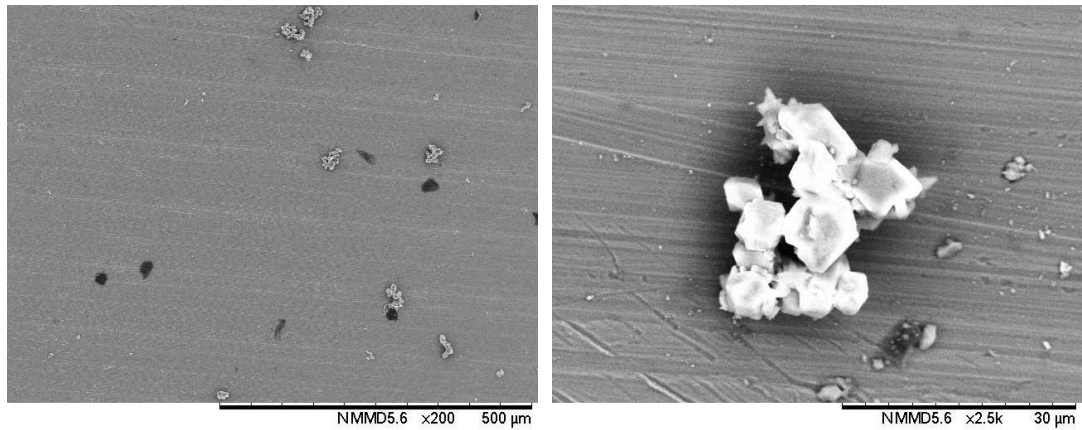


Figure 4.4g: CrN – The formation of calcite crystals with rounded edges as a lump of crystals over the surface.

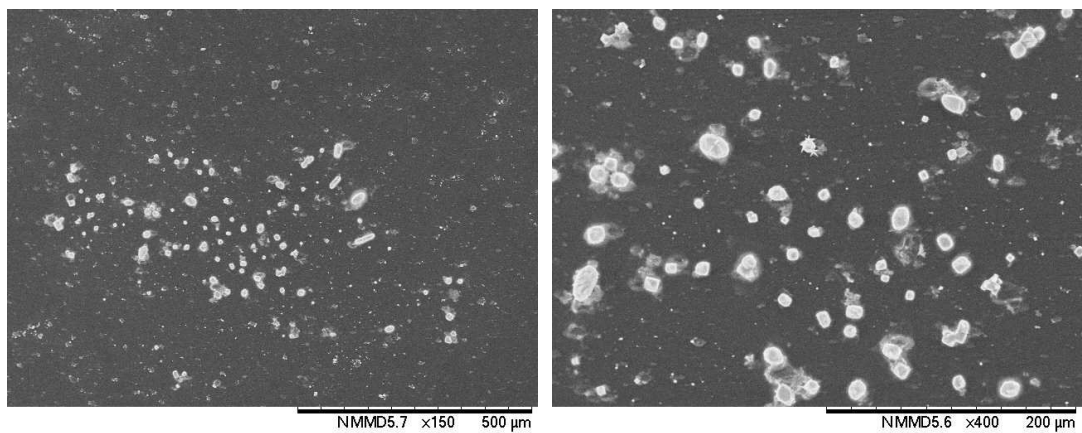


Figure 4.4h: DHS – The formation of scattered single calcite crystals with round edges onto the surface, heterogeneous nucleation is occurring.

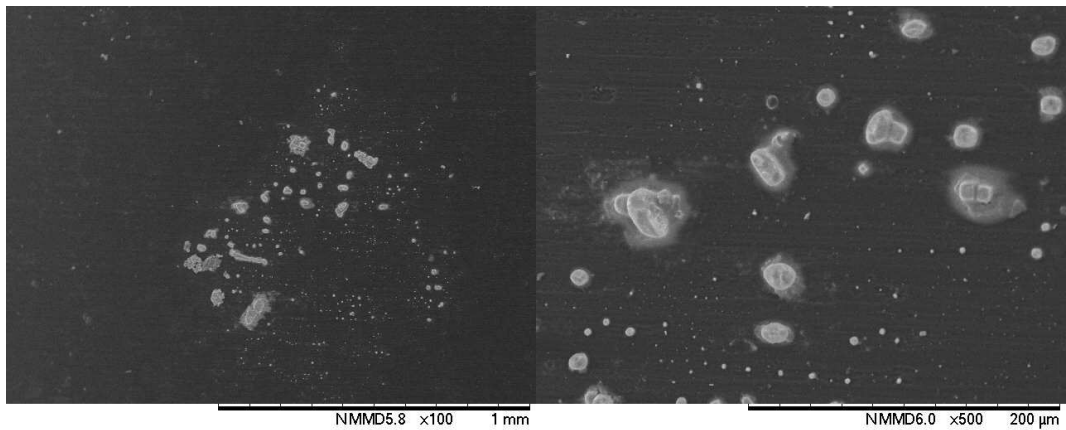


Figure 4.4*i*: DLC – Localised scale formation of scale crystals on the surface, heterogeneous nucleation is occurring.

The scale deposits on some modified surfaces (e.g. Figure 4.4*a*, Figure 4.4*f*, Figure 4.4*i*, Figure 4.4*j* and Figure 4.4*k*) are formed as localised scale deposition. Localised scale deposition forms as a result of heterogeneous nucleation and crystal growth.

It can be attributed to the fact that as the heterogeneous nucleation starts on the surface and such sites result in the crystal growth, the surface area adjacent to the formed crystals on the surface would be more susceptible to further surface scaling. As a result, the surface scaling rate near to pre-deposited surface areas would be escalated and lead to localised formation of scale deposits.

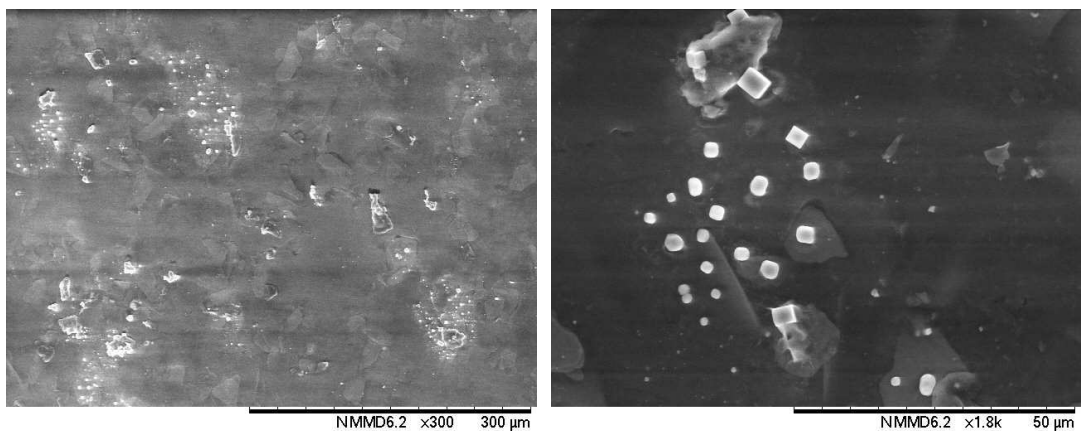


Figure 4.4*j*: ETFE – Localised formation of single calcite crystals on the surface.

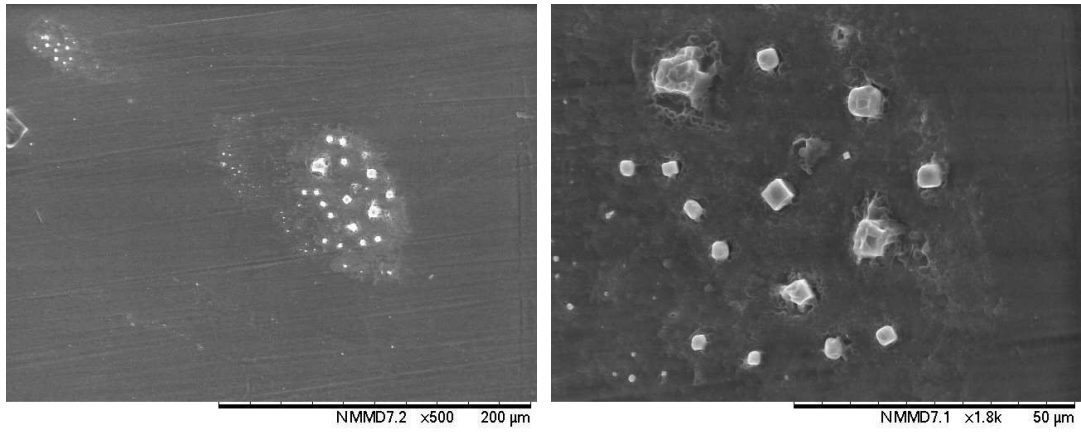


Figure 4.4k: PTFE – Localised formation of scale deposits as calcite crystals, heterogeneous nucleation is occurring in the adhesion process.

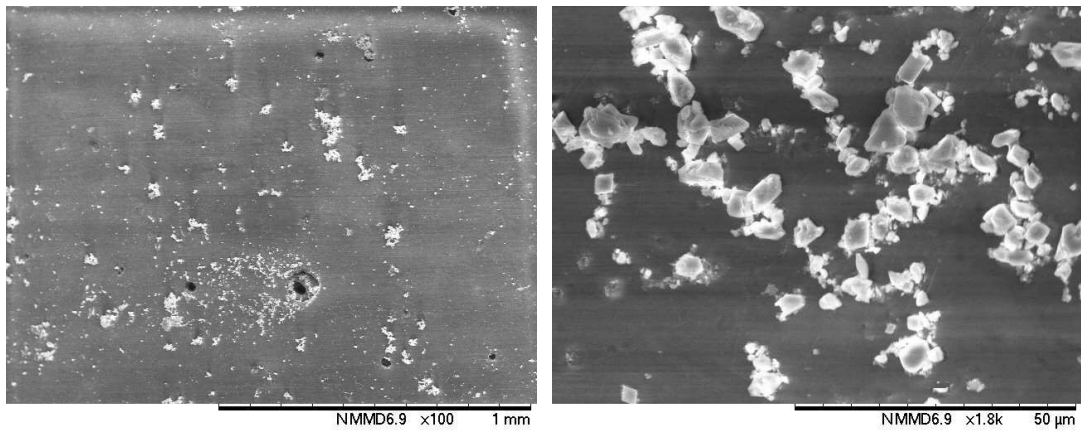


Figure 4.4l: FEP – The formation of amorphous and calcite crystals on the surface.

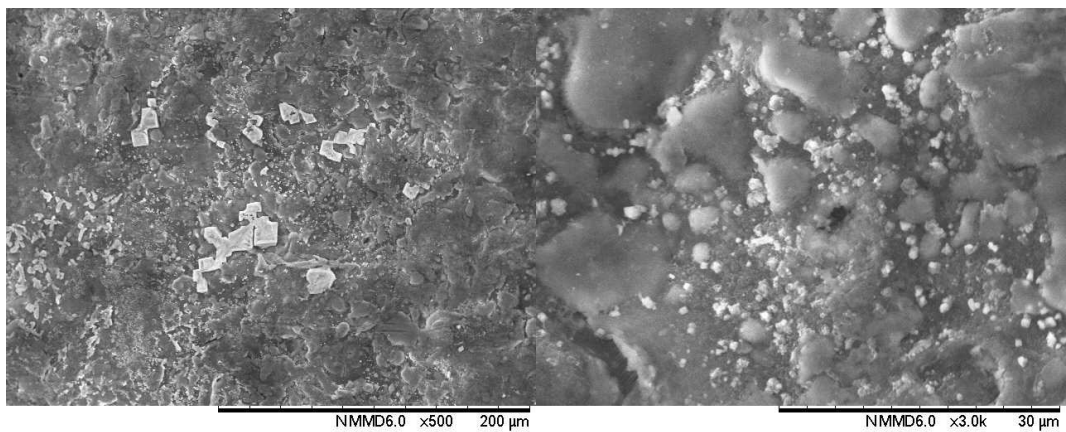


Figure 4.4m: “One” – Scattered formation of the lump of calcite crystals on the surface.

The crystals formed in turbulent conditions are mainly calcite crystals with a little amount of amorphous calcium carbonate crystals on some of the surfaces. In turbulent conditions, the adhesion of the pre-precipitated crystals onto the surface is easier in regions where they are less influenced by the shear forces induced by the flow regime, e.g. in the valleys and grooves of the surface.

For example, the surfaces with higher texture complexities, such as “B1391”, “B5891”, “B5891exp” and “One”, the calcite crystals adhere themselves uniformly all over the surfaces. Or, as shown in Figure 4.4n and Figure 4.4o, the scale deposits are formed in the grooves of “SS416 and “TiN”, respectively, while the convex areas (i.e. peaks) of the surface have fewer scale deposits.

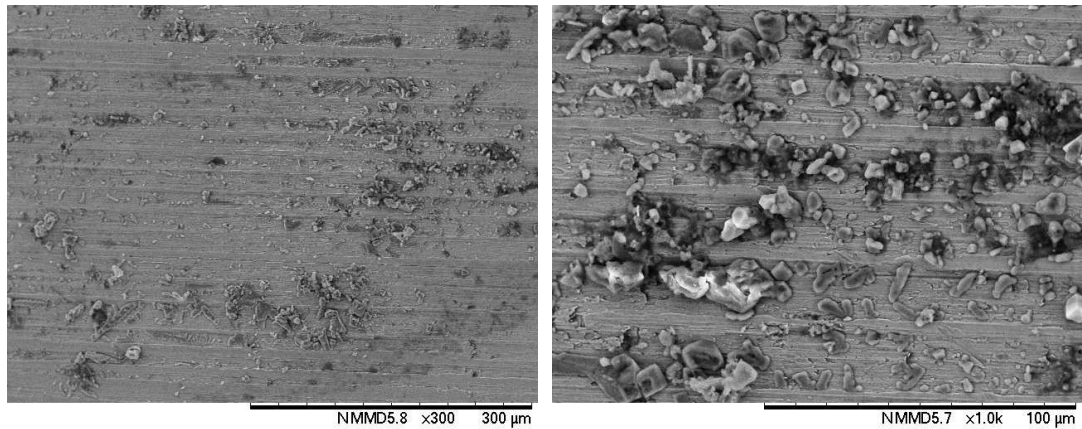


Figure 4.4n: SS 416 – Scale deposits are predominantly formed in the concave areas of the surface.

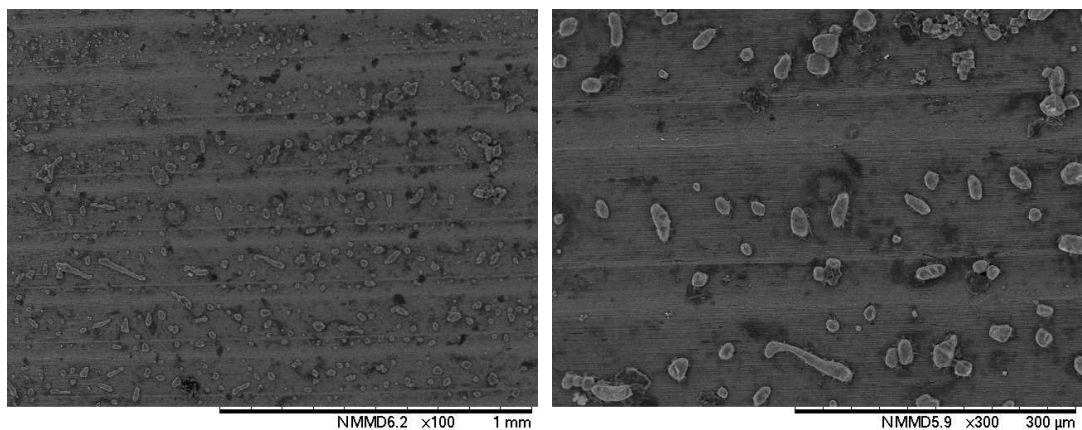


Figure 4.4o: TiN – Scale deposits are mainly formed in the grooves of the surface.

Figure 4.4. SEM images of the scale deposits formed on different modified surfaces at different magnification range in the adhesion process for turbulent flow regime.

In conditions where the gravitational forces are dominant and against the adhesion of the crystals onto the surfaces, the process of surface scaling is mainly governed by heterogeneous nucleation and crystal growth. The zoomed-in image of such localised scale deposition is shown in Figure 4.5. It can be implied that the heterogeneous nucleation and crystal growth is always taking place, although the crystals are already pre-precipitated in the bulk. Such occurrence is also noticeable in the SEM images of Figure 4.4-*a,e,f,h, i* and *k*.

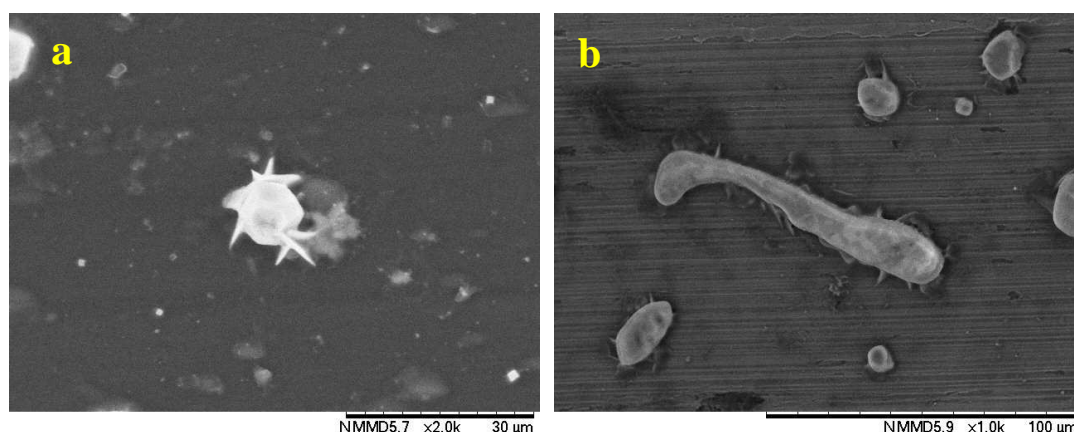


Figure 4.5. The SEM image of scale deposits in the adhesion process in the turbulent conditions. Heterogeneous nucleation and crystal growth still occurring onto the surface: (a) DLC and (b) TiN.

In other words, there are so many connections around the formed scale deposits and the modified surfaces which indicate a strong affinity between these two entities. The author believes that such occurrence can be attributed to the fact that heterogeneous nucleation is taking place although it is the adhesion process. However, the author cannot distinguish the occurrence sequence of these processes, i.e. whether it is the heterogeneous nucleation and crystal growth process that facilitates the adhesion of pre-precipitated scale deposits onto the surface or vice versa.

4.4.2. SEM images in the *deposition* process

Since the fluoropolymer and epoxy coatings are not conductive, the platinum layer is coated on the surface for a better assessment of the crystal morphology on such surfaces.

As shown in Figure 4.6, there are mainly calcite and aragonite crystals formed on the B1341 coating as scale deposits. The small aragonite crystals formed as a single crystal but as they start to grow up, they will grow up as a bundle of aragonite (see Figure 4.6-left, Figure 4.7-c and Figure 4.9). Such behaviour is also evident on other modified surfaces.

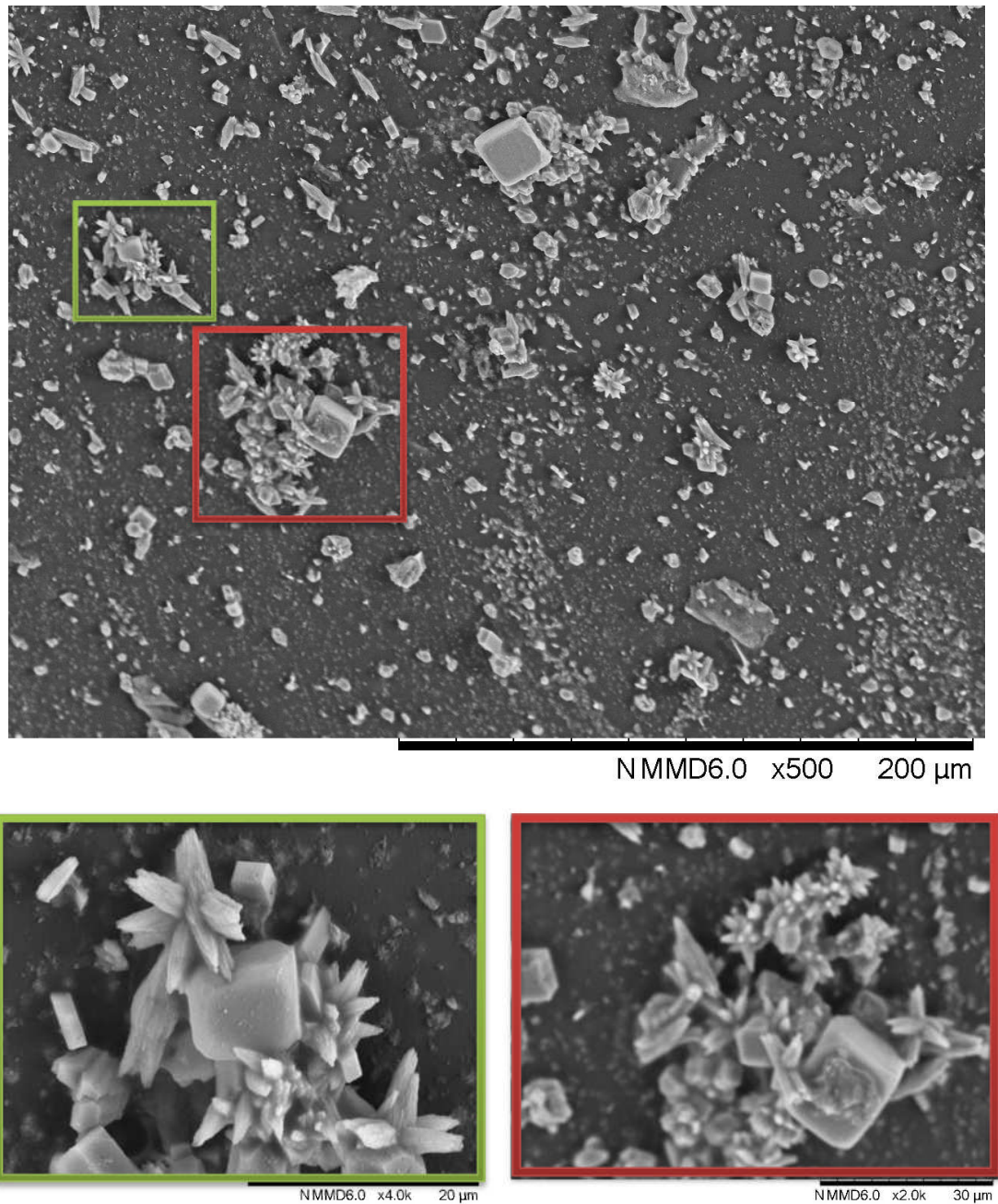


Figure 4.6. The SEM image of scale deposits on the “B1341” coating in the *deposition* process.

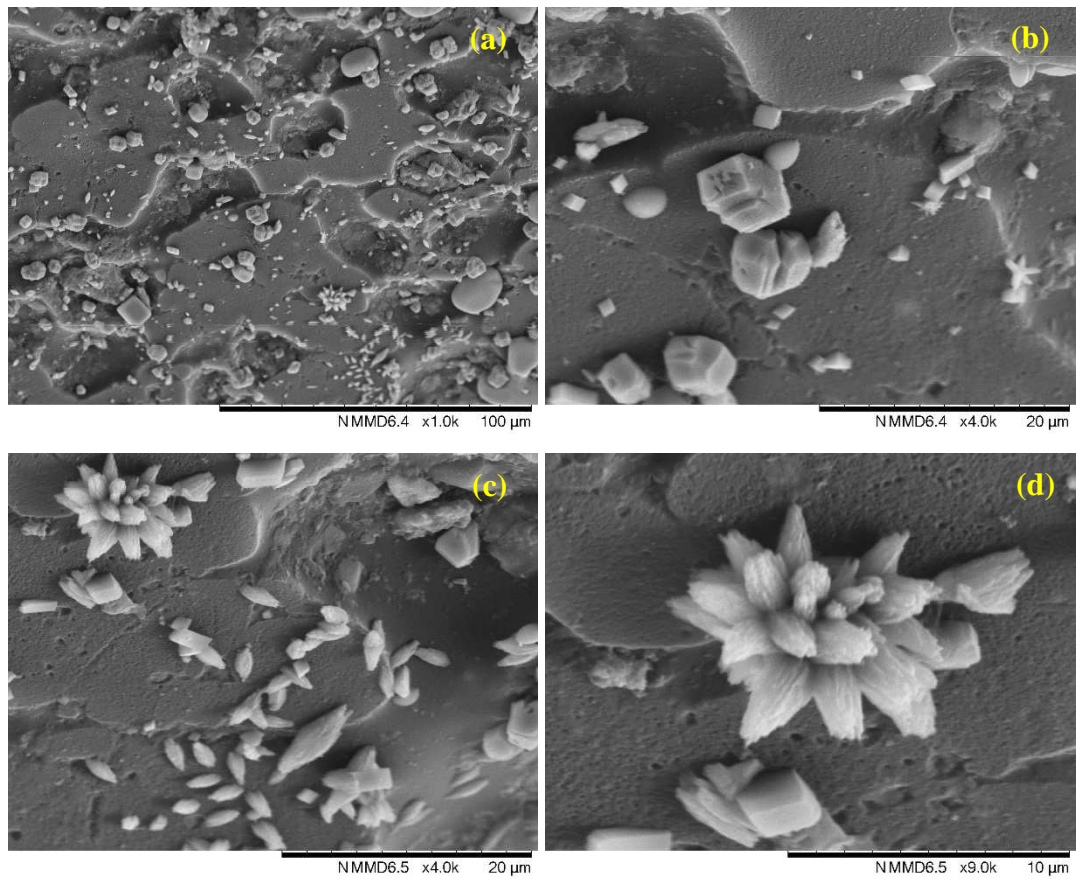


Figure 4.7. The SEM image of scale deposits on the “B1391” coating in the *deposition* process.

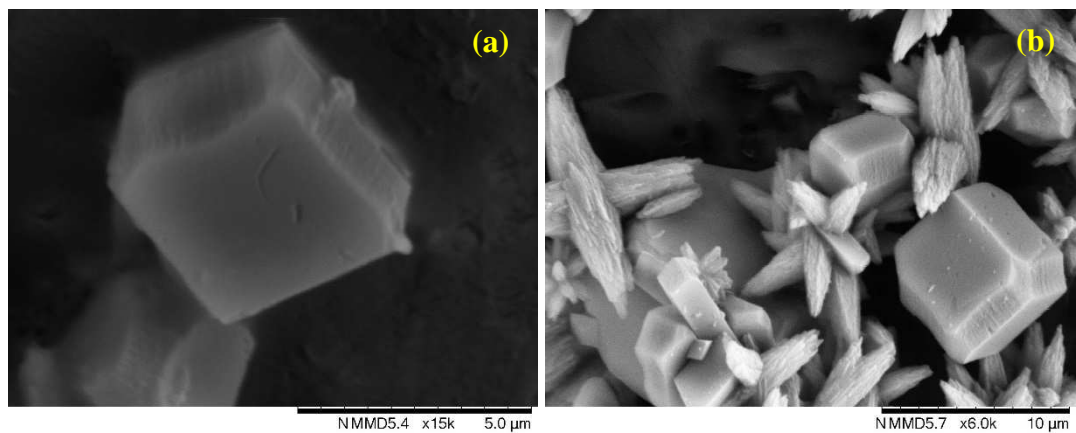


Figure 4.8. The sharp edges of calcite are rounded on different modified surfaces: (a) ETFE and (b) PFA.

Secondary nucleation phenomenon is also observable on the surface of the calcite crystal (Figure 4.6-right and Figure 4.7-b). Secondary nucleation formation and the dissolution of the crystals mainly at the edges of the calcite crystals, where the ion transfer is at its highest rate (see Figure 4.8), will lead to the formation of lump crystals onto the surfaces (see Figure 4.5 or Figure 4.4-*a, b, h, i, n, o*).

It can explain clearly why the formed crystals on the modified surfaces in the *adhesion* process do not follow the shape of the known morphologies of carbonate scale deposits. In other words, in terms of time sequence, the *deposition* tests are occurring in the first 2 hours that the brines were mixed, while the *adhesion* tests are starting after 2 hours of the time that the brines were mixed together. Therefore, the latter is at later stages compared to the former process.

The effect of the substrate on the morphology of the scale deposits has not fully determined, yet. The SEM images (see Figure 4.9 and Figure 4.10) show that the morphology of the formed scale deposits will be affected by the chemical composition of the substrate, however, the author believes that much more systematic research should be conducted in future to study such effects.

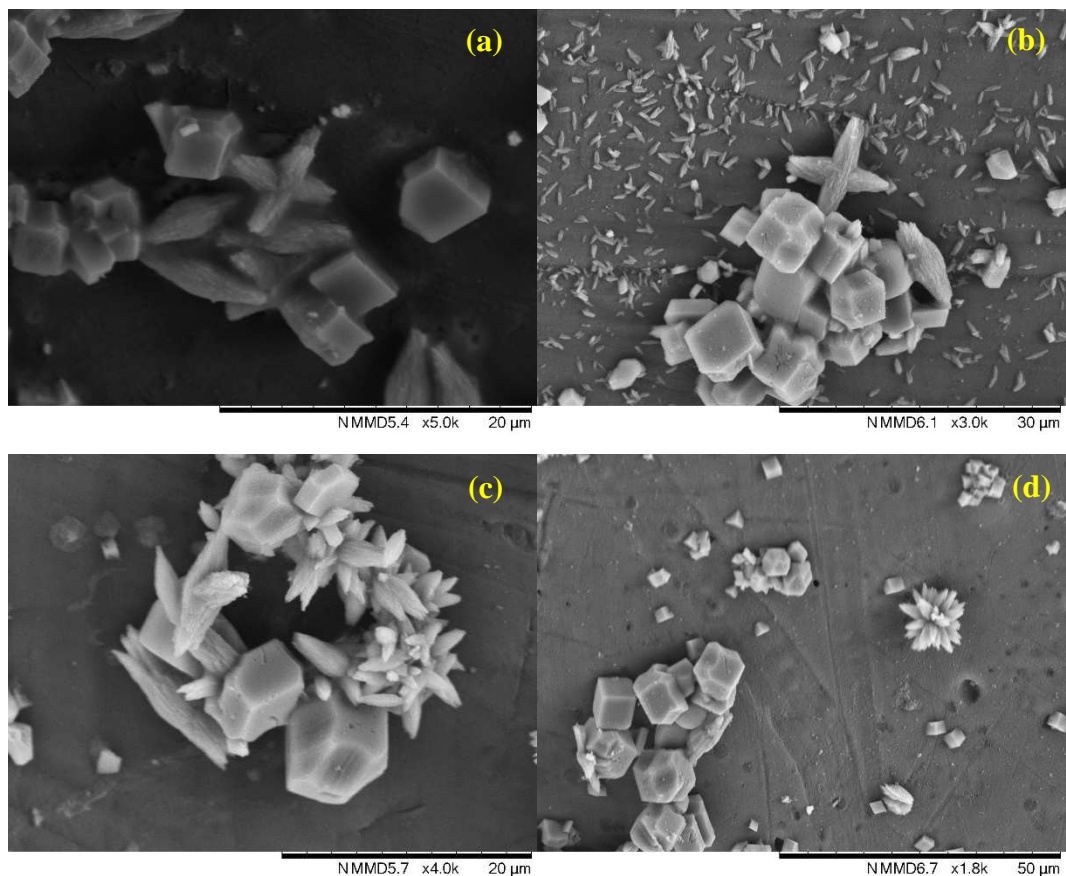


Figure 4.9. The formation of needle-like aragonite bundle with low aspect ratio and calcite formation and dissolution at their edges in the *deposition* tests on the fluoropolymer surfaces: (a) ETFE, (b) FEP, (c) PFA and (d) PTFE.

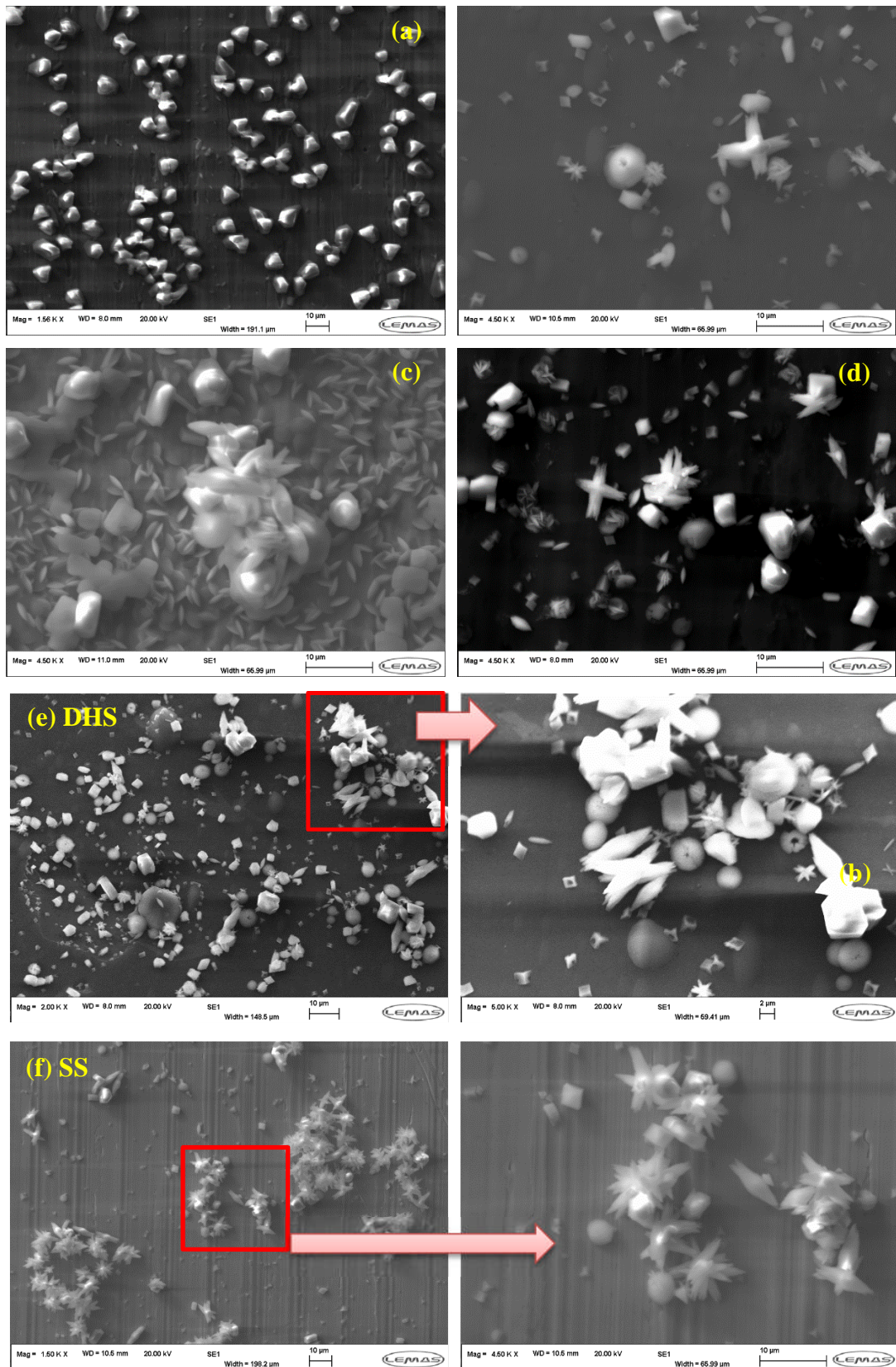


Figure 4.10. The formation of rounded edges calcite, needle-like aragonite with low aspect ratio and round shape and/or di-pyramidal vaterite formed in the *deposition* tests on different modified surfaces: (a) CrN, (b) DLC, (c) TiN, (d) DLC, (e) DHS and (f) Stainless steel.

As shown in Figure 4.9, the dominant morphology of the scale deposits formed on the fluoropolymer-based surfaces are the needle-like aragonite bundles and calcite with rounded edges, while the morphology of the scale deposits formed on the ceramic-based surfaces and the stainless steel include all three main morphologies of the calcium carbonate crystals: calcite crystals with rounded edges, aragonite crystals with low aspect ratio which are formed mainly as a bundle, and vaterite crystals which are shaped as either round crystals or dipyramidal crystals (see Figure 4.10).

By comparing the surface scale deposits between the epoxy coatings and the fluoropolymer coatings, there is not much difference in terms of the morphology of the crystals formed on surfaces, while in ceramic coatings the existence of the vaterite crystals on such surfaces are quite apparent and forms in different known shapes of the vaterite crystals.

Apart from the known morphologies, there is a type of uncommon calcite crystal with sharp edges but a hollow in the middle, as shown in Figure 4.11.

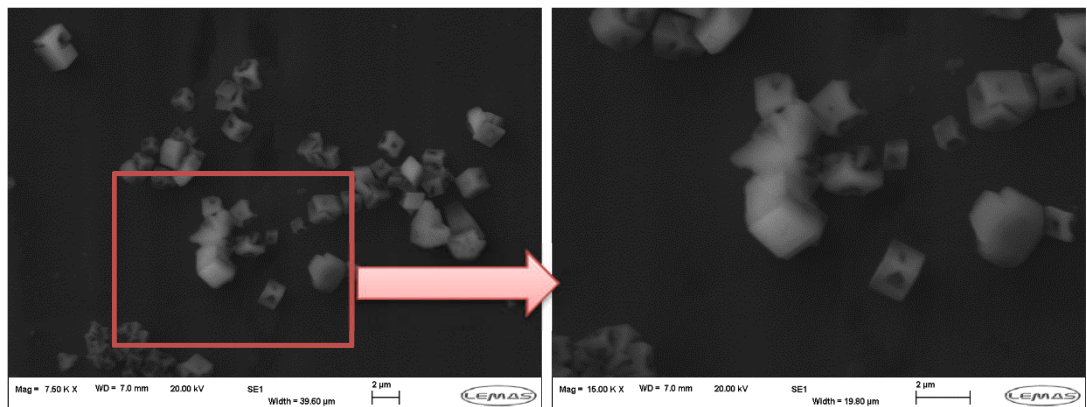


Figure 4.11. SEM images of CaCO₃ deposited on DLC: showing deformity at the centre of the cubical structure.

Figure 4.12 shows the crystals formed on one specific substrate (TiN) for both turbulent and laminar conditions. In both cases, both calcite (polyhedron) and aragonite (needle-like but thicker in the middle) are formed, however, the dimension of the crystals are relatively different.

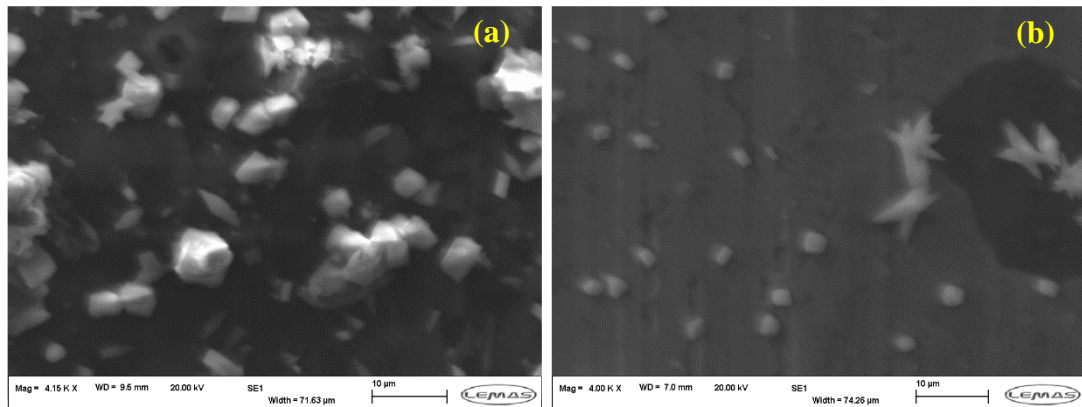


Figure 4.12. SEM images of the crystal morphologies of scale deposits on a specific substrate (TiN) in different flow regimes: (a) Turbulent conditions (b) Laminar conditions

Aragonite crystals in laminar conditions are relatively longer than that of in turbulent conditions but this discrepancy is not much; on the other hand, the calcite crystals in the turbulent flow conditions are 1.5 to 2 times bigger than that of in the laminar flow conditions. Such occurrence can be associated with the kinetics formation rate of aragonite versus calcite crystals.

The aragonite crystals formed in the laminar conditions are formed as needle-like bundles, while in the turbulent conditions these crystals are solely formed and scattered. The reason can be attributed to the way that crystals are formed with regard to gravitational forces: in laminar conditions crystallization takes place in more localized way on the surface and begins to grow, while in turbulent conditions crystals would grow up to a level and then they will be affected by shear stress induced by the brine solution.

The zoomed-out SEM images of scale formation on different substrates after 2-hour experiments in laminar and turbulent flow conditions are shown in Figure 4.13 and Figure 4.14, respectively. In turbulent conditions, the scale deposits are formed evenly all over the surface, while the scale deposits are formed locally and then have grown locally in the laminar conditions.

Such behaviour can be attributed to the fact that the heterogeneous nucleation and crystal growth is primarily governed by the transport of the ions of interest from the bulk solution onto the crystal interface. In laminar conditions, the mass transfer is controlled by diffusion, while in turbulent conditions it is mainly controlled by advection.

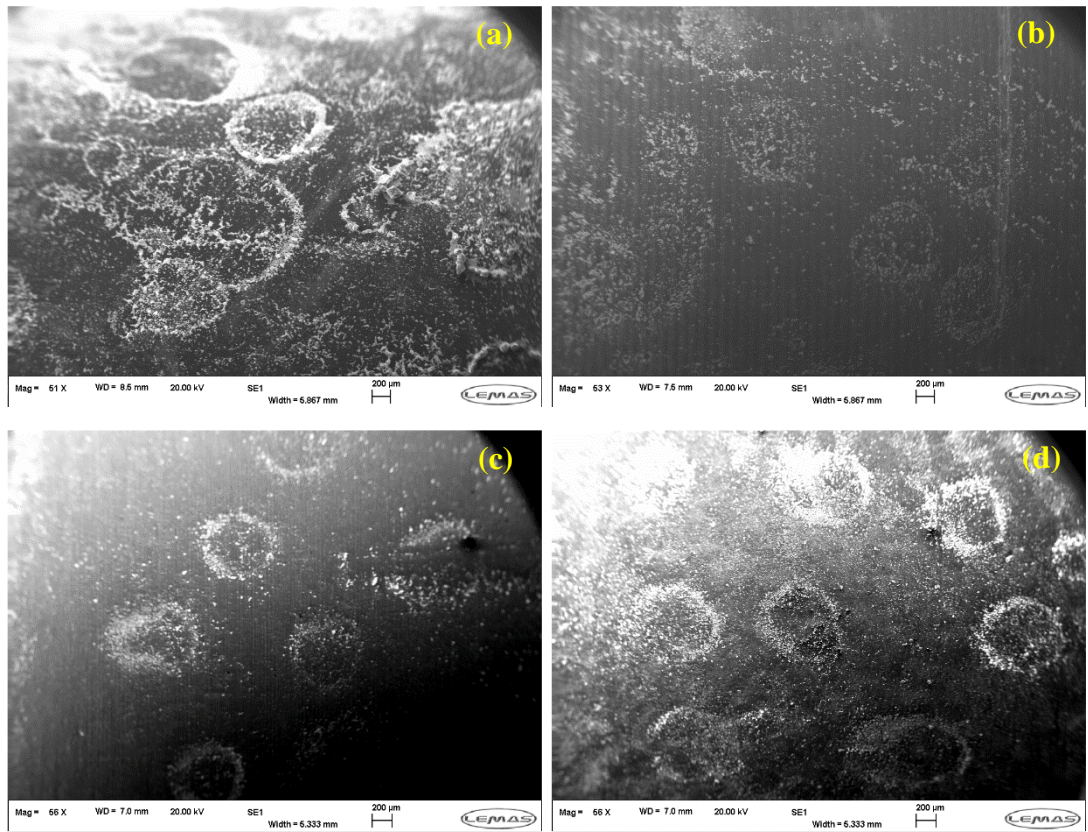


Figure 4.13. SEM images of carbonate scale formation in laminar conditions (zoomed out): (a) DHS, (b) TiN, (c) Stainless steel, and (d) DLC.

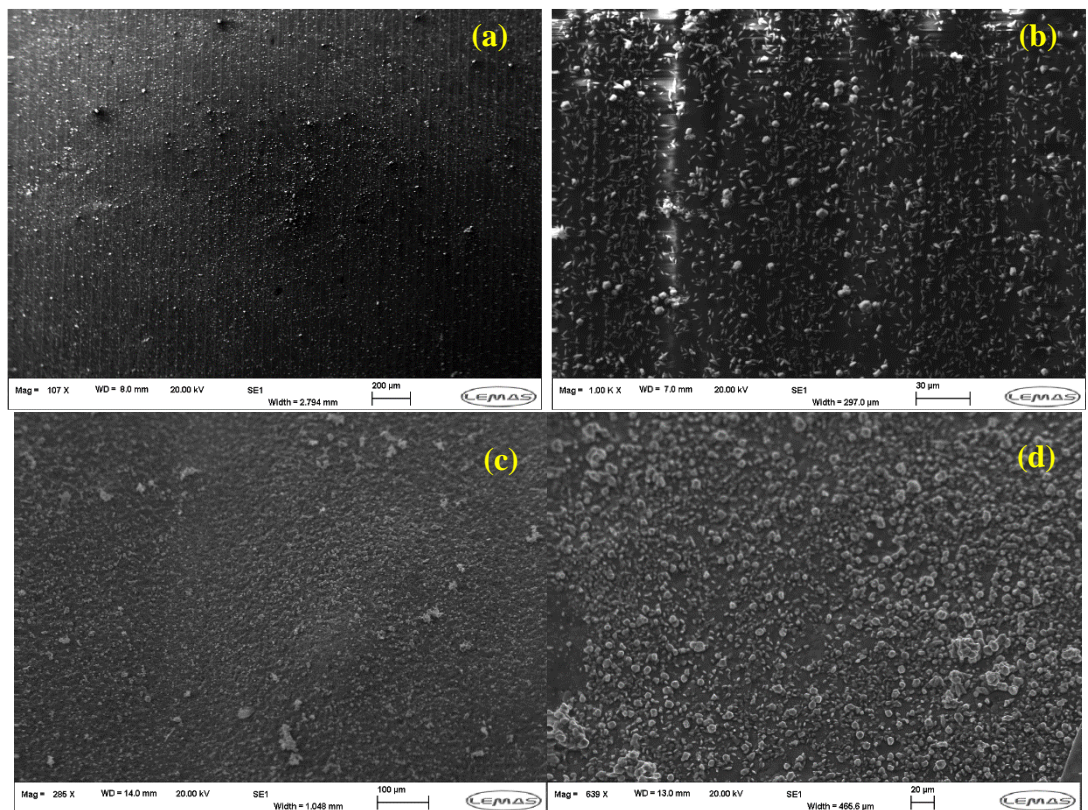


Figure 4.14. SEM images of scale formation in turbulent conditions (zoomed out): (a) DLC, (b) DTi, (c) B1541 and (d) Black.

As a result, in laminar conditions, where the mass transfer diffusion is higher, local scale deposition occurs more often, while in turbulent conditions the advection (or convection) effects overcome the diffusion effects and more uniform scale deposition occurs.

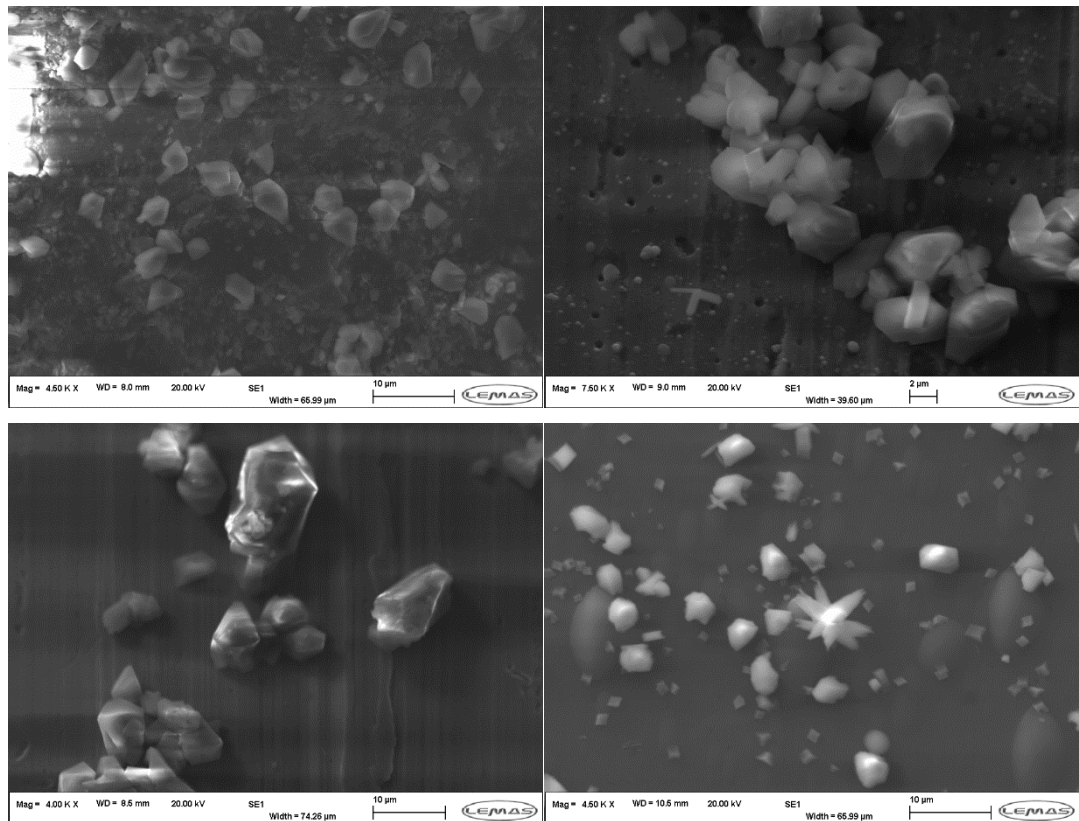


Figure 4.15. SEM images of scale deposits on different modified surface, the formation of polyhedron calcite due to the existence of Mg^{2+} crystals: (a) B5891, (b) CrN, (c) Stainless steel, and (d) DHS.

SEM images of scale deposits, affected by the existence of Mg^{2+} in the system, formed on different modified surfaces are shown in Figure 4.15. The existence of Mg^{2+} in the bulk solution has affected the morphology of the calcite crystals on different modified surfaces. In addition, Mg^{2+} has affected the aragonite crystals by having such crystals with low aspect ratio formed as needle-like bundles all over the surface (see Figure 4.16).

More discussions on the morphological studies of the carbonate-dominated scale deposits will be presented in Chapter-7. However, the author believes that more work

needs to be done to assess the effect of the modified surfaces on the morphology of the crystals forms on surfaces.

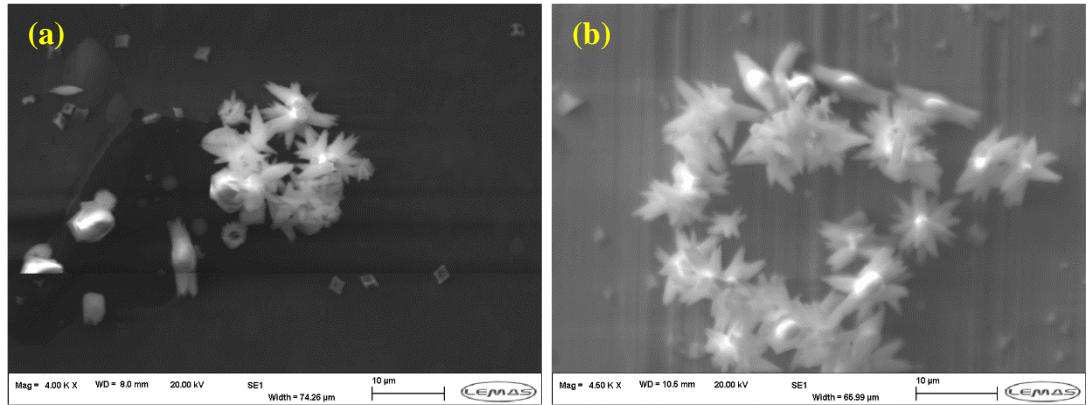


Figure 4.16. SEM images of scale deposits on modified surfaces: (a) DHS and (b) Stainless steel; formation of aragonite (needle-like bundles) with low aspect ratio with an orientation parallel to the surface.

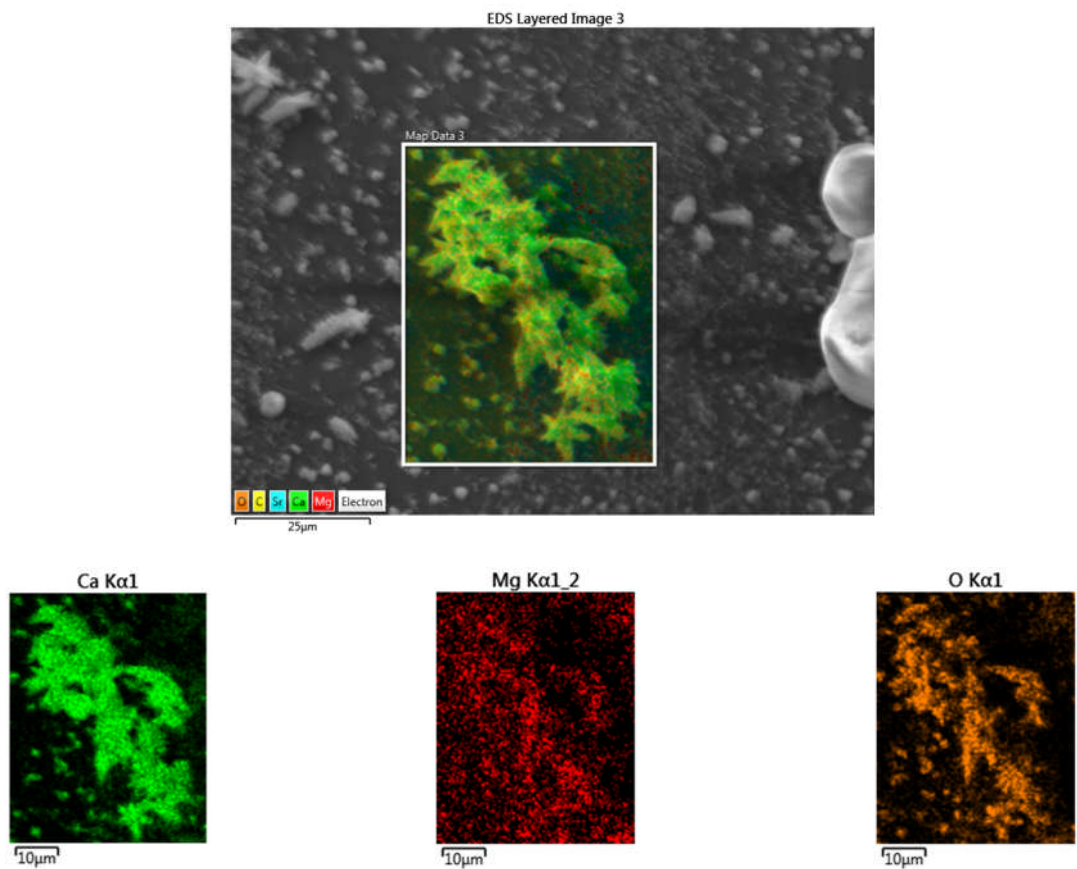


Figure 4.17. EDX images of scale deposits: the presence of magnesium in the lattice of calcium carbonate (aragonite).

4.5. EDX analysis of scale deposits

By using the EDX technique, the elemental composition of the scale deposits formed on the surface is shown in Figure 4.17., and it seems that the existence of Mg^{2+} not only affects the morphology of calcite crystals (see Figure 4.15), but also the morphology of aragonite crystals (see Figure 4.17), e.g. the formed aragonite crystals have low aspect ratio.

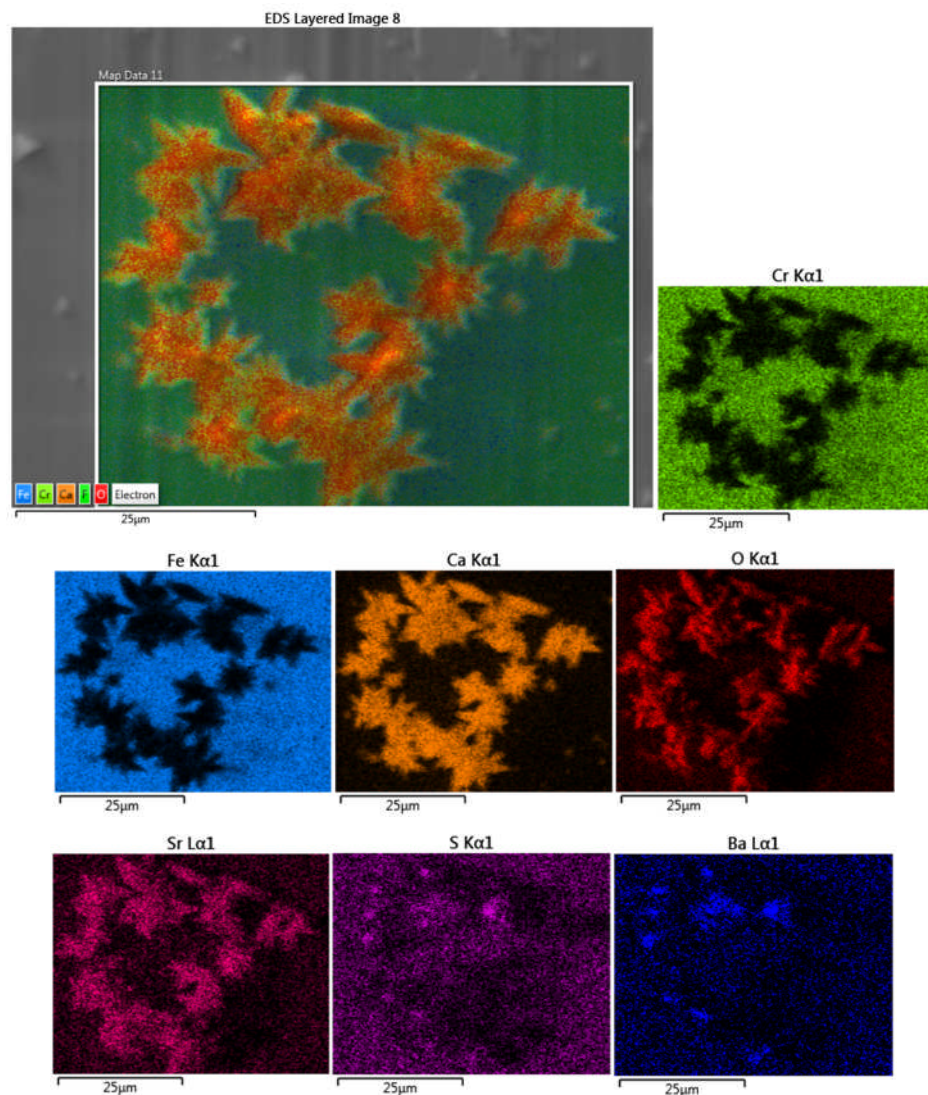


Figure 4.18. EDX analysis of surface scale formation (surface deposition of $CaCO_3$, $SrCO_3$ and $BaSO_4$)

As shown in Figure 4.18, by using the EDX technique, the scale deposits formed on the surface are characterised and apart from calcium carbonate, the existence of elements such as barium, strontium, sulphate are evident that can be accounted for the

formation of BaSO_4 and SrSO_4 (which are in agreement with their supersaturation ratio value) or the co-precipitation of such crystals together.

The EDX images of the scale deposits formed on stainless steel and DHS are shown in Figure 4.19 and Figure 4.20, respectively. The incorporation of the strontium in the lattice of calcite and aragonite are different, irrespective of the modified surfaces. The incorporation of strontium in the lattice of the latter is higher than that of the former crystals on both surfaces.

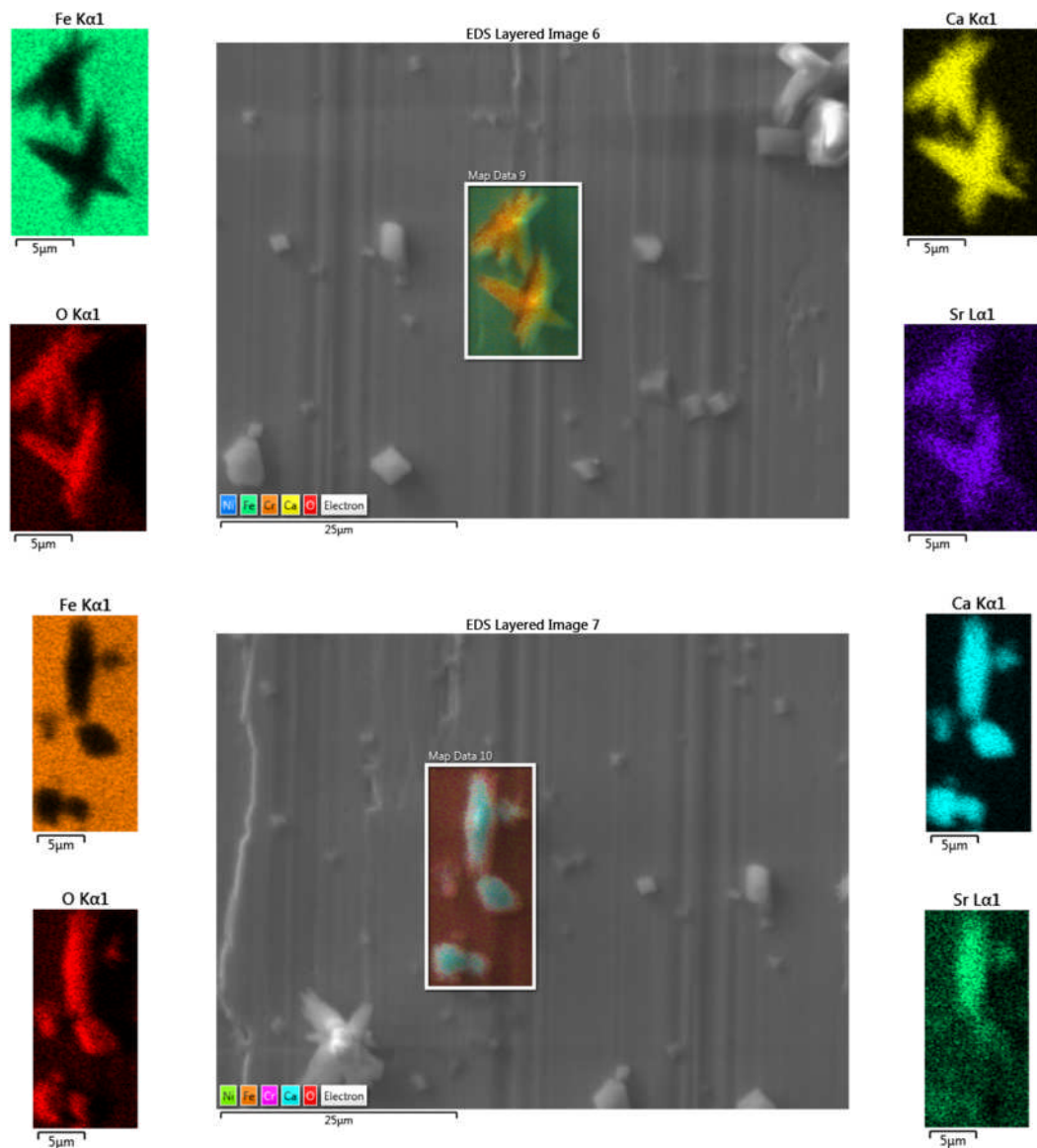


Figure 4.19. EDX images of scale deposited on the stainless steel surface: the incorporation of strontium in the lattice of aragonite, but not the calcite.

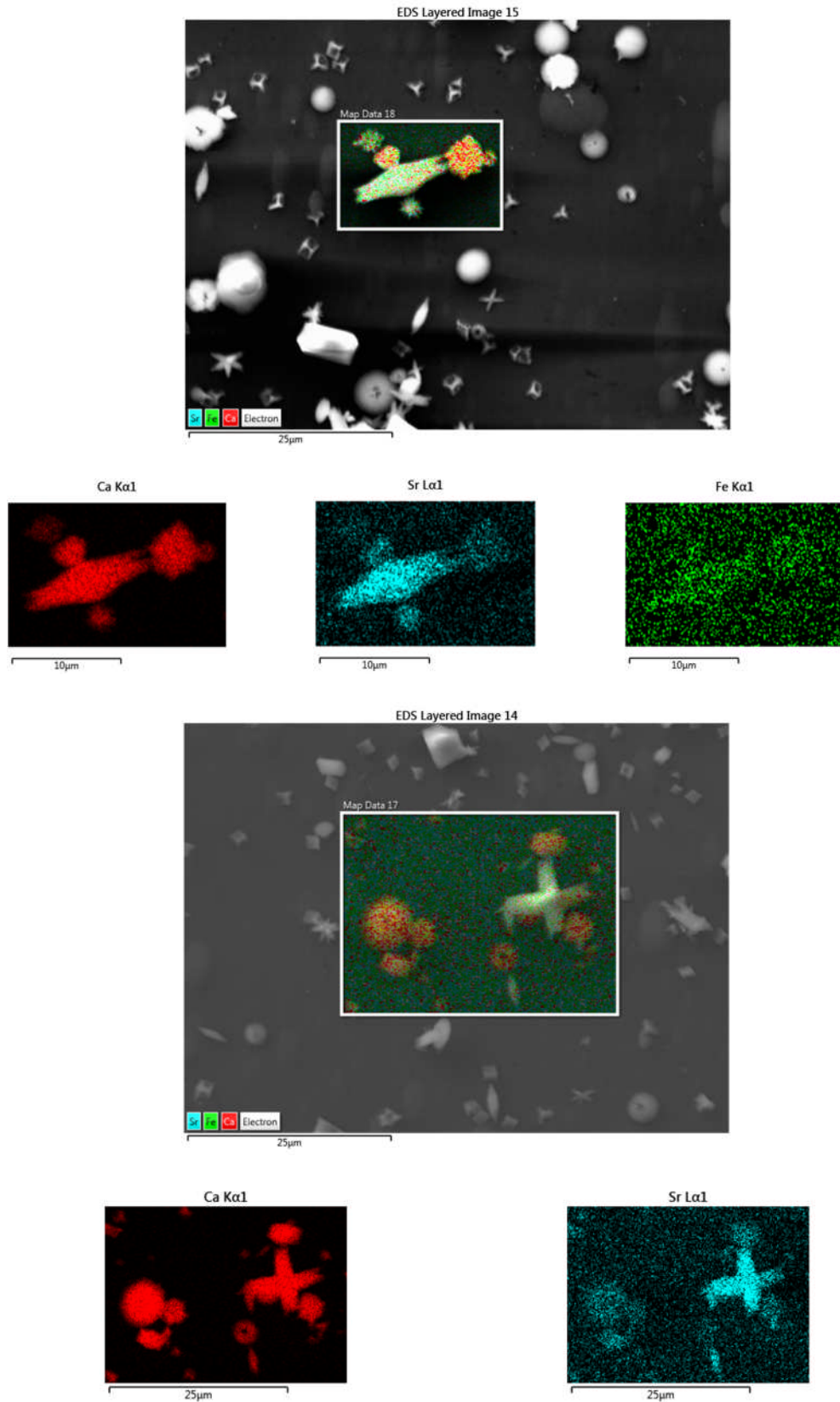


Figure 4.20. EDX images of scale deposits on DHS surface: incorporation of strontium in the lattice of aragonite is higher compared to both calcite and vaterite.

The author will discuss the co-precipitation of the scale deposits in more details in chapter-7.

4.6. ICP analysis of scale deposits

In order to demonstrate the ion concentration of the scale deposits on the surface, Inductively Coupled Plasma (ICP) measurements were made.

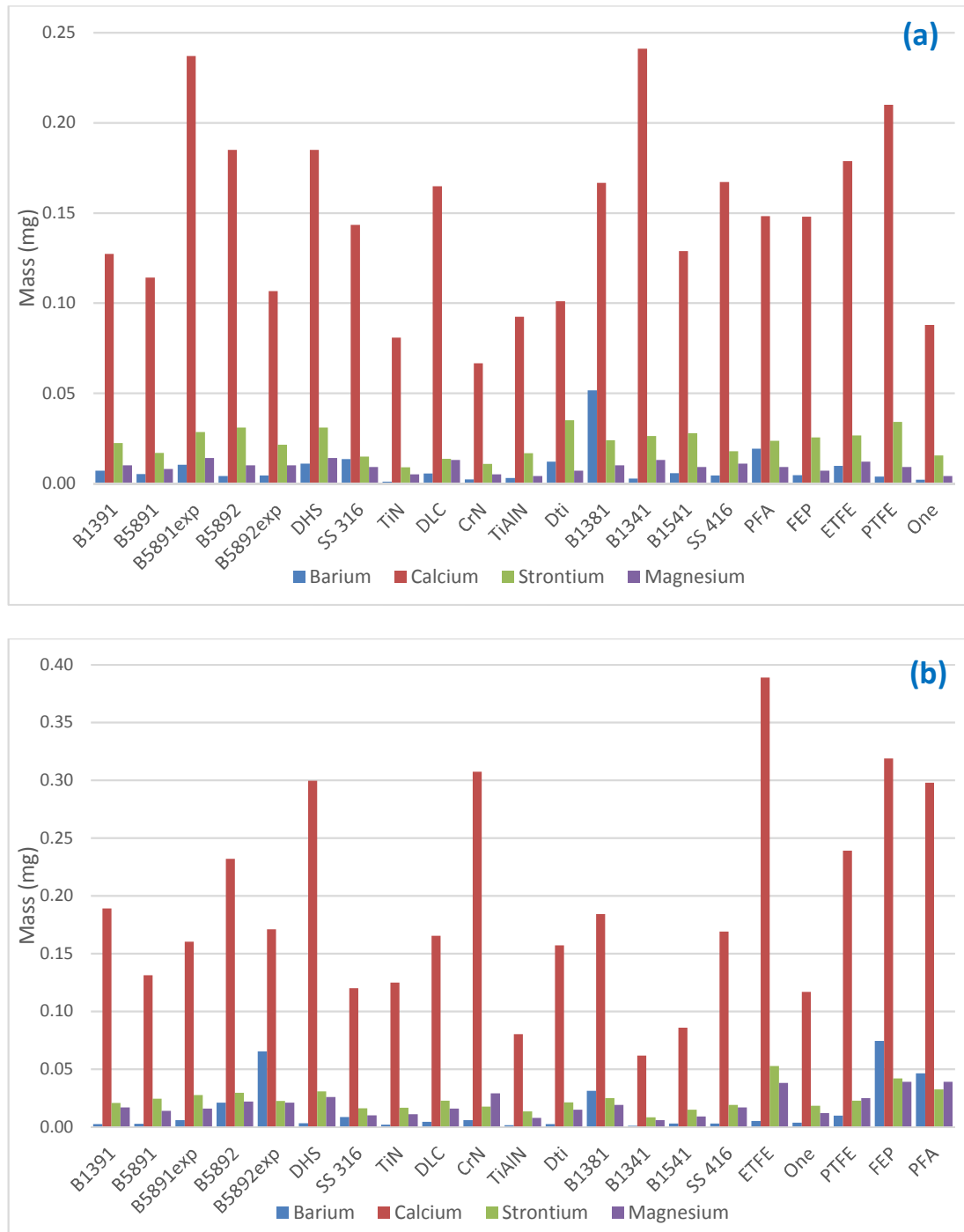


Figure 4.21. ICP results of the scale deposits in the *deposition* tests presented in mass gain: (a) Laminar and (b) Turbulent flow conditions.

The ion concentration of calcium, magnesium, strontium and barium in both laminar and turbulent flow conditions are shown in Figure 4.21 and Figure 4.22 by their mass gain values for the *deposition* and *adhesion* processes, respectively.

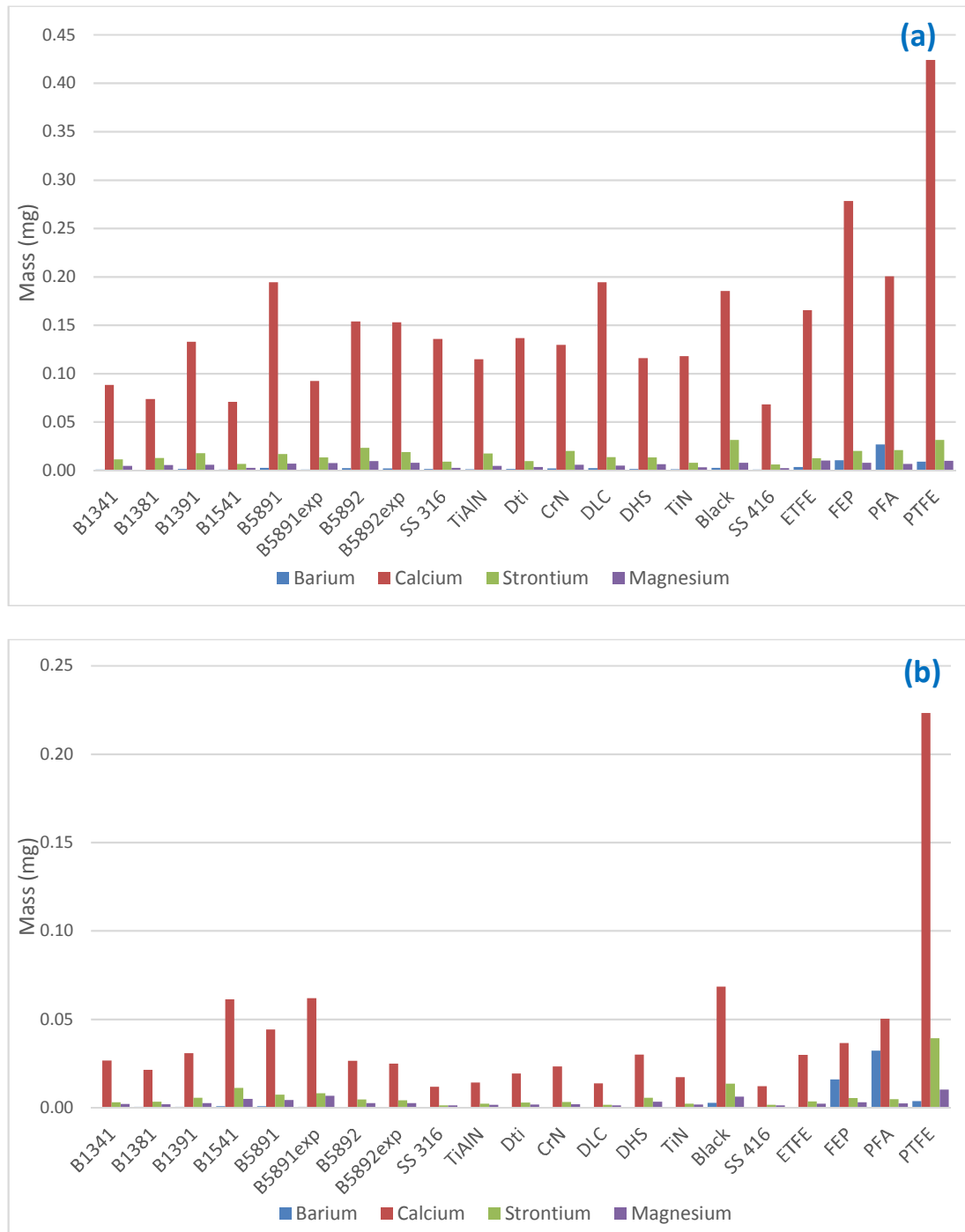


Figure 4.22. ICP results of the scale deposits in the *adhesion* tests presented in mass gain: (a) Laminar and (b) Turbulent flow conditions.

By comparing the results in both the *deposition* (see Figure 4.21) and the *adhesion* (see Figure 4.22) tests, the following findings can be addressed:

- The predominant existence of the calcium ions in the carbonate-dominated brine is quite distinguishable.
- In the *deposition* tests, the calcium ratio in the formed scale deposits on the modified surfaces is higher in the *adhesion* tests.

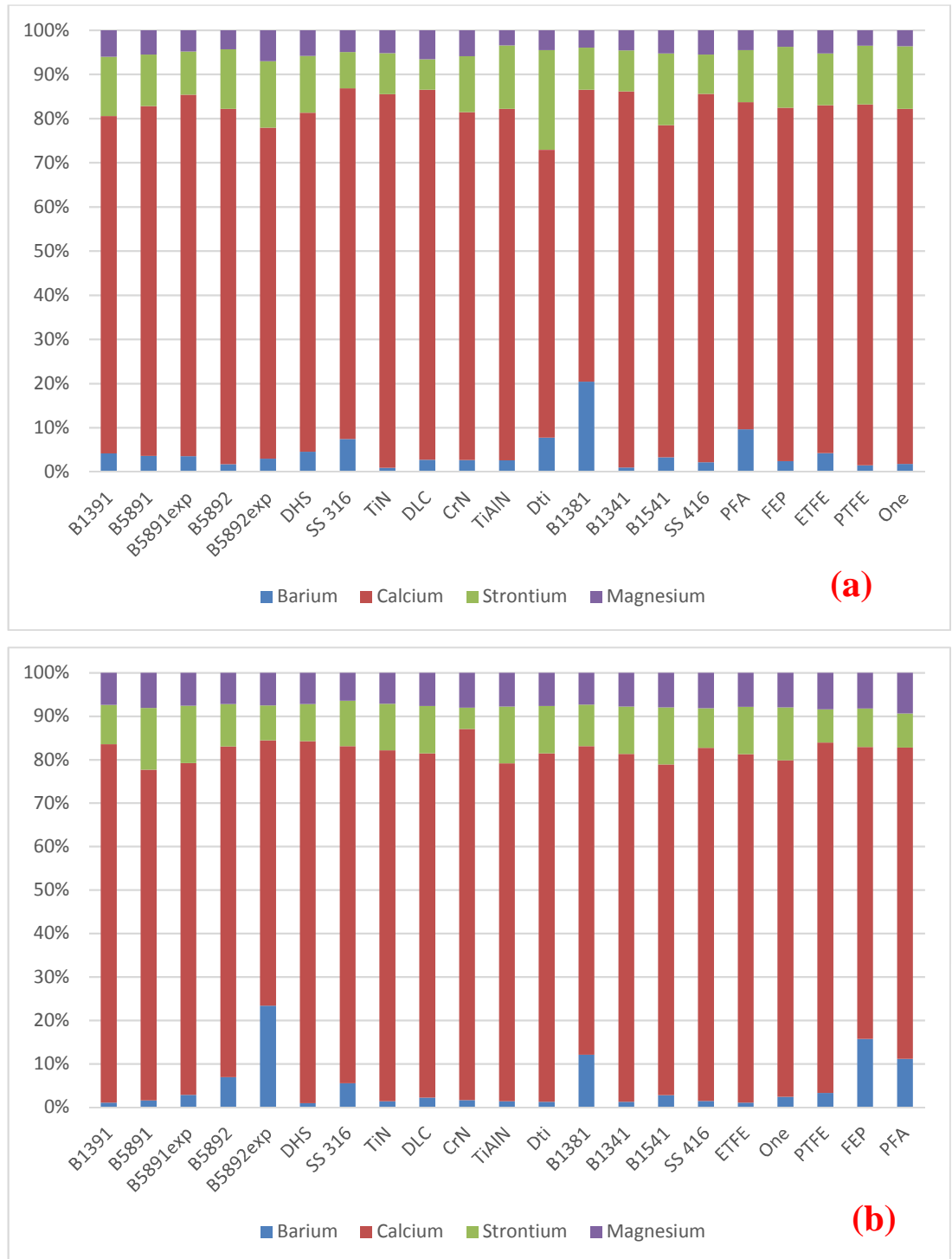


Figure 4.23. Mole percentage of barium, calcium, strontium and magnesium existing on the surface as scale deposits in the *deposition* process: (a) Laminar and (b) Turbulent flow conditions.

- The magnesium ions play a major role in the mechanism and the morphology of the carbonate-dominated scale deposits.
- The agitation level or the turbulence level of the flow has a low impact on the ratio of the ions formed in the scale deposits in processes.

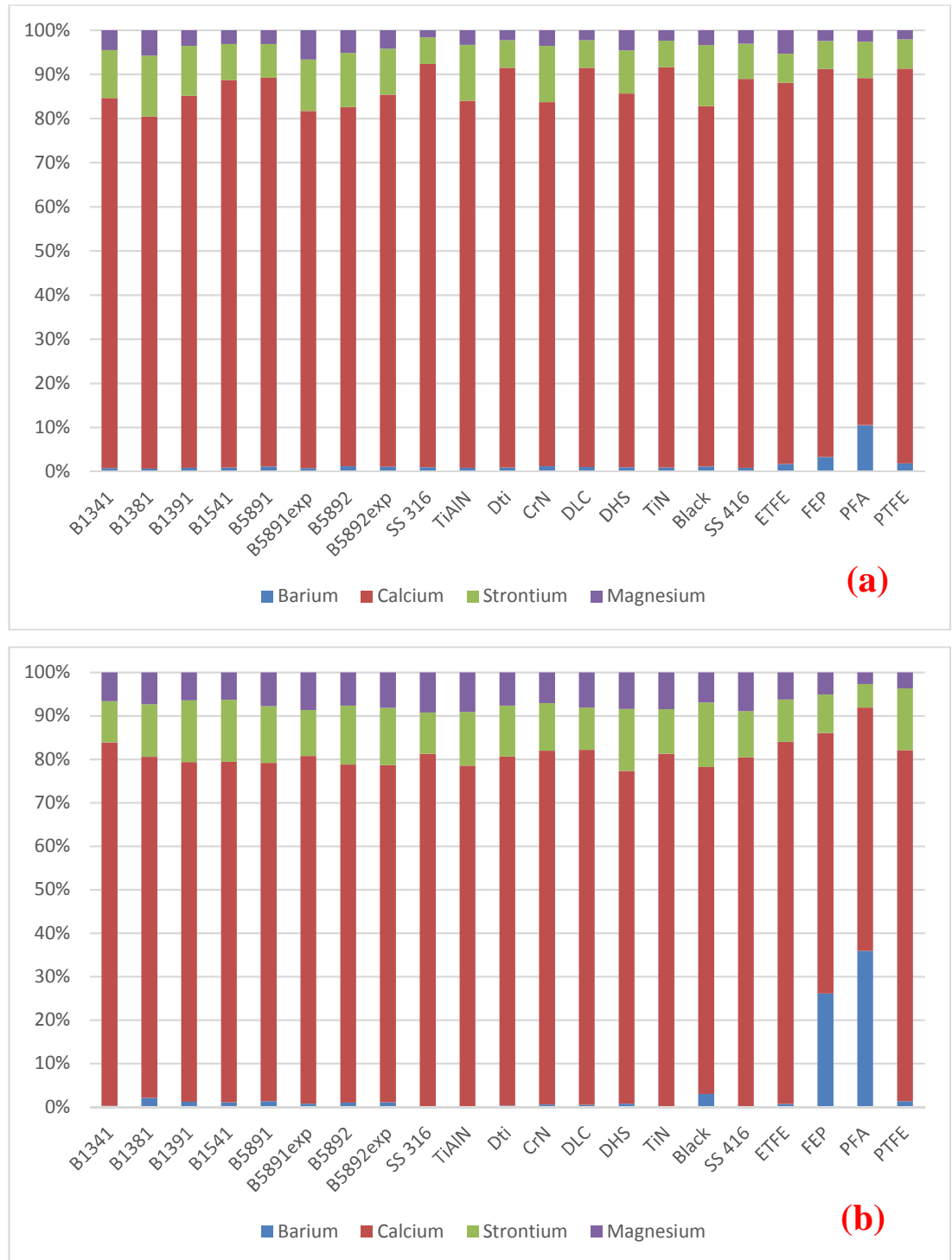


Figure 4.24. Mole percentage of barium, calcium, strontium and magnesium existing on the surface as scale deposits in the *adhesion* process: (a) Laminar and (b) Turbulent flow conditions.

The mole percentage of the ions, e.g. barium, calcium, strontium and magnesium, presented in the scale deposits on different modified surfaces for laminar and turbulent flow conditions are shown in Figure 4.23 and Figure 4.24 for *deposition* and *adhesion* processes, respectively.

Considering the formation of calcium carbonate, barium sulphate and strontium sulphate as scale deposits on modified surfaces, as shown in Figure 4.23 and Figure 4.24, the following aspects can be addressed:

- Calcium is the most abundant ion which conveys the idea that the calcium carbonate is the predominant scale deposits formed on the surface.
- The existence of barium can be attributed to the fact that the supersaturation ratio of the barium sulphate is more than unity and thermodynamically there is a chance of the precipitation of such crystals in the bulk and its deposition onto the surface.
- The hydrodynamic effects have not affected the incorporation of strontium ions in the scale deposits, while the density coefficient of the magnesium ions has increased by the agitation level of the bulk solution.
- The modified surfaces do not have much effect on the chemical composition of the scale deposits, but the author believes that more studies need to be conducted in this area to reach to a conclusive assessment.

4.7. Summary

The surface scale formation tests for a wide range of modified surfaces, which are commercially-available, were carried out as two different processes known as “deposition process” or heterogeneous nucleation and crystal growth, and “adhesion process” or the adherence of the pre-crystallized particles onto the surface in two hydrodynamic conditions known as laminar and turbulent flow conditions. The scaling tests have been done in a carbonate-dominated brine which is supersaturated with respect to calcium/strontium carbonate and barium sulphate and is prepared to provide the same brine composition as in the Brazilian oil basins. This chapter can be summarised as the followings:

- Due to the high supersaturation ratio of the carbonate-dominated brine, the induction period of the bulk is within a minute and the nucleation process is instantaneous for all the tests.

- The scaling tendency of the ceramic coatings in both the *adhesion* and the *deposition* tests in both laminar and turbulent conditions were the lowest. In other words, ceramic coatings had the best performance and mainly the fluoropolymer coatings had poorer performance.
- The scaling tendency of the heterogeneous nucleation and crystal growth is higher than the adherence of the pre-crystallised scale particles.
- To enhance the feasibility of certain modified surfaces, the scaling tendency rate has been translated into the scaling growth in a year.
- The level of turbulence favours the rate of scaling in the *deposition* tests, while in the *adhesion* tests it reduces the scaling rate.
- The behaviour of scale formation on the surface will change with respect to the level of turbulence of the bulk, i.e. in the *deposition* process, the surface scale deposits are formed rather scattered in turbulent flow conditions and localised in laminar flow conditions, and in the *adhesion* process, the surface scale deposits in both flow conditions are formed in scattered formation, however, in turbulent conditions the presence of localised scale sites is noticeable.
- There are diverse morphologies formed on different modified surfaces. The surface chemistry will affect the morphology of the crystals on the surfaces.
- The most dominant crystals formed on the surfaces in the *adhesion* process are calcite crystals with rounded edges. There is a trace of needle-like aragonite on some surfaces (e.g. DTi and One).
- In the *deposition* process, all three main polymorphs of crystals exist, i.e. calcite, aragonite and vaterite. Unlike the *adhesion* tests, the dominant crystals

formed on the surfaces are aragonite and vaterite. The needle-like aragonite crystals formed on the surfaces have a lower aspect ratio compared to the literature and they tend to form on the surfaces as a bundle.

- Even in the *adhesion* process, the heterogeneous nucleation and crystal growth is in progress and is distinguishable for most of the modified surfaces.
- In the *deposition* tests, the occurrence of secondary nucleation on calcite crystals is apparent.
- The calcium ion ratio in the scale deposits in the *deposition* tests is higher compared to the *adhesion* tests.
- The flow conditions have low effect on the ratio of the ions formed in the scale deposits.

Chapter 5

Results of Sulphate-dominated Brine

5.1. Introduction

In this chapter, both the *deposition* and *adhesion* processes are applied in a supersaturated brine referred to as the sulphate-dominated brine. Since the supersaturation ratio of such brine is more than unity, the formation of BaSO₄, SrSO₄, CaCO₃ and SrCO₃ scale deposits are thermodynamically possible.

The mass gain of each modified substrate is presented for both flow regimes in *deposition/adhesion* processes. The scale deposits on the surfaces are analysed by SEM, EDX and ICP analyses to have a better understanding of the morphology of the crystals and chemical composition of them, as well as having an insight into the co-precipitation/co-deposition of the formed crystals.

5.2. Surface scale deposition of sulphate-dominated brine

Deposition tests: The scaling tendency test for the *deposition* tests have been carried out for all the modified surfaces for the period time of 90 minutes which starts from the time that the brines were mixed together and the samples were submerged into the sulphate dominated brine composition. In the *deposition* tests, when the coupon is immersed into the brine solution, the saturation ratio is at its highest rate initially and then progressively decreases during the test. The mass gain of scale deposits formed on different modified surfaces in the *deposition* process, where the focus is on heterogeneous nucleation and crystal growth is shown in Figure 5.1.

As shown in Figure 5.1, the chemical composition has not much effect on the scaling tendency of the modified surfaces in the *deposition* process for the sulphate-dominated brine composition. In other words, in both the laminar and turbulent conditions for the *deposition* process, the anti-scaling performance of different groups of coatings does not follow a specific trend. For instance, in both laminar and turbulent conditions, the performance of the ceramic coatings in terms of anti-scaling characteristics can be defined with both good (e.g. TiN or DLC) and bad (CrN-Ag or DTi) quality.



Figure 5.1. Scale deposits formed on different modified substrates in the deposition tests, where the focus is on heterogeneous nucleation and crystal growth, in (a) laminar and (b) turbulent conditions.

As a result, the performance of each coating needs to be assessed separately according to its surface characteristics. In laminar conditions, the “B1381” coating has a poor performance while in the turbulent conditions its anti-fouling characteristic has shown promising results, or the best anti-scaling performance can be attributed to the “B5891” coating in both laminar and turbulent conditions in the *deposition* process. The good anti-scale performance of DLC and TiN is independent of the bulk flow regime, while PFA has poor performance in both flow conditions.

In order to show the measured mass gains of different modified substrates to a better indicator, the results can be interpreted into the annual scale deposits thickness growth, at both laminar and turbulent conditions. Based on the ICP and SEM results, it has been assumed that the scale deposits are made of the mixture of 40% of BaSO₄ with a density of 4.5 g.cm⁻³, and 60% of SrSO₄ with a density of 9.96 g.cm⁻³. As a result, the density of the scale formed on the surface is around 4.176 g.cm⁻³, provided that the deposited scale on the substrates is fully dense. Therefore, each value of the mass gain per area can be multiplied by 0.71 to get the value as the growth rate of scale deposits on the surface in cm.year⁻¹.

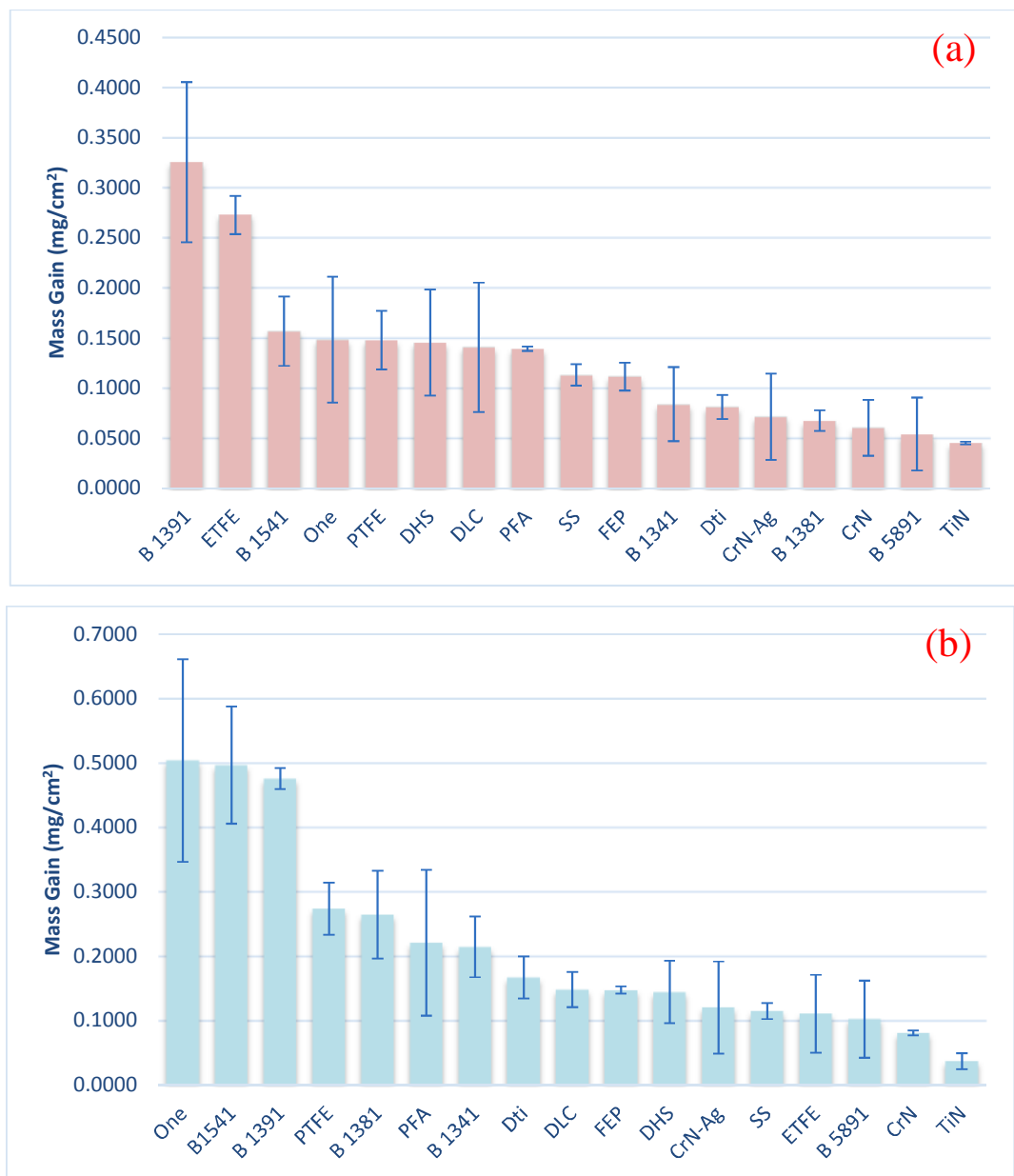


Figure 5.2. Scale deposits thickness growth of different modified substrates in the *adhesion* tests, where the focus is on *adhesion* of pre-precipitated of scale crystals, in (a) laminar and (b) turbulent conditions.

The scale deposit thickness growth rate ($\text{cm}\cdot\text{year}^{-1}$) for the *deposition* process in the laminar flow conditions ranges from 0.159 (B5891, epoxy coating), to 0.388 (ETFE, Fluoropolymer coating), while in the turbulent flow conditions the scale deposits thickness growth ranges between 0.257 (B5891, epoxy coating) and 0.974 (One, fluoropolymer coating). By comparing the results, it conveys the idea that the agitation level of the bulk solution is in favour of surface scale deposition in the *deposition* process.

Adhesion tests: The scaling tendency test for the *adhesion* tests have been carried out for all the modified surfaces for the period time of 90 minutes. The main difference with the previous scenario can be attributed to the time of the submergence of the coupon in the mixed sulphate-dominated brine. At this time, the brine solutions were already mixed together and the mixed brine composition has reached to an equilibrium state where the rate of the scale formation (i.e. crystal formation) in the brine is in balance with the crystal dissolution in the brine. In such tests, the saturation ratio has reached a stable value before the insertion of the coupons into the brine solution.

The mass gain of scale deposits formed on different modified surfaces in the *adhesion* process, where the focus is on the adhesion of the pre-precipitated scale onto the surface, are shown in Figure 5.2.

Like the *deposition* process, in the *adhesion* process not certain groups of coatings have better performance, however, the ceramic coatings' performance is much better compared to another type of coatings. It is also noticeable that the anti-scaling characteristics performance of the coatings in the sulphate-dominated brine composition is independent of the scaling mechanism. In other words, the coatings with good anti-scaling characteristics in the *deposition* process, have the same performance in the *adhesion* process, and vice versa. For instance, the "B5891", which is an epoxy coating, and TiN, which is a ceramic coating, have a good anti-scaling tendency performance in both *adhesion* and *deposition* processes, while the "One", which is a fluoropolymer coating has poor anti-scaling performance in both processes. However, the anti-scaling performance of some coatings, such as the coating "B1391", is depending on the scaling mechanisms. For example, "B1391" has a good anti-scaling performance in the *deposition* process, while in the *adhesion* process it can be categorised as one of the coatings with poor performance.

The results can be expressed as scale thickness growth ($\text{cm}\cdot\text{year}^{-1}$) by multiplying the mass gain results ($\text{mg}\cdot\text{cm}^{-2}$) by the value of 0.71. Therefore, for the *adhesion* process in the laminar flow regime it ranges from 0.063 (TiN, ceramic coating) to 0.455 (B1391, epoxy coating), while in the turbulent flow regime the scale deposits thickness growth ranges in between of 0.052 (TiN, ceramic coating) – 0.705 (One, fluoropolymer coating). Like the *deposition* process, the agitation level is in favour of surface scale *deposition* in the *adhesion* process.

More discussions on the hydrodynamic effects on the surface scale depositions in both *adhesion* and *deposition* processes will be presented in chapter-7.

5.2.1. SEM and EDX study of scale deposits

As part of the qualitative assessment, the Scanning Electron Microscopy (SEM) technique has been applied to study the morphology of the crystals and the way that they are formed on the surfaces for both laminar and turbulent flow conditions in the sulphate-dominated brine composition.

Adhesion process: The scale crystals formed on the surfaces in the sulphate-dominated brine in the turbulent conditions are shown in almost most of the modified surfaces from Figure 5.3a to Figure 5.3n.

As shown in Figure 5.3 (*a, b, g, h, j, k, and l*) most of the crystals formed onto the surface are needle-like crystals which has not propagated and widen from their both ends, yet; while in Figure 5.3 (*e, f, i, m, and n*) the crystals have started to propagate from their both ends to shape like a dumbbell (or bowtie).

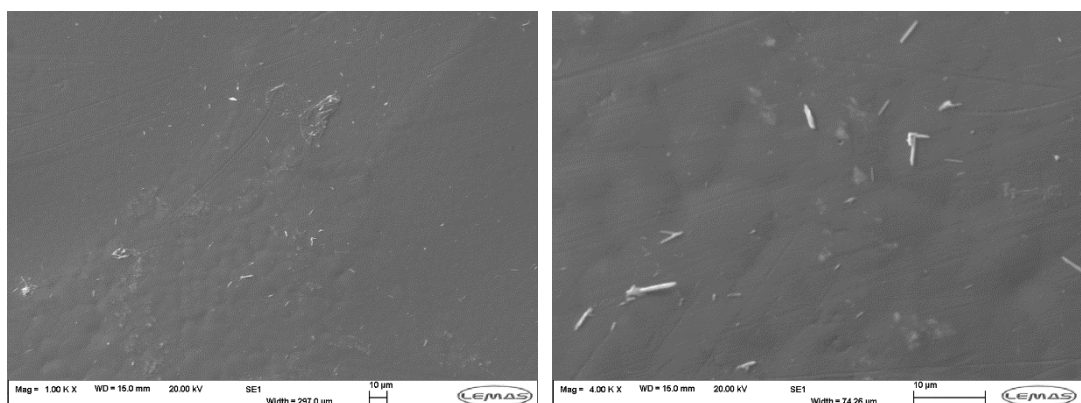


Figure 5.3a: B1341 – SEM images of scale deposits at different magnitudes, the formation of needle-like crystals with high aspect ratio.

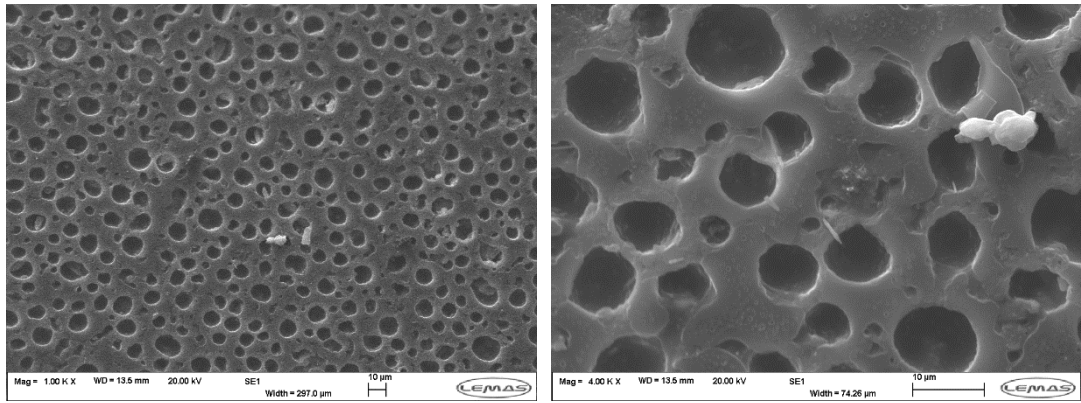


Figure 5.3b: B1381 – SEM images of scale deposits at different magnitudes, the formation of needle-like crystals with high aspect ratio.

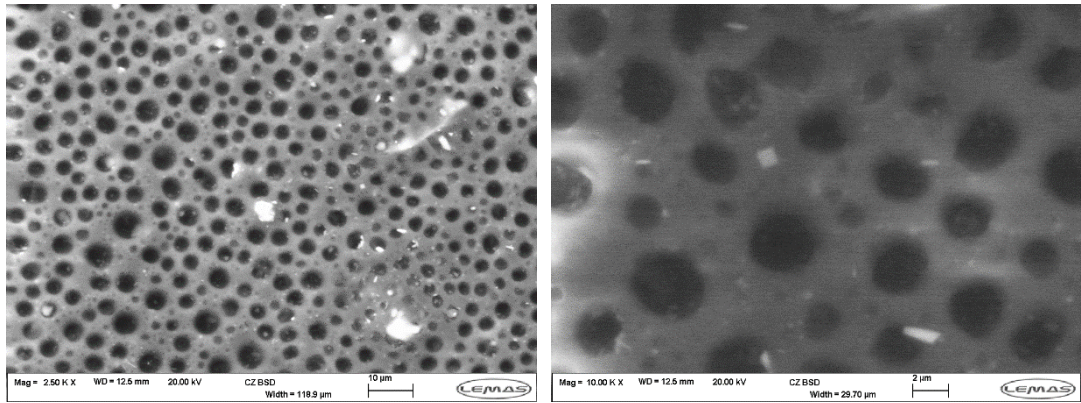


Figure 5.3c: B1391 – SEM images of scale deposits at different magnitudes, irregularities on the surface reduce the anti-fouling performance of the coating.

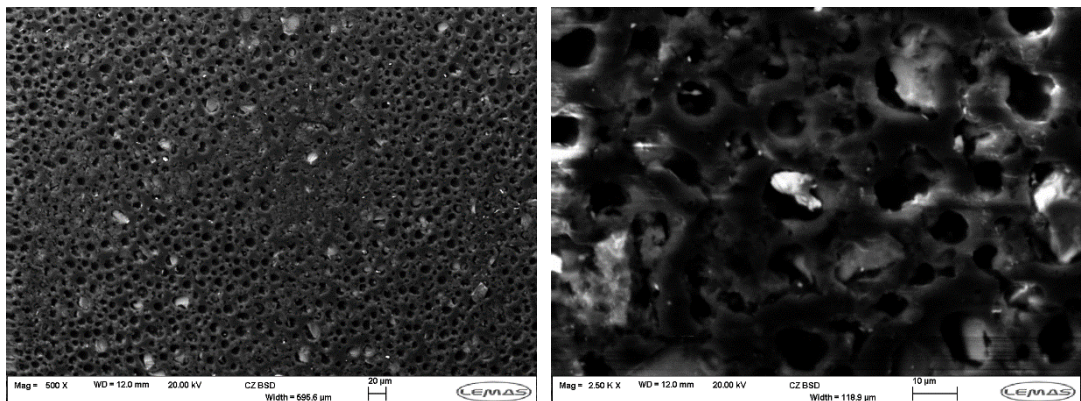


Figure 5.3d: B1541 – SEM images of scale deposits at different magnitudes, irregularities on the surface reduce the anti-fouling performance of the coating.

A good surface finish will improve the anti-scaling tendency of a modified surface. As shown in Figure 5.3 (b, c, d and e), in such surfaces (mostly epoxy coatings) the scale crystals are formed mainly at the edges of such irregularities on the surfaces.

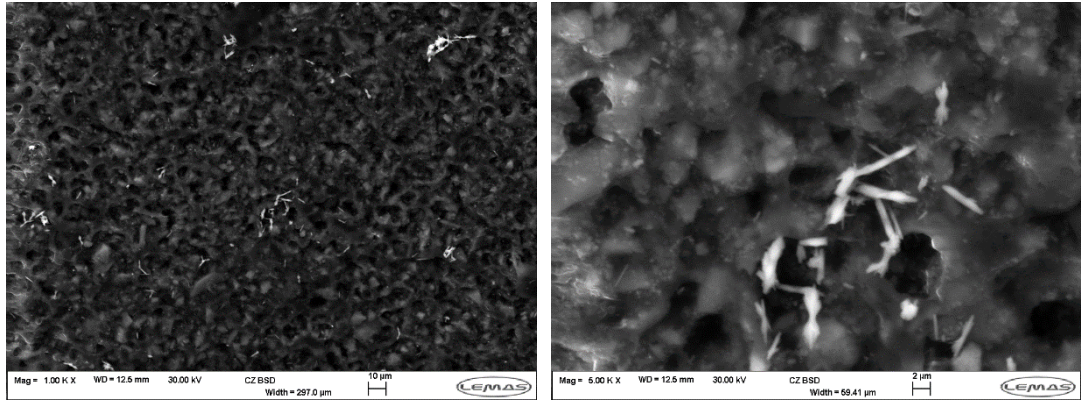


Figure 5.3e: B5891 – SEM images of scale deposits, the formation of scale crystals shaped as a dumbbell or bowtie.

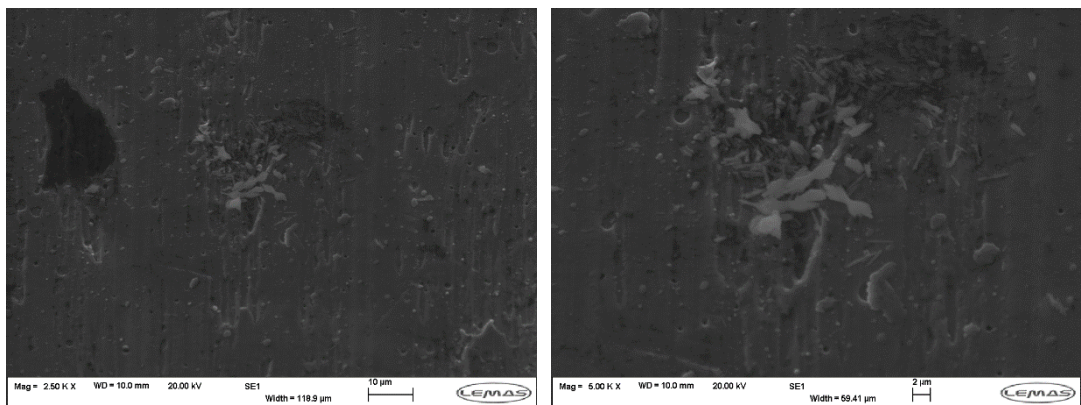


Figure 5.3f: CrN – SEM images of scale deposits, needle-like crystals have propagated from their both ends to shape a bowtie.

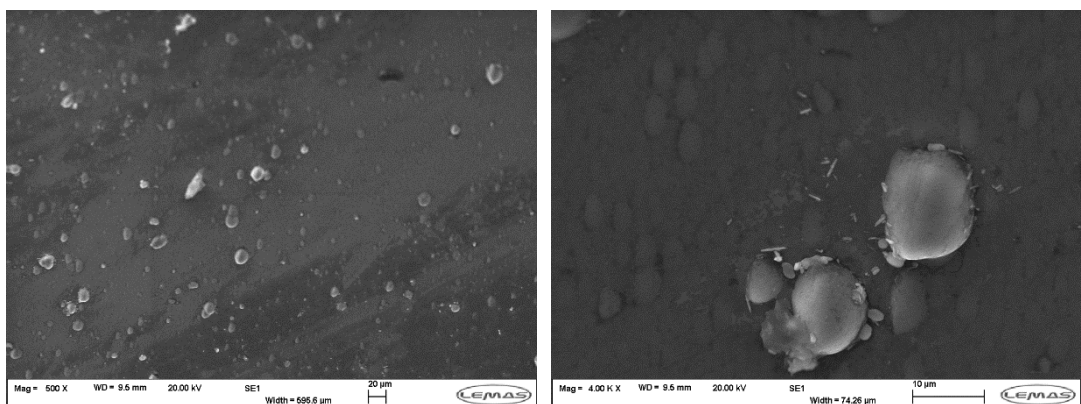


Figure 5.3g: DHS – SEM images of scale deposits, surface imperfections can entangle scale deposits on the surface.

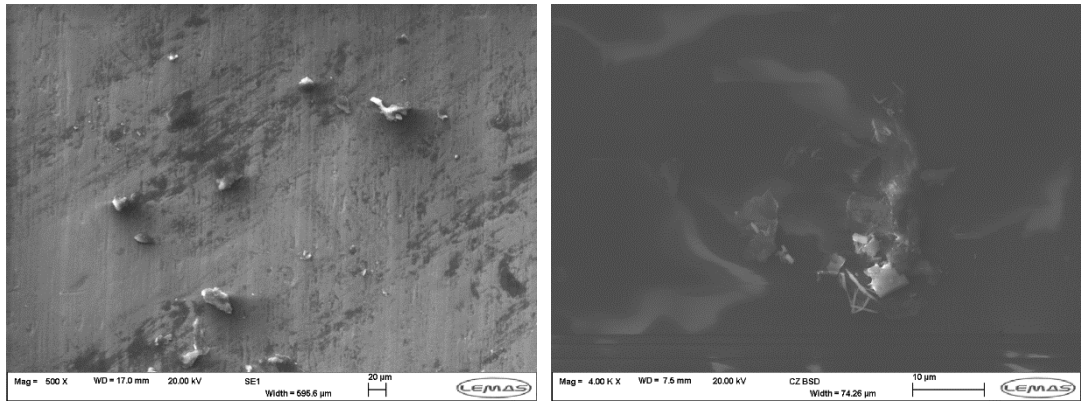


Figure 5.3h: DTi – SEM images of scale deposits, surface imperfections has undermined scaling performance of the surface.

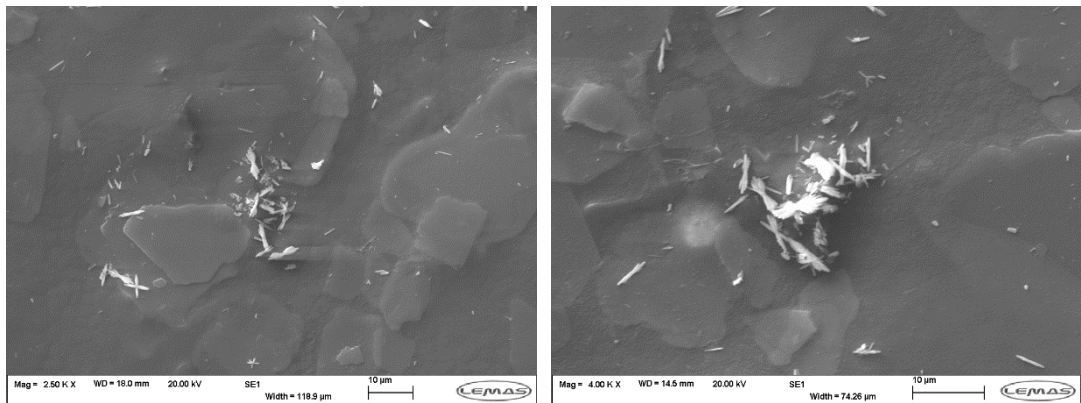


Figure 5.3i: ETFE – SEM images of scale deposits, crystals shape like needle-like crystals up to a limit, then starts to grow at both ends.

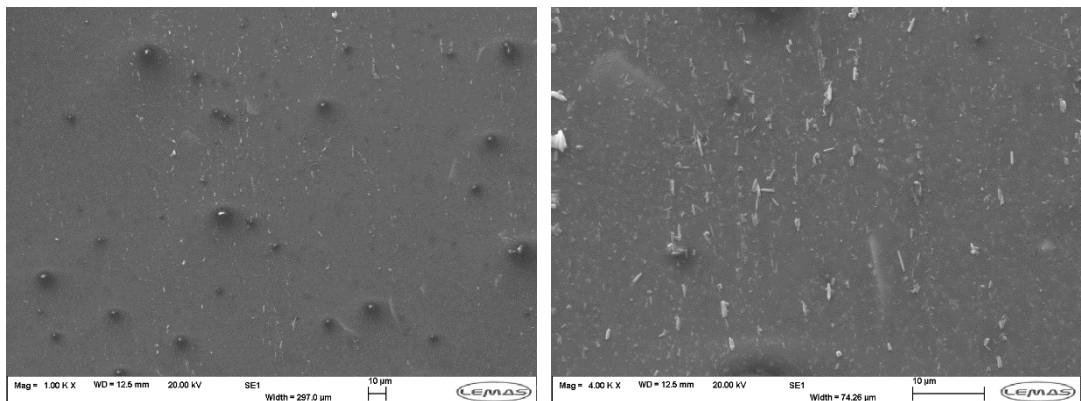


Figure 5.3j: FEP – SEM images of scale deposits, the formation of scattered needle-like crystals all over the surface.

It can be attributed to the fact that in such irregularities, esp. on the tips, the surface energy is at its highest rate and also the asperities of a surface is more exposed to the active ions in the bulk solution which will result in higher surface scaling rate at such regions.

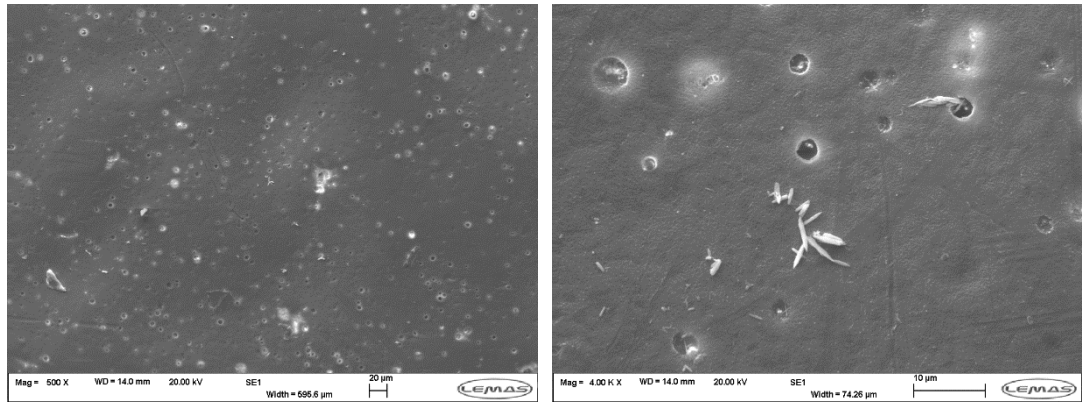


Figure 5.3k: PFA – SEM images of scale deposits, the formation of scattered needle-like crystals all over the surface.

In addition, surface imperfections cause the same problem. As shown in Figure 5.3 (g and h), the scale crystals are either formed or entangled by the imperfection sites on the surface.

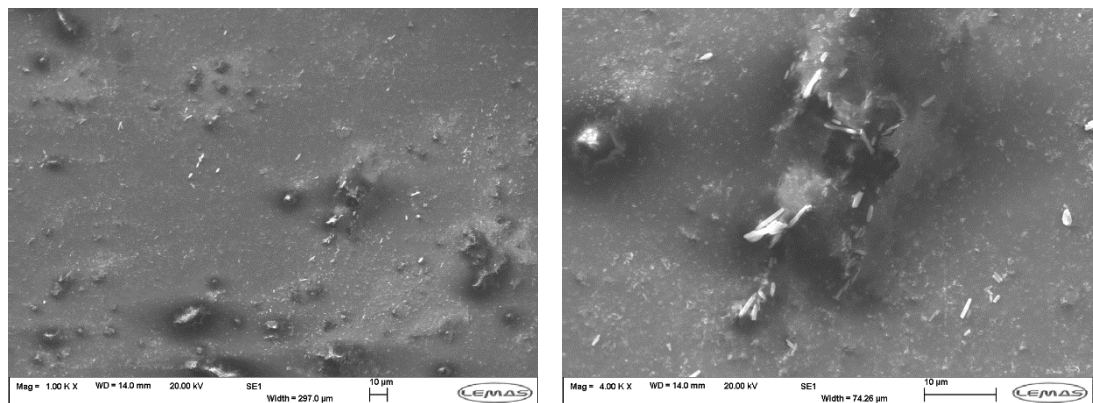


Figure 5.3l: PTFE – SEM images of scale deposits, surface imperfections and irregularities entangle the scale deposits in between of such irregularities, and increase the scaling tendency of the surface.

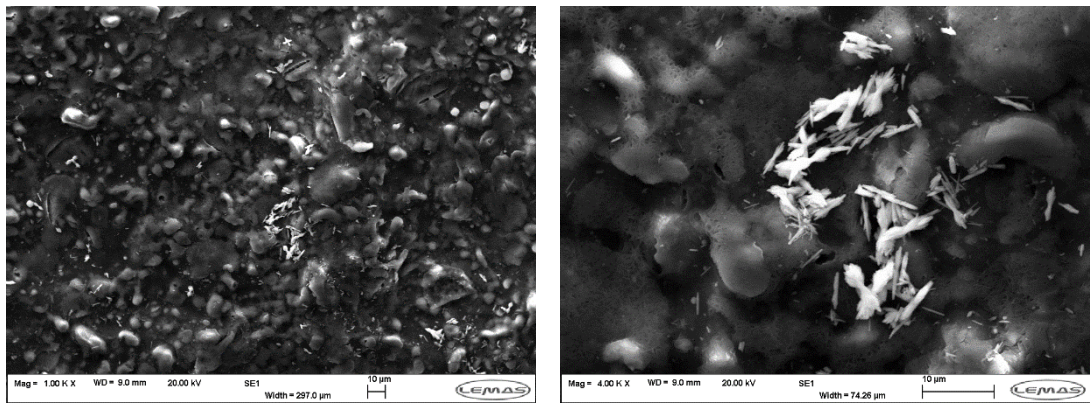


Figure 5.3m: “One” – SEM images of scale deposits, a rough surface (high in a number of peaks and valleys) increase the scaling tendency of the surface.

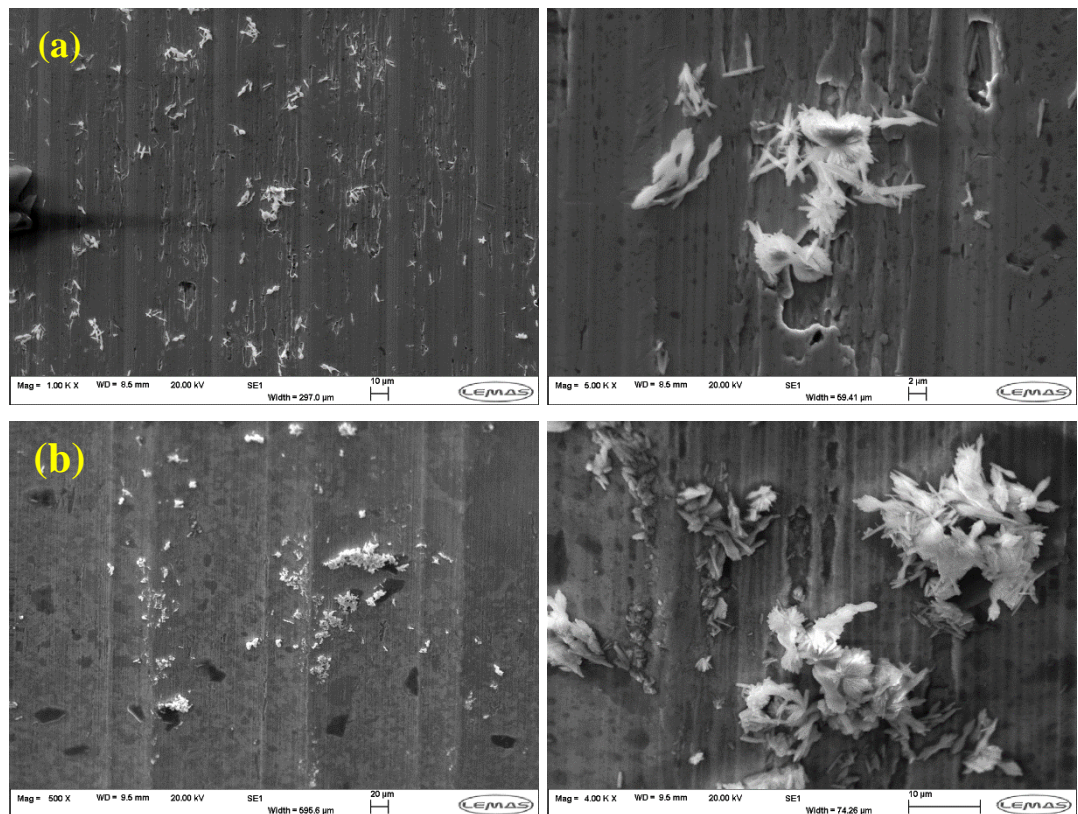


Figure 5.3n: (a) SS and (b) TiN – SEM images of the scale deposits, bundle scale deposits formed in concave regions of surfaces

Figure 5.3. SEM images of the scale deposits formed on different modified surfaces at different magnification range in the *adhesion* process for turbulent flow regime.

As shown in Figure 5.3, most of the crystals formed on the surfaces are predominantly needle-like with a proportion of bowtie-shape crystals. The scale deposits formed on

surfaces in the turbulent conditions are predominantly scattered all over the surfaces, not as a clump of crystals; rather, they are forming as a single crystal or a couple of crystals lying on the surfaces. However, on surfaces with a uniform periodic convex-concave topography (e.g. SS and TiN), there is a chance of scale formation as a bundle which occurs in the concave regions of the surface (see Figure 5.3n).

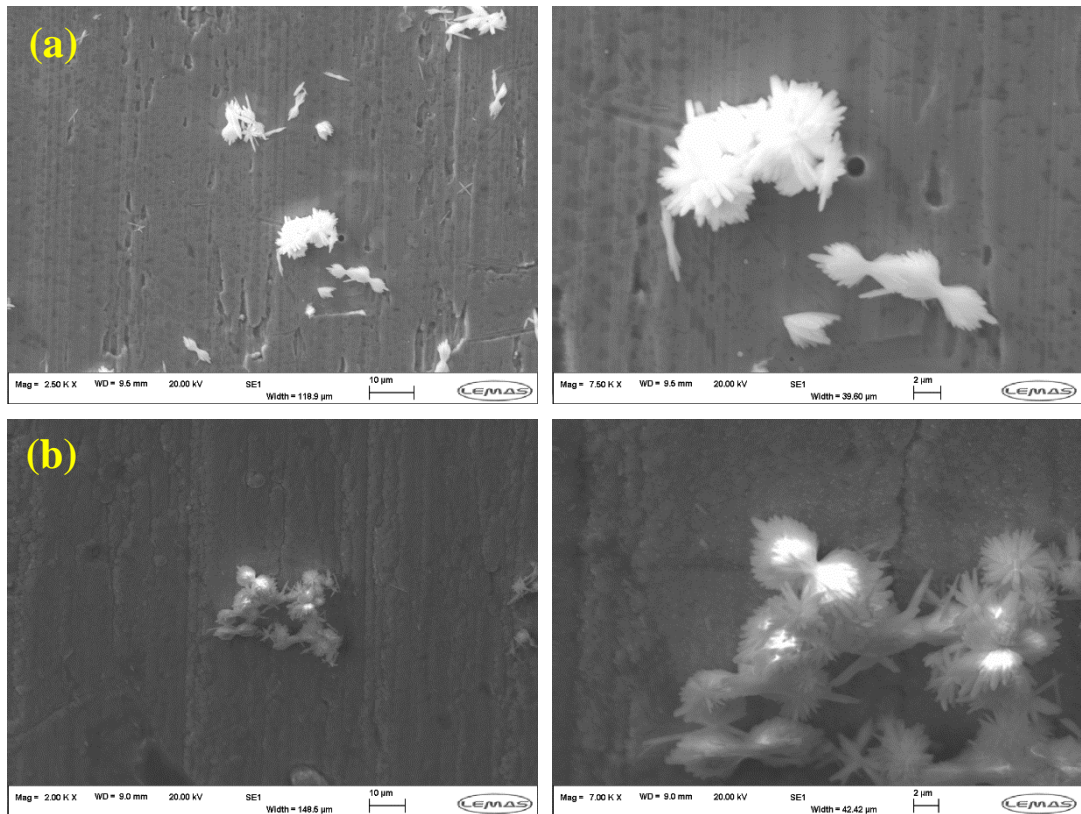


Figure 5.4a: (a) CrN and (b) CrNAg – SEM images of scale deposits, the formation of scale deposits as bowtie and sisal-like crystals.

As shown in Figure 5.4a to Figure 5.4c, the formation of scale deposits in the sulphate-dominated brine in the *adhesion* process in laminar flow conditions is rather more regional (less scattered) than in turbulent flow conditions. However, the author cannot come to a conclusion that such an occurrence can just be attributed to the effect of flow regime on the surface scaling behaviour. The rate of surface scaling on modified surfaces in the laminar flow conditions in the *adhesion* process was comparatively lower compared to the turbulent conditions, and all the SEM images are captured from a low quantity of existing scales on surfaces.

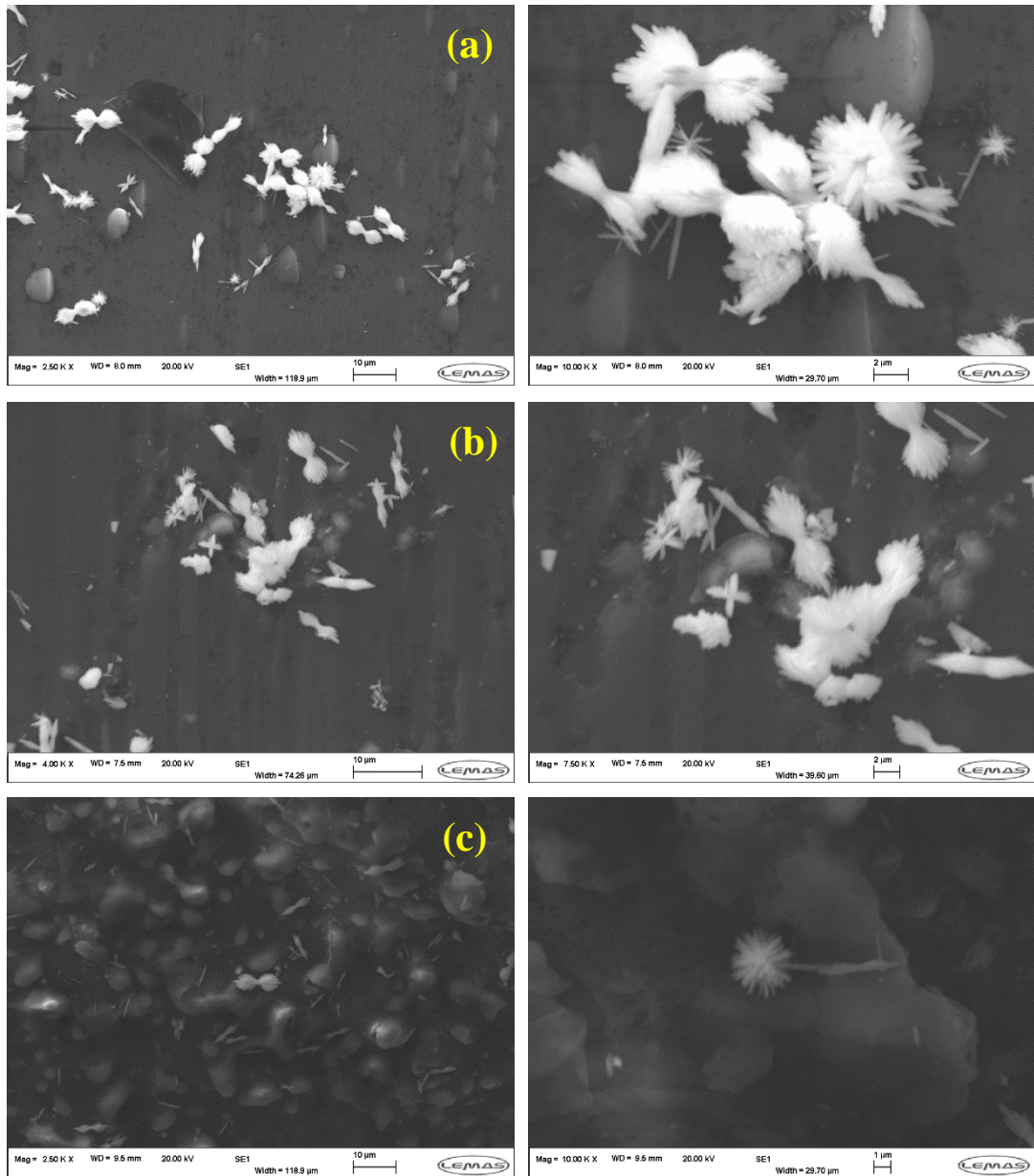


Figure 5.4b: SEM images of scale deposits for different modified surfaces: (a) DHS, (b) DLC, and (c) One – Surface has not much effect on the morphology of the scale deposits.

As shown in Figure 5.4 (a to c), in laminar flow conditions, a new shape of scale deposits, other than the turbulent flow conditions, formed on different modified surfaces, which is called “sisal-like” crystals. It seems that due to the lower agitation level of the bulk, the induced shear forces from the bulk to the crystals are relatively lower compared to turbulent conditions. In such systems, the crystals have the opportunity to propagate normal to the surface and still stick onto the surface, while in the turbulent flow conditions the propagated crystals in z-direction are already detached from the surface by relative high shear forces of the bulk, unless the scaling phenomena occurs either fast enough to bond with adjacent crystals (is true at higher

saturation ratio value) or heterogeneous nucleation starts all over the surface (is true when there is a *deposition* process, not *adhesion* process).

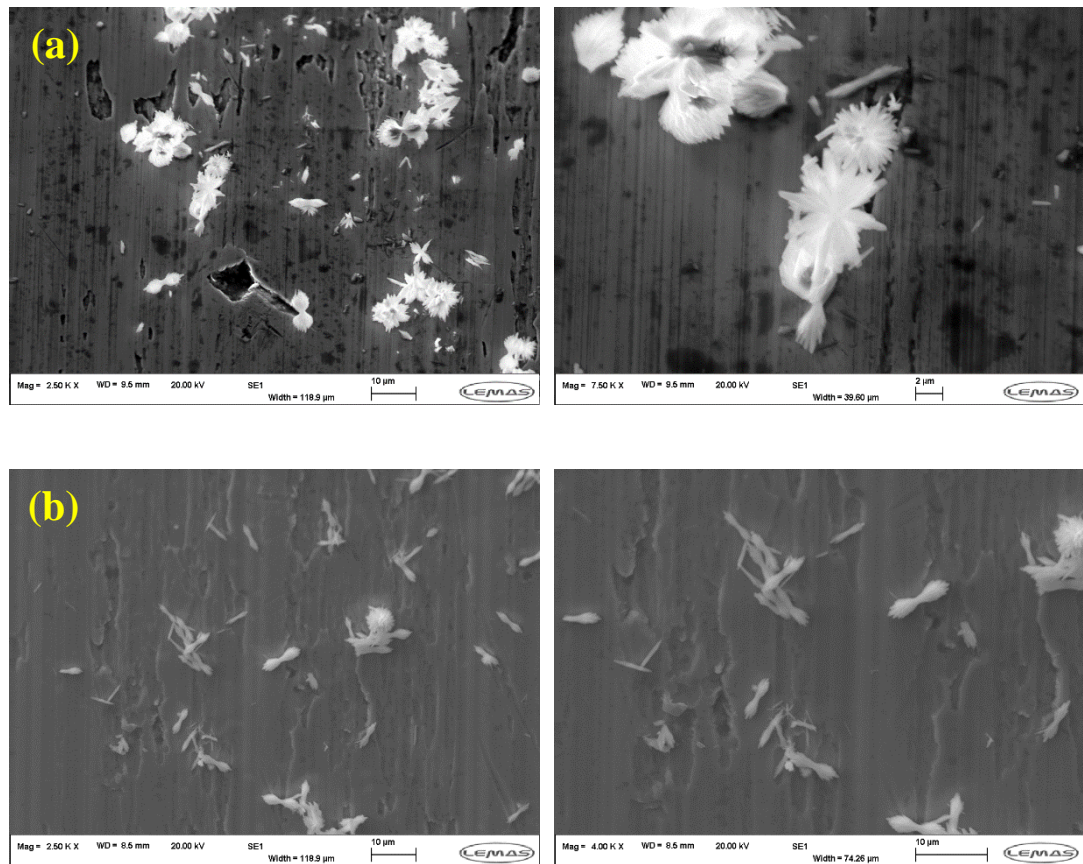


Figure 5.4c: SEM images of scale deposits on modified surfaces:(a) SS and (b) TiN, scale deposits occurring all over the surfaces either as a bundle or singular.

Figure 5.4. SEM images of the scale deposits formed on different modified surfaces at different magnification range in the *adhesion* process for laminar flow regime.

Unlike the turbulent flow conditions, in the laminar flow conditions, the scale deposits are forming all over the surface irrespective of the topography of the substrate (see Figure 5.4c). It can be contributed to the fact that in the laminar flow conditions the mass transfer and the surface shear stresses induced by the bulk solution are relatively lower than those of in the turbulent flow conditions. Therefore, there is not much difference between the concave and convex regions on the surface for the scale deposits to adhere themselves onto the surface.

Deposition Process: As expected, the surface coverage by scale crystals in the *deposition* process is higher compared to the *adhesion* process; however, in terms of morphology there is no noticeable difference between the crystals formed on the

modified surface in both processes neither in the laminar flow conditions nor in the turbulent flow regimes, while the hydrodynamic conditions have affected the pattern of the carbonate-based scale deposits formed on the surface.

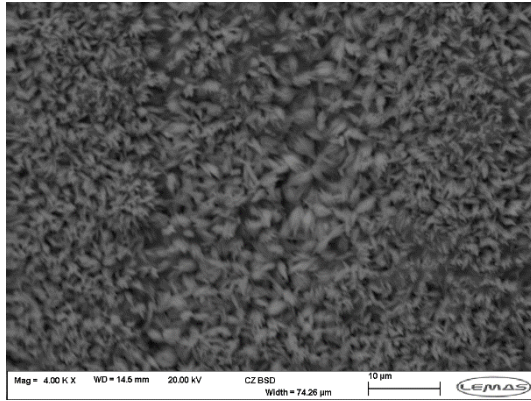


Figure 5.5a: CrNAg

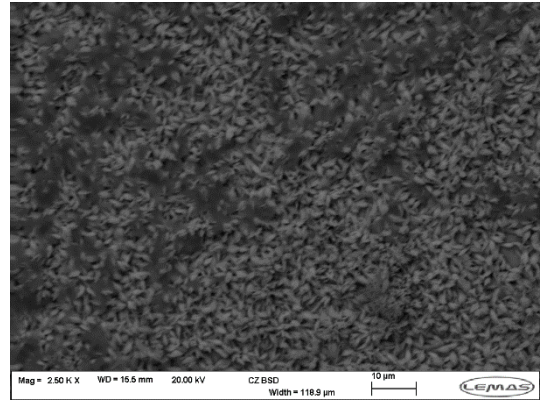


Figure 5.5b: CrN

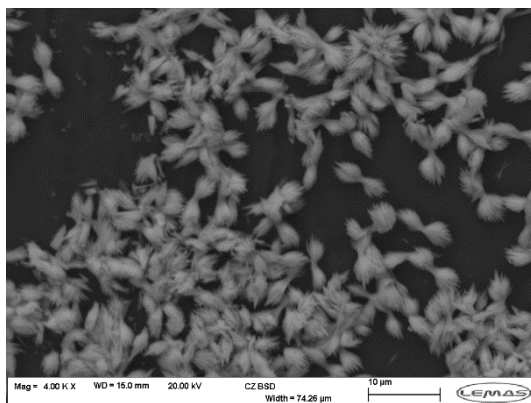


Figure 5.5c: DLC

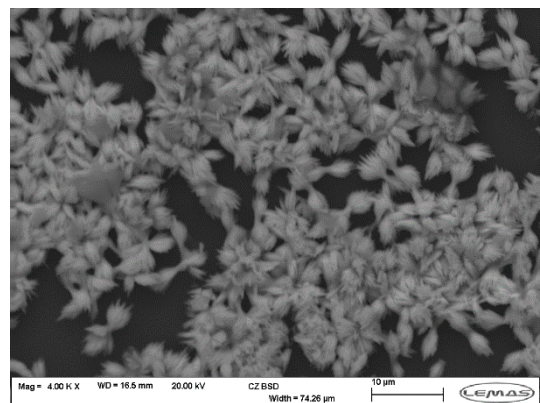


Figure 5.5d: DTi

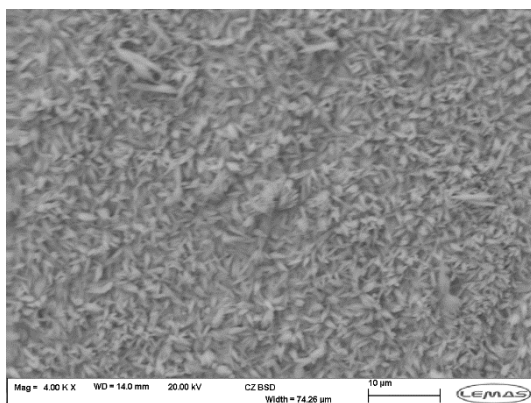


Figure 5.5e: SS

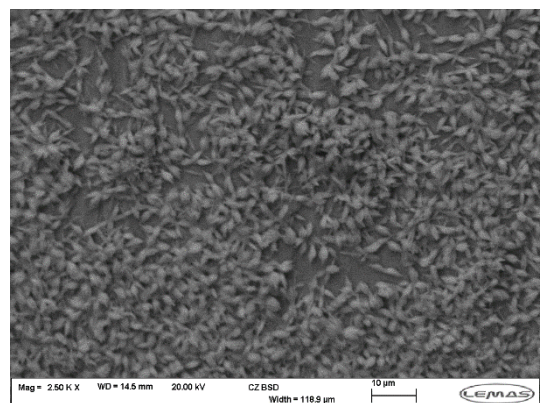


Figure 5.5f: TiN

Figure 5.5. The SEM images of the scale deposits on different modified surfaces in the *deposition* tests in the turbulent flow conditions.

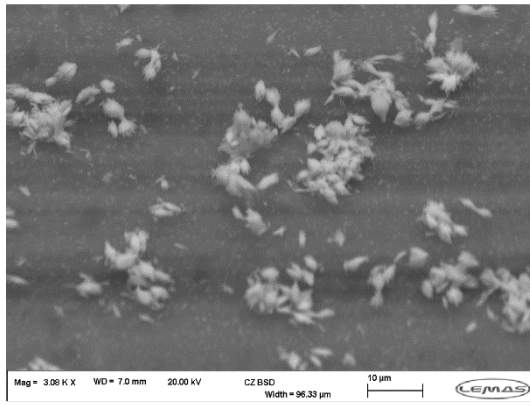


Figure 5.6a: B1341

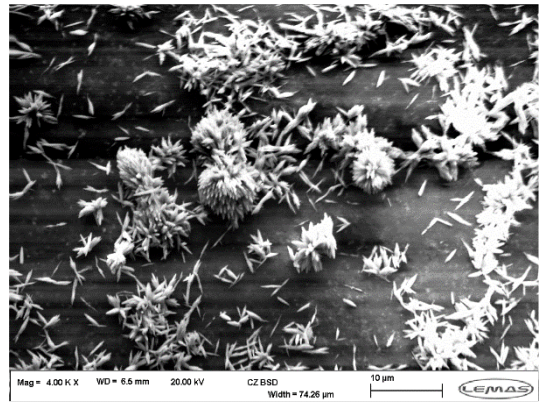


Figure 5.6b: B1381

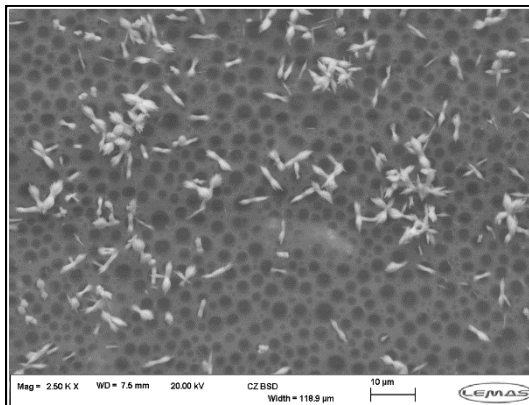


Figure 5.6c: B1391

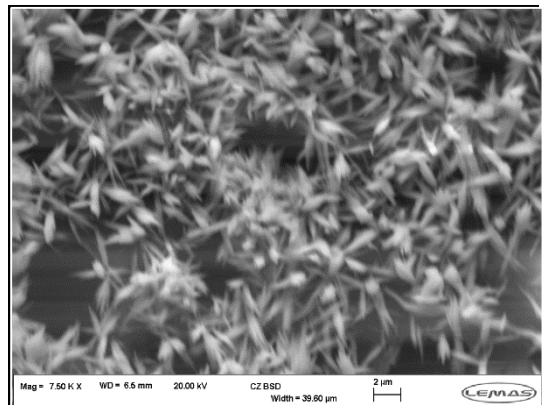


Figure 5.6d: B1541

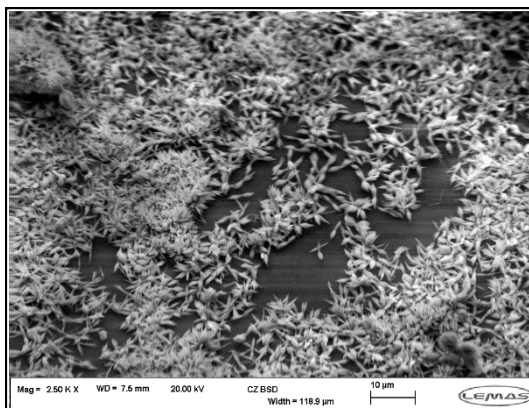


Figure 5.6e: CrNAg

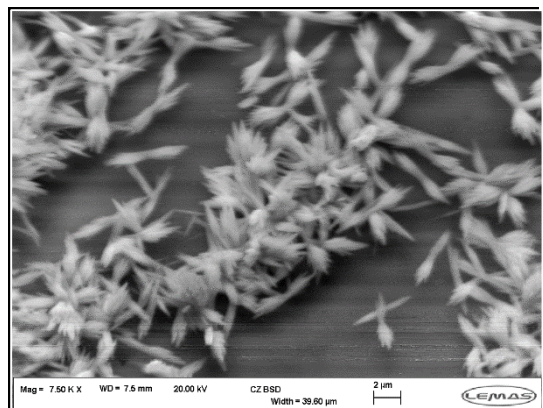


Figure 5.6f: FEP

As shown in Figure 5.5 (a to f) and Figure 5.6 (a to n), almost all the scale crystals formed on different modified surfaces in the *deposition* tests are shaped as bowtie (same as the *adhesion* tests), and the surface chemistry does not have much effect on the morphology of the crystals.

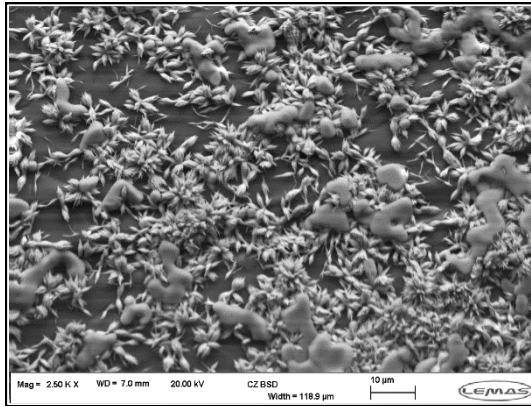


Figure 5.6g: PFA

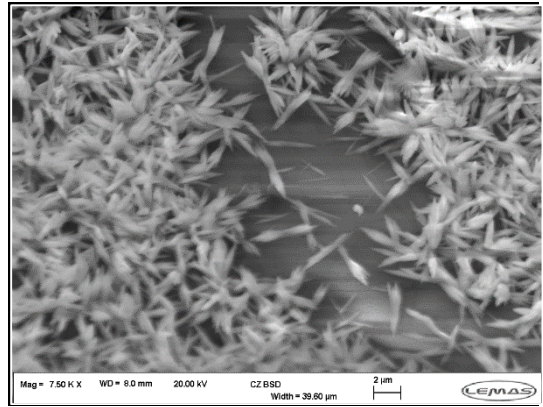


Figure 5.6h: PTFE

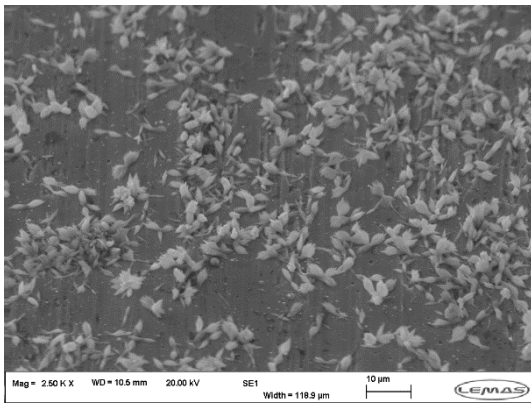


Figure 5.6i: CrN

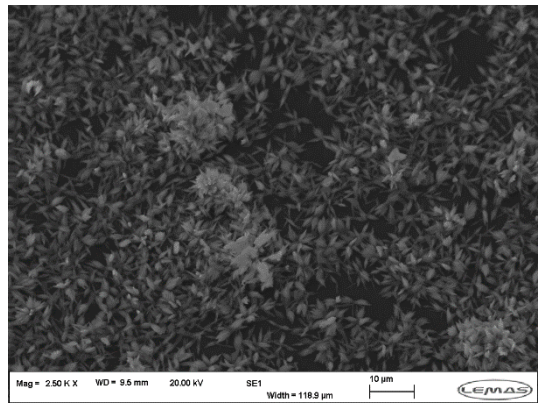


Figure 5.6j: DHS

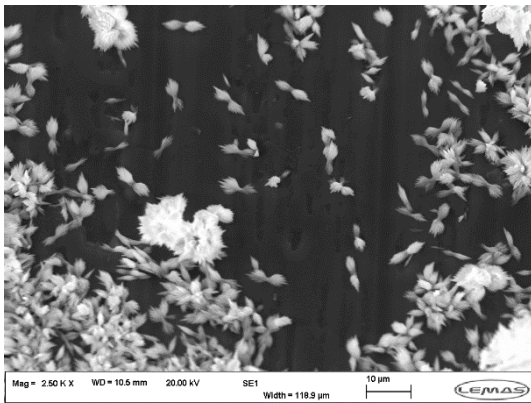


Figure 5.6k: DLC

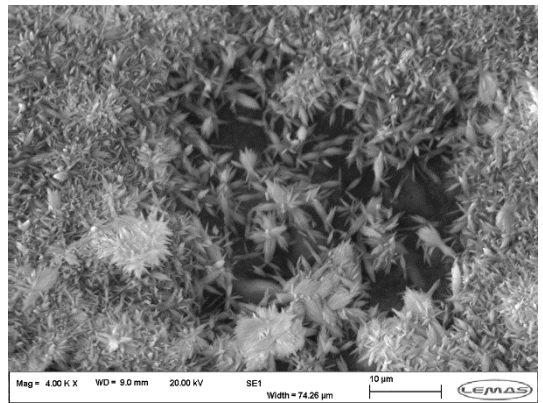


Figure 5.6l: One

Figure 5.6 (a to n) illustrate the SEM images of the scale deposits formed on different modified surfaces in the *deposition* process in the laminar flow conditions. Like the *adhesion* process in laminar flow conditions, the existence of sisal-like crystals on different modified surfaces in the *deposition* process in laminar flow conditions is noticeable. Such occurrence will accentuate the role of the agitation level or shear

forces of the bulk on the morphology of the sulphate-dominated crystals formed on surfaces.

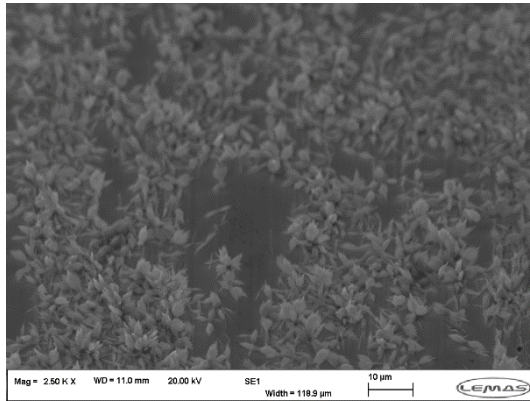


Figure 5.6m: SS

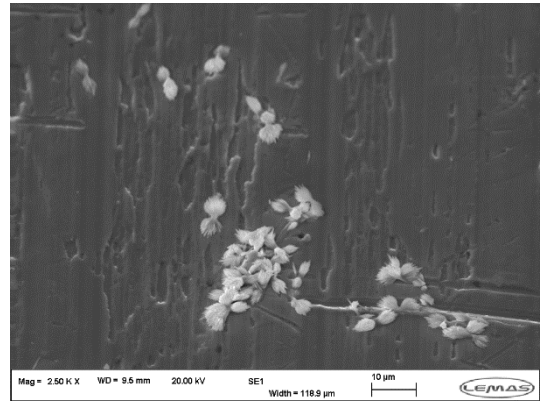


Figure 5.6n: TiN

Figure 5.6. The SEM images of the scale deposits on different modified surfaces in the *deposition* tests in the laminar conditions.

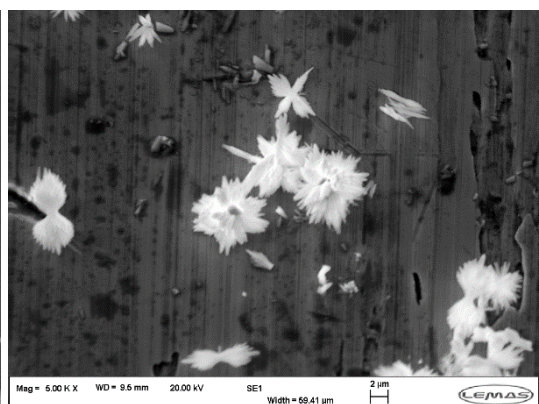
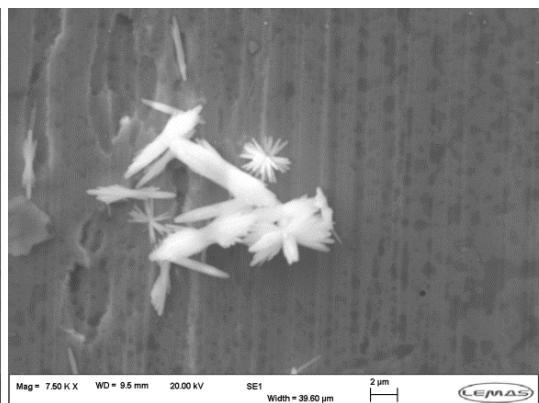
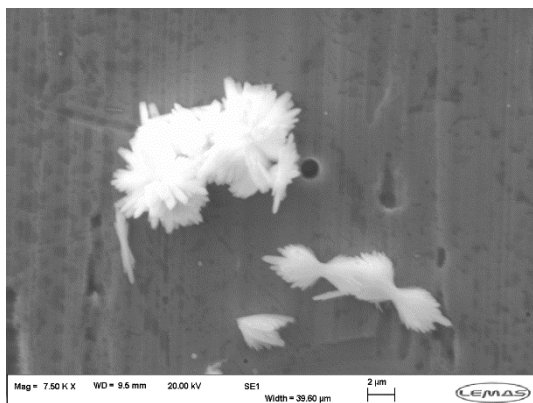


Figure 5.7. The SEM images of scale deposits on different modified surfaces: the size of each morphology of the sulphate-dominated scale deposits is in the same range.

In summary, the two predominant morphologies of the scale deposits formed on different modified surfaces in the sulphate-dominated brine composition, are sisal-like hierarchical structure and the bowtie structure, as shown in Figure 5.7. In all cases, the morphology of the majority of the formed crystals is shaped like a “bowtie” which their size reaches to around 6-9 μm in length and 1.5-2 μm in width on both sides. The sisal-like hierarchical structure is composed of the same needle-like crystals but with various orientations and is in a range of 6-9 μm in diameter.

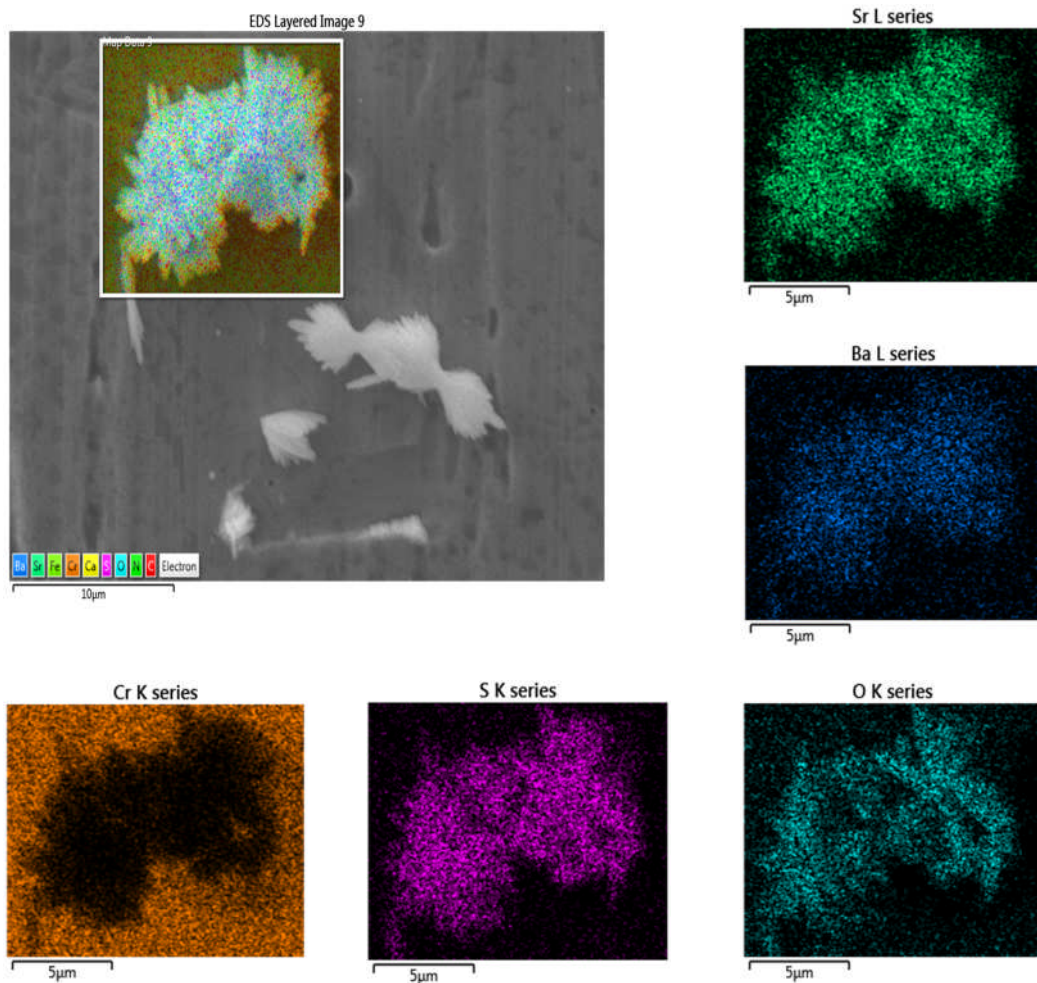


Figure 5.8. EDX images of the sisal-like hierarchical structure morphology.

The elemental composition of both morphologies is analysed with using the Energy Dispersive X-ray (EDX) technique as shown in Figure 5.8 and Figure 5.9. In both morphologies, the presence of sulphate along with strontium and barium is noticeable, where the amount of strontium is higher compared to barium which is confirmed by the ICP measurements.

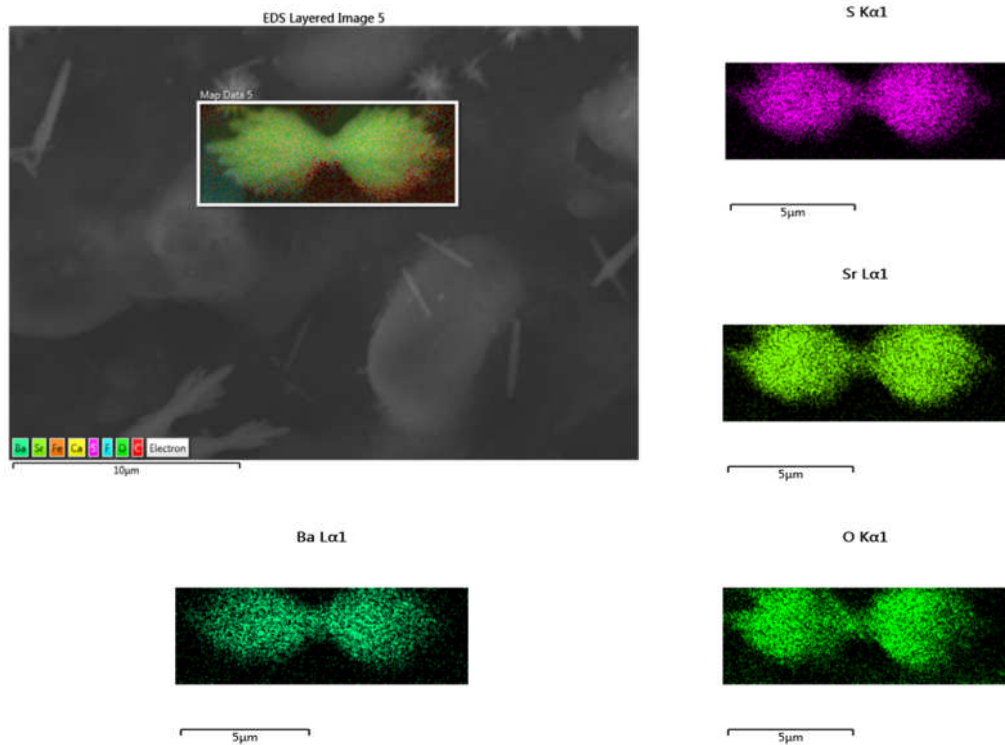


Figure 5.9. EDX images of the bowtie structure morphology.

5.2.2. Inductively Coupled Plasma (ICP) of scale deposits

To understand more about the chemical composition of the deposited crystals on the surface, the Inductively Coupled Plasma (ICP) spectroscopy technique is employed to measure the relative amount of calcium, barium and strontium by dissolving the formed scale deposits.

The ion concentration of calcium, barium and strontium in both the laminar and turbulent flow conditions are shown in Figure 5.10 and Figure 5.11 by their mass gain values for the *deposition* and *adhesion* processes, respectively. By comparing the results in both the *deposition* and the *adhesion* processes, the following findings can be addressed:

- In the *deposition* process, the predominance ion concentration can be ranked as strontium and barium, respectively, in both flow regime conditions; while in the *adhesion* process, the calcium ion concentration is higher than that of in the *deposition* process, and in the turbulent flow condition its concentration is even higher compared to strontium and barium ion concentrations.



Figure 5.10. ICP results of the scale deposits in the *deposition* tests presented in mass gain: (a) Laminar and (b) Turbulent flow conditions.

- In sulphate dominated scale, where strontium and barium incorporate in the lattice of the scale crystals, the ion concentration of the strontium found in the scale deposits on different modified surfaces is higher than that of the barium in the *deposition* process.

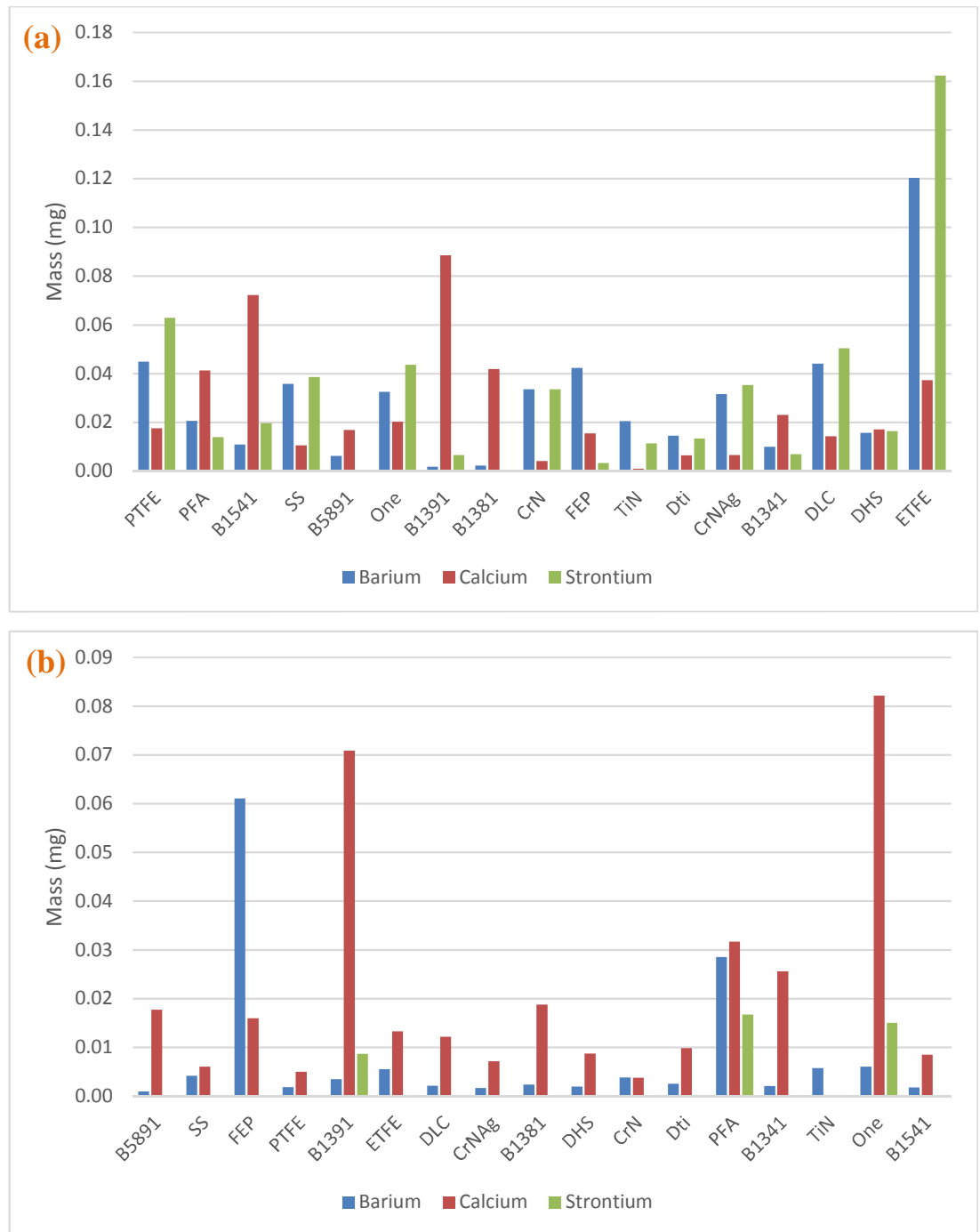


Figure 5.11. ICP results of the scale deposits in the *adhesion* tests presented in mass gain: (a) Laminar and (b) Turbulent flow conditions.

- The flow regime, or the agitation level, has little effect on the ion concentration of the scale deposits form on the surface in the *deposition* process, while in the *adhesion* process the hydrodynamic effect is influential in the formation of scale deposits on the surfaces. For example, in the *adhesion* process, the trace of barium, strontium and calcium is evident in the laminar flow conditions,

while in the turbulent flow conditions there is a little trace of strontium in the scale deposits.



Figure 5.12. Mole percentage of calcium, barium and strontium existing on the surface as scale deposits in the *deposition* process: (a) Laminar and (b) Turbulent flow conditions.

The mole percentage of calcium, barium and strontium for the laminar and turbulent flow conditions for *deposition* and *adhesion*, respectively, are shown in Figure 5.12

and Figure 5.13. More discussion on the chemical composition of the scale deposits will be given in chapter-7.

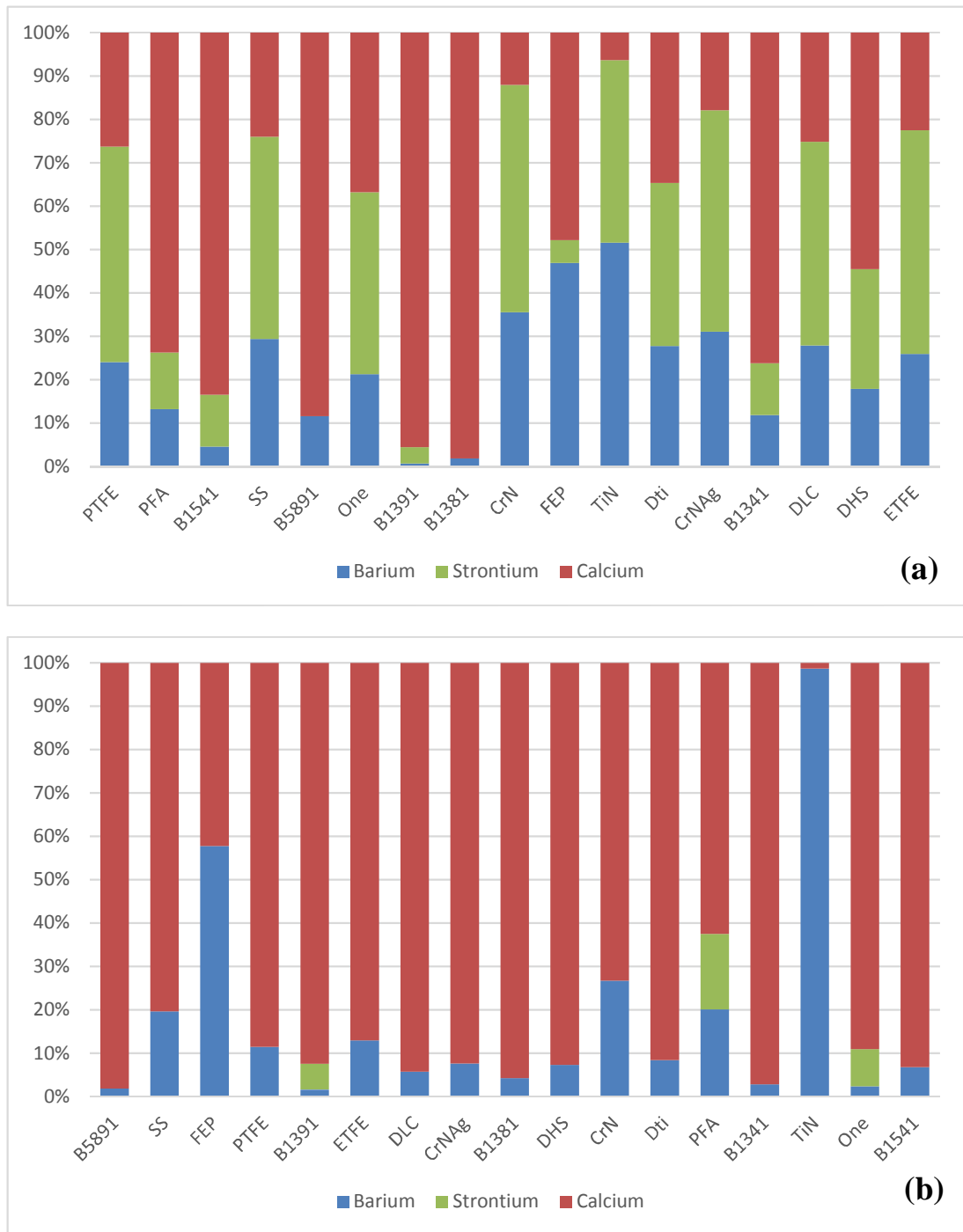


Figure 5.13. Mole percentage of calcium, barium and strontium existing on the surface as scale deposits in the *adhesion* process: (a) Laminar and (b) Turbulent flow conditions.

5.3. Summary

The presented work surveyed the effect of the hydrodynamic conditions on the rate of inorganic scale of a wide range of commercially-available coatings in a complex brine

solution, e.g. the sulphate-dominated brine composition, in two processes: heterogeneous nucleation and crystal growth as “deposition process”, and the adherence of the pre-crystallised particles to the surface as “adhesion process”. The brine composition is provided by PETROBRAS to assess the scaling tendency of modified surfaces in the same condition in the oil basins of Brazil. The key findings of this chapter are:

- In the sulphate-dominated brine composition, the anti-scaling performance of different groups of coatings in both the *adhesion* and *deposition* processes in both flow regimes does not follow a specific trend. In other words, a specific group of coatings cannot guarantee good anti-scaling characteristics.
- The performance of some coatings in the *deposition* process can be assessed as good anti-scaling characteristics, while the same coating has not necessarily shown promising results in the *adhesion* process. In other words, the performance of the coatings in sulphate-dominated brine compositions is affected by the surface scale mechanism.
- An increase in the level of the turbulence in the bulk would increase the scale formation rate on the surface in both *deposition* and *adhesion* processes.
- The surface scale formation rate is more dominantly controlled by the heterogeneous nucleation and crystal growth rather than the adherence of the pre-crystallised particles; however, the level of agitation could have inverse effects on one process to another.
- The predominant morphology of the scale crystals formed on the modified surfaces is mainly needle-like or bowtie (dumbbell) shape crystals.
- The scale deposits formed on the modified surfaces are normally scattered all over the surface in the turbulent flow conditions, while in the laminar flow conditions they rather form regionally than being scattered.

- The chemical composition of the modified surfaces has not much effect on the morphology of the crystals formed on the surfaces. However, the surface finish and surface irregularities/imperfections will affect the rate of surface scale formation.
- The morphology of the scale deposits on the modified surfaces is affected by the bulk flow regime in both the *adhesion* and *deposition* processes, wherein the laminar flow conditions the existence of sisal-like crystals is evident while in the turbulent flow conditions it is mainly the needle-like and bowtie crystals.
- The relative chemical composition of scale deposits would be affected by different mechanisms of scale formation on the surface (i.e. from the *deposition* process to *adhesion* process), while the morphology of the scale deposits has not changed.
- The hydrodynamic conditions have not much effect on the relative ion composition of the surface scale deposits in the *deposition* process, but the relative ion concentration of scale deposits in the *adhesion* process is affected by the agitation level.

Chapter 6

Field Data

6.1. Introduction

Mineral scale deposition on surfaces of oil production equipment has been recognised as a major flow assurance problem. Most of the mineral scale deposition studies published have solely focused on laboratory experiments and very little data are available that demonstrate such results are relevant and can be scaled-up to field environments. This chapter presents the real data obtained from an oilfield rig situated in one of the oilfield basins in Brazil. The obtained results and post-processing of the data would help the author to understand and link the systematic laboratory work to the real-time data in the field.

6.2. Oilfield rig

The Carmapolis oilfield is located in the Sergipe-Alagoas basin 30km of Aracaju, Sergipe State, Brazil. The oilfield flow rig is situated at the end of the line of the multi oil-water separation facilities.



Figure 6.1. Onshore oilfield flow rig.

As a result, the formation water coming out of the separation tank has less than 0.1% of the oil. The system has been running for about 5 months and the temperature inside

the pipe system has been in a range of 55-60°C. The onshore oilfield rig is shown in Figure 6.1.

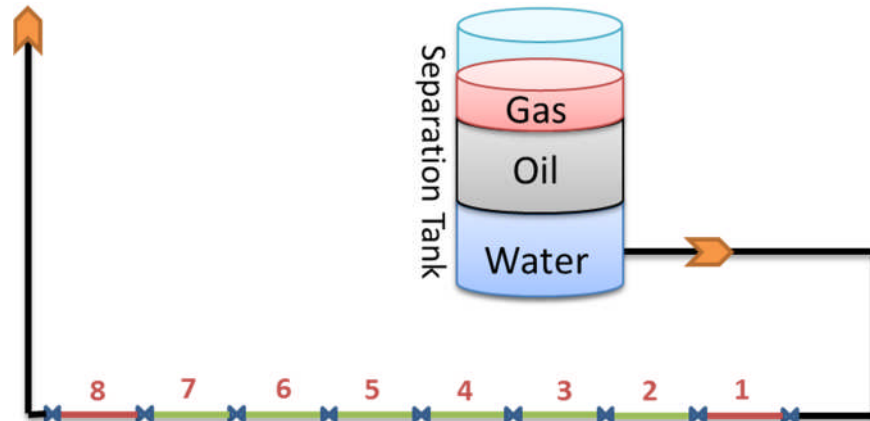


Figure 6.2. Schematic of oilfield site flow rig: green lines are coated pipes, red lines are uncoated pipes.

Each pipe spools has a length of 1 metre and a diameter of 3.5 inches (or 89 mm). The first (number 1) and the last (number 8) pipe spools are uncoated carbon steel pipes and the pipe spools in between (number 2 to number 7) are internally coated with commercially-available coatings (e.g. epoxies and fluoropolymer coatings). Such configuration is designed so that the rate of surface scaling tendency along the pipe can be characterised by comparing the surface scaling tendency of the uncoated pipe spools at the inlet and outlet of the flow rig.

Table 6.1. The order number of the commercial coatings positioned from the inlet of the oilfield rig.

Order Number	Company	Order Number	Company
1	Uncoated	5	IPC ME35
2	Belzona 5891	6	Belzona 1391
3	3MSK 6258	7	IPC Magna
4	Belzona 1341	8	Uncoated

The schematic of the oilfield site flow rig along with the corresponding commercial coatings are shown in Figure 6.2 and Table 6.1, respectively.

The water composition of the water running in the oilfield rig is shown in Table 6.2.

Table 6.2. Ion composition of the water in the oilfield rig.

Field Brine

Ion	Amount (mg/L)	Ion	Amount (mg/L)
Na ⁺	42000	Cl ⁻	71613.48
K ⁺	493	Br ⁻	195
Mg ²⁺	1160	SO ₄ ²⁻	390
Ca ²⁺	2953.07	HCO ₃ ⁻	383.74
Ba ²⁺	8.24	CH ₃ COO ⁻	10
Sr ²⁺	85.64	CH ₃ CH ₂ COO ⁻	5
Fe ³⁺	14.44	CH ₃ CHOHCOO ⁻	5
Li ⁺	2.5	NH ₄ ⁺	29
B ³⁺	16	NO ₃ ⁻	1
Si ⁴⁺	14	NO ₂ ⁻	1

The saturation ratio of the field is calculated by the Multiscale® software, where no oil or gas phase is present. The saturation ratio is calculated at the temperature of 56°C and the results are shown in Table 6.3. Based on the calculations, the scale formation of barium sulphate is thermodynamically possible. Furthermore, the calcite formation could be possible due to the inhomogeneity of the water composition.

Table 6.3. Saturation ratio calculations of the oilfield water composition.

Temperature	SR (FeCO ₃)	SR (CaCO ₃)c	SR (BaSO ₄)	SR (SrSO ₄)
56°C	0.2619	0.9998	5.9088	0.2071

6.3. Oilfield results

The weight of the pipe spools was measured before installing them in the oilfield flow rig. After the scale tendency test in the field, the pipe spools were dismantled and taken out to put in the oven to remove all the moisture. Toluene was used to dissolve the residuals of the oil on the scale deposits. The weight of the pipe spools was measured. As a result, the difference in the weight shows a number of scale deposits which were deposited on the internal surface of the pipes, as shown in Figure 6.3 and Table 6.4. The lower scaling tendency of coated pipes compared to uncoated pipelines is expected, however such discrepancy between two uncoated pipes is not fully understood. The author believes that due to the U-turn of pipeline, the flow conditions at the first pipe spool is more turbulent, since it is not fully developed, which leads to higher rate of scale formation on the first pipe spool compared to the last uncoated pipe spool.

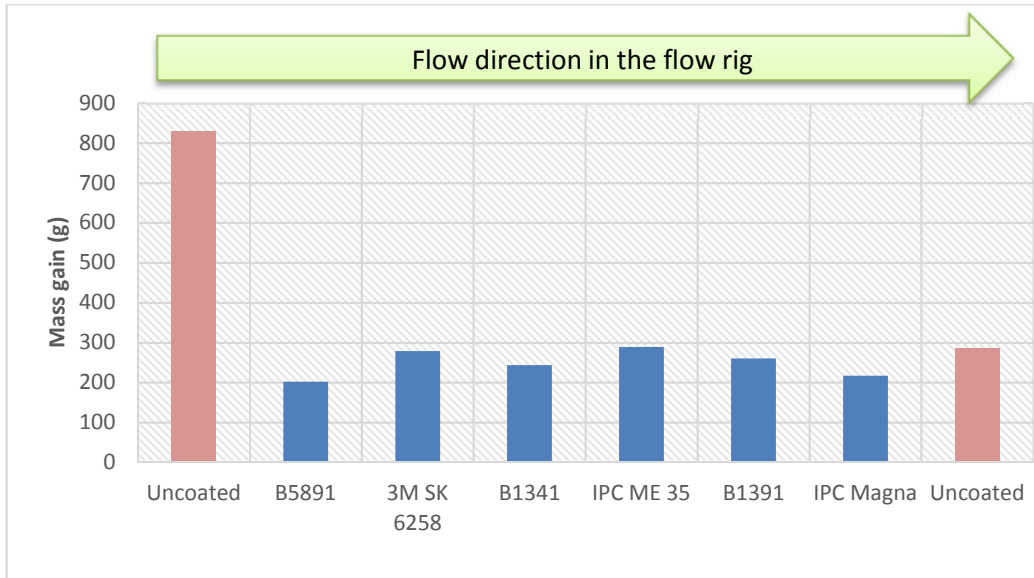


Figure 6.3. The scale deposits mass gain of each substrate along the flow rig.

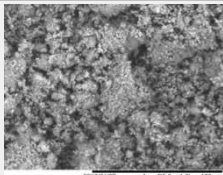
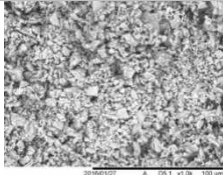
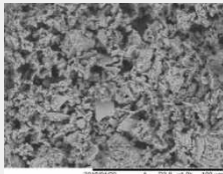
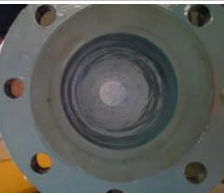
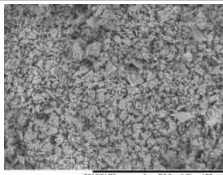
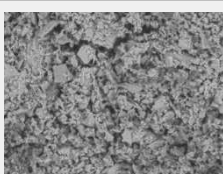
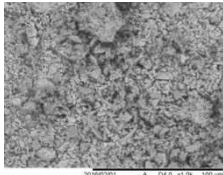
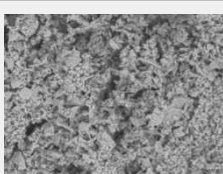
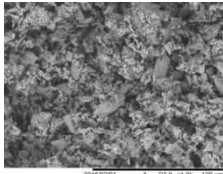
The mass gain of scale deposits of each substrate is divided by the area, and it is assumed that the scale deposits formed on the surface are fully dense barium sulphate with the density of 4.5 g.cm^{-3} . As a result, the annual thickness growth of scale deposits on these modified substrates can be determined and the results are shown in Table 6.4.

Table 6.4. The scale deposits mass gain of the pipes along the pipeline

Order No.	Company	Mass gain (g)	Thickness (cm/year)
1	Uncoated	830.13	0.678
2	B5891	202.1	0.165
3	3M SK 6258	279.14	0.228
4	B1341	243.18	0.198
5	IPC ME 35	288.88	0.236
6	B1391	260.61	0.213
7	IPC Magna	216.85	0.177
8	Uncoated	287.09	0.234

As shown in Table 6.4, all of the modified surfaces have shown their antifouling properties and reduced the mass gain on the surface to some extent. In addition, as the flow passes through the piping system, its potential to scale formation will decrease (i.e. first pipe is facing to more active ions to scale formation than the last pipe).

Table 6.5. Images of the modified pipe spools in the flow rig before (Stage 1) and after (Stage 2&3) running the test along with post processing (Stage 4).

No.	Stage 1	Stage 2	Stage 3	Stage 4
1	-		-	
2				
3				
4				
5				
6				
7				
8				

This occurrence is well-distinguishable where the performance of two uncoated pipe spools are so different. Since the material of the uncoated pipes is carbon steel, the corrosion would be highly probable for the uncoated pipe spools. Therefore, there is no surprise if the amount of mass gain of the uncoated pipe is drastically higher compared to the coated pipes, as indicated in Table 6.4.

As shown in Table 6.5, the modified pipe spools along with the uncoated ones are shown before implementing in the flow rig (stage 1), after dismantling the pipe spools from the flow rig with the presence of oil on the scale deposits (stage 2), cleaning up the oil from the scale deposits (stage 3), and the post-processing of the scale deposits with EDX and XRD techniques (stage 4).

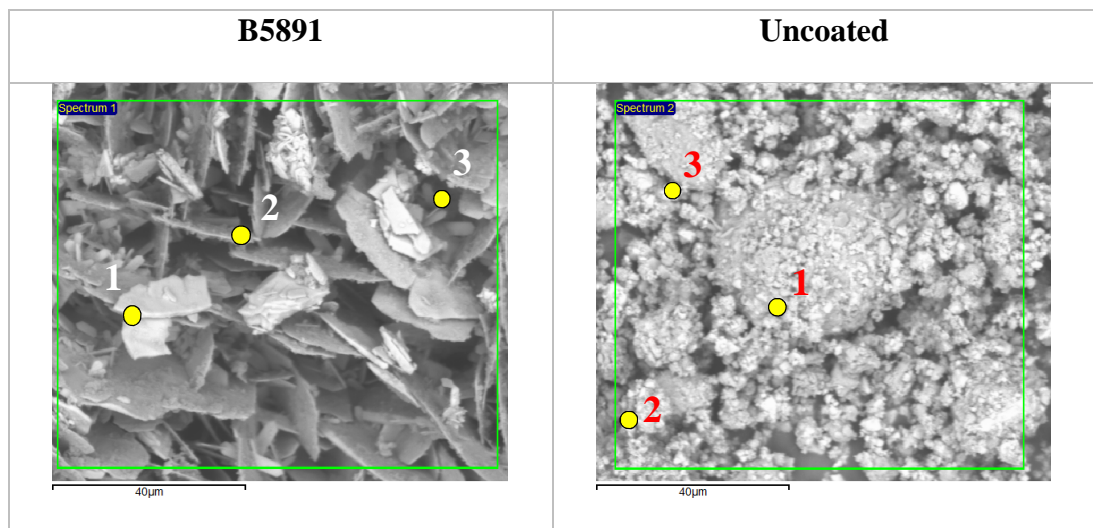


Figure 6.4. SEM images of scale deposits formed on the pipe surfaces along with three random points analysed by EDX technique.

By comparing the images in Table 6.5, it can be clearly seen that how effective can be the surface modifications. It should be noted that both uncoated pipe spools are subjected to not only scaling but also corrosion; however, the product of the corrosion is a type of scaling and as time passes by, it would lead to the clogging of the pipes. In order to have a better understanding of the difference between the scale deposits on uncoated and coated pipes' surface, the scale deposits are studied with the SEM and EDX techniques, as shown in Table 6.6 and Figure 6.4. The coated sample that has been selected is the B5891 coating which has shown the best scaling tendency performance amongst all other coatings in the sulphate-dominated brine.

Table 6.6. Elemental results of the surface scale deposits on surface “B5891” and uncoated (or “UC”) on three random points along with their whole mapping area.

Element	Weight% point 1		Weight% point 2		Weight% point 3		Weight% Overall	
	B5891	UC	B5891	UC	B5891	UC	B5891	UC
Oxygen	11.792	32.300	2.949	30.640	14.716	35.717	16.712	24.790
Sulphur	8.664	4.504	3.387	4.041	10.058	---	9.090	4.988
Chlorine	0.663	2.845	0.435	3.407	3.819	5.997	3.238	3.667
Calcium	0.938	0.719	0.818	0.909	1.391	0.971	0.904	1.355
Iron	1.090	26.503	1.717	29.370	10.310	30.609	3.293	33.390
Strontium	1.664	---	---	---	2.428	---	2.382	---
Barium	49.245	12.310	87.519	10.390	45.582	2.451	51.213	15.739
Gold	25.079	20.819	2.538	19.860	10.371	17.012	10.596	14.430

As shown in Table 6.6 and Figure 6.4, the elemental results of the surface scale deposits on both B5891 and the uncoated pipe of three random points along with their whole mapping area are presented.

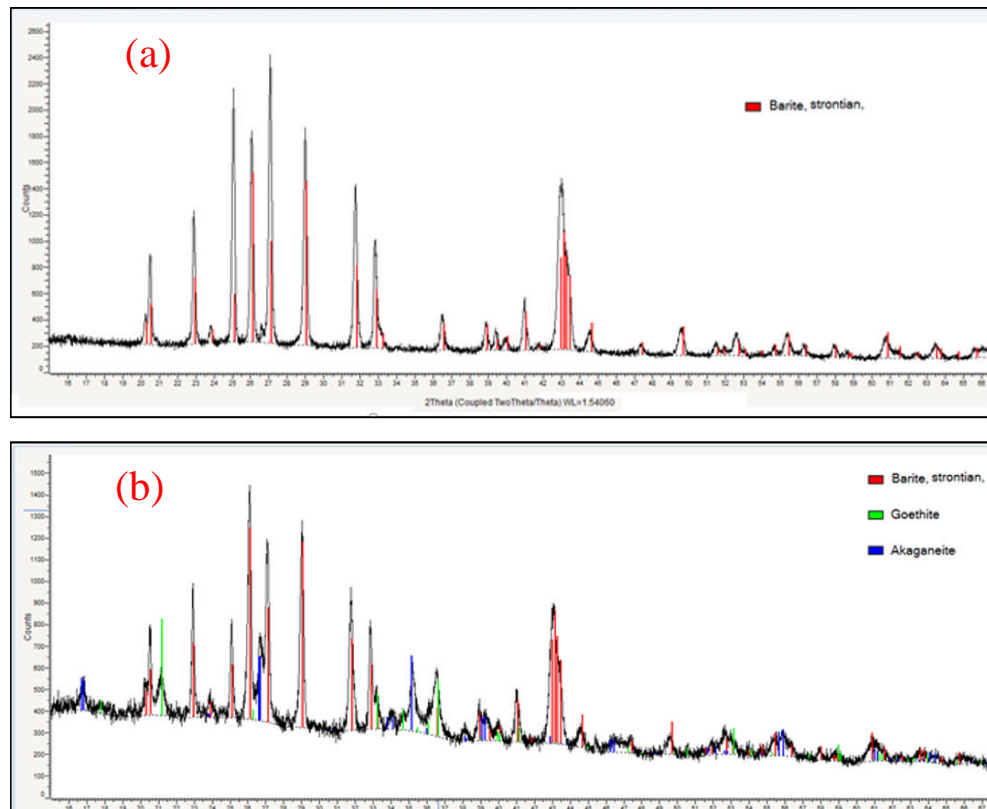


Figure 6.5. The X-ray diffraction analysis of the scale deposits in the rig: (a) coated pipe and (b) uncoated pipe.

As shown in Table 6.6, the dominant scale deposits formed on the surface is mainly made up of barium sulphate (as expected by its relative high supersaturation ratio), and a substantial presence of iron elements is distinguishable in the scale deposits of the uncoated substrates, while there are not much of iron elements on the B5891 coating. The presence of iron elements onto the surface demonstrating that the corrosion process has taken place widely on the uncoated surfaces and its products accumulated on the surface as scaling deposits. In addition, the presence of iron elements on the B5891 coating is primarily attributed to the detachment of the corrosion products that has occurred in the upstream of the coated pipe and have the chance to adhere themselves onto the pipe surface.

The scale deposits residuals collected from inside the pipe spools have been analysed with the X-ray diffraction technique. As shown in Figure 6.5-(b), apart from the barite scale deposits, the corrosion products detected on the surface of the uncoated pipes are Akaganeite ($\text{Fe}^{3+}\text{O} [\text{OH}, \text{Cl}]$) and Goethite ($\text{FeO}(\text{OH})$), and as expected barite is the dominant scale deposits formed on the modified surfaces (Figure 6.5-(a)).

Table 6.7. The mass gain of the modified pipe spools without the presence of iron-based compounds.

No.	Coating	Mass gain (g)	(%) Fe	Mass gain (g) (without corrosion products)
1	Uncoated	830.13	32.2	405.1
2	B5891	202.1	2.2	193.1
3	3M SK 6258	279.14	0.8	274.7
4	B1341	243.18	1.2	237.3
5	IPC ME 35	288.88	0.9	283.9
6	B1391	260.61	1.1	255.1
7	IPC Magna	216.85	1.4	210.9
8	Uncoated	287.09	7.5	252.9

Most of the iron elements found on the pipe surfaces are initiated from the upstream of the whole facility. The aim of this research is to assess the effect of surface engineering on the rate of surface scale formation. Therefore, in a system where all the valve and pipe component systems are fully coated internally, the results can be re-assessed without the presence of corrosion products (i.e. iron-based compounds) for each pipe spool, as shown in Table 6.7.

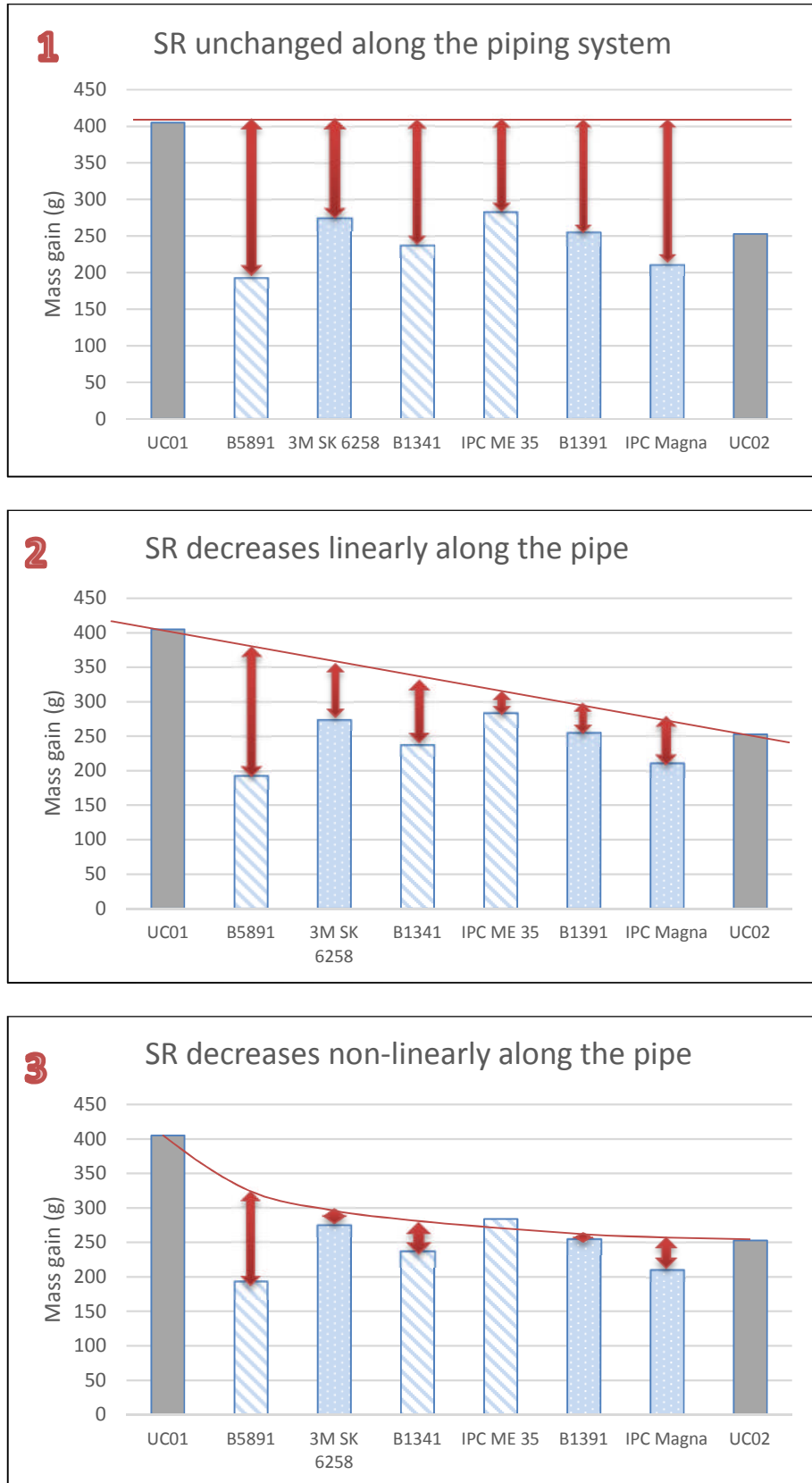


Figure 6.6. The comparison of the mass gain of each substrate with regard to hypothetical SR: (1) SR does not change, (2) SR decreases linearly, (3) SR decreases non-linearly along the piping system.

The efficiency of the coatings can be calculated in different ways depending on the parameters that are taken into considerations. These calculations can be divided into two groups: based on the average performance of the uncoated pipes or based on the scale potentiality of brine, characterised as supersaturation ratio.

The efficiency of the coatings can be calculated with the following formula:

$$Efficiency = \left(\frac{M - m}{M} \right) * 100 \quad \text{Eq (6.1)}$$

where, M is the average mass gain of the uncoated tubes and m is a number of scale deposits formed on the modified substrates.

The supersaturation ratio (SR) of the brine along the flow rig can be either unchanged or decreasing. The decrease of the SR can be either linear or non-linear, as shown in Figure 6.6.

By considering the fact that the precipitation ratio has reached to an equilibrium state, where the dissolution of crystals is in balance with the crystallisation process, the first scenario of Figure 6.6, e.g. unchanged SR along the eight pipe spools, is more logical.

The scaling tendency performance efficiency of the modified substrates are shown in Table 6.8.

Table 6.8. The scaling tendency performance efficiency of modified substrates with regard to (a) the average performance of uncoated substrates and (b) hypothetical SR value along the piping system.

No.	Coating	Efficiency (%)			
		Mass average	SR const.	SR (lin.)	SR (non-lin)
1	Uncoated-1	-	-	-	-
2	B5891	41.31	52.35	49.63	44.21
3	3M SK 6258	16.50	32.20	24.03	12.98
4	B1341	27.87	41.43	30.18	19.76
5	IPC ME 35	13.71	29.93	10.76	0
6	B1391	22.46	37.04	13.93	5.42
7	IPC Magna	35.90	47.95	23.21	19.02
8	Uncoated-2	-	-	-	-

As shown in Table 6.8, in all scenarios the B5891 by far has the best performance, as well as its promising performance in the laboratory results.

6.4. Summary

Most of the literature in the field of flow assurance and the management of scaling problems in the oil and gas industry investigating similar mineral fouling mechanism mainly focused on either a laboratory framework under well-controlled conditions or from field conditions with no systematic investigations.

The comparison of field data with systematic laboratory two sets of results facilitates a better understanding of the controlling parameters in scaling formation in both laboratory conditions and field conditions. In addition, there have been some doubts about employing surface engineering as a mean to mitigate the flow assurance problems in the oil and gas industry. The work presented in this chapter clearly shows the effectiveness of the surface engineering to reduce the rate of surface scale formation.

Chapter 7

Discussion of the Results

7.1. Introduction

The work presented in this chapter is primarily focused on understanding the mechanisms of surface scale formation on different modified surfaces, commercially-available coatings, with stainless steel as a reference substrate in different complex brine compositions, i.e. carbonate/sulphate-dominated brine composition. The effect of hydrodynamic conditions is studied as laminar and turbulent flow conditions.

To have a better insight into the mechanism of surface scale formation, it has been divided into two interlinked mechanisms as heterogeneous nucleation and crystal growth, which is addressed in this thesis as a “Deposition process” and the adhesion of the pre-crystallised particles onto the surface which is called in this study as an “Adhesion process”.

Many aspects of the surface scale formation are studied but still, some areas need further work. For example, the effect of some surface parameters such as surface roughness and surface energy on the rate of surface scale formation will be discussed in all the surface scaling tendency conditions.

Due to the complexity of the brine solutions, the nature and morphology of the formed surface scale deposits which are the products of co-precipitation process will be discussed in this chapter for both brine solutions.

Extensive laboratory research works [107, 108, 112, 113, 124, 128] and oilfield reports [10-12, 129] have been carried out on the rate of scaling tendency of modified surfaces in dynamic conditions. Therefore, there always has been a gap which can connect the understanding and findings from the laboratory results to a corresponding real-time oilfield. In this chapter, these two aspects, laboratory experiments and field data, are presented and compared. Some modified surfaces along with unmodified surfaces have been tested in an oilfield which is prone to scaling. The oilfield results have been compared with some of the coatings surfaces that are supposed to affect the surface scale formation in the laboratory. Observations relating to the performance of these modified surfaces and comparison of them with unmodified surfaces in the field are discussed.

7.2. Hydrodynamic effects on surface scale deposition

7.2.1. Carbonate-dominated scale formation

The mass gain comparisons of different modified surfaces in the carbonate-dominated brine composition between the laminar and turbulent flow conditions in both the *deposition* and *adhesion* processes are shown in Figure 7.1.

In the turbulent flow conditions, the surface scaling phenomenon is controlled predominantly with heterogeneous nucleation and crystal growth rather than the adhesion of pre-crystallised particles onto the surface. It can be recognised from big discrepancies between the mass gain of the *deposition* process with the *adhesion* process for all the modified surfaces. In the laminar flow conditions, not only are there comparatively lower differences in the mass gain between the two processes, but also for some modified surfaces where the surface scaling rate of the *deposition* process is lower the surface scaling is mainly controlled by the *adhesion* scaling process, e.g. the rate of surface scaling of the four out of five best coatings in the laminar flow conditions for the *adhesion* process is higher than that of for the *deposition* process.

The big discrepancies in a mass gain of the modified surfaces in the turbulent flow conditions compared to the laminar flow conditions can be explained by the importance of the hydrodynamic conditions, in particular for the *adhesion* process. In the *adhesion* process, there is always a trade-off between the adhesion of the particles that are already formed in the bulk onto the surface and the shear stress induced by the flow to the crystal onto the surface to detach. In turbulent flow conditions, the surface shear force is higher compared to laminar flow conditions, and it can exceed the attachment force of the crystal with the surface. However, the higher flow rate of the bulk solution would result in a higher mass transfer rate, i.e. the surface is exposed to a higher amount of active ions to build up the scale crystals.

Having said that, the author cannot determine either the pre-crystallised particles adhere onto the surface and reach a critical size to be detached due to relatively higher gravitational forces by the bulk, or the pre-crystallised particles bigger than a certain size cannot adhere onto the surface in the first place due to high shear stresses.

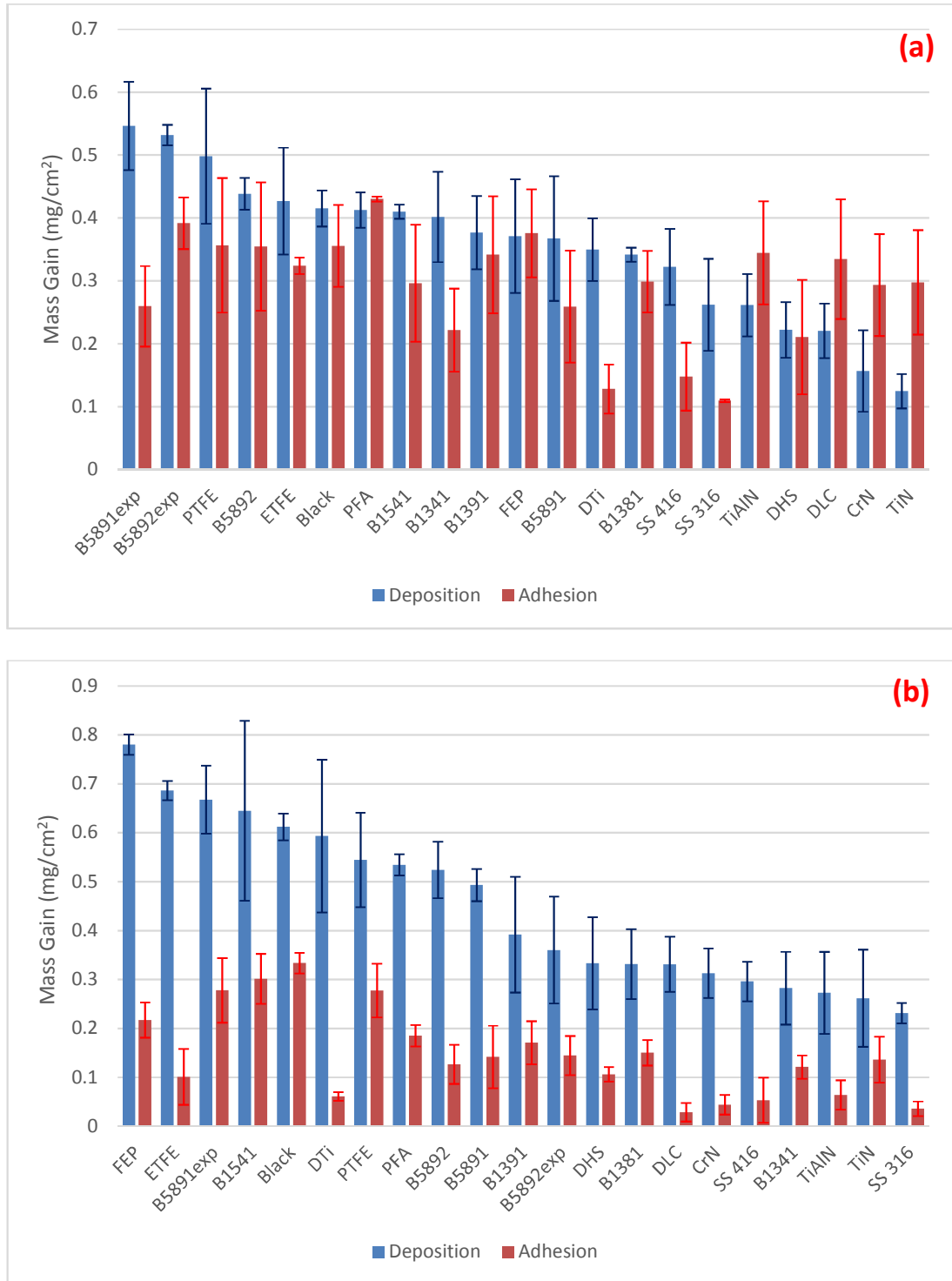


Figure 7.1. The comparison of the surface scale mass gain between the *deposition* and *adhesion* processes for (a) Laminar and (b) Turbulent flow conditions.

The mass gain comparisons of different modified surfaces in the carbonate-dominated brine composition between the *deposition* and *adhesion* processes in both laminar and turbulent flow conditions are shown in Figure 7.2.

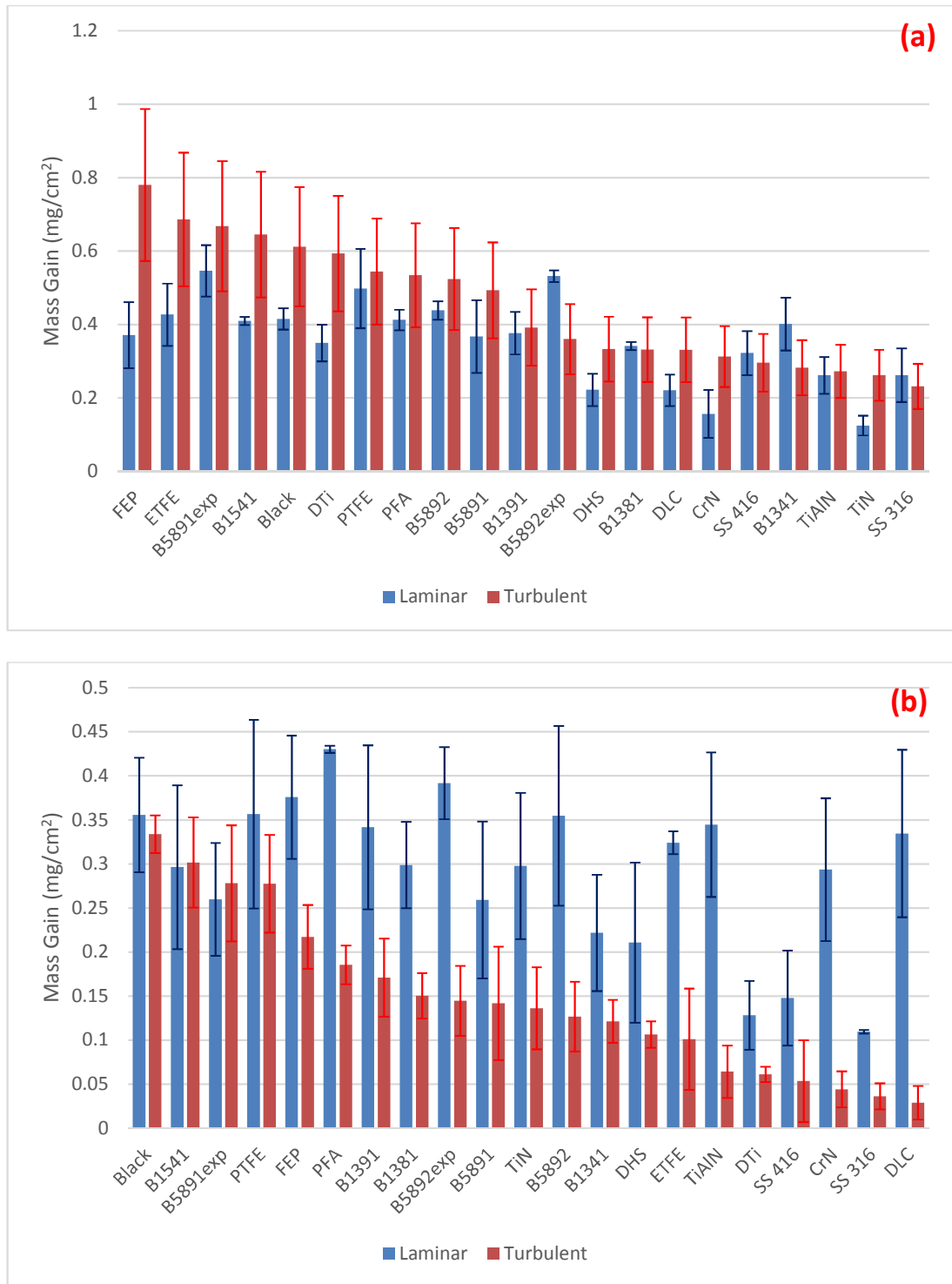


Figure 7.2. The comparison of the surface scale mass gain between the laminar and turbulent flow conditions for (a) Deposition and (b) Adhesion processes.

As shown in Figure 7.2-a, in the *deposition* process, by having a comparison between the surface mass gain results in turbulent and laminar flow conditions, the scaling deposition tendency increases as the hydrodynamic condition rises (e.g. FEP, ETFE

& B1541). However, the hydrodynamic effect seems not to be a dominant parameter at lower scaling tendency (e.g. SS-316, SS416 and TiAlN). As shown in Figure 7.2-a, the scale surface deposition for surfaces with lower scaling tendency in both flow regimes are relatively in the same range, but as the rate of scale surface deposition increases, the discrepancies of scaling tendency between turbulent and laminar flow conditions enhances. This occurrence can be attributed to the fact that the surface scale deposition is inhibited by the surface modifications, but as soon as the surface is fully coated by the scale, the hydrodynamic effects, which in fact increases the rate of mass transfer, would enhance the scaling rate by helping the build-up of scale on the pre-deposited scale on the surface.

In so many of the previous studies [109, 111, 128, 130] it has been reported that an increase in the level of the fluid hydrodynamics will favour the rate of scale formation in the bulk and on the surface due to a higher rate of mass transfer. As shown in Figure 7.2-b, the mass gain of the modified surfaces in the laminar flow conditions is relatively lower than that of in the turbulent flow conditions in the *adhesion* process, which is in contrast with what the general perception considers. In such studies, the surface scale formation whether has not divided into the two interlinked processes (e.g. *adhesion* and *deposition* processes) or other than carbonate-dominated scale has been studied [128].

It can be explained that the precipitation in the bulk solution has reached to an equilibrium condition where the crystallisation rate is in balance with the dissolution rate of the crystals in the bulk. Therefore, the crystals are developed and have reached a size that will be affected by the gravitational forces. As a result, in the turbulent flow conditions, it will be harder for the pre-precipitated particles to adhere onto the surface and stick to the surface while they are under the influence of bulk shear forces to detach from the surface. It has been also reported that in carbonate-dominated scaling tendency tests where the samples are immersed in a bulk solution which its precipitation has reached to steady-state conditions, the rate of the surface in laminar flow conditions is higher than that of in the turbulent flow conditions [127], although the author has not pointed out the reason of such occurrence.

In order to have a better understanding of the mass gains presented in Figure 7.1 and Figure 7.2, the mass gain ratio of the laminar to turbulent flow regimes in both processes and the mass gain ratio of *adhesion* to *deposition* processes in both flow regimes are presented in Table 7.1.

It can be concluded from Table 7.1 that in laminar flow regimes, both heterogeneous nucleation and crystal growth, and the *adhesion* of the pre-crystallised particles onto the surface are controlling the surface scaling (i.e. the adh/dep ratio is around unity), while in the turbulent flow regimes the surface scaling is predominantly controlled by the former process (i.e. adh/dep = 0.319). In addition, the *deposition* process is less affected by the hydrodynamic conditions compared to the *adhesion* process, and such trends are also in contrast with each other. In other words, an increase in the level of bulk turbulence will increase the rate of surface scaling to some extent in the *deposition* process (i.e. lam/turb = 0.832), while it would drastically decrease the surface scaling in the *adhesion* process (i.e. lam/turb = 2.871).

Table 7.1. The comparison of the surface scale mass gains ratio for different flow regimes and surface scale processes, in carbonate-dominated brine.

No.1	Coating	Deposition	Adhesion	Laminar	Turbulent
		Lam/Turb	Lam/Turb	Adh/Dep	Adh/Dep
1	B1341	1.421	1.828	0.552	0.429
2	B1381	1.030	1.987	0.875	0.453
3	B1391	0.961	1.998	0.907	0.436
4	B1541	0.636	0.982	0.723	0.468
5	B5891	0.745	1.827	0.706	0.288
6	B5891exp	0.818	0.934	0.475	0.416
7	B5892	0.837	2.798	0.809	0.242
8	B5892exp	1.476	2.707	0.736	0.402
9	Black	0.678	1.066	0.857	0.545
10	CrN	0.501	6.643	1.873	0.141
11	DHS	0.667	1.980	0.949	0.320
12	DLC	0.666	11.564	1.516	0.087
13	DTi	0.589	2.095	0.367	0.103
14	ETFE	0.622	3.205	0.759	0.147
15	FEP	0.476	1.729	1.012	0.278
16	PFA	0.772	2.320	1.042	0.347
17	PTFE	0.915	1.285	0.716	0.510
18	SS 316	1.132	3.026	0.418	0.157
19	SS 416	1.088	2.764	0.459	0.181
20	TiAlN	0.958	5.366	1.318	0.235
21	TiN	0.476	2.186	2.386	0.520
Average		0.832	2.871	0.926	0.319

The summary of the mass gain results of the carbonate-dominated scale for both the *adhesion* and *deposition* processes with regard to the flow regimes are shown in Figure 7.3.

As shown in Figure 7.3a, the mass gain in the *deposition* process increases as the flow regime increases while in the *adhesion* process an increase in the agitation level of the bulk solution is against the surface scale formation. On the other hand, as shown in

Figure 7.3b, the *adhesion* and *deposition* processes have the same effect on different flow regimes of the bulk solution with different impact in terms of the magnitude, i.e. as the flow regime of the bulk solution increases from the laminar flow conditions to fully turbulent conditions, the surface scale formation increases with a higher magnitude from the *adhesion* process to the *deposition* process.

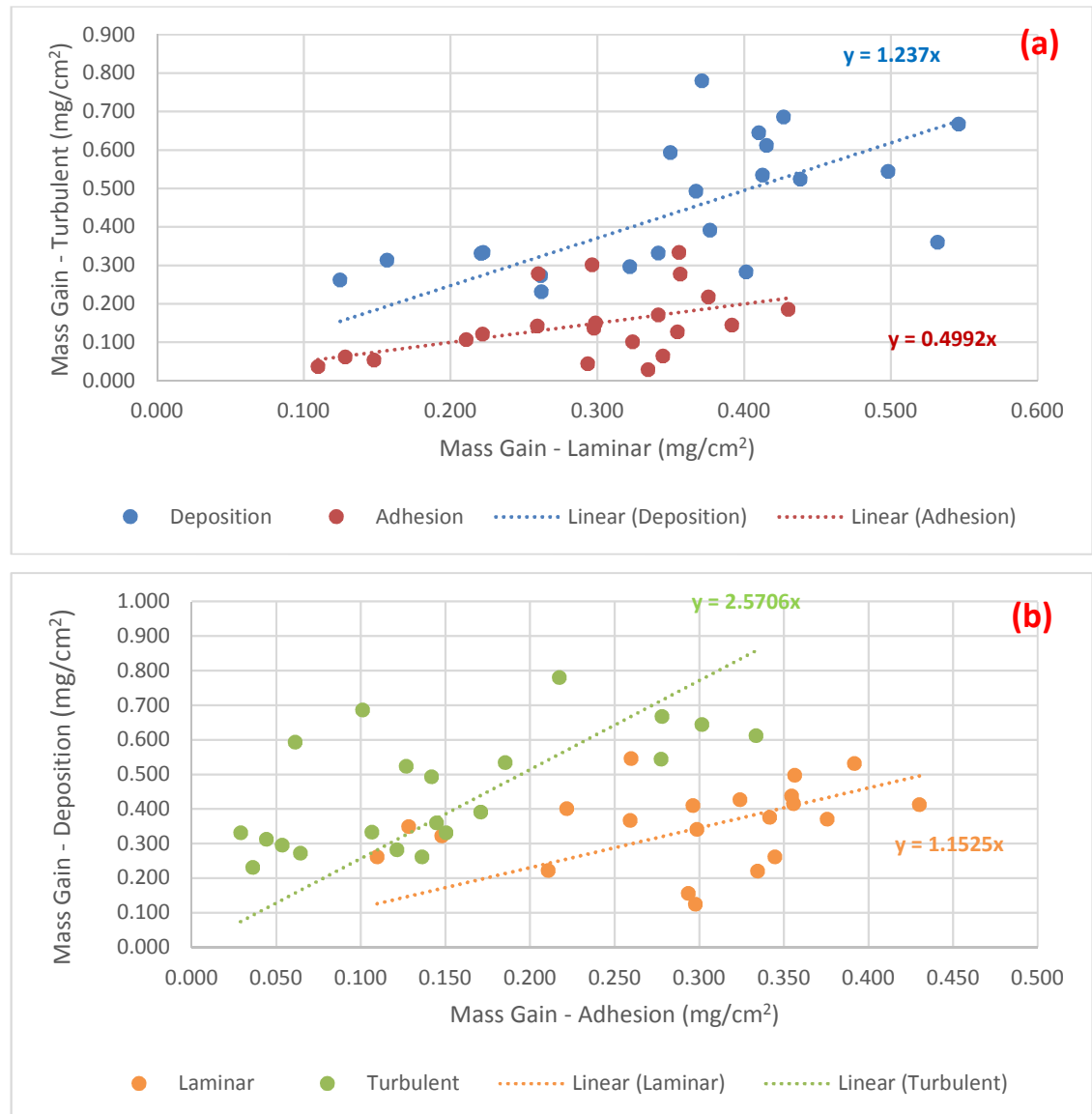


Figure 7.3. The summary mass gain comparison of the *adhesion* and *deposition* processes with regard to the flow regimes in carbonate-dominated brine: (a) the flow regimes have different behaviour toward the *adhesion/deposition* processes, (b) the processes have the same effect on the flow regimes of the bulk solution with different magnitude.

7.2.2. Sulphate-dominated scale formation

The mass gain comparisons of different modified surfaces in the sulphate-dominated brine composition between the laminar and turbulent flow conditions for both *adhesion* and *deposition* processes are shown in Figure 7.4.

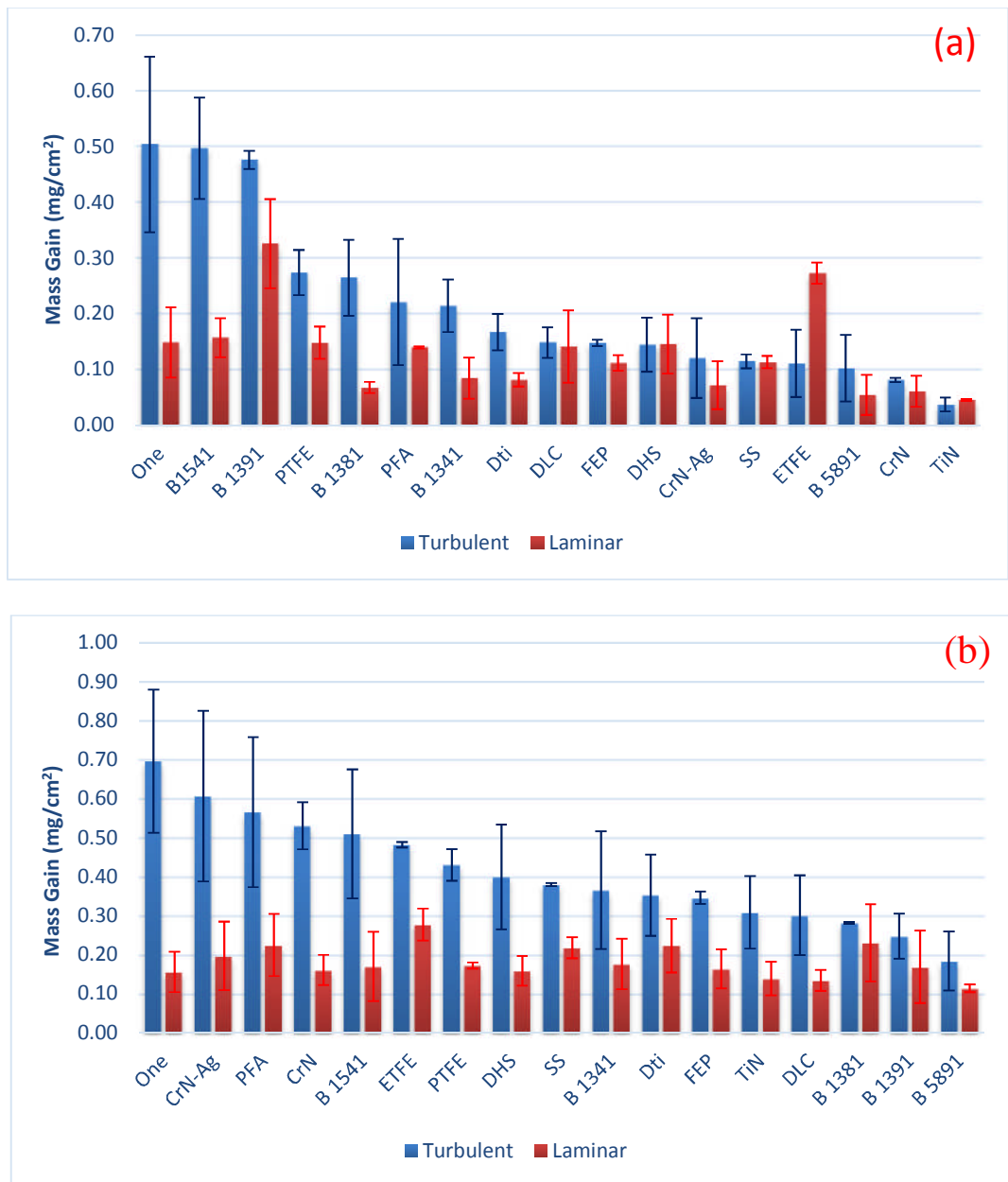


Figure 7.4. Comparison of scaling tendency in different levels of agitation in the (a) Adhesion and (b) Deposition processes.

As shown in Figure 7.4, generally there is a higher rate of mass formation in the turbulent conditions compared to laminar conditions in both *adhesion* and *deposition* processes. It can be explained as in the *deposition* process due to the higher rate of

mass transfer the heterogeneous nucleation sites are more exposed to active ions, to form scales and grow on the surface.

One of the fluoropolymer coatings coded as “One” has unique scaling characteristics among the other coatings. It is the roughest coating, whilst being the most hydrophobic. There is a trade-off between these two parameters in surface scale formation phenomena. With a closer investigation into its performance, it is observed that in turbulent conditions for both *adhesion* and *deposition* tests, this type of coating has the worst performance while in the laminar conditions; it has a relatively good performance. In other words, in laminar conditions where the mass transfer mainly occurs due to the diffusion, hydrophobic effects could have higher effects on hindering the scale formation on the surface while in turbulent conditions such effects are negligible compared to surface roughness which increases the rate of surface scale formation.

Many studies [109-111, 130] have shown that the level of agitation (or hydrodynamic conditions) would affect the rate of scaling, no matter what the chemical composition of the scale. In laminar conditions, the mass transport is mainly controlled by diffusion, while in turbulent conditions it is controlled by advection. Advection (or convection) has a higher effect on the scale formation on the surface compared to diffusion; which is in agreement with our both *adhesion* and *deposition* test results.

However, these changes in the *adhesion* process are not as noticeable as in the *deposition* process which can be referred to the mechanism of scale formation on the surface. In the *adhesion* process, due to the size of the pre-crystallised particles, the effect of momentum is significant; therefore, in turbulent conditions, there is a close rivalry between the settlement of the particles and their adhesion to the surfaces (which is in favour of scale formation) and the effect of momentum and shear stress induced by the brine to the particles to detach them from the surfaces (which are against the scale formation). As a result, there is a lower possibility for particles to settle and adhere to the surface in a turbulent condition. As the level of agitation rises to a critical point, the detachment forces (critical shear stress) exceeds the adhesion forces which results in self-cleaning or removing the scale deposits on the surface by hydrodynamic effects.

The mass gain comparisons of different modified surfaces in the sulphate-dominated brine composition between the *deposition* and *adhesion* processes in both laminar and turbulent flow conditions are shown in Figure 7.5. In the turbulence flow conditions,

the mass gain discrepancies between the heterogeneous nucleation and crystal growth, and the adhesion of the pre-precipitated particles onto the surface are higher than those of in the laminar flow conditions.

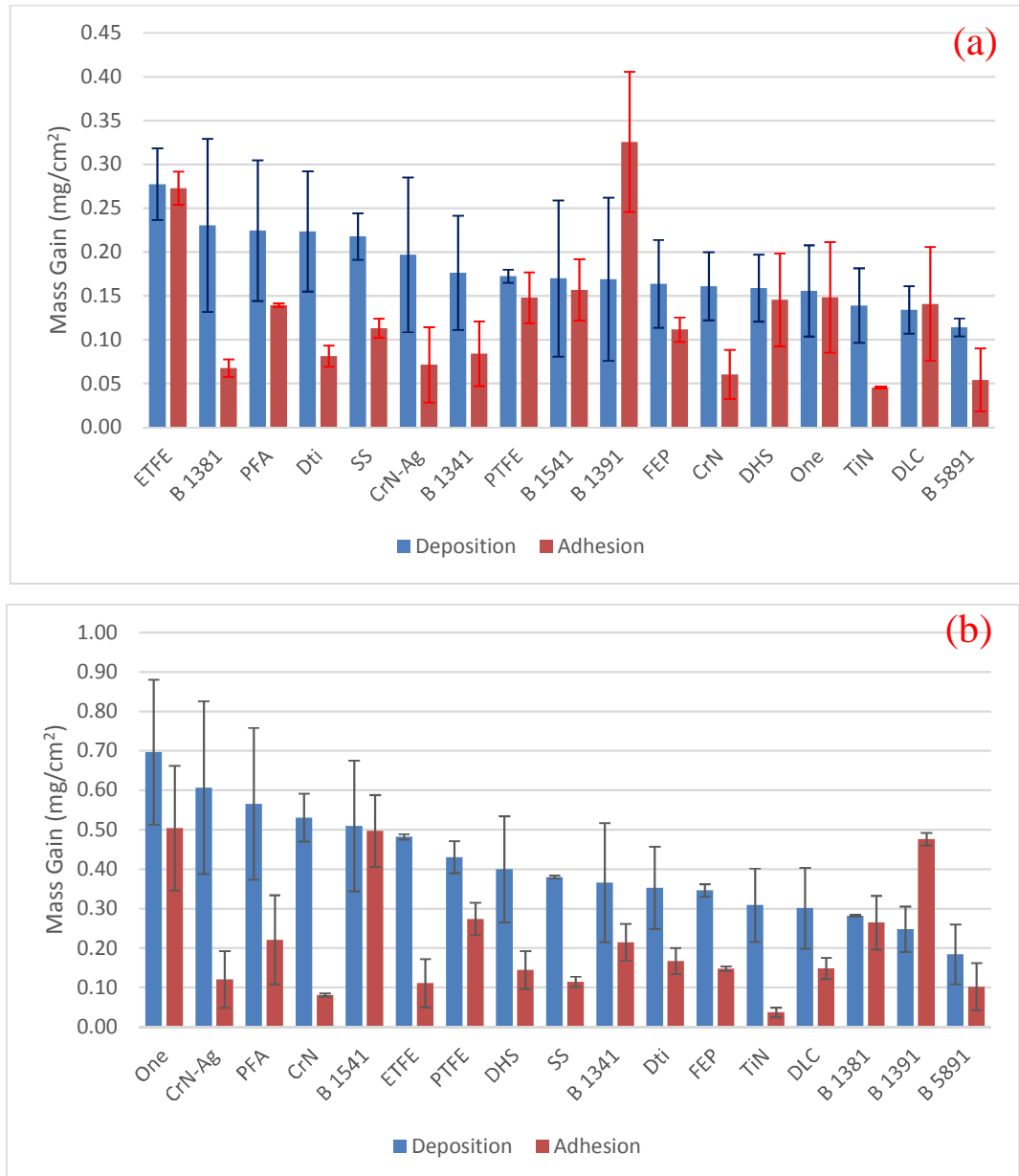


Figure 7.5. Comparison of scaling tendency in different processes of scale formation in (a) Laminar and (b) Turbulent flow conditions.

As shown in Figure 7.5, the surface scale formation is predominantly controlled by the heterogeneous nucleation and crystals growth, i.e. *deposition* process, rather than the adhesion of pre-crystallised particles onto the surface, i.e. *adhesion* process, in both laminar and turbulent flow conditions.

One of the epoxy coatings (e.g. “B1391”) has a distinctive behaviour in both flow regimes, having higher rates of scale formation on the surfaces in the *adhesion* tests. Such occurrence can be explained by its particular topography, i.e. the presence of lumps (e.g. rigid silicon carbide particles) on its surface resulting in the escalation of the effect of particle adhesion to the surface.

In order to have a better understanding of the mass gains presented in Figure 7.4 and Figure 7.5, the mass gain ratio of the laminar to turbulent flow regimes in both processes and the mass gain ratio of *adhesion* to *deposition* processes in both flow regimes are presented in Table 7.2.

Table 7.2. The comparison of the surface scale mass gain ratio for different flow regimes and surface scale processes in sulphate-dominated brine.

No.1	Coating	Deposition	Adhesion	Laminar	Turbulent
		Lam/Turb	Lam/Turb	Adh/Dep	Adh/Dep
1	B 1341	0.482	0.392	0.984	0.586
2	B 1381	0.817	0.255	0.293	0.937
3	B 1391	0.683	0.684	0.621	1.924
4	B 1541	0.333	0.315	0.363	0.200
5	B 5891	0.620	0.531	0.519	2.703
6	CrN	0.303	0.747	0.363	0.152
7	CrN-Ag	0.324	0.594	0.477	0.198
8	DHS	0.398	1.008	0.857	0.361
9	DLC	0.445	0.951	0.923	0.492
10	Dti	0.634	0.486	1.928	0.473
11	ETFE	0.575	2.465	0.681	0.230
12	FEP	0.473	0.756	0.375	0.426
13	One	0.224	0.294	0.916	0.723
14	PFA	0.397	0.631	0.953	0.390
15	PTFE	0.401	0.540	0.326	0.636
16	SS	0.573	0.989	1.050	0.301
17	TiN	0.450	1.227	0.475	0.120
Average		0.478	0.757	0.712	0.638

It can be concluded from Table 7.2 that as the level of agitation increases from the laminar flow condition to turbulent flow conditions, the importance of the *adhesion* process with regard to the *deposition* process in the surface scale formation diminishes. In other words, the mass gain ratio of *adhesion* to *deposition* in laminar flow conditions from 0.712 reduces to 0.638 in the turbulent flow conditions. It can be attributed to the fact that as the bulk hydrodynamics increases the shear forces will increase and it gets more difficult for the pre-precipitates to attach themselves to the surface.

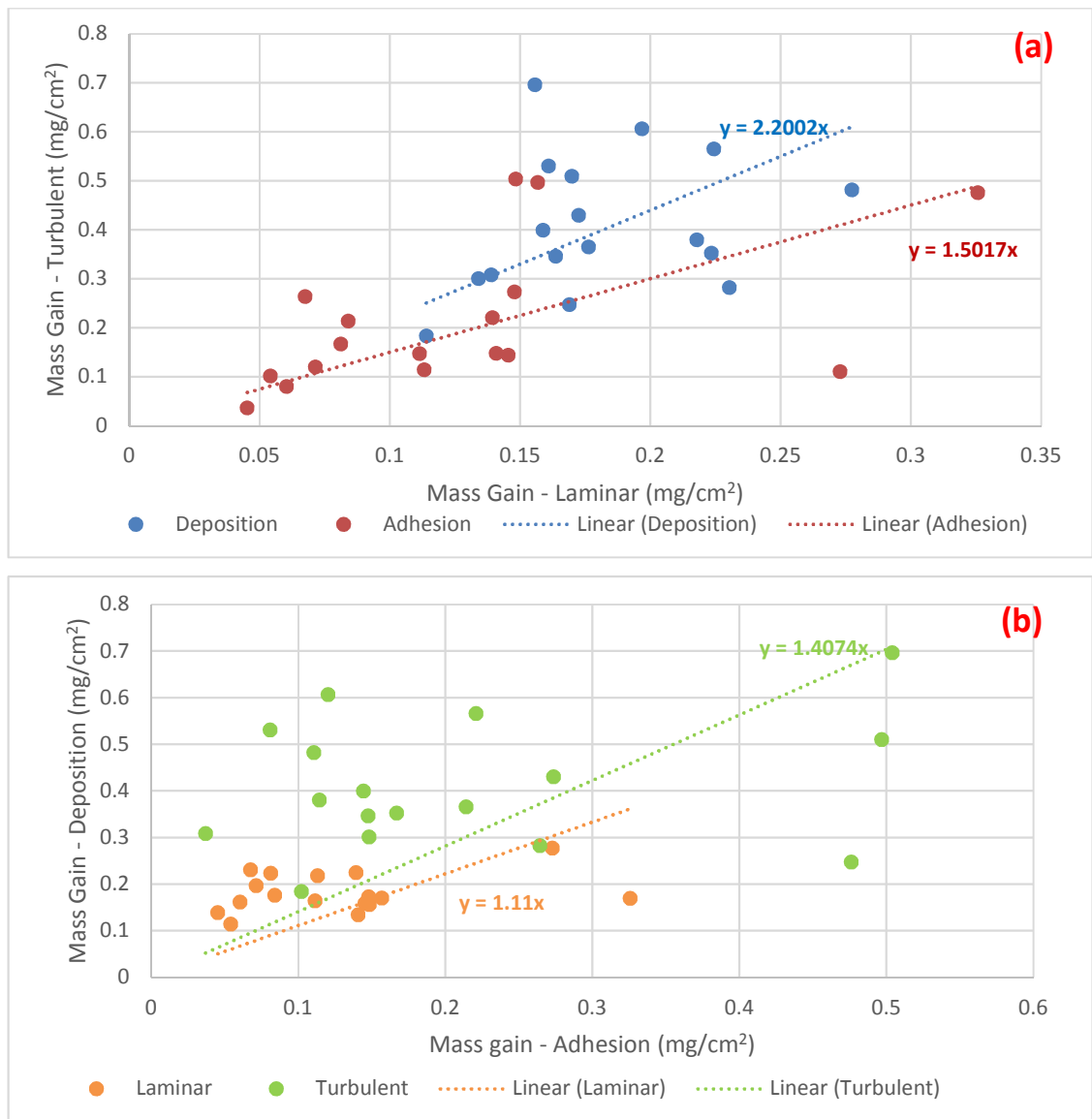


Figure 7.6. The summary mass gain comparison of the *adhesion* and *deposition* processes with regard to the flow regimes in sulphate-dominated brine: (a) the flow regimes have the same behaviour toward the *adhesion/deposition* processes, (b) the processes have the same effect on the flow regimes of the bulk solution with different magnitude.

As explained before, the surface scale formation in the *deposition* process is affected by the convection term, while in the *adhesion* process the diffusion term is primarily controlling the surface scale formation. Such effects are evident in Table 7.2. The mass gain ratio of laminar to turbulent flow conditions increases in the *deposition* process from 0.478 to 0.757 in the *adhesion* process. Such an increase conveys the fact that the surface scale mechanism can change the *adhesion* process in laminar flow conditions to the *deposition* process in turbulent flow conditions in the sulphate-dominated scale systems.

The summary of the mass gain results of the sulphate-dominated scale for both the *adhesion* and *deposition* processes with regard to the flow regimes are shown in Figure 7.6.

As shown in Figure 7.6a, the mass gain in both the *deposition* and *adhesion* processes increase as the flow regime increase. In addition, the former process is more influenced by the flow regimes due to its higher gradient value. On the other hand, as shown in Figure 7.6b, both of the processes have the same effect on the flow regimes of the bulk solution, however, the effect of *deposition* process on turbulent flow regime is higher. It can be attributed to the fact that the heterogeneous nucleation rate is proportional to mass transfer rate, while in the *adhesion* process the surface shear stress which acts as a detachment force increases as the agitation level escalates.

7.2.3. Conclusion summary

In conclusion, the surface scaling performance of sulphate-dominated scale is different from the carbonate-dominated scale with regard to hydrodynamic effects in the *adhesion* process. For example, surface scaling tendency in laminar conditions is higher than turbulent flow conditions in the *adhesion* process for carbonate-dominated scale, while for the sulphate-dominated scale it is vice versa.

The obtained results can be explained by the research conducted by Sanni et al. [131] and Bukuaghangin et al. [132] on the kinetics and surface scale deposition for carbonate and sulphate scales, respectively. By comparing their results, it can be inferred that the size of the scale deposits formed on the surface in the carbonate case is bigger while the number of the nucleation sites for the sulphate case is higher. In the *adhesion* process, the pre-precipitated crystals in the bulk solutions are more affected by the flow conditions, i.e. either by gravitational forces or surface shear stresses. As a result, in the turbulent flow conditions, it is more difficult for the carbonate-based crystals, which are bigger in size, to attach themselves to the surface compared to sulphate-based crystals. Therefore, the surface scaling rate in the carbonate-based scales in the turbulent flow conditions is lower than that of in the laminar flow conditions, although the higher mass transfer of active ions is in favour of scale formation.

Therefore, this study will also help to understand and apply right strategies to mitigate the flow assurance problems in the oilfields, as follows:

- (a) **Carbonate-dominated scale:** in an oil production system that is prone to carbonate-dominated scale, the flow conditions in the downhole, where scaling is dominantly controlled by the *deposition* process, can be maintained at low flow regimes (i.e. laminar flow conditions), where the scaling is rather lower than that of in the turbulent flow conditions. On the other hand, at ground level, where the scaling is controlled up to a point by the *adhesion* process, the flow conditions can be increased drastically, so the high flow conditions inhibit the adhesion of the pre-precipitated particles onto the wall of the oil pipe.
- (b) **Sulphate-dominated scale:** in an oil production system that is prone to sulphate-dominated scale, unlike the previous case, the flow conditions both in the downhole and on the ground level should be controlled at low flow conditions to maintain the mass transfer rate of the active ions to avoid speeding up the surface scale formation. Coating Belzona 5891 is considered as the best coating in sulphate-dominated scale, however this type of coating can withstand up to 90°C and due to its thickness, it cannot apply in valve and pump applications.

7.3. Surface roughness/energy effects on surface scale deposition

7.3.1. Carbonate-dominated scales

One of the many surface parameters that can affect the surface scaling tendency is the surface roughness. The mass gain of scale deposits on the surface versus the surface roughness in both laminar and turbulent conditions are shown in Figure 7.7 and Figure 7.8 for the *deposition* and *adhesion* processes, respectively.

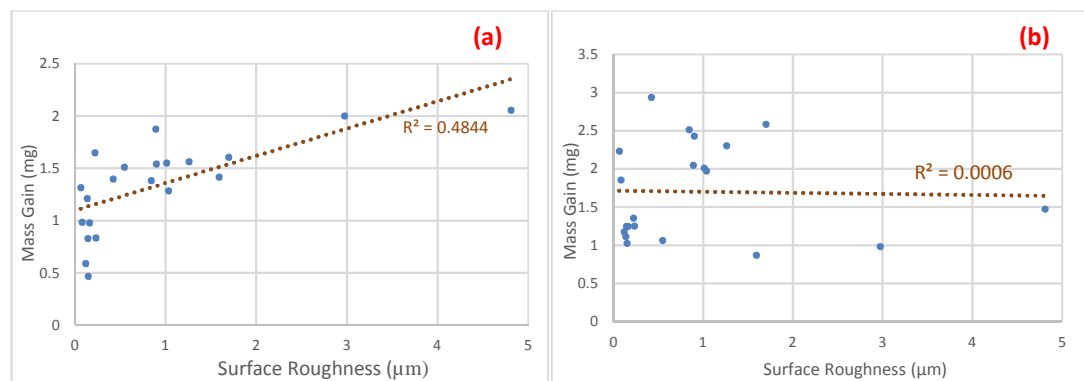


Figure 7.7. The effect of surface roughness on a number of surface scale deposits in the *deposition* process in (a) laminar, and (b) turbulent flow conditions.

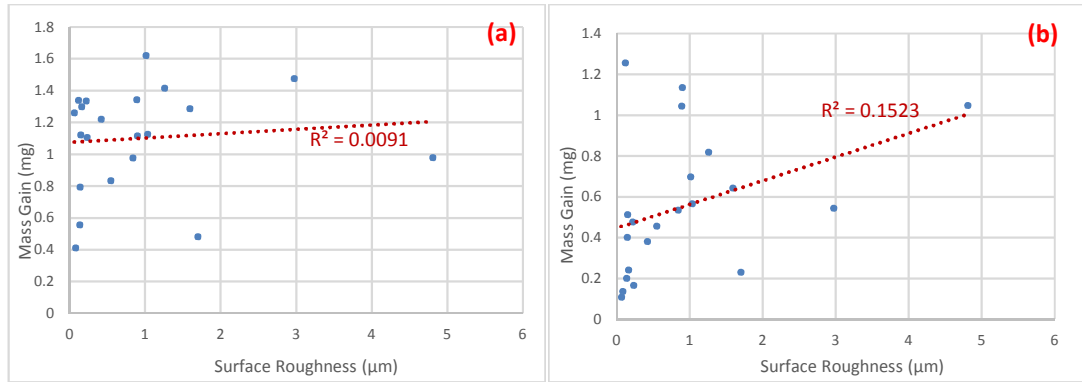


Figure 7.8. The effect of surface roughness on a number of surface scale deposits in the *adhesion* process in (a) laminar, and (b) turbulent flow conditions.

The surface roughness seems has not much effect on the rate of surface scale formation in both *adhesion* and *deposition* processes. Although the effect of surface roughness in the *deposition* process is more distinguishable in the laminar flow conditions compared to the turbulent flow conditions, the surface roughness cannot merely determine the scaling tendency, as there are so many parameters needed to be considered, such as the density of peaks on the surface.

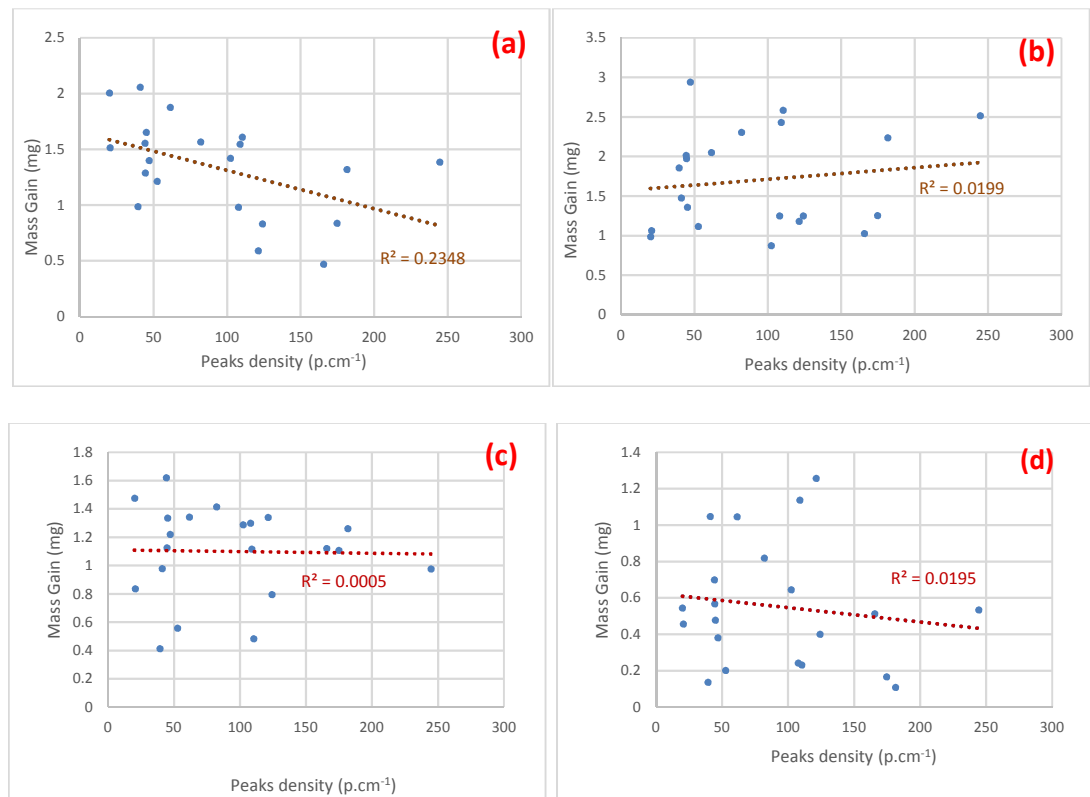


Figure 7.9. The effect of surface peaks density on a number of surface scale deposits in the *deposition* process in (a) laminar, and (b) turbulent flow conditions; and in the *adhesion* process in (c) laminar, and (d) turbulent flow conditions.

As shown in Figure 7.9, the effect of surface peaks density against the mass gain of different modified surfaces for both flow regimes does not show a uniform trend, although the effect of the surface peaks density like the surface roughness is more evident in the laminar flow regimes compared to the turbulent flow regime. For a better understanding of the effect of the surface peaks density, it can be assessed for a certain group of coating, e.g. the ceramic coatings, in laminar flow regimes, where the effect of the surface is more evident on the surface scaling rate.

As shown in Figure 7.10, in ceramic coatings (except the DTi) as the density of peaks (p.cm^{-1}) increases in the laminar flow conditions the rate of surface scale formation decreases. It seems that the high number of peaks, acting as nucleation sites, with regard to the smoothness of the substrates will lead to low scaling tendency. Extensive studies have been conducted on the kinetic of the surface scale formation for both calcium carbonate [131] and barium sulphate[132]. They have shown that in a carbonate-dominated brine, there is a lower number of nucleation sites and bigger crystals compared to a sulphate-dominated brine. It can be concluded from their work that carbonate crystals tend to nucleate and grow in the valleys which are in agreement with the fact that the crystal growth can be faster in the valleys compared to the peaks due to the lower shear forces. In addition, such an argument can be supported by the overgrowth of the carbonate crystals deposited on the surface.

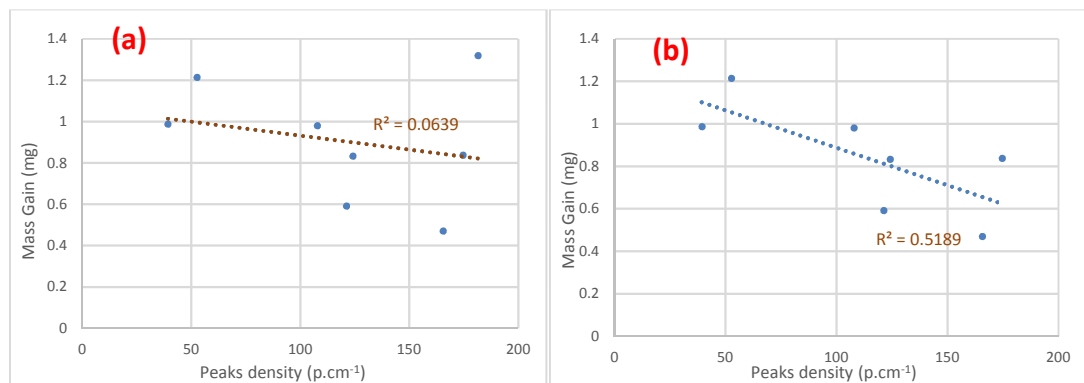


Figure 7.10. The effect of surface peaks density on ceramic surface scale deposits in laminar flow conditions in the *deposition* process for (a) all the ceramic coatings, and (b) ceramic coatings except DTi.

As a result, the high number of peaks on a surface would decrease the possibility of contact between the carbonate nuclei and potential sites on the substrate, known as valleys, as shown in Figure 7.11.

$$(d_1 < d_2) \Rightarrow (pks_1 > pks_2)$$



Figure 7.11. Schematic of two surfaces with a different number of peaks in a specific length.

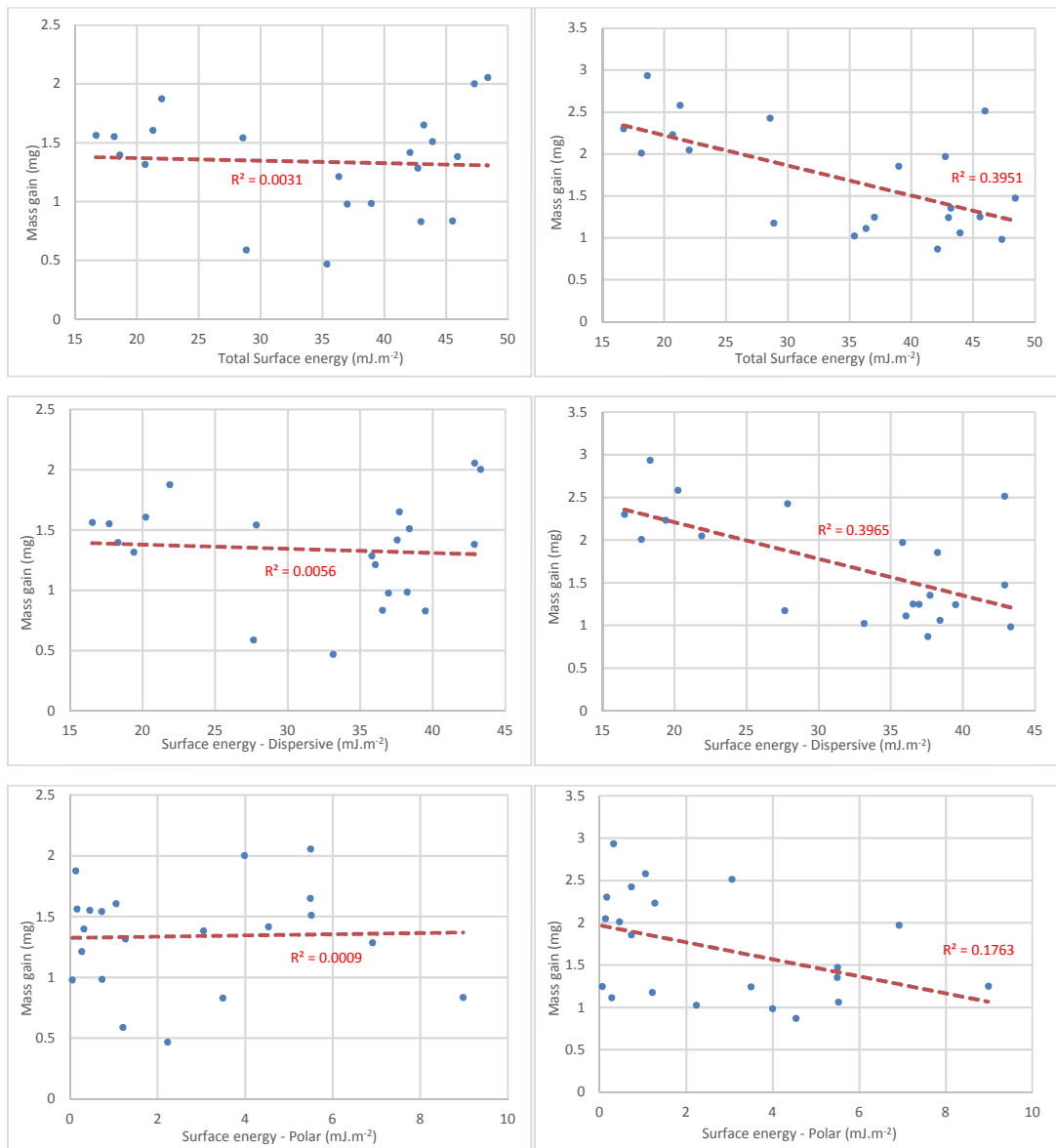


Figure 7.12. The effect of surface energy components on the scaling tendency rate in the *deposition* process using liquid probes for diiodomethane and water for laminar (left column) and turbulent (right column) flow conditions.

The effect of the surface energy along with its dispersive and polar components of the scaling tendency rate of substrates in the *deposition* process for the laminar and turbulent flow conditions are shown in Figure 7.12 and Figure 7.13 for diiodomethane/water and diiodomethane/ethylene glycol liquid probes, respectively.

As shown in Figure 7.12 and Figure 7.13, in both sets of liquid probes, in the turbulent conditions, an increase in the total surface energy would lead to lower scaling tendency ratio. However, this trend is not clear in the laminar conditions in both sets.

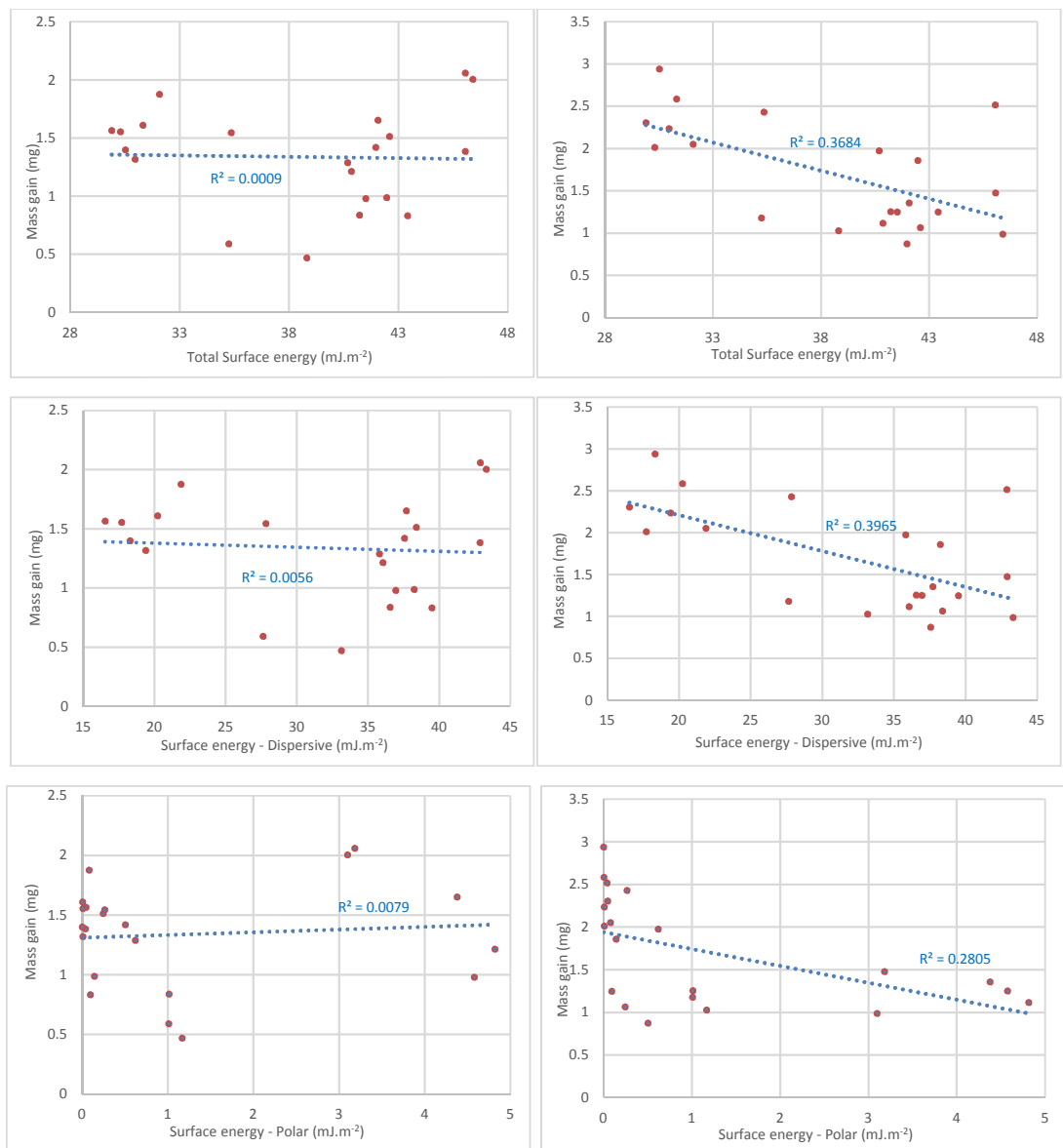


Figure 7.13. The effect of surface energy components on the scaling tendency rate in the *deposition* process using liquid probes for diiodomethane and ethylene glycol for laminar (left column) and turbulent (right column) flow conditions.

An increase in the polar component of surface energy would result in an escalation in the scaling tendency rate in the diode-EG set, however, in the diode-water set such trend is opposite. As a result, the dispersive component of the surface energy is the dominant parameters which control the trend between the surface energy and scaling tendency ratio.

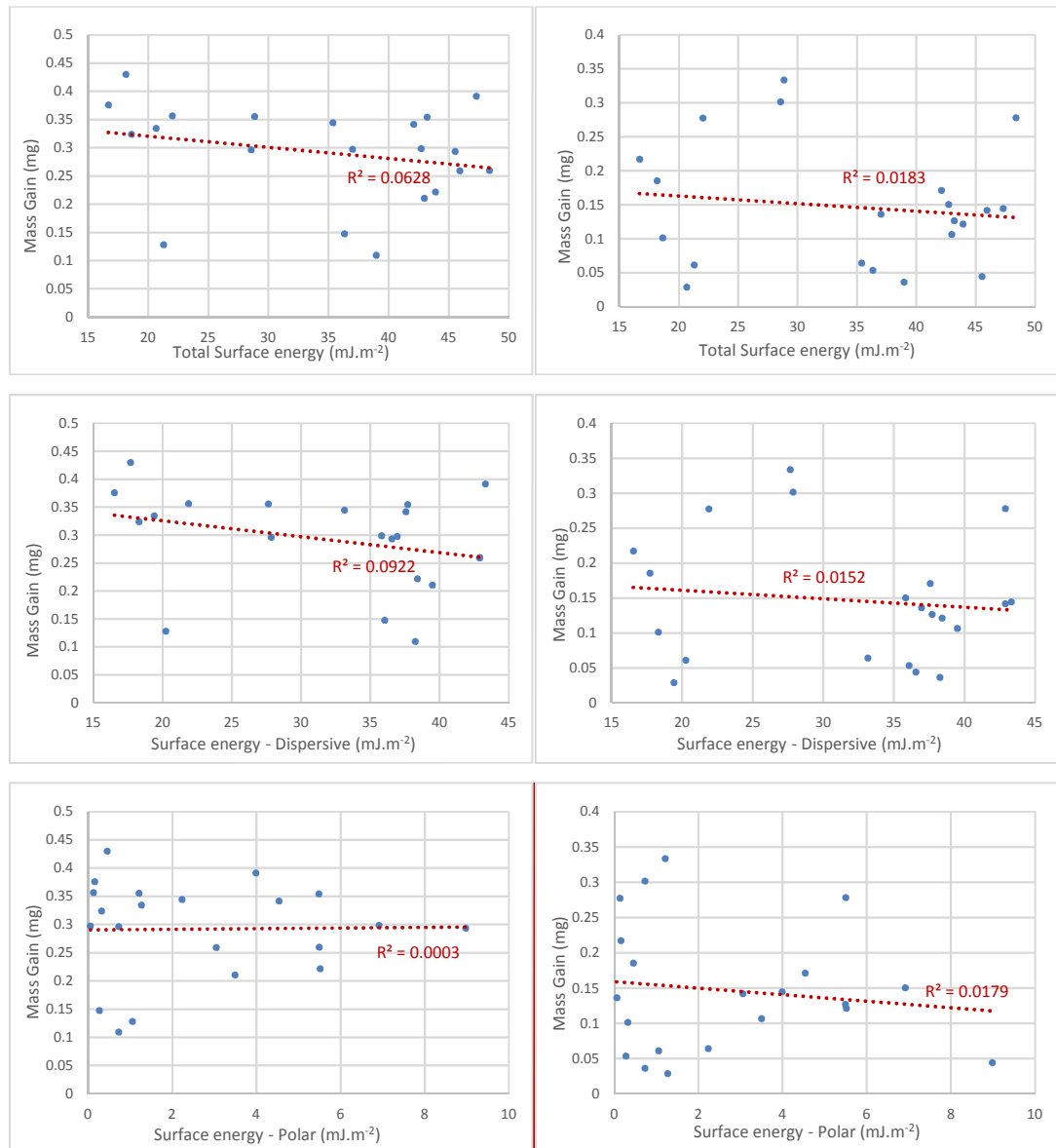


Figure 7.14. The effect of surface energy components on the scaling tendency rate in the *adhesion* process using liquid probes for diodomethane and water for laminar (left column) and turbulent (right column) flow conditions.

The effect of the surface energy along with its dispersive and polar components of the scaling tendency rate of substrates in the *adhesion* process for the laminar and

turbulent flow conditions are shown in Figure 7.14 for diiodomethane/water liquid probes. By taking into the consideration of the trend line of the effect of the surface energy components on the surface mass gain of the *adhesion* process, it is evident that the surface energy has no impact on the surface scale formation in all flow regimes.

7.3.2. Sulphate-dominated scales

In general, the parameters such as surface chemistry, surface roughness, surface energy, and surface hydrophobicity are known as the criteria that play a major role in the scale formation process. However, it is not fully understood how each of these parameters affects the scaling process.

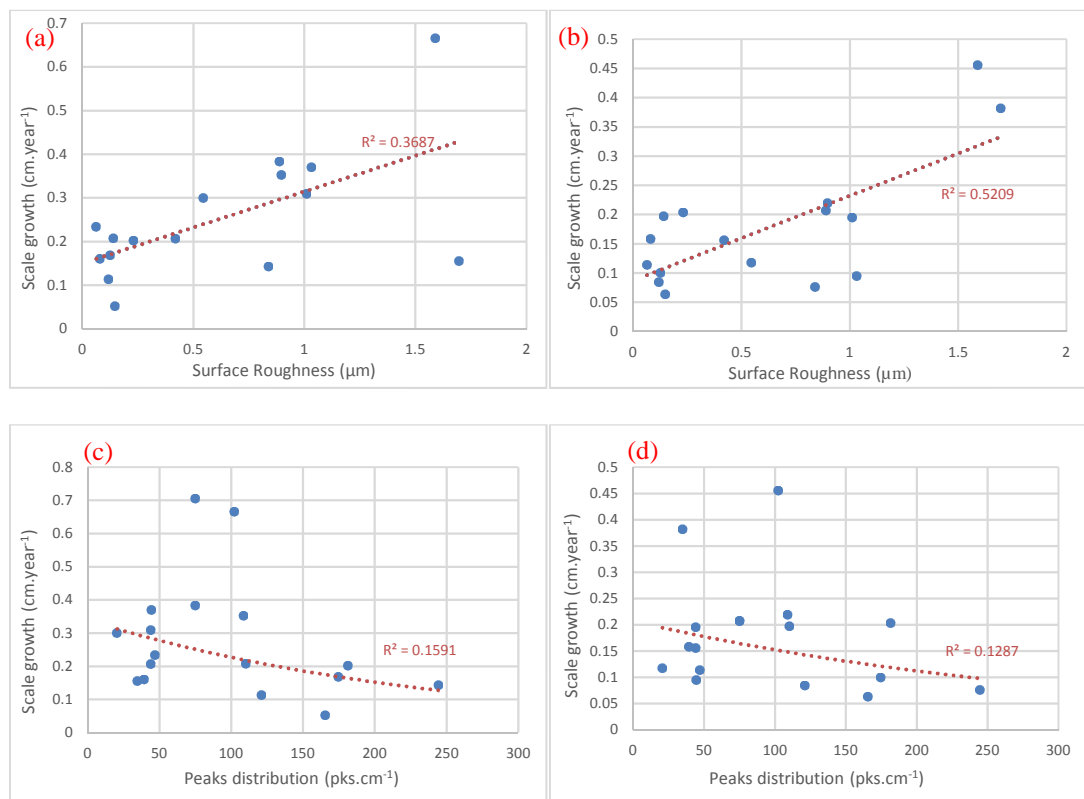


Figure 7.15. The effect of surface roughness and peak distribution on the surface scale growth rate in the *adhesion* process, for (a) & (c) Turbulent and (b) & (d) Laminar flow conditions respectively.

For instance, low surface energy is known as one of the parameters which decreases the scale deposition rate on a surface. However, Forster et al. [100] showed that the deposition rate of a substrate PTFE coating is higher than that with DLC coating, although the latter one has higher surface energy. Eroini et al. [133] surveyed surface resistance to scaling over a diverse range of substrates and reported that there is no

strong correlation between the surface roughness/hydrophobicity and the scaling deposition. Rankin and Adamson [103] mentioned that roughness increases contact surface area; therefore, a rough surface has a greater effective surface energy comparing to a smooth surface, and as a result, a stronger adhesion can occur on rough surfaces.

Keysar [63] tested the effect of roughness (0.1 μm - 24 μm) of the mild steel under well-controlled conditions on calcite scale formation and found that the adhesion force of rough surfaces is much higher than that for smooth surfaces. Herz et al. [102] also conducted the scale *deposition* test on a substrate with roughnesses range from 0.18 μm to 1.55 μm and accentuated that as the surface roughness increases the deposited scale enhances on the surface. They reported that such behaviour can be contributed to the reduction of local shear forces at the valleys and the increase in primary heterogeneous nucleation rate on the surface. However, Cheong [64] reported that rougher surfaces do not necessarily end up with higher scale deposits. The author indicated that in polymer surfaces the roughness effects found to be of secondary importance and other characteristics such as surface chemistry and surface energy could be more important.

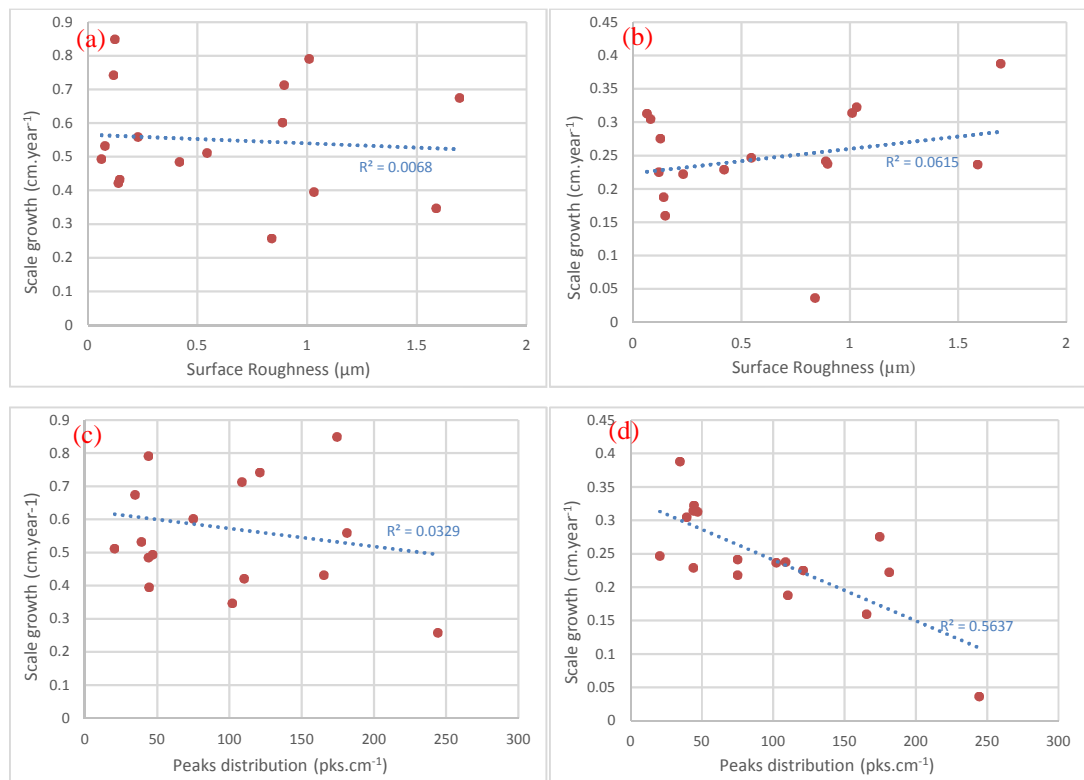


Figure 7.16. The effect of surface roughness and peak distribution on the surface scale growth rate in the *deposition* process for (a) & (c) Turbulent and (b) & (d) Laminar flow conditions, respectively.

The roughness of the majority of tested coated surfaces ranges from $0.063\mu\text{m}$ to $1.697\mu\text{m}$, except the coating “One” with a roughness of $3.6029\mu\text{m}$. Due to its particular roughness, the coating “One” is excluded in both Figure 7.15 and Figure 7.16 to be assessed separately. As shown in Figure 7.15 and Figure 7.16, the effect of surface roughness and the surface peak distribution on the surface scale growth rate are assessed separately in both *adhesion* and *deposition* processes for both turbulent and laminar conditions. In the *deposition* tests, there is no noticeable correlation between the surface roughness and the surface scale growth rate, while in the *adhesion* process there is a trend, although it is a weak one. It also shows that in the *deposition* tests the effect of roughness in such scale (i.e. lower than $2\mu\text{m}$) is diminishing, while in the *adhesion* process it is strengthening.

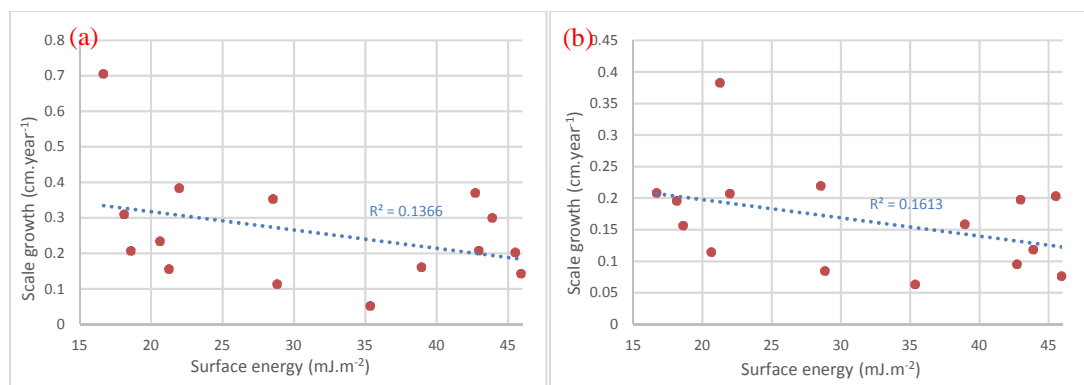


Figure 7.17. The effect of surface energy on the surface scale growth rate in the *adhesion* process for (a) Turbulent and (b) Laminar flow conditions.

The effect of surface peak distribution in all of the flow conditions in both processes on the surface scale growth rate appears unchanged. An increase in the number of peaks in a specific dimension will lead to a lower surface scale growth rate. The reason can be attributed to the kinetics and the way that sulphate-based scale forms on the surface. The mechanism of the surface scale formation in the *deposition* process is mainly directed by the heterogeneous nucleation and the crystal growth. Unlike the general perception as a higher number of nucleation sites, a higher number of potential points for scale formation, the higher number of peaks has resulted in the lower amount of scale formation which needs to be assessed and analysed in more details. Such results are more obvious in the laminar flow regime where the surface

topography plays a more dominant parameter compared to the turbulent flow regime, where the bulk effect on the surface scale formation is more prevalent.

Surface energy is often quoted as a parameter which when it is increased on the surface would have an enhanced rate of scale formation on the surface. The *deposition/adhesion* test results are plotted in Figure 7.17 and Figure 7.18 and the weak trend seems to oppose the literature and conventional thinking. However, it is important to remember that there are many more variables here other than surface energy.

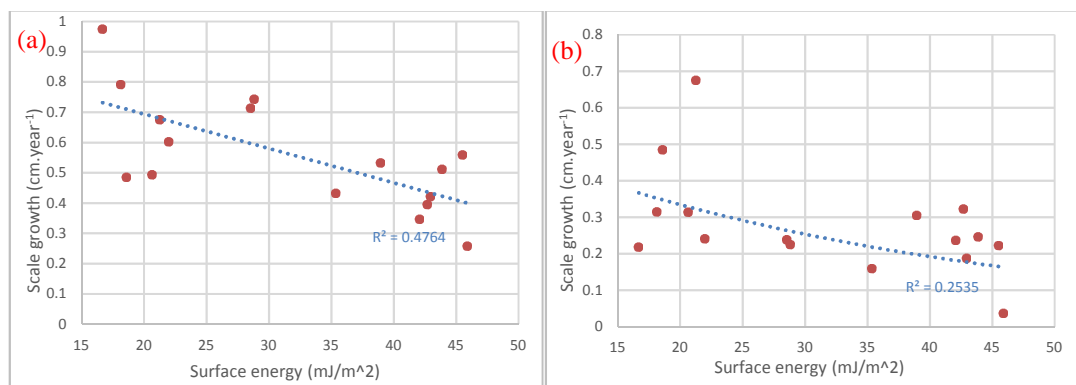


Figure 7.18. The effect of surface energy on the surface scale growth rate in the *deposition* process for (a) Turbulent and (b) Laminar flow conditions.

Surface energy and surface roughness show how they would behave in *adhesion* and *deposition* processes however these parameters along with surface chemical compositions are not the main factors affecting the scale formation on the surface.

7.3.3. Conclusion summary

Based on the results presented in both the *adhesion* and *deposition* processes, it seems that one parameter cannot merely affect the surface scale formation rate, i.e. neither the surface roughness nor the surface energy has not shown a definitive impact on the rate of surface scale tendency. Although characterising such parameters one at a time can help to have a better understanding to improve the surface performance and mitigate the flow assurance problems.

For example, no trend is observed between the peak density and the surface scaling rate; however, assessing such a trend in a system with the same surface finish characteristics (e.g. ceramic coatings) has shown a more evident result.

In carbonate-dominated case, the trend between the surface scaling and the surface roughness is proportional in laminar flow conditions in the *deposition* process, while it is not the case for turbulent flow conditions in the *adhesion* process, although such trends in both processes are weak.

It has been observed that if the liquid probes system in measuring the surface energy changes, the proportionality between the surface energy and the surface scaling rate does not change considerably.

In sulphate-dominated case, it has been observed in the *adhesion* process that the rougher the surface, the more surface scaling rate; and also the higher is the value of the peak density, the lower surface scaling rate. In the *deposition* process, such trends are only true for laminar flow conditions.

The similarity between both of the sulphate/carbonate-dominated brine compositions is in the effect of surface energy on the rate of surface scaling, where in both cases, higher surface energy is inversely proportional to the surface scaling rate in both processes in laminar and turbulent flow conditions, although they are weak trends.

7.4. Morphology of scale deposits

7.4.1. Carbonate-dominated scales

Calcium carbonate (CaCO_3) is the most abundant inorganic biomaterial with different polymorphs, e.g. three anhydrate and three hydrated polymorphs. With the increasing order of the thermodynamic stability, these polymorphs are amorphous calcium carbonate (ACC), calcium carbonate hexahydrate ($\text{CaCO}_3 \cdot 6\text{H}_2\text{O}$), calcium carbonate monohydrate ($\text{CaCO}_3 \cdot \text{H}_2\text{O}$), vaterite, aragonite and calcite. [134, 135]

As shown in Figure 4.10, all morphologies of calcium carbonate (calcite, aragonite and vaterite) have been formed and deposited on modified surfaces. The SEM examinations have revealed that various crystal structures comprising the needle-like structure as aragonite, the rhombohedral structure as calcite and spherical structure as vaterite. In addition, some unusual morphologies are distinguishable that are either formed as one crystal or as the result of the aggregations of crystals together (e.g. centred deformed calcite crystal or clump of crystals shaped like a star or rod-like aggregates). But what are the most interesting morphological findings in the results are the dominant presence of amorphous crystals which are thermodynamically the least stable form of calcium carbonate polymorphs [134].

Tang et al. [135] suggest that in conditions where a rich variety of CaCO_3 polymorphs exist it can be attributed to the amorphous character of amorphous calcium carbonate (ACC) that enables it to easily shape itself into many different polymorphs.

Figure 4.11 shows the deformity at the centre of the cubical structure of calcite crystals. Such unusual morphology has been reported with different names such as concave terraced calcite [136], pitting on the surface due to the characteristics of resolution of the crystallites [137], or the deformity in the centre of the calcite crystals due to the fact that vaterite is formed from calcite precursor in stages, and such crystals are at middle stages.[138]

As shown in Figure 4.12, the aragonite crystals are less affected by the hydrodynamic effects compared to the calcite crystals. By considering the fact that aragonite precipitates more rapidly compared to calcite, [139, 140] the size of the aragonite crystals would be less affected by the hydrodynamic conditions, which is reasonable due to its needle-like shape and the orientation that such crystals have grown on the surface. Burton and Walter [140] have reported that the aragonite precipitation rate is equivalent to those of calcite at 5°C , while aragonite precipitation rates increase up to a factor of 4 compared to calcite at a temperature of 37°C , irrespective of the degree of saturation. In addition, the existence of Mg^{2+} decreases the crystal growth of calcite to about 50% [141], but it seems that such impact would affect the calcite crystals in laminar conditions.

As shown in Figure 4.15, the presence of Mg^{2+} ions in the bulk solution have affected the morphology of calcite crystals. In many systems, Mg^{2+} and Ca^{2+} ion coexist. Mg^{2+} ion has attracted much attention among the inorganic mineralizers because of its abundance in seawater and its critical role in the formation CaCO_3 . [142] Therefore, there have been so many studies assess the effect of Mg^{2+} ions in the bulk on the morphologies of calcium carbonate.

Tang et al. [135] reported that as the molar ratio of Mg^{2+} to Ca^{2+} increases, the morphology of calcium carbonate changes from well-defined rhombohedral crystals to rough rhombohedral crystals and eventually to peanut-like aggregates. In addition, in this study instead of water, ethanol, as a solvent was used to increase the influence of magnesium ions on the morphology of CaCO_3 and the crystals, changed from rhombohedral crystals to irregular polyhedrons and bundles. Yang et al. [134] found that by an increase in the ratio of $n_{\text{Mg}^{2+}}/n_{\text{Ca}^{2+}}$ in the system, the average size of

nanocrystals of calcite decreases which results in a decrease and disordering in the lattice of calcite.

As shown in Figure 4.17, the existence of magnesium ions in the lattice of aragonite is clear. It has been shown that the distribution coefficient of Mg^{2+} in calcite (k_{Mg}^C) rises by an increase in temperature, [97, 143] however, the temperature effect on the distribution coefficient of Mg^{2+} in aragonite (k_{Mg}^A) is insignificant.[97] The existence of Mg^{2+} ions in a system not only affect the calcite morphology but also have impact on the nucleation process and inhibit the crystal growth.[141, 142, 144-147]

Davis et al. [148] have shown that the Mg^{2+} ions inhibit the calcite crystal growth by incorporating into the calcite lattice. Furthermore, many studies have reported that Mg^{2+} inhibits the growth rate of calcite but not aragonite. [141, 149-151] Dawe and Zhang has reported that the existence of Mg^{2+} at a ratio of $[Mg^{2+}] / [Ca^{2+}]$ between 0.1 and 0.5 affects the kinetics of calcite and causes a 50% reduction of calcite growth rate. [141] In the brine composition tested in this thesis, the ratio of Mg^{2+} (mMol) to Ca^{2+} (mMol) is around 0.24.

Mucci and Morse [152] have shown that the amount of $MgCO_3$ would result in the overgrowth of calcium carbonate crystals and is determined by the Mg^{2+} to Ca^{2+} concentration ratio in the solution which they precipitated.

Park et al. [153] reported that the existence of the Mg^{2+} ions in the brine solution would lead to the formation of Mg-calcite and as Mg^{2+} ion concentrations increase the amount Mg-calcite crystals decreases and a number of aragonite increases. In addition, the longitude and aspect ratio of the formed aragonite crystals decreases due to an increase in Mg^{2+} ion concentration. [153, 154]

As shown in Figure 4.16, aragonite crystals formed on the surface normally shaped as rod-like bundles with a relative lower aspect ratio compared to normal needle-like aragonite crystals that were reported before. [154, 155]

Xu et al. [156] also reported that at room temperature the high concentration of Mg^{2+} ion favours the aragonite precipitations rather than calcite. Magnesium ions can incorporate into the lattice of calcite while the aragonite lattice is unaffected by the magnesium ions. In addition, the incorporation of magnesium into the lattice of the calcite will cause it to be more soluble than pure calcite. As a result, the increased amount of aragonite with respect to the increase of magnesium ions can be described in terms of selective adsorption of magnesium onto the calcite crystals which

effectively reduces the crystal growth of calcite and increases the relative stability of aragonite.[157]

7.4.2. Sulphate-dominated scales

As shown in Figure 5.3 - Figure 5.7, the size and the basic morphology of the scale deposits have altered neither by the effect of the hydrodynamic conditions nor by the employment of different scale processes. Such observation is also reported by Todd and Yuan.[158]

The sisal-like hierarchical structure is also reported and analysed the formation process of SrSO_4 . Wang et al. [29] speculated the morphology evolution steps of the strontium sulphate from a SrSO_4 small monopod to grow into SrSO_4 multi-pods, in which the adjacent crystals are oriented by sharing a common crystallographic orientation and docking of these crystals at a planar interface, as shown in Figure 7.19.

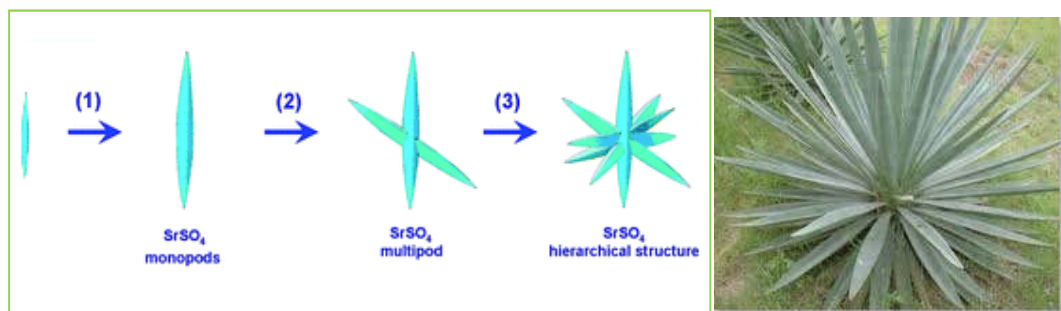


Figure 7.19. Schematic illustration of the formation process of the SrSO_4 sisal-like hierarchical structures [29] and the natural shape of a sisal plant.

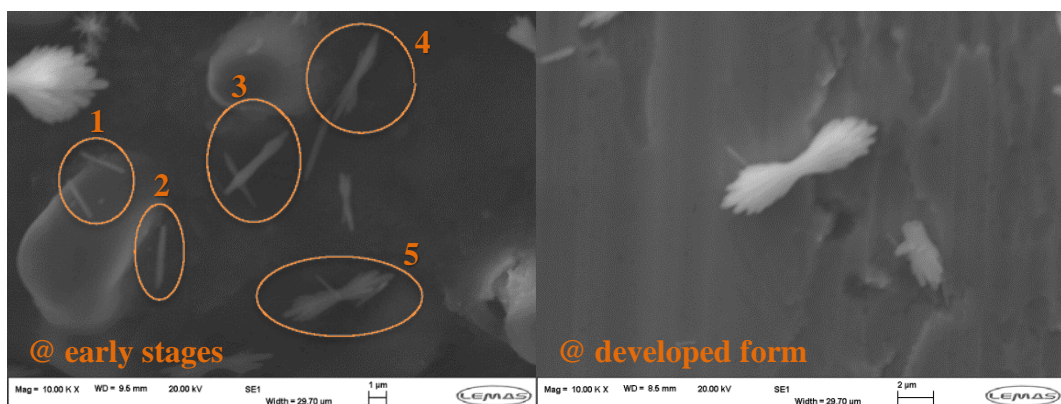


Figure 7.20. The SEM image of the scale deposits showing the evolution steps of the bowtie structure morphology.

The morphology evolution steps of the bowtie structure cannot be fully determined, due to the limitation in observing the *in situ* orientation process. However, the author believes that it can be explained as shown in Figure 7.20. Tang et al. [135] reported that the existence of the magnesium in the brine will lead to the formation of calcium carbonate with the morphology of peanut-like aggregates. They also suggested the same formation process of peanut-like CaCO₃ aggregates.

7.5. Co-precipitation of scale deposits

7.5.1. Carbonate-dominated scales

As shown in Figure 4.18, the deposited scale on the surface is the deposition of CaCO₃, SrCO₃ and BaSO₄ scale deposits. Therefore, understanding the chemistry and morphology of the scale deposits originated from a complex brine solution is essential. Although the importance of the co-precipitation phenomenon, not many studies have been conducted to characterise the co-precipitation and co-deposition of the scale deposits in the oilfield.

There have been so many studies that surveyed the incorporation of strontium into the lattice of calcium carbonate. [90, 93-96, 152, 159, 160] Katz et al. [159] have shown that the distribution coefficient of strontium in calcite has affected slightly by the temperature, but not affected by the presence of NaCl. In addition, the strontium incorporated in the calcite recrystallized from aragonite.

As shown in Figure 4.19 and Figure 4.20, the co-precipitation of Sr²⁺ in the lattice of aragonite has a higher ratio compared to both calcite and vaterite on both modified surfaces. Plummer and Busenberg [160] have demonstrated that the exchange of calcium in strontianite (SrCO₃) and strontium in aragonite initially enhance the stability of the precipitate.

It has been showed in the SEM images section that the existence of magnesium in the complex brine solution and the lattice of the calcium carbonate crystal will result in the formation of calcite with round edges or the formation of aragonite crystals with relative lower aspect ratio. In addition, in the EDX section, the existence of strontium in the lattice of the aragonite crystals is evident.

By considering the fact that in the complex brine composition with relative high supersaturation ratio of calcium carbonate, where there is an abundant amount of magnesium and strontium ions in the solution, the incorporation of such ions in the

CaCO₃ is not surprising. As a result, by integrating the dominant morphologies of the calcium carbonate, e.g. calcite and aragonite, into one entity as calcium carbonate scale deposits, the compound can be written as $(Ca_x Sr_y Mg_z)CO_3$ for which $0 < x, y, z < 1$. Therefore the results can be presented in Table 7.3.

Table 7.3. The chemical compound of the carbonate-dominated scale deposits on the surface, analysed by ICP in turbulent and laminar flow conditions in the *adhesion* and *deposition* processes.

Coating	Deposition Process		Adhesion Process	
	Turbulent*	Laminar*	Turbulent*	Laminar*
B1391	Ca _{0.83} Sr _{0.09} Mg _{0.07}	Ca _{0.8} Sr _{0.14} Mg _{0.06}	Ca _{0.79} Sr _{0.14} Mg _{0.07}	Ca _{0.85} Sr _{0.11} Mg _{0.04}
B5891	Ca _{0.77} Sr _{0.14} Mg _{0.08}	Ca _{0.82} Sr _{0.12} Mg _{0.06}	Ca _{0.79} Sr _{0.13} Mg _{0.08}	Ca _{0.89} Sr _{0.08} Mg _{0.03}
B5891exp	Ca _{0.79} Sr _{0.14} Mg _{0.08}	Ca _{0.85} Sr _{0.10} Mg _{0.05}	Ca _{0.81} Sr _{0.11} Mg _{0.09}	Ca _{0.82} Sr _{0.12} Mg _{0.07}
B5892	Ca _{0.82} Sr _{0.10} Mg _{0.08}	Ca _{0.82} Sr _{0.14} Mg _{0.04}	Ca _{0.79} Sr _{0.14} Mg _{0.07}	Ca _{0.82} Sr _{0.12} Mg _{0.05}
B5892exp	Ca _{0.79} Sr _{0.11} Mg _{0.10}	Ca _{0.77} Sr _{0.16} Mg _{0.07}	Ca _{0.79} Sr _{0.13} Mg _{0.08}	Ca _{0.85} Sr _{0.11} Mg _{0.04}
DHS	Ca _{0.84} Sr _{0.09} Mg _{0.07}	Ca _{0.80} Sr _{0.13} Mg _{0.07}	Ca _{0.77} Sr _{0.14} Mg _{0.09}	Ca _{0.86} Sr _{0.10} Mg _{0.04}
SS 316	Ca _{0.82} Sr _{0.11} Mg _{0.07}	Ca _{0.86} Sr _{0.09} Mg _{0.05}	Ca _{0.81} Sr _{0.09} Mg _{0.09}	Ca _{0.92} Sr _{0.06} Mg _{0.02}
TiN	Ca _{0.82} Sr _{0.11} Mg _{0.07}	Ca _{0.85} Sr _{0.09} Mg _{0.06}	Ca _{0.81} Sr _{0.10} Mg _{0.09}	Ca _{0.92} Sr _{0.06} Mg _{0.02}
DLC	Ca _{0.81} Sr _{0.11} Mg _{0.08}	Ca _{0.86} Sr _{0.07} Mg _{0.05}	Ca _{0.82} Sr _{0.10} Mg _{0.08}	Ca _{0.91} Sr _{0.06} Mg _{0.03}
CrN	Ca _{0.87} Sr _{0.05} Mg _{0.08}	Ca _{0.81} Sr _{0.13} Mg _{0.06}	Ca _{0.82} Sr _{0.11} Mg _{0.07}	Ca _{0.83} Sr _{0.13} Mg _{0.04}
TiAlN	Ca _{0.79} Sr _{0.13} Mg _{0.08}	Ca _{0.82} Sr _{0.15} Mg _{0.03}	Ca _{0.79} Sr _{0.12} Mg _{0.09}	Ca _{0.84} Sr _{0.13} Mg _{0.03}
Dti	Ca _{0.81} Sr _{0.11} Mg _{0.08}	Ca _{0.71} Sr _{0.24} Mg _{0.05}	Ca _{0.80} Sr _{0.12} Mg _{0.08}	Ca _{0.91} Sr _{0.06} Mg _{0.03}
B1381	Ca _{0.81} Sr _{0.11} Mg _{0.08}	Ca _{0.83} Sr _{0.12} Mg _{0.05}	Ca _{0.80} Sr _{0.13} Mg _{0.07}	Ca _{0.80} Sr _{0.14} Mg _{0.06}
B1341	Ca _{0.81} Sr _{0.11} Mg _{0.08}	Ca _{0.86} Sr _{0.09} Mg _{0.05}	Ca _{0.83} Sr _{0.10} Mg _{0.07}	Ca _{0.84} Sr _{0.11} Mg _{0.05}
B1541	Ca _{0.78} Sr _{0.14} Mg _{0.08}	Ca _{0.78} Sr _{0.17} Mg _{0.05}	Ca _{0.80} Sr _{0.14} Mg _{0.06}	Ca _{0.89} Sr _{0.08} Mg _{0.03}
SS 416	Ca _{0.82} Sr _{0.09} Mg _{0.08}	Ca _{0.85} Sr _{0.09} Mg _{0.06}	Ca _{0.80} Sr _{0.11} Mg _{0.09}	Ca _{0.89} Sr _{0.08} Mg _{0.03}
PFA	Ca _{0.81} Sr _{0.09} Mg _{0.11}	Ca _{0.82} Sr _{0.13} Mg _{0.05}	Ca _{0.88} Sr _{0.08} Mg _{0.04}	Ca _{0.88} Sr _{0.09} Mg _{0.03}
FEP	Ca _{0.80} Sr _{0.11} Mg _{0.10}	Ca _{0.82} Sr _{0.14} Mg _{0.04}	Ca _{0.81} Sr _{0.12} Mg _{0.07}	Ca _{0.91} Sr _{0.06} Mg _{0.03}
ETFE	Ca _{0.80} Sr _{0.11} Mg _{0.08}	Ca _{0.82} Sr _{0.12} Mg _{0.06}	Ca _{0.84} Sr _{0.10} Mg _{0.06}	Ca _{0.88} Sr _{0.07} Mg _{0.05}
PTFE	Ca _{0.83} Sr _{0.08} Mg _{0.09}	Ca _{0.83} Sr _{0.13} Mg _{0.04}	Ca _{0.82} Sr _{0.14} Mg _{0.04}	Ca _{0.91} Sr _{0.07} Mg _{0.02}
One	Ca _{0.79} Sr _{0.13} Mg _{0.08}	Ca _{0.82} Sr _{0.14} Mg _{0.04}	Ca _{0.78} Sr _{0.15} Mg _{0.07}	Ca _{0.83} Sr _{0.14} Mg _{0.03}
Average	Ca _{0.81} Sr _{0.11} Mg _{0.08}	Ca _{0.82} Sr _{0.13} Mg _{0.05}	Ca _{0.81} Sr _{0.12} Mg _{0.07}	Ca _{0.87} Sr _{0.09} Mg _{0.04}
<ul style="list-style-type: none"> The counterpart of the carbonate is written in the table: $(Ca_x Sr_y Mg_z)-CO_3$ 				

As shown in Figure 4.23, Figure 4.24 and Table 7.3, in both the *deposition* and *adhesion* processes, the bulk hydrodynamics have affected the chemical composition of the scale deposits in the same way. In both processes, as the agitation level of the bulk increases, both the magnesium and strontium proportion in the calcium carbonate scale deposits increases.

An increase in the rate of mass transfer in the bulk will facilitate the incorporation of both the magnesium ions in the lattice of the calcite crystals and the strontium ions in the lattice of the aragonite crystals. Such effect is more evident in the *adhesion* process from the laminar (87% of calcium) to turbulent (81% of calcium) flow conditions compared to the *deposition* process.

7.5.2. Sulphate-dominated scales

As shown in Figure 5.12 and Figure 5.13, in the *adhesion* tests calcium is the dominant ion that is present in the scale deposits on the surface, while in the *deposition* tests strontium and barium ions are more dominant. According to the DLVO theory, adhesion is determined by the balance between Van der Waals attractions and electrostatic double layer repulsion which is depending on the size, geometry and weight of the formed molecules. [50]

In the *deposition* process, the attractive Van der Waals forces even for bigger and heavier molecules (e.g. BaSO₄ and SrSO₄) is predominant, while in the *adhesion* process the repulsive electrostatic double layer forces for heavy particulates are high enough to prevent the adhesion of scale deposits on the surface. Furthermore, due to the importance of the momentum and gravitational forces in the *adhesion* process, it is easier for lighter scale crystals (e.g. CaSO₄ or CaCO₃) to adhere to the surface, while for heavier scale crystals formed by barium and strontium ions there are higher detachment forces. As a result, this trend is less obvious in the laminar flow regime compared to the turbulent condition due to lower critical shear stress induced by the brine to remove the crystal from the surface. In terms of heterogeneous nucleation and crystal growth (*deposition* process), the hydrodynamic effects do not affect the chemical composition of the scale deposits, while the level of agitation would change the nature of scale deposits in the *adhesion* process.

Sulphate scale causes more severe production problems compared to the carbonate scale due to its comparably higher adhesion between the scale and the substrates and also its solubility resistance against most of the common acids used to remove the

carbonate scales, such as hydrochloric acid.[2] Barium sulphate is normally accompanied by strontium sulphate to form a completely mixed scale called “barite celestine sulphate scale” as $(Ba_x Sr_{1-x})SO_4$ for which $0 < x < 1$. Todd and Yuan, 1992, [158] found that as the temperature increases from 20°C to 70°C, the contribution of the $SrSO_4$ enhances the scale formation which is predicted due to the supersaturation decrease of $BaSO_4$. The sulphate scale deposits formed on different modified surfaces for the *deposition* process in both laminar and turbulent flow conditions are shown in Table 7.4 based on the ICP analysis.

Table 7.4. The chemical compound of the sulphate scale deposits on the surface, analysed by ICP in turbulent and laminar flow conditions in the *deposition* process.

Coating	Turbulent flow condition			Laminar flow condition		
	Mole (%)			Mole (%)		
	Barium	Strontium	Compound	Barium	Strontium	Compound
B1541	37%	63%	$(Sr_{0.63}Ba_{0.37})SO_4$	35%	65%	$(Sr_{0.65}Ba_{0.35})SO_4$
FEP	40%	60%	$(Sr_{0.60}Ba_{0.40})SO_4$	43%	57%	$(Sr_{0.57}Ba_{0.43})SO_4$
ETFE	39%	61%	$(Sr_{0.61}Ba_{0.39})SO_4$	35%	65%	$(Sr_{0.65}Ba_{0.35})SO_4$
CrNAg	40%	60%	$(Sr_{0.60}Ba_{0.40})SO_4$	41%	59%	$(Sr_{0.59}Ba_{0.41})SO_4$
B1341	39%	61%	$(Sr_{0.61}Ba_{0.39})SO_4$	37%	63%	$(Sr_{0.63}Ba_{0.37})SO_4$
Dti	39%	61%	$(Sr_{0.61}Ba_{0.39})SO_4$	39%	61%	$(Sr_{0.61}Ba_{0.39})SO_4$
B1381	39%	61%	$(Sr_{0.61}Ba_{0.39})SO_4$	39%	61%	$(Sr_{0.61}Ba_{0.39})SO_4$
One	39%	61%	$(Sr_{0.61}Ba_{0.39})SO_4$	40%	60%	$(Sr_{0.60}Ba_{0.40})SO_4$
DHS	38%	62%	$(Sr_{0.62}Ba_{0.38})SO_4$	39%	61%	$(Sr_{0.61}Ba_{0.39})SO_4$
SS	40%	60%	$(Sr_{0.60}Ba_{0.40})SO_4$	38%	62%	$(Sr_{0.62}Ba_{0.38})SO_4$
CrN	39%	61%	$(Sr_{0.61}Ba_{0.39})SO_4$	33%	67%	$(Sr_{0.67}Ba_{0.33})SO_4$
PFA	42%	58%	$(Sr_{0.58}Ba_{0.42})SO_4$	30%	70%	$(Sr_{0.70}Ba_{0.30})SO_4$
TiN	39%	61%	$(Sr_{0.61}Ba_{0.39})SO_4$	40%	60%	$(Sr_{0.60}Ba_{0.40})SO_4$
B1391	39%	61%	$(Sr_{0.61}Ba_{0.39})SO_4$	40%	60%	$(Sr_{0.60}Ba_{0.40})SO_4$
B5891	50%	50%	$(Sr_{0.50}Ba_{0.50})SO_4$	62%	38%	$(Sr_{0.38}Ba_{0.62})SO_4$
DLC	39%	61%	$(Sr_{0.61}Ba_{0.39})SO_4$	48%	52%	$(Sr_{0.52}Ba_{0.48})SO_4$
PTFE	39%	61%	$(Sr_{0.61}Ba_{0.39})SO_4$	38%	62%	$(Sr_{0.62}Ba_{0.38})SO_4$

In such scale deposits, the strontium ions contribution in the sulphate scale is higher compared to the barium ions. The author calls such compound as “celestite bariumian sulphate”. As shown in Table 7.4, there is not much difference in terms of the ion

contribution in the sulphate scale compound between the barium and strontium in both laminar and turbulent conditions. In other words, the hydrodynamic effect has not altered the nature of the scale deposits on the different modified substrates, although there are some exceptions, specifically B5891 which its performance is quite different compared to other coatings in both laminar and turbulent flow conditions.

7.6. Field data

Mineral scale deposition on surfaces of oil production equipment has been recognised as a major flow assurance problem. Most of the mineral scale deposition work published has solely focused on laboratory experiments and very little data are available that demonstrate such results are relevant and can be scaled-up to field environments.

The current study focuses on mineral scale formation on surfaces and compares laboratory results with field data.[161, 162] A field test has been running for half a year on commercially-coated pipe spools along with uncoated ones. The different pipe sections were positioned along a water line injection system in an oilfield. In the laboratory, a standard bulk jar test was used and the ability of a range of chemically and morphologically modified coatings to prevent/reduce mineral scale surface fouling were assessed under different flow conditions (ranging from laminar to turbulent flow).

The current study shows that if properly selected, surface engineering offers great promise as an approach to prevent mineral scale deposition in the piping system of oilfields.

Table 7.5. The comparison between the supersaturation ratio of the brine composition tested in the laboratory setup and the field data.

Laboratory setup				Real	
Sulphate dominant brine		Carbonate dominant brine		Field data	
Species	SR	Species	SR	Species	SR
CaCO ₃	10.79	CaCO ₃	12.54	CaCO ₃	1.00
BaSO ₄	121.50	BaSO ₄	3.03	BaSO ₄	5.91
SrCO ₃	4.09	SrCO ₃	4.67	SrSO ₄	0.21
SrSO ₄	11.70	SrSO ₄	0.29	FeCO ₃	0.26

As shown in Table 6.3, the flow assurance problem of the oilfield mainly originates from the formation of sulphate scales in the oil pipe. To relate the laboratory results with the oilfield data and have a better assessment of the obtained results from the surface mass gain of the coatings, two types of complex brine composition which their salinity range is in the same range were selected but with different scale formation characteristics as a “carbonate-dominated brine” and a “sulphate-dominated brine” compositions. The comparison of the complex brine composition tested in the laboratory setup with the real conditions in the field is shown in Table 7.5.

As shown in Table 7.5, the supersaturation ratio range of the scale deposits in the laboratory setup are higher compared to the brine composition in the oilfield to compensate the discrepancies of the time interval between the field and the laboratory setup.

Three out of the six coatings employed in the oilfield test are fluoropolymer coatings and the rest are epoxy coatings. These epoxy coatings, e.g. B1341, B1381 and B5891, are the same coatings from the same manufacturer that are used in the laboratory setup.

As shown in Table 7.6, the rotational speed that has been set in the laboratory setup for the scaling tendency tests is comparable to the range of flow conditions in the oilfield. In other words, the 2000rpm of the RCE will simulate the flow condition with the Reynolds number of 17,845 which is in the range 100-120 (m³/day) flow rate in the oilfield which gives a Reynolds number in the range of 16,000-20,000.

Table 7.6. The comparison of the flow regimes between the laboratory setup and the field data.

Laboratory Setup			Field data
Rotational Speed	Reynolds Number	Surface Shear Stress	Reynolds Number
2000 rpm	17,845	7.851 Pa	16,884 – 20,242

7.6.1. Mass gain

As addressed before in chapter-6, eight pipe spools (2 uncoated, 3 epoxy coatings, and 3 fluoropolymer coatings) in the oilfield were employed to assess their scale tendency characteristics in real conditions. In Table 7.7, the surface scale deposits rate is compared with the laboratory results for both the sulphate/carbonate-dominated brine compositions for both the *adhesion* and *deposition* processes.

Due to the fact that the field data is obtained in multiphase flow conditions where crude oil is present in the brine, while the experimental results are primarily obtained from single-phase flow condition, the author’s analysis is based on ideal simplified conditions with systematic approach rather than result-end parameters. Such study can be a benchmark for further researches in future to conduct more realistic multiphase flow scale tendency experiments.

Table 7.7. The comparison of scale deposits growth in the oilfield with the laboratory setup for both carbonate/sulphate-dominated brine compositions for *adhesion* and *deposition* processes.

No.	Company	Real	Scale Thickness Growth (cm/year)			
			Carbonate		Sulphate	
			Adhesion	Deposition	Adhesion	Deposition
1	Uncoated	0.678	---	---	---	---
2	B5891	0.165	0.219	0.759	0.143	0.257
3	3M SK 6258	0.228	---	---	---	---
4	B1341	0.198	0.187	0.435	0.300	0.511
5	IPC ME 35	0.236	---	---	---	---
6	B1391	0.213	0.263	0.603	0.666	0.346
7	IPC Magna	0.177	---	---	---	---
8	Uncoated	0.234	---	---	---	---

Although the final result of surface scale deposits rate of the field data and experimental results are not comparable, the ranking of the surfaces is one of the parameters that is worth to consider. As a result, Table 7.7 can be summarised based on the scale tendency performance ranking of the epoxy coatings in Table 7.8.

Table 7.8. The scale tendency performance ranking of the epoxy coating in the oilfield and the laboratory.

Company	Real	Scale deposit rate ranking			
		Carbonate		Sulphate	
		Adh	Dep	Adh	Dep
B5891	1	2	3	1	1
B1341	2	1	1	2	3
B1391	3	3	2	3	2

As shown in Table 7.8, by comparing the ranking of the coatings, this is the *adhesion* process in the sulphate-dominated brine composition that matches the field data. The results match due to the following aspects:

1. The dominant scale deposits found in the field data is sulphate-based, which matches to the sulphate-dominated brine setup in the laboratory.
2. The oilfield site is situated at the end of the line of the re-injecting water facility to pump the fluid into the oil well. In other words, the precipitation rate in the brine has reached to an equilibrium state, which matches to the *adhesion* process that is defined in the laboratory setup.

As a result, by using the obtained results in the *adhesion* process in the sulphate-dominated brine, the relative scaling tendency of other coatings can be assessed, although the author believes that more experimental results need to be validated by the field data to have a better understanding and prediction of a modified surface.

7.6.2. Conclusion

It can be inferred from this study that the standard bulk jar scaling test combined with RCE to assess the hydrodynamic effects in the laboratory, is an acceptable approach to study the surface scaling in different flow conditions, provided that the chemical composition of the brine solution itself is in agreement with the nature of scale deposits formed in the field; however, the obtained field data has been run for one time with the presence of oil, while the conducted experimental tests were done in one phase condition.

The current study shows that if properly selected, surface engineering offers great promise as an approach to prevent mineral scale deposition in the piping system of oilfields.

Based on the presented results, the author has recommended specifically this type of coating (e.g. B5891) to PETROBRAS, and to the best knowledge of the author, PETROBRAS is going to apply this type of coating in their piping systems where they are facing with the sulphate-based flow assurance problems.

Chapter 8

Conclusion

8.1. Conclusion summary

In this thesis, the surface scale deposition of commercially-available coatings for carbonate-dominated/sulphate-dominated scale formation with regard to the flow regimes of the bulk solution for two interlinked processes, as *deposition* and *adhesion* processes, have been studied. This chapter has mainly focused on the following aspects:

1. The surface scale formation as *deposition* and *adhesion* processes.
2. The hydrodynamic effects on surface scale formation.
3. Morphology and co-precipitation of scale deposits
4. Characterising a good anti-fouling surface.
5. Correlating of the systematic laboratory results to field data.

This chapter gives a general summary of the finding of each aspect and recommends future works.

8.2. Surface scale formation

Due to the complexity in understanding the surface scale formation mechanism, it is proposed to divide it to two interlinked processes as: *deposition* process, or the heterogeneous nucleation and crystal growth, and *adhesion* process, or the attachment of pre-precipitated particles in the bulk solution to the surface. Such strategy also helps to understand the predominant process taking place in the oil production line. In other words, in the downhole, where the bulk solution is considered as fresh, the surface scale formation mainly occurs as the *deposition* process, while on ground level, due to the time interval it takes for the bulk solution travels from the downhole up to the ground level, the bulk solution carries the pre-precipitated particles. As a result, the surface scale formation occurring in this region is predominantly controlled by the *adhesion* process.

At early stages of the oil production, due to thermodynamic changes in the bulk solution the problematic scale deposits are mainly carbonate based, and at late stages of the oil production when EOR is employed, due to the incompatibility of the seawater and aquifer, sulphate based scales are causing flow assurance problems.

Since at different stages of the oilfield production the nature of problematic scale changes, the laboratory setup is designed based on two brine solution with the same salinity as carbonate-dominated scale and sulphate-dominated scale setups.

It is found that the surface scale formation rate in the *deposition* process increases with an increase in the agitation level of the bulk solution for both the sulphate/carbonate-dominated brine solutions; however, in the *adhesion* process, as the bulk solution changes from the laminar to turbulent flow conditions, the rate of surface scale formation increases in the sulphate-dominated brine solution but decreases in the carbonate-dominated brine solution.

The scaling tendency of heterogeneous nucleation and crystal growth is higher than the adherence of the pre-crystallised scale particles for both brine solutions, however, the level of agitation could have inverse effects on one process to another. Even in the *adhesion* process, it is found that the heterogeneous nucleation is in progress and is distinguishable for most of the modified surfaces. It is also found that the behaviour of scale formation on the surface will change with respect to the level of turbulence of the bulk, i.e. in the *deposition* process, the surface scale deposits are formed rather scattered in turbulent flow conditions and localised in laminar flow conditions, and in the *adhesion* process, the surface scale deposits in both flow conditions are formed in scattered formation, however, in turbulent conditions the presence of localised scale sites is noticeable.

8.3. Good anti-fouling surfaces

In general, the parameters such as surface chemistry, surface roughness, surface energy, and surface hydrophobicity of the surface known as the criteria that play a major role in scale *deposition* process, but the effects of such parameters all together in a process is not fully understood.

To study the effect of surface aforementioned parameters, stainless steel (SS316) samples are coated with 21 different commercially available types of coatings which cover a variety of surface roughness and surface energy values with different surface compositions.

Although categorising the coated substrates as good anti-scaling surfaces, considering the fact that their surface parameters are quite diverse, is not a methodical approach,

the anti-scaling performance of a certain group of coatings in different brine solutions in different flow regimes are promising, e.g. ceramic coatings, esp. TiN. It is found that having a good anti-scaling performance in a carbonate-dominated brine composition necessarily does not guarantee a promising performance in the sulphate-dominated brine solutions. Amongst the epoxy coatings which have shown fair anti-scaling characteristics, the Belzona B5891 had the best performance in the sulphate-dominated tests, however its performance in the carbonate-dominated tests is not quite promising. Even in sulphate-dominated tests, the scale deposits formed on this coating is high in calcium which predicts its susceptibility in calcium-based scale environment.

Although low surface energy characteristic of a surface is considered as an anti-scaling parameter, the results have shown that this parameter cannot merely assure a low rate of surface scaling, and in some scenarios, high surface energy can lead to a better anti-scaling performance.

It has been found that the role of surface roughness is more evident in laminar flow conditions compared to the turbulent flow conditions irrespective of the nature of the surface scale deposits. It is found that the number of peaks can adversely affect the surface scaling ratio of the modified surfaces for both the sulphate/carbonate-dominated brine compositions. Such an adverse effect is more evident in the laminar flow conditions compared to the turbulent flow conditions.

The chemical composition of the modified surfaces has not much effect on the morphology of the crystals formed on the surfaces. However, the surface finish and surface irregularities/imperfections will affect the rate of surface scale formation.

8.4. Morphology and co-precipitation of scale deposits

In the carbonate-dominated scale deposits: There are diverse morphologies formed on different modified surfaces. The surface chemistry will affect the morphology of the crystals on the surfaces. The most dominant crystals formed on the surfaces in the *adhesion* process are calcite crystals with rounded edges. There is a trace of needle-like aragonite on some surfaces (e.g. DTi and One). In the *deposition* process, all three main polymorphs of crystals exist, i.e. calcite, aragonite and vaterite. Unlike the *adhesion* tests, the dominant crystals formed on the surfaces are aragonite and vaterite.

The needle-like aragonite crystals formed on the surfaces have a lower aspect ratio compared to the literature and they tend to form on the surfaces as a bundle. In the *deposition* tests, the occurrence of secondary nucleation on calcite crystals is apparent. The calcium ion ratio in the scale deposits in the *deposition* tests is higher compared to the *adhesion* tests. The flow conditions have low effect on the ratio of the ions formed in the scale deposits.

Due to the complexity of the brine solutions, the scale deposits formed on the surface are the complex crystals with the incorporation of the cations in their lattice, e.g. Mg^{2+} and Sr^{2+} in the lattice of calcite and aragonite or the co-precipitation of Sr^{2+} in barite.

It is found that the formed calcite under the influence of Mg^{2+} formed as cubic crystals with rounded edges or irregular polyhedrons and bundles. In addition, the incorporation ratio of strontium ions in the lattice of the aragonite is higher than that of the calcite crystals, and as a result, the formed aragonite have lower aspect ratio compared to the literature. Vaterite crystals are also observed either as a spherical shape or cubic crystal with a hollow in the centre. SEM images of the crystals have shown that in the *adhesion* process, the heterogeneous nucleation and crystal growth is in progress, as well. The flow conditions also have affected the scale deposition pattern in the *deposition* process on the surface, i.e. scale deposits are scattered all over the surface in the turbulent flow conditions while in the laminar flow conditions it is more localised.

In the case of co-precipitation of magnesium and strontium in the lattice of the calcium carbonate, it is found that the density ratio of these cations is increased by an increase in the bulk hydrodynamic conditions in both the *deposition* and *adhesion* processes.

In the sulphate-dominated scale deposits, the majority of the formed crystals are shaped either as bowtie or sisal-like; however, it is shown that the latter crystal only appears in the laminar flow conditions, which conveys the idea that the flow conditions can affect the morphology of the scale deposits on the surface. It is found that the morphology of the scale deposits on the modified surfaces is affected by the bulk flow regime in both the *adhesion* and *deposition* processes, wherein the laminar flow conditions the existence of sisal-like crystals is evident while in the turbulent flow conditions it is mainly the needle-like and bowtie crystals. It has been observed that the relative chemical composition of scale deposits would be affected by different mechanisms of scale formation on the surface (i.e. from the *deposition* process to *adhesion* process), while the morphology of the scale deposits has not changed. In

addition, it has been understood that the hydrodynamic conditions have not much effect on the relative ion composition of the surface scale deposits in the *deposition* process, but the relative ion concentration of scale deposits in the *adhesion* process is affected by the agitation level.

Formed scale deposits are mainly formed from the co-precipitation of strontium and barium with the sulphate ions.

In such scale deposits, the strontium ions contribution in the sulphate scale is higher compared to the barium ions. The hydrodynamic effect has not altered the nature of the scale deposits on the different modified substrates, although there are some exceptions, specifically B5891 which its performance is quite different compared to other coatings in both laminar and turbulent flow conditions.

8.5. Correlating the laboratory studies to field data

Unlike most of the studies that are merely focused either on the laboratory results or reporting the field data, in this thesis, the comparison of field data with systematic laboratory is studied. In addition, there have been some doubts about employing surface engineering as a mean to mitigate the flow assurance problems in the oil and gas industry. The work presented clearly shows the effectiveness of the surface engineering to reduce the rate of surface scale formation.

Also, it has been shown that the standard bulk jar scaling test combined with RCE to assess the hydrodynamic effects in the laboratory, is an acceptable approach to study the surface scaling in different flow conditions, provided that the chemical composition of the brine solution itself is in agreement with the nature of scale deposits formed in the field.

The outcome of this thesis has helped PETROBRAS to identify the surface scaling problem they are facing in the oilfield and recommended to choose the optimum commercially-available coating in the market with regard to its application to mitigate the flow assurance problems in Brazilian oilfields. To the best knowledge of the author, PETROBRAS is going to apply this type of coating in their piping systems where they are facing with the sulphate-based flow assurance problems.

8.6. Future work

Surface scale formation: Most of the studies conducted so far to understand the surface scale formation have been focused on one entity as the *deposition* process or heterogeneous nucleation and crystal growth. This thesis is one of the first studies that is mainly focused on these two interlinked processes. Future studies need to be focused on the comparison of these mechanisms in different flow conditions, pressure, temperature, pH level, bulk alkalinity, CO₂ level, brine composition, SR ratio, the addition of impurities, hydrodynamic conditions and the effect of inhibitors. Like this thesis, such studies can be applied in different supersaturated brine composition such as sulphide studies and also wax formation. For further studies of the *adhesion* process, it is advisable to filter the brine solution when the crystallisation rate is in balance with the dissolution rate and calculate the saturation ratio and start assessing the modified surfaces.

Good anti-scaling formation: Surface has a crucial role in the formation of scale on the substrate, as a result understanding the surface parameters is vital to mitigate the flow assurance problems. Unfortunately, there are so many surface parameters involve in surface scaling, but as a future work, an extensive study needs to be conducted to maintain all the parameters at a time, and start to change one parameter and start to characterise one parameter at a time.

Morphology and co-precipitation of scale deposits: The morphology of the scale deposits are so dependent on the chemical composition of the scale deposits. Although co-precipitation theory has been proposed more than 80 years ago, not much attention has been focused on this matter which greatly affects the surface scaling. It can be associated with the fact that such mechanism is so complicated. In this study, the effect of flow conditions and *adhesion/deposition* processes on the co-precipitated scale deposits have been studied. However, the author believes that this study can be supported by co-precipitation theory in well-controlled conditions in the laboratory. Due to the abundant cases of calcium carbonate co-precipitation with cations, there are so many studies in this field, but the co-precipitation of sulphate based compound has been neglected despite its importance in surface scale formation.

Correlating and laboratory studies with field data: This is the first study that has been systematically conducted to correlate the laboratory results with the field data. As a result, there are so many parameters that can be improved in future studies:

- **Field:** The reference pipe spools employed in the field were carbon steel pipes. Although corrosion products can be categorised as scale deposits, applying stainless steel would be advisable. Not all the coatings employed in the field were available in the laboratory. Online monitoring the brine solution is a good methodology to observe the flow conditions in the field.
- **Laboratory:** The scaling tests have been carried out in a complex brine solution. In future, the surface scaling tests can be done with the presence of oil in the brine solution. The batch tests have been used to assess the anti-scaling performance of the coatings, which can be substituted with in-situ rigs.

Bibliography

1. Dickinson, S.R., G. Henderson, and K. McGrath, *Controlling the kinetic versus thermodynamic crystallisation of calcium carbonate*. Journal of Crystal Growth, 2002. **244**(3): p. 369-378.
2. Crabtree, M., et al., *Fighting scale—removal and prevention*. Oilfield Review, 1999. **11**(3): p. 30-45.
3. API. *Oil and Natural gas, from the Well to You*. 2013 [21.08.2013]; Available from: <http://www.adventuresinenergy.org/index.html>.
4. California-CCS-coalition. *Advanced Resources International (ARI) study on CO2 and EOR*. 2013 [07/10/2013]; Available from: <http://caccscoalition.org/presentations/study-shows-ccs-enhanced-oil-recovery-could-slash-u-s-dependence-on-foreign-oil/>.
5. Brown, M., *Full Scale Attack review*. The BP Technology Magazine, 1998: p. 30-32.
6. Eltaib, E. and A.A. Rabah, *Crude Oil Pipeline Scale Deposition: Causes and Removal Methods*. Khartoum University Engineering Journal, 2012.
7. Vetter, O., *Oilfield Scale---Can We Handle It?* Journal of Petroleum Technology, 1976. **28**(12): p. 1,402-1,408.
8. Bader, M., *Sulfate scale problems in oil fields water injection operations*. Desalination, 2006. **201**(1): p. 100-105.
9. Schlumberger. *Carbonate Reservoirs*. 2014 [19 February 2014]; Available from: http://www.slb.com/services/technical_challenges/carbonates.aspx.
10. Jordan, M., et al. *Life Cycle Management of Scale Control within Subsea Fields and its Impact on Flow Assurance Gulf of Mexico and the North Sea Basin*. in *SPE Annual Technical Conference and Exhibition*. 2001. Society of Petroleum Engineers.
11. Moghadasi, J., et al. *Scale formation in oil reservoir and production equipment during water injection (Kinetics of CaSO4 and CaCO3 crystal growth and effect on formation damage)*. in *SPE European Formation Damage Conference*. 2003. Society of Petroleum Engineers.
12. Moghadasi, J., et al. *Scale formation in Iranian oil reservoir and production equipment during water injection*. in *International Symposium on Oilfield Scale*. 2003. Society of Petroleum Engineers.
13. Vetter, O. and W. Farone. *Calcium carbonate scale in oilfield operations*. in *SPE Annual Technical Conference and Exhibition*. 1987. Society of Petroleum Engineers.
14. Bezemer, C. and K.A. Bauer, *Prevention of Carbonate Scale Deposition - a Well-Packing Technique with Controlled Solubility Phosphates*. Journal of Petroleum Technology, 1969. **21**(Apr): p. 505-&.
15. Moghadasi, J., et al. *Formation damage in Iranian oil fields*. in *International Symposium and Exhibition on Formation Damage Control*. 2002. Society of Petroleum Engineers.
16. Hardy, J. and I. Simm, *Low sulfate seawater mitigates barite scale*. Oil and Gas Journal, 1996. **94**(50): p. 64-67.
17. Plummer, L.N. and E. Busenberg, *The solubilities of calcite, aragonite and vaterite in CO₂-H₂O solutions between 0 and 90 C, and an*

- evaluation of the aqueous model for the system CaCO₃-CO₂-H₂O*. *Geochimica et Cosmochimica Acta*, 1982. **46**(6): p. 1011-1040.
18. Gabrielli, C., et al., *In situ Raman spectroscopy applied to electrochemical scaling. Determination of the structure of vaterite*. *Journal of Raman Spectroscopy*, 2000. **31**(6): p. 497-501.
 19. Mukkamala, S.B., C.E. Anson, and A.K. Powell, *Modelling calcium carbonate biomineralisation processes*. *Journal of inorganic biochemistry*, 2006. **100**(5): p. 1128-1138.
 20. Brečević, L. and D. Kralj, *On calcium carbonates: from fundamental research to application*. *Croatica Chemica Acta*, 2007. **80**(3-4): p. 467-484.
 21. Eroini, V., *Kinetic study of calcium carbonate formation and inhibition by using an in-situ flow cell*, 2011, University of Leeds.
 22. Wang, Z., *Mineral scale formation-aspects of surface energy and adhesion*, 2006, University of Leeds.
 23. Bader, M., *Sulfate removal technologies for oil fields seawater injection operations*. *Journal of Petroleum Science and Engineering*, 2007. **55**(1): p. 93-110.
 24. Guimaraes, Z., et al. *Case Histories of Barium Sulfate Scale Removal in Offshore Wells Brazil Using a New Engineered Combination of Coiled-Tubing Tools*. in *SPE/ICoTA Coiled Tubing and Well Intervention Conference and Exhibition*. 2007. Society of Petroleum Engineers.
 25. Pauling, L. and P.H. Emmett, *The crystal structure of barite*. *Journal of the American Chemical Society*, 1925. **47**(4): p. 1026-1030.
 26. Massi, M., et al., *Tetrazoles: a new class of compound for crystallization modification*. *CrystEngComm*, 2010. **12**(12): p. 4205-4207.
 27. Rautaray, D., et al., *Influence of alcohol on the morphology of BaSO₄ crystals grown at the air-water interface*. *CrystEngComm*, 2002. **4**(106): p. 626-630.
 28. Blount, C., *Barite solubilities and thermodynamic quantities up to 300/sup 0/C and 1400 bars*. *Am. Mineral.*; (United States), 1977. **62**.
 29. Wang, W.-S., et al., *Synthesis and formation process of SrSO₄ sisal-like hierarchical structures at room temperature*. *CrystEngComm*, 2011. **13**(2): p. 620-625.
 30. Sheikh, A.R. and S.R. Patel, *Ultrasound assisted reactive crystallization of strontium sulfate*. *Journal of Crystal Growth*, 2014. **390**: p. 114-119.
 31. Duggirala, P.Y., *Formation of calcium carbonate scale and control strategies in continuous digesters*. CD del II Coloquio Internacional sobre Celulosa de Eucalipto, Concepción, Chile, Mayo, 2005.
 32. Mullin, J.W., *Crystallization*. 2001: Butterworth-Heinemann.
 33. Wang, Z., *Mineral scale formation - aspect of surface energy and adhesion*. 2006.
 34. Ghizellaoui, S., et al., *Etude de l'inhibition du pouvoir entartrant des eaux du Hamma par précipitation contrôlée rapide et par un essai d'entartrage accéléré*. *Desalination*, 2004. **166**: p. 315-327.
 35. Söhnel, O. and J. Garside, *Precipitation: basic principles and industrial applications*. 1992: Butterworth-Heinemann.

36. Klepetsanis, P.G., et al., *The effect of mineral deposits on stainless steel*, in *Mineral Scale Formation and Inhibition*. 1995, Springer. p. 131-144.
37. Sun, Y., *Controlled synthesis of colloidal silver nanoparticles in organic solutions: empirical rules for nucleation engineering*. Chemical Society Reviews, 2013. **42**(7): p. 2497-2511.
38. Best, B., *Lessons for Cryonics from Metallurgy and Ceramics*. LESSONS FOR CRYONICS FROM METALLURGY AND CERAMICS, 1990.
39. Nancollas, G. *Oilfield scale: "Physical chemical studies of its formation and prevention,"*. in *Symposium on 'Chemicals in the Oil Industry*. 1985.
40. Beaunier, L., et al., *Investigation of electrochemical calcareous scaling: Nuclei counting and morphology*. Journal of Electroanalytical Chemistry, 2001. **501**(1): p. 41-53.
41. Frawley, P.J., et al., *The effects of supersaturation, temperature, agitation and seed surface area on the secondary nucleation of paracetamol in ethanol solutions*. Chemical Engineering Science, 2012. **75**: p. 183-197.
42. Myerson, A., *Handbook of industrial crystallization*. 2002: Butterworth-Heinemann.
43. Söhnel, O. and J. Mullin, *Precipitation of calcium carbonate*. Journal of Crystal Growth, 1982. **60**(2): p. 239-250.
44. He, S., A.T. Kan, and M.B. Tomson, *Inhibition of calcium carbonate precipitation in NaCl brines from 25 to 90 C*. Applied Geochemistry, 1999. **14**(1): p. 17-25.
45. Stamatakis, E., et al., *An improved predictive correlation for the induction time of CaCO₃ scale formation during flow in porous media*. Journal of colloid and interface science, 2005. **286**(1): p. 7-13.
46. Koutsoukos, P.G. and C.G. Kontoyannis, *Precipitation of calcium carbonate in aqueous solutions*. Journal of the Chemical Society, Faraday Transactions 1: Physical Chemistry in Condensed Phases, 1984. **80**(5): p. 1181-1192.
47. Shaw, D.W. and C. Goodman, *Crystal growth theory and techniques*. Vol. 1 Plenum, London, 1974: p. 1.
48. Noyes, A.A. and W.R. Whitney, *Drug Dissolution*. Journal of the American Chemical Society, 1897. **19**: p. 930-934.
49. Packham, D.E., *Handbook of adhesion*. 2006: John Wiley & Sons.
50. Oliveira, R., *Understanding adhesion: a means for preventing fouling*. Experimental Thermal and Fluid Science, 1997. **14**(4): p. 316-322.
51. Merdhah, A.B.B. and A.A.M. Yassin, *Laboratory Study on Precipitation of Barium Sulphate in Malaysia Sandstone Cores*. Open Petroleum Engineering Journal, 2009. **2**: p. 1-11.
52. Han, Y.S., et al., *Factors affecting the phase and morphology of CaCO₃ prepared by a bubbling method*. Journal of the European Ceramic Society, 2006. **26**(4-5): p. 843-847.
53. Kitamura, M., *Controlling factor of polymorphism in crystallization process*. Journal of Crystal Growth, 2002. **237**: p. 2205-2214.
54. Yu, J., et al., *Facile preparation of calcium carbonate particles with unusual morphologies by precipitation reaction*. Journal of crystal growth, 2004. **261**(4): p. 566-570.

55. Dyer, S.J. and G.M. Graham, *The effect of temperature and pressure on oilfield scale formation*. Journal of Petroleum Science and Engineering, 2002. **35**(1–2): p. 95-107.
56. Peyvandi, K., A. Haghtalab, and M.R. Omidkhan, *Using an electrochemical technique to study the effective variables on morphology and deposition of CaCO₃ and BaSO₄ at the metal surface*. Journal of Crystal Growth, 2012. **354**(1): p. 109-118.
57. Hewitt, G.F. and J. Barbosa, *Heat exchanger design handbook*. Vol. 98. 2008: Begell House.
58. Alahmad, M., *Factors Affecting Scale Formation in Sea Water Environments—An Experimental Approach*. Chemical engineering & technology, 2008. **31**(1): p. 149-156.
59. Millero, F.J., *Chemical oceanography*. 2013: CRC press.
60. Al-Anezi, K. and N. Hilal, *Scale formation in desalination plants: effect of carbon dioxide solubility*. Desalination, 2007. **204**(1–3): p. 385-402.
61. Wada, N., K. Yamashita, and T. Umegaki, *Effects of divalent cations upon nucleation, growth and transformation of calcium carbonate polymorphs under conditions of double diffusion*. Journal of Crystal Growth, 1995. **148**(3): p. 297-304.
62. Chen, T., A. Neville, and M. Yuan, *Assessing the effect of on scale formation—bulk precipitation and surface deposition*. Journal of Crystal Growth, 2005. **275**(1–2): p. e1341-e1347.
63. Keysar, S., et al., *Effect of surface roughness on the morphology of calcite crystallizing on mild steel*. Journal of colloid and interface science, 1994. **162**(2): p. 311-319.
64. Cheong, W.C., P.H. Gaskell, and A. Neville, *Substrate effect on surface adhesion/crystallisation of calcium carbonate*. Journal of Crystal Growth, 2013. **363**(0): p. 7-21.
65. Rankin, B.H. and W.L. Adamson, *Scale formation as related to evaporator surface conditions*. Desalination, 1973. **13**(1): p. 63-87.
66. Herz, A., M.R. Malayeri, and H. Müller-Steinhagen, *Fouling of roughened stainless steel surfaces during convective heat transfer to aqueous solutions*. Energy Conversion and Management, 2008. **49**(11): p. 3381-3386.
67. Briscoe, B. and S. Panesar, *The effect of surface topography on the adhesion of poly (urethane)-metal contacts*. Journal of Physics D: Applied Physics, 1992. **25**(1A): p. A20.
68. Tabor, D., *Surface forces and surface interactions*. Journal of Colloid and Interface Science, 1977. **58**(1): p. 2-13.
69. Zisman, W.A., *Relation of the equilibrium contact angle to liquid and solid constitution*. 1964.
70. Fowkes, F.M., *Attractive forces at interfaces*. Industrial & Engineering Chemistry, 1964. **56**(12): p. 40-52.
71. Owens, D.K. and R. Wendt, *Estimation of the surface free energy of polymers*. Journal of applied polymer science, 1969. **13**(8): p. 1741-1747.
72. Wu, S., *Surface tension of solids: an equation of state analysis*. Journal of Colloid and Interface Science, 1979. **71**(3): p. 605-609.
73. Van Oss, C., R. Good, and M. Chaudhury, *The role of van der Waals forces and hydrogen bonds in “hydrophobic interactions” between*

- biopolymers and low energy surfaces*. Journal of Colloid and Interface Science, 1986. **111**(2): p. 378-390.
74. Förster, M., W. Augustin, and M. Bohnet, *Influence of the adhesion force crystal/heat exchanger surface on fouling mitigation*. Chemical Engineering and Processing: Process Intensification, 1999. **38**(4–6): p. 449-461.
75. Eroini, V., et al., *Preventing Scale Formation Using Modified Surfaces*. CORROSION 2011, 2011.
76. Zhao, Q. and X. Wang, *Heat transfer surfaces coated with fluorinated diamond-like carbon films to minimize scale formation*. Surface and Coatings Technology, 2005. **192**(1): p. 77-80.
77. Butter, R., et al., *Production and wetting properties of fluorinated diamond-like carbon coatings*. Thin Solid Films, 1997. **311**(1): p. 107-113.
78. Trojan, K., M. Grischke, and H. Dimigen, *Network Modification of DLC Coatings to Adjust a Defined Surface Energy*. physica status solidi (a), 1994. **145**(2): p. 575-585.
79. Bargir, S., et al., *The use of contact angle measurements to estimate the adhesion propensity of calcium carbonate to solid substrates in water*. Applied Surface Science, 2009. **255**(9): p. 4873-4879.
80. Geddert, T., W. Augustin, and S. Scholl, *Induction time in crystallization fouling on heat transfer surfaces*. Chemical Engineering & Technology, 2011. **34**(8): p. 1303-1310.
81. Geddert, T., et al., *Extending the induction period of crystallization fouling through surface coating*. Heat Transfer Engineering, 2009. **30**(10-11): p. 868-875.
82. Jaouhari, R., et al., *Influence of water composition and substrate on electrochemical scaling*. Journal of The Electrochemical Society, 2000. **147**(6): p. 2151-2161.
83. Gabrielli, C., et al., *Study of the Electrochemical Deposition of CaCO₃ by In Situ Raman Spectroscopy I. Influence of the Substrate*. Journal of the Electrochemical Society, 2003. **150**(7): p. C478-C484.
84. Koch, K., B. Bhushan, and W. Barthlott, *Diversity of structure, morphology and wetting of plant surfaces*. Soft Matter, 2008. **4**(10): p. 1943-1963.
85. Cheng, Y.T., et al., *Effects of micro-and nano-structures on the self-cleaning behaviour of lotus leaves*. Nanotechnology, 2006. **17**(5): p. 1359.
86. Kolthoff, I., *Theory of Coprecipitation. The Formation and Properties of Crystalline Precipitates*. The Journal of Physical Chemistry, 1932. **36**(3): p. 860-881.
87. Sheikholeslami, R., *Mixed salts—scaling limits and propensity*. Desalination, 2003. **154**(2): p. 117-127.
88. Doerner, H. and W.M. Hoskins, *CO-PRECIPIATION OF RADIUM AND BARIUM SULFATES*. Journal of the American Chemical Society, 1925. **47**(3): p. 662-675.
89. Kushnir, J., *The coprecipitation of strontium, magnesium, sodium, potassium and chloride ions with gypsum. An experimental study*. Geochimica et Cosmochimica Acta, 1980. **44**(10): p. 1471-1482.
90. Lorens, R.B., *Sr, Cd, Mn and Co distribution coefficients in calcite as a function of calcite precipitation rate*. Geochimica et Cosmochimica Acta, 1981. **45**(4): p. 553-561.

91. Brower, E., *Synthesis of barite, celestite and barium-strontium sulfate solid solution crystals*. *Geochimica et Cosmochimica Acta*, 1973. **37**(1): p. 155-158.
92. Dietzel, M., N. Gussone, and A. Eisenhauer, *Co-precipitation of Sr²⁺ and Ba²⁺ with aragonite by membrane diffusion of CO₂ between 10 and 50 C*. *Chemical Geology*, 2004. **203**(1): p. 139-151.
93. Holland, H., et al., *The coprecipitation of Sr²⁺ with aragonite and of Ca²⁺ with strontianite between 90 and 100 C*. *Geochimica et Cosmochimica Acta*, 1963. **27**(9): p. 957-977.
94. Kinsman, D.J. and H. Holland, *The co-precipitation of cations with CaCO₃—IV. The co-precipitation of Sr²⁺ with aragonite between 16 and 96 C*. *Geochimica et Cosmochimica Acta*, 1969. **33**(1): p. 1-17.
95. Holland, H., H. Holland, and J. Munoz, *The coprecipitation of cations with CaCO₃—II. The coprecipitation of Sr²⁺ with calcite between 90° and 100° C*. *Geochimica et Cosmochimica Acta*, 1964. **28**(8): p. 1287-1301.
96. Pingitore, N.E. and M.P. Eastman, *The coprecipitation of Sr²⁺ with calcite at 25 C and 1 atm*. *Geochimica et Cosmochimica Acta*, 1986. **50**(10): p. 2195-2203.
97. Oomori, T., et al., *Distribution coefficient of Mg²⁺ ions between calcite and solution at 10–50°C*. *Marine Chemistry*, 1987. **20**(4): p. 327-336.
98. Liu, Y., et al., *Investigation of adhesion of CaCO₃ crystalline fouling on stainless steel surfaces with different roughness*. *International Communications in Heat and Mass Transfer*, 2011. **38**(6): p. 730-733.
99. Zhao, Q., et al., *Effect of surface free energy on the adhesion of biofouling and crystalline fouling*. *Chemical Engineering Science*, 2005. **60**(17): p. 4858-4865.
100. Förster, M. and M. Bohnet, *Influence of the interfacial free energy crystal/heat transfer surface on the induction period during fouling*. *International journal of thermal sciences*, 1999. **38**(11): p. 944-954.
101. Azimi, G., et al., *Scale-resistant surfaces: Fundamental studies of the effect of surface energy on reducing scale formation*. *Applied Surface Science*, 2014. **313**: p. 591-599.
102. Herz, A., M. Malayeri, and H. Müller-Steinhagen, *Fouling of roughened stainless steel surfaces during convective heat transfer to aqueous solutions*. *Energy conversion and management*, 2008. **49**(11): p. 3381-3386.
103. Rankin, B. and W. Adamson, *Scale formation as related to evaporator surface conditions*. *Desalination*, 1973. **13**(1): p. 63-87.
104. Dyer, S. and G. Graham, *The effect of temperature and pressure on oilfield scale formation*. *Journal of Petroleum Science and Engineering*, 2002. **35**(1): p. 95-107.
105. Han, Y.S., et al., *Factors affecting the phase and morphology of CaCO₃ prepared by a bubbling method*. *Journal of the European Ceramic Society*, 2006. **26**(4): p. 843-847.
106. Eroini, V., et al., *New insight into the relation between bulk precipitation and surface deposition of calcium carbonate mineral scale*. *Desalination and water treatment*, 2013. **51**(4-6): p. 882-891.
107. Wang, Z., A. Neville, and A. Meredith. *How and Why does Scale Stick- Can the Surface be Engineered to Decrease Scale Formation and*

- Adhesion?* in *SPE International Symposium on Oilfield Scale*. 2005. Society of Petroleum Engineers.
108. Cheong, W.C., et al. *Using nature to provide solutions to calcareous scale deposition*. in *SPE International Oilfield Scale Conference, Aberdeen, UK*. 2008.
 109. Quddus, A., *Effect of hydrodynamics on the deposition of CaSO₄ scale on stainless steel*. *Desalination*, 2002. **142**(1): p. 57-63.
 110. Quddus, A. and L.M. Al-Hadhrami, *Hydrodynamically deposited CaCO₃ and CaSO₄ scales*. *Desalination*, 2009. **246**(1–3): p. 526-533.
 111. Quddus, A. and I.M. Allam, *BaSO₄ scale deposition on stainless steel*. *Desalination*, 2000. **127**(3): p. 219-224.
 112. Morizot, A., A. Neville, and T. Hodgkiess, *Studies of the deposition of CaCO₃ on a stainless steel surface by a novel electrochemical technique*. *Journal of Crystal Growth*, 1999. **198–199, Part 1**(0): p. 738-743.
 113. Neville, A. and A. Morizot, *A combined bulk chemistry/electrochemical approach to study the precipitation, deposition and inhibition of CaCO₃*. *Chemical engineering science*, 2000. **55**(20): p. 4737-4743.
 114. Zarga, Y., et al., *Study of calcium carbonate and sulfate coprecipitation*. *Chemical Engineering Science*, 2013. **96**: p. 33-41.
 115. Kan, A.T. and M.B. Tomson. *Scale prediction for oil and gas production*. in *International Oil and Gas Conference and Exhibition in China*. 2010. Society of Petroleum Engineers.
 116. McKeen, L.W., *Fluorinated Coatings and Finishes Handbook: The Definitive User's Guide*. 2006: William Andrew.
 117. Robertson, J., *Diamond-like amorphous carbon*. *Materials Science and Engineering: R: Reports*, 2002. **37**(4): p. 129-281.
 118. Dong-Hyeok, L. and C. Nahm-Gyoo, *Assessment of surface profile data acquired by a stylus profilometer*. *Measurement Science and Technology*, 2012. **23**(10): p. 105601.
 119. Sheng, Y.-J., S. Jiang, and H.-K. Tsao, *Effects of geometrical characteristics of surface roughness on droplet wetting*. *The Journal of chemical physics*, 2007. **127**(23): p. 234704.
 120. Yuan, Y. and T.R. Lee, *Contact angle and wetting properties*, in *Surface science techniques*. 2013, Springer. p. 3-34.
 121. Bohnet, M., *Influence of the transport properties of the crystal/heat transfer surface interfacial on fouling behavior*. *Chemical engineering & technology*, 2003. **26**(10): p. 1055-1060.
 122. Van Oss, C.J., *Interfacial forces in aqueous media*. 2006: CRC press.
 123. Gabe, D., *The rotating cylinder electrode*. *Journal of Applied Electrochemistry*, 1974. **4**(2): p. 91-108.
 124. Vazirian, M.M., et al., *Surface inorganic scale formation in oil and gas industry: As adhesion and deposition processes*. *Journal of Petroleum Science and Engineering*, 2016. **137**: p. 22-32.
 125. Foundation, G.E.C. *Automatic analyzer for water pollution monitoring station*. 2016 03.10.2016]; Available from: http://nett21.gec.jp/CTT_DATA/WMON/CHAP_4/html/Wmon-101.html.
 126. Zhang, Y., et al., *The kinetics of carbonate scaling—application for the prediction of downhole carbonate scaling*. *Journal of Petroleum Science and Engineering*, 2001. **29**(2): p. 85-95.

127. Charpentier, T., A. Neville, and S. Baraka-Lokmane. *Evaluation of Anti-fouling Surfaces for Prevention of Mineral Scaling in Sub-surface Safety Valves*. in *SPE International Oilfield Scale Conference*. 2014.
128. Vazirian, M. and A. Neville, *An investigation into the effect of hydrodynamic conditions and surface characteristics on adhesion/deposition processes of carbonate/sulphate scales in the oil and gas industry*. Proceedings of Oilfield Chemistry Symposium, Geilo, Norway., 2015.
129. Liu, X., et al., *The analysis and prediction of scale accumulation for water-injection pipelines in the Daqing Oilfield*. Journal of Petroleum Science and Engineering, 2009. **66**(3–4): p. 161-164.
130. Johnston, C.J., W. Taylor, and L. Sutherland. *The Influence of Turbulence (or Hydrodynamic Effects) on Barium Sulphate Scale Formation and Inhibitor Performance*. in *SPE International Symposium on Oilfield Chemistry*. 2013. Society of Petroleum Engineers.
131. Sanni, O., et al., *Study of Surface Deposition and Bulk Scaling Kinetics in Oilfield Conditions Using an In-Situ Flow Rig*, NACE International.
132. Bukuaghangin, O., et al., *A Kinetic Study of Barium Sulphate Formation in Presence of Scale Inhibitor in a Flowing System*, NACE International.
133. Eroini, V., et al. *Preventing Scale Formation Using Modified Surfaces*. in *CORROSION 2011*. 2011. NACE International.
134. Yang, X., et al., *The influence of O-carboxymethylchitosan on the crystallization of calcium carbonate*. Powder Technology, 2010. **204**(2–3): p. 228-235.
135. Tang, H., J. Yu, and X. Zhao, *Controlled synthesis of crystalline calcium carbonate aggregates with unusual morphologies involving the phase transformation from amorphous calcium carbonate*. Materials Research Bulletin, 2009. **44**(4): p. 831-835.
136. Keum, D.-K., K. Naka, and Y. Chujo, *Unique crystal morphology of hydrophobic CaCO₃ composite by sodium trisilanolate in a mixture of a water-miscible organic solvent and water*. Journal of Crystal Growth, 2003. **259**(4): p. 411-418.
137. Dinamani, M., P.V. Kamath, and R. Seshadri, *Electrochemical synthesis of calcium carbonate coatings on stainless steel substrates*. Materials Research Bulletin, 2002. **37**(4): p. 661-669.
138. Gopi, S.P., P. Vijaya, and V.K. Subramanian, *Morphological and crystallization process of CaCO₃ in the presence of Aqua soft 330 (AS 330)*. Powder Technology, 2012. **225**: p. 58-64.
139. Bischoff, J.L., *Kinetics of calcite nucleation: magnesium ion inhibition and ionic strength catalysis*. Journal of Geophysical Research, 1968. **73**(10): p. 3315-3322.
140. Burton, E.A. and L.M. Walter, *Relative precipitation rates of aragonite and Mg calcite from seawater: Temperature or carbonate ion control?* Geology, 1987. **15**(2): p. 111-114.
141. Dawe, R.A. and Y. Zhang, *Kinetics of calcium carbonate scaling using observations from glass micromodels*. Journal of Petroleum Science and Engineering, 1997. **18**(3–4): p. 179-187.
142. Zhu, L., et al., *Formation of star-shaped calcite crystals with Mg²⁺ inorganic mineralizer without organic template*. Journal of Solid State Chemistry, 2006. **179**(4): p. 1247-1252.

143. Katz, A., *The interaction of magnesium with calcite during crystal growth at 25–90°C and one atmosphere*. *Geochimica et Cosmochimica Acta*, 1973. **37**(6): p. 1563-1586.
144. Sondi, I., S.D. Škapin, and B. Salopek-Sondi, *Biomimetic precipitation of nanostructured colloidal calcite particles by enzyme-catalyzed reaction in the presence of magnesium ions*. *Crystal Growth and Design*, 2007. **8**(2): p. 435-441.
145. De Leeuw, N., *Molecular dynamics simulations of the growth inhibiting effect of Fe²⁺, Mg²⁺, Cd²⁺, and Sr²⁺ on calcite crystal growth*. *The Journal of Physical Chemistry B*, 2002. **106**(20): p. 5241-5249.
146. Compton, R.G. and C.A. Brown, *The Inhibition of Calcite Dissolution/Precipitation: Mg²⁺ Cations*. *Journal of Colloid and Interface Science*, 1994. **165**(2): p. 445-449.
147. Nancollas, G.H. and K. Sawada, *Formation of scales of calcium carbonate polymorphs: The influence of magnesium ion and inhibitors*. *Journal of Petroleum Technology*, 1982. **34**(03): p. 645-652.
148. Davis, K.J., P.M. Dove, and J.J. De Yoreo, *The role of Mg²⁺ as an impurity in calcite growth*. *Science*, 2000. **290**(5494): p. 1134-1137.
149. Paquette, J., H. Vali, and A. Mucci, *TEM study of Pt-C replicas of calcite overgrowths precipitated from electrolyte solutions*. *Geochimica et Cosmochimica Acta*, 1996. **60**(23): p. 4689-4699.
150. Akin, G.W. and J.V. Lagerwerff, *Calcium carbonate equilibria in solutions open to the air. II. Enhanced solubility of CaCO₃ in the presence of Mg²⁺ and SO₄²⁻*. *Geochimica et Cosmochimica Acta*, 1965. **29**(4): p. 353-360.
151. Mucci, A., *Influence of temperature on the composition of magnesian calcite overgrowths precipitated from seawater*. *Geochimica et Cosmochimica Acta*, 1987. **51**(7): p. 1977-1984.
152. Mucci, A. and J.W. Morse, *The incorporation of Mg²⁺ and Sr²⁺ into calcite overgrowths: influences of growth rate and solution composition*. *Geochimica et Cosmochimica Acta*, 1983. **47**(2): p. 217-233.
153. Park, W.K., et al., *Effects of magnesium chloride and organic additives on the synthesis of aragonite precipitated calcium carbonate*. *Journal of Crystal Growth*, 2008. **310**(10): p. 2593-2601.
154. Hu, Z. and Y. Deng, *Synthesis of needle-like aragonite from calcium chloride and sparingly soluble magnesium carbonate*. *Powder technology*, 2004. **140**(1): p. 10-16.
155. Wang, L., I. Sondi, and E. Matijević, *Preparation of Uniform Needle-Like Aragonite Particles by Homogeneous Precipitation*. *Journal of Colloid and Interface Science*, 1999. **218**(2): p. 545-553.
156. Xu, S., et al., *Structure and Morphology of Electrodeposited CaCO₃: X-Ray Diffraction and Microscopy Studies*. *Journal of the Electrochemical Society*, 1999. **146**(9): p. 3315-3323.
157. Berner, R.A., *The role of magnesium in the crystal growth of calcite and aragonite from sea water*. *Geochimica et Cosmochimica Acta*, 1975. **39**(4): p. 489-504.
158. Todd, A. and M. Yuan, *Barium and strontium sulfate solid-solution scale formation at elevated temperatures*. *SPE production engineering*, 1992. **7**(01): p. 85-92.

159. Katz, A., et al., *Strontium behavior in the aragonite-calcite transformation: An experimental study at 40–98°C*. *Geochimica et Cosmochimica Acta*, 1972. **36**(4): p. 481-496.
160. Plummer, L.N. and E. Busenberg, *Thermodynamics of aragonite-strontianite solid solutions: Results from stoichiometric solubility at 25 and 76°C*. *Geochimica et Cosmochimica Acta*, 1987. **51**(6): p. 1393-1411.
161. Vazirian, M.M., et al., *Scale Deposition in the Oil and Gas Industry: From a Systematic Experimental Scale Study to Real-Time Field Data*, 2016, NACE International.
162. Vazirian, M.M., et al., *Assessing Surface Engineering Solutions for Oilfield Scale; Correlating Laboratory Tests to Field Trials*, 2016, Society of Petroleum Engineers.